FILM THINNING IN OIL/WATER COALESCENCE

by

ALBERTUS J. S. LIEM

A Thesis

Submitted to the Faculty of Graduate Studies

in Partial Fulfilment of the Requirements

for the Degree

Doctor of Philosophy

McMaster University

June, 1975

FILM THINNING IN OIL/WATER COALESCENCE

DOCTOR OF PHILOSOPHY (1975) McMASTER UNIVERSITY

(CHEMICAL ENGINEERING) Hamilton, Ontario

TITLE: Film thinning in oil/water coalescence

AUTHOR: Albertus J.S. Liem, B.E. (University of Queensland)

M.E.Sc. (University of Queensland)

SUPERVISOR: Professor D.R. Woods, Ph.D.

NUMBER OF PAGES: xx, 285

ABSTRACT: This thesis is a study of the effect of surfactant on the film thinning behaviour of small, single droplets coalescing at a planar interface in oil/water systems. There are two major parts in this thesis. The first is the mathematical modelling of film thinning, and the second is the experimental measurement of the variation of film thickness during thinning.

The mathematical modelling consists of:

(i) the development of a film thinning model in which the interface mobility is calculated and not assumed arbitrarily,

(ii) the numberical solution of this film thinning model based on a polynomial representation of the pressure in the film,

(iii) the extension of the parallel disc model to describe the thinning at the barrier ring for uneven thinning, by allowing the interfaces to have varying degrees of partial mobility, and

(iv) the algebraic analysis of a postulate for the conditions for even and uneven thinning, based on the assumption that the pressure in the film is a parabolic function of the radial distance.

To verify these models, their predictions are compared with experimental observations.

In the experimental part, the effect of additions of palmitic acid and the effect of drop size and bulk interface age on the film thinning behaviour of toluene drops have been investigated using the white light interference technique. A novel drop forming technique has been developed, by which one drop forming nozzle can be used to form drops of different sizes without piercing the bulk interface; this technique eliminates the possibility of surfactant transfer between the bulk and drop interfaces.

New observations of film thinning behaviour are reported. These are the uneven thinning pattern that occurs when both the drop and bulk interfaces have the same surface concentration, and new thinning patterns which occur when drops are released to the bulk interface in rapid succession.

ACKNOWLEDGEMENTS

The author wishes to thank Dr. D.R. Woods for his supervision; Drs. T.W. Hoffman and P. Dawson for their service on the advisory committee; Dr. I. Feuerstein for his supervision during Dr. Woods absence on sabbatical leave; and, Dr. K.A. Burrill for the suggestions and ideas he raised during many useful discussions.

Many of the experimental difficulties would not have been overcome without the assistance of the staff of the Chemical Engineering Workshop, the Glassblower's Shop and the Audiovisual Department.

The editorial assistance of Mr. R.A. Knowles is also acknowledged with thanks.

The financial assistance of the National Research Council is gratefully acknowledged.

TABLE OF CONTENTS

PAGE

PAGE

LIST OF FIGURES

PAGE

PAGE

PAGE

APPENDIX A

APPENDIX B

APPENDIX C

APPENDIX D

LIST OF TABLES

EQUATION, FIGURE AND TABLE NUMBERING

For convenience, the following convention has been adopted for reference to equations, figures and tables. Within each chapter references to equations, etc. are made without the prefatory chapter number; references to equations, etc. from other chapters, however, do include the chapter number.

LIST OF SYMBOLS

A	Contact area between the interfaces
A_n	Coefficient of r^n in the polynomial representation of the pressure (normalized) in the film
A^*, B^*, C^*	Parameters for calculating ζ, defined in Appendix E
b	Drop radius
B_1	Coefficient for the linear representation of U_1^+
c	Bulk surfactant concentration
C_1	Symbol for integration constant
D_1	Coefficient for the linear representation of U_2^+
F	Force acting on the film; in this thesis F is the drop buoyancy force
g	Gravitational accelaration
h	Film thickness h_o : h at the initial time h_r : critical thickness at rupture
H_0, H_2	Coefficients for the parabolic representation of Γ_2^+
G_0, G_2	Coefficients for the parabolic representation of Γ_1^+
j_n	Rate of surfactant adsorption to an interface
k_3	Rate constant for the linear expression for j_n
k^*	Constant for the ideal surface equation of state
$k^*\Gamma$	Lowering of interfacial tension of an interface with a surfactant concentration of Γ
K	Constant for the linear isotherm
L_n	Coefficient of r^n in the polynomial representation of the film thickness (normalized); L_0 denotes the normalized film thickness at the barrier ring in Chapter 5

n_G	Geometrical factor, defined in Eq. (5-7)
n_I	Number of completely immobile interfaces
n_M	Number of fully mobile interfaces; extended in its meaning to the degree of interface mobility
N	The highest order of r^n in the polynomial representation of the pressure in the film
p	Pressure in the film
P	Normalizing constant for pressure
(r,z)	Axi-symmetrical cylindrical coordinates; r = radial distance and z = axial distance
r_c	Barrier ring radius
R	Normalizing constant for radial distance
ℝ	Symbol denoting the instant of film rupture
R'	Radial distance where the interfaces are not influenced by the flow in the film, and where the surface concentration is equal to Γ_s
R_p	Radial distance where the pressure and its gradient are zero
t	Interface age t_a : t for a sufficiently aged interface t_c : critical t when instantaneous coalescence no longer occurs t_e : t when the equilibrium interfacial tension is reached
T	Normalizing constant for time
U	Normalizing constant for interface velocity
$\underline{U}$	General interface velocity vector
U_1, U_2	Interface velocities of interfaces 1 and $2^{(x)}$, respectively
$\underline{V}$	General velocity vector
V_r, V_z	Radial and axial components of $\underline{V}$, respectively
y(r)	General expression for a curved interface

Y	Normalizing constant for film thickness
z_1, z_2	Bulk and drop interfaces, respectively

Greek characters

β	A measure of the radial location, βR_p where the interface is not influenced by the flow in the film
β_1, β_2	Principal radii of curvature
γ	Interfacial tension γ_1, γ_2 : γ for interfaces 1 and 2 respectively γ_o : γ for an uncontaminated interface γ_{eq} : Equilibrium interfacial tension
Γ	Surface concentration Γ_1, Γ_2 : Γ for interfaces 1 and 2, respectively Γ_{1o}, Γ_{2o}: Γ_1 and Γ_2 at the initial time Γ_s : Γ for an aging stationary interface Γ_{s1}, Γ_{s2}: Γ_s for interfaces 1 and 2, respectively
θ	Elapsed time
θ_o	Initial time
Θ	Rest time
μ	Film viscosity
ν	Kinematic viscosity
ξ	General symbol for an independent variable
ρ	Density of the film
$\Delta\rho$	Density difference between the two phases
$\underline{\tau}$	General shear stress tensor
τ_n, τ_t	Normal and tangential components of the shear stress tensor at a curved interface
τ_{rr}, τ_{rz} τ_{zr}, τ_{zz}	Cylindrical coordinates components of the shear stress tensor
X	General symbol for a dependent variable

ϕ_7 Ratio of Γ_{s2} to Γ_{s1}

ϕ_9 Dimensionless group proportional to $k^* \Gamma_{s1}$; in Chapter 2 it is defined by $(k^* \Gamma_{s1}/\gamma)$ and in Chapter 4, by $(k^* \Gamma_{s1}/P\,Y)$

Φ Parameter to characterize the number of mobile or immoblile interfaces, defined in Eq. (5-3)

Script characters

$\mathcal{D}$ Bulk diffusion coefficient

$\mathcal{D}$ Surface diffusion coefficients

Superscripts

$\bullet$ Dimensionless variables defined by Eq. (2-9)

$\blacksquare$ Dimensionless variables defined by Eq. (2-69)

$+$ Normalized variables defined by Eq. (4-1)

Vector notation

∇c Gradient, defined by $\frac{dc}{dx_i}\,\hat{i} + \frac{dc}{dx_j}\,\hat{j} + \ldots$

$\nabla \cdot \underline{V}$ Divergence, defined by $\frac{dV_i}{dx_i} + \frac{dV_j}{dx_j} + \ldots$

$\nabla^2 c$ Laplacian, defined by $\frac{d^2c}{dx_i^2} + \frac{d^2c}{dx_j^2} + \ldots$

$\underline{V}.\underline{V}$ Dyadic product, a tensor with $(i,j)^{th}$ element equals to $V_i V_j$

where

x_i , x_j .... coordinate axes.

$\hat{i}$, $\hat{j}$ ..... unit vectors in x_i, x_j ...

V_i , V_j .... components of $\underline{V}$ in x_i, x_j ...

Note:

(x) In Chapter 2, interface 1 refers to the bulk interface; however, in general, interface 1 refers to the interface with the larger value of Γ_s.

CHAPTER 1

INTRODUCTION

Coalescence is the process by which two or more bodies of the same fluid, separated by another immiscible fluid, join together. One of the fluids must be a liquid, the other can be a liquid or a gas. Examples of the three possible cases are shown in Figs. 1a to 1c. In the collapse of foams, the coalescing fluid is a gas and the other fluid is a liquid; in the formation of rain drops, the coalescing fluid is water and the other fluid is air; and in a settling process the two fluids are liquid. Fig. 1c also shows that coalescence can take place between drops or between a drop and its already formed bulk phase.

In certain cases, coalescence should not take place; for example, where a stable emulsion is to be sustained. Conversely, in a distillation column, where persistent foaming is undesirable, coalescence must take place quite readily. These examples serve to illustrate the two types of coalescence studies. The first deals with emulsion stability; typified by the studies of thin soap film behaviour[1-4] and forces - such as the van der Waals[5-10] and electrical double layer forces[9-11] - which act on surfaces that are close together. The second deals with unstable systems, where the main interest is the rate at which coalescence takes place. This thesis belongs to the second type of study.

In a settling tank, the two liquids separate completely when all the drops have coalesced with their bulk phases; hence the rate of coa-

lescence determines the efficiency of the settling tank. The separation of two immiscible liquids is, of course, a common chemical engineering process. When a reaction or mass transfer is to take place between two immiscible liquids, these liquids are first dispersed to enhance the process by increasing the contact area. After the reaction or mass transfer is completed, these liquids must then be separated. The rate of coalescence, and hence the separation rate, is often the controlling step in the process.

Settling is just one example where coalescence can be important. In general, coalescence plays an important role in processes that involve two-phase systems with large contact area.

Two approaches can be adopted in coalescence studies. The first is to design experiments which resemble the real situation as closely as possible so as to obtain results that are usable from a practical point of view. However, the design and analysis of such experiments are difficult because of the large number of variables - some of which may still be unknown - that have to be controlled and/or measured. The second approach is to use a simple experiment in which the important variables can be more easily identified and controlled, and their effects measured. By this means, a fundamental understanding of the process can be gained and then used as a basis for dealing with the more complex and realistic cases.

The simplest case of coalescence is one that occurs between a drop and a bulk phase at a planer interface. This thesis deals only with this simplest case in liquid/liquid systems.

1.1. Qualitative description of single drop coalescence

Consider again the coalescence in a settling tank. Following the path of a drop in isolation - in this instance for a drop that is lighter

than the surrounding liquid - one would observe that the drop will:

(i) rise rapidly to the interface,

(ii) appear to be arrested at the interface,

(iii) join the bulk phase, and sometimes

(iv) leave behind a smaller drop.

The sequence is shown in Fig. 2. Steps (i) to (iii) are referred to as the first stage of coalescence. The first stage of coalescence is sometimes followed by the formation of a smaller drop, called a secondary or satellite drop, as shown in step (iv). However, the study of the behaviour of secondary drops is beyond the scope of this thesis.

The time during which the drop appears to be arrested at the interface is called the rest time. For practical purposes, rest time and coalescence time can be considered equal. Since step (ii) is the rate determining step, let us consider in more detail what actually happens when the drop appears to be arrested at the interface.

In this instance, the drop is an oil that is lighter than the surrounding liquid, water. The water is the continuous phase and the oil which the drop eventually joins is the bulk phase. Thus there are three phases - the drop, the continuous and the bulk phases - which are separated by two interfaces. The bulk interface separates the bulk and continuous phases and the drop interface, the continuous phase and the drop.

When the drop is close to the bulk interface, a film of the continuous phase is formed between the bulk and the drop interfaces. (The definitions of the terminology and the geometry of the problem are shown in Fig. 3). Because of its buoyancy force, the drop continues to approach the bulk interface causing the film to thin. Finally when the

the film reaches its critical thickness, the film ruptures and the contents of the drop flow into the bulk phase, thus completing the first stage of coalescence. It is during the film thinning that the drop appears to be arrested at the bulk interface.

For the film to thin, there must be a fluid flow in the film, which implies the existence of a pressure gradient in the film. Because the interfaces are liquid/liquid interfaces, they must deform and hence the film is not uniform in thickness. The radial location of the minimum film thickness is called the barrier ring.

The flow in the film, caused by the pressure gradient, exerts shear stresses at the interfaces which might cause the interfaces to move tangentially. Therefore, the rate of film thinning depends - amongst other factors - on the rate at which the interfaces move. If the interfaces are completely immobile - which is the property of a solid interface or one where the interfaces cannot move - thinning occurs at the slowest possible rate. Conversely, if the interfaces are fully mobile - which is the property of an uncontaminated fluid/fluid interface - thinning occurs at the fastest possible rate.

A completely immobile or fully mobile interface is a special case. In general, surfactants or surface active contaminants are present at an interface. These surface active substances, which lower the interfacial tension of the interface, alter the mobility and the flow properties of the interface. A simplified illustration of how surfactants act in altering interface mobility is shown in Fig. 4. Initially the surfactant molecules are uniformly distributed at the interface. When the interface moves from A to B (for example, as a result of an application of a shear

stress), it will carry surfactant molecules. Thus the surfactant concentration will no longer be uniform; it is now larger at B. This retards the interface movement because the interfacial tension at A is greater than that at B. In summary, surfactants alter the flow properties of an interface by means of setting up an interfacial tension gradient at the interface. This surfactant effect is referred to as the surface elasticity and the Marangoni effect[12].

The extent of the surfactant effect is determined by the factors which govern the distribution of the surfactant concentration at the interface. These factors are the rate at which the interface moves (because of convective transfer of surfactant molecules), the surface diffusion due to the non-uniform concentration, and the rate of adsorption/desorption of surfactant between the interface and the bulk phase.

From the foregoing description, one can deduce the probable variables which affect film thinning:

(i) densities and viscosities, which affect the flow properties of the film, the drop and the bulk phase,

(ii) interfacial tensions, which affect the deformability of the bulk and drop interfaces,

(iii) drop size and density difference, and the van der Waals and electrical double layer forces, which affect the force acting on the film,

(iv) the properties of the adsorbed surfactant, which affect the flow properties of the bulk and drop interfaces.

The surfactant properties of interest are:

(i) the 'strength' , that is, the degree of lowering the interfacial tension for a given surfactant concentration distribution, and

(ii) the surface diffusion coefficient and the rate of adsorption/desorption between the interface and the bulk fluid: these are the properties which affect the surfactant concentration distribution for a given flow system.

In this thesis, the effect of surfactants composed of large molecules, such as a protein or a long chain polymer, and the effect on the deformability of an interface are assumed negligible, because only low concentrations of relatively small surfactants are considered.

1.2. Previous work

This section is not an exhaustive literature survey; it is a review of the development of research in coalescence to show the present state of knowledge, so that the scope and the contributions of this thesis can be more cearly defined.

1.2.1. Experimental studies

In early studies[13-16] only rest times were measured. The aim was to correlate rest time with system physical properties, such as drop size, viscosity, density and interfacial tension. Rest times were found to vary - in some cases from 1 to 30 seconds - even though the experimental conditions appeared to be identical. This variation was attributed mainly to the randomness of the film rupture process.

Rest time was therefore regarded as a distributional quantity, which had a mean and a standard deviation. This lead to the use of a Gaussian distribution to describe rest time data, and proposals for equations correlating the mean rest time with system physical properties [17,18].

An important contribution to the explanation of the scatter and poor reproducibility of rest time data was made by Hodgson and Lee[19] who developed new techniques for cleaning the bulk interface and forming drops accurately. They introduced a new variable, the bulk interface age, and showed that the rest time was a function of this new variable. (The interface age is an indirect measure of the surface concentration at the interface. When the age is zero, which corresponds to the instant when the interface has just been formed or cleaned, the surface concentration is also zero. As the age increases so does the surface concentration because of the surfactant adsorption to the interface.) Therefore, the scatter of the rest time data could be partly due to the interface aging effect, or in more general terms - the variation in surface concentration at the bulk and/or the drop interfaces.

The work of Hodgson and Lee also showed that coalescence is extremely sensitive to minute traces of surfactant at the interface. Even when thorough cleaning and purification procedures were exercised, the interface aging effect was still observed for 'pure' systems.

The next development in coalescence research was the attempt to gain a basic understanding of how coalescence takes place by measuring the change in film thickness during thinning[20-23]. The findings of Hodgson and Lee were confirmed by others who identified at least four patterns of film thinning behaviour for the same liquids and drop size [22,23]. These patterns were:

(i) Pattern I: rapid thinning and instantaneous coalescence,

(ii) Pattern II: rapid thinning, arrest, dimple formation (an increase in the film thickness with elapsed time) and thinning,

(iii) Pattern III: uneven thinning (unsymmetrical about an axis which passes through the drop centre at right angle to the bulk interface), and

(iv) Pattern IV: slow even thinning, where the approach of the drop to the bulk interface is arrested at a large film thickness, and the subsequent thinning occurs mainly in the barrier ring region.

The occurrence of one pattern depended mainly on the surfactant concentration. Therefore, the scatter of rest time data for seemingly identical conditions can be explained partly by the existence of these different thinning patterns, because the rate of film thinning for one pattern is different from that for another.

The mechanisms that lead to the different film thinning behaviour have been proposed in terms of the distribution of surfactant concentration at the bulk interface and the consequent interface movement[23].

Hartland[24] also observed dimple formation, even and uneven thinning in very viscous systems. His explanation was given in terms of the internal circulation in the drop, which he measured by photographing the motion of tracer particles inside the drop, in the film and in the bulk phase.

It has now become apparent that to understand coalescence, the change in film thickness during thinning must be measured; the measurement of rest times alone is not adequate. Moreover, because of the sensitivity of coalescence to minute traces of surfactant, the surfactant concentration must be carefully controlled. Consider now some of the experimental techniques that have been used.

Film thickness measurements

So far only optical methods have been used. (An electrical capacitance method[25] can only be used to measure 'average' thicknesses) These are the side photography and light interference techniques.

In the side photography, the film is observed at one cross-sectional plane from a direction parallel to the bulk interface; that is, the film is observed two-dimensionally. The obtain the angular variation in film thickness, which is necessary in identifying uneven thinning, either more than one camera must be used, or the camera must be rotated around the drop during film thinning. In this respect, the light interference is a better technique because the film is observed from the direction perpendicular to the bulk interface; hence both the radial and angular variation in film thickness can be observed simultaneously.

The choice between the two techniques is often dictated by the restrictions imposed on the refractive indices of the two fluids, and the range of film thicknesses to be measured. Consider these restrictions in turn.

In the side photography, the film is viewed through the bulk phase since the bulk phase deforms during film thinning. Therefore, to minimize distortion, the refractive indices of the two fluids should be as close as possible without rendering the interfaces invisible. On the other hand, with the light interference technique, the difference in the refractive indices should be as large as possible because reflections from the bulk and drop interfaces must occur. This requires that the minimum difference in refractive indices be about 0.1.

The side photography and the light interference techniques have different ranges of measurable film thicknesses. With the former, there is no upper limit; the lower limit is determined by the resolution power of the camera lens and the grain size of the camera film. For commercially available products, this lower limit is about 0.001 cm. The side photography technique has been used extensively by Hartland[21] and his co-workers for viscous systems where the rate of thinning was small even at large film thicknesses. When the lower limit was reached, they then used the electrical capacitance method .

In the light interference technique, either monochromatic or white light can be used. When monochromatic light is used, the interference results are the appearance of dark and light regions. The interpretation of the results is ambiguous because no reference thickness is available, and moreover because the shape of the film (that is, whether the film is increasing or decreasing in thickness) is in general not known. This difficulty can be overcome by using white light which produces interference colours. From the sequence of these colours the shape of the film as well as the film thickness can be determined. The theory which relates film thickness to interference colour is given elsewhere[26,27].

The range of measurable film thicknesses for the white light interference technique is from 400 A^{o} to 16,000 A^{o}; therefore this technique is suitable for most oil/water and air/water systems[20,22,23].

Methods for cleaning the bulk interface

Although thorough cleaning and purification procedures have been exercised, there are still surface active contaminants present in the

coalescence apparatus. By cleaning the bulk interface, these contaminants (and the deliberately added surfactant) can be temporarily removed from the bulk interface. Therefore, interface cleaning is a form of an indirect control of surface concentration.

The three types of cleaning technique that have been used are:

(i) spilling technique[13,17,20], in which the interface is 'spilled' in order to form a fresh interface,

(ii) adsorption by talc powders[15], in which talc powders are introduced to the interface to adsorb the contaminants, and subsequently removed after the adsorption is completed, and

(iii) suction technique[15,19], in which a suction probe is used to remove the bulk fluids in the vicinity of the interface, thereby providing a cleaning action.

For the suction technique to be effective, both fluids must be removed simultaneously. This simultaneous removal is difficult to achieve because usually the suction probe is wetted by only one of the fluids. Thus when suction is applied, only the fluid that wets the probe is removed; for example, if a glass probe is used to clean an oil/water interface, only the water is removed by the suction. Hodgson[19] developed a cleaning technique which ensured this simultaneous removal - shown diagramatically in Fig. 5. To clean an oil/water interface, the probe is made of glass, and a teflon thread is placed inside the probe at its tip. Therefore, the probe is wetted by one fluid and the thread by the other fluid. Because of these wetting properties, both fluids can be removed simultaneously: one fluid flows through the probe, and the other flows over the thread.

The effectiveness of an interface cleaning technique is not easily determined because of the difficulties in measuring the concentration of the contaminants before and after cleaning. Nevertheless, one can use rest time measurements to give some indication of the effectiveness of an interface cleaning technique. If coalescence occurs instantaneously (zero rest time) for a period of time after the cleaning has been completed, this indicates that the technique used is effective because zero rest time corresponds to fully mobile - hence uncontaminated - interfaces. By this criterion, Hodgson's technique is the most effective technique.

Drop forming technique

The drop-volume method[28] has been the most commonly used method. The drop size is calculated from the balance between the drop buoyancy and the surface forces; hence by the density difference, the interfacial tension and the nozzle dimensions. The measurement of the drop size is often complicated by the formation of a satellite drop at the instant the drop detaches from the nozzle. There is also the inconvenience of having to change the nozzle to form drops of different sizes.

Hodgson[19] developed a technique, whereby one nozzle can be used to form drops of different sizes. Fig. 6 shows this technique. To form a drop, the nozzle tip is inserted into the bulk phase, and the desired volume of the drop is metered by using a micrometer syringe. The nozzle, now containing the drop, is then withdrawn from the bulk phase. With this technique the drop size can be measured directly using the micrometer syringe because the drop does not wet the nozzle and hence the drop size is not determined by the balance between drop buoyancy and surface forces.

A further advantage of Hodgson's technique is that the drop and and the bulk phase have the same temperature and bulk surfactant concentration. Therefore, any effect on the film thinning behaviour that may result from differences in temperature or bulk surfactant concentration is minimized. However, Hodgson's technique has a disadvantage in that the bulk interface is disturbed by the insertion and withdrawal of the drop forming nozzle tip, exactly at the location where the coalescence takes place. As a result, surfactant molecules and contaminants may be transferred between the bulk interface and the nozzle tip and hence the drop interface. This means that it is impossible to control the surfactant concentration at the drop interface.

1.2.2. Mathematical modelling of film thinning

The basis for developing a film thinning model is the description of the flow in the film. However, since the film is bounded by liquid/liquid interfaces which deform under pressure and may move tangentially under shear stress, it is also necessary to describe the interface movements and the flow in the bulk phase and inside the drop. The simultaneous solution of these flow equations is difficult. Hence in the past, various assumptions for the interface movements have been made to avoid the need of solving the flow equations at the bulk and drop interfaces, in the bulk phase and inside the drop. These assumptions were:

(i) completely immobile interface, that is $U = 0$, where U is the interface velocity, and

(ii) fully mobile interaface, that is $\partial V/\partial z = 0$, where z is the direction normal to the interface, and V is the velocity profile parallel to the interface.

These assumptions have been made despite the known fact that in general a liquid/liquid interface is neither completely immobile nor fully mobile (cf. Fig. 4). The interface velocity should be calculated from the balance between the shear stresses that act at the interface and the interfacial tension gradient that is set up by the non-uniform distribution of surfactant concentration at the interface[29]. Hence the constant-mobility assumption further simplifies the modelling of film thinning since the surfactant mass balance equations need not be considered.

To simplify further the modelling of film thinning, the assumption that the interfaces are non-deformable has also been made. The resulting model cannot describe the change in film curvature with elapsed time during thinning. Such a model is usually used to describe film thinning only at a particular location in the film, for example the barrier ring; that is, the model is used for predicting rest times.

Consider now some of the models that have been developed. The most widely used model is the parallel disc model, originally developed by Reynolds[30] and Stefan[31]. In the parallel disc model, the interfaces are assumed to be non-deformable, completely immobile and parallel. The rate of thinning is given by

$$-\frac{dh}{d\theta} = \frac{2\pi}{3\mu}\frac{F}{A^2}h^3 \qquad (1)$$

where h is film thickness, θ is elapsed time, μ is film viscosity, F is the force acting on the film, and A is the contact area of the interfaces. The rest time can thus be calculated integrating Eq. (1) between the limits of $\theta=0$ at $h=\infty$, and $\theta=\Theta$ at $h=h_1$, the critial film thickness. The result is

$$\theta = \frac{3\mu}{4\pi} \frac{A^2}{F} \frac{1}{h_1^2} \qquad (2)$$

For the case of a drop approaching a planar interface, the simplest expression for F is the drop buoyancy force, and for A is the area calculated from the equilibrium barrier ring radius (see, for example Ref. 32). The parallel disc model overestimates the rest times of liquid/liquid systems.

To account for the properties of a liquid/liquid interface, various modifications to the parallel disc model have been made. These include allowing one of the interfaces to be fully mobile[33] and obtaining more accurate estimates for the value of F/A^2 (see, for example Refs. 34 to 37). These modified models can only describe the observed thinning rates over a narrow range of film thicknesses. A review of these models is given elsewhere[38].

Charles and Mason[32] derived the general equation for the rate of thinning for a film bounded by non-deformable, completely immobile interfaces of any geometry. From this general equation, the rate of thinning for, for example the approach of a spherical drop to a planar interface can be readily obtained.

The modifications to the parallel disc model that have just been described were directed towards the obtaining of more accurate shapes for the film geometry. A different way of modifiying the parallel disc model is to allow the interfaces to be partially mobile instead of completely immobile or fully mobile[36,37] . This is the subject of Chapter 5.

Other non-deformable models are those of Hodgson and Woods[22] and Marucci[38]. The former was developed for one particular case of

film thinning behaviour, the slow even thinning Pattern IV. This model predicts well the thinning at the barrier ring, provided that it is applied to the same thinning pattern. It is worth noting that the dependence of the rate of thinning on system physical properties for this model is different from that for the parallel disc model.

Marucci[44] suggested that film thinning was a two-stage process: rapid thinning to a quasi-equilibrium thickness, followed by slow thinning until the film critical thickness is reached. He derived the equations for calculating the quasi-equilibrium thickness (if it is less than the expected critical thickness, instantaneous coalescence occurs) and the rate of thinning for the slow thinning. However, no comparison with experimental data was given.

Non-deformable models do not give a fundamental understanding of film thinning behaviour because they do not describe the observed variation in film curvature during thinning. Hence deformable models have also been developed: the approach of a solid drop to a deformable bulk interface[39], a deformable drop to a solid bulk interface[40], a deformable drop to a deformable bulk interface[41,42] and a drop to another drop[43]. In all these models, except that of Burrill[42], the interfaces were assumed to be completely immobile or fully mobile. In Burrill's model the mobility of the bulk interface was calculated, but the drop interface was assumed to be fully mobile or completely immobile. These previous models did not satisfactorily describe the experimental observations, nor could they explain the existence of different types of film thinning behaviour. Even when the mobility of the bulk interface was calculated (Burrill's model), the predicted rates of dimple formation and thinning were about ten times faster than those observed.

It appears reasonable to conclude that the main cause of failure of these previously developed models is the incorrect assumption that the interfaces are either completely immobile or fully mobile, because of the sensitivity of film thinning behaviour to minute traces of surfactant. Hence, to model film thinning successfully the mobility of the bulk and the drop interfaces should be calculated and not preset.

1.2.3. Summary of previous work

1. The measurement of rest times only is not adequate in the study of coalescence; the film thinning behaviour and how it is affected by surfactant must also be studied.

2. The white light interference technique is a useful method for measuring film thicknesses during thinning, and detecting even and uneven thinning behaviour.

3. Hodgson's interface cleaning technique is effective for cleaning the bulk interface.

4. There is a need for a drop forming technique, by which drops of different sizes can be formed in one nozzle (Hodgson's technique) and the possibility of surfactant transfer between the bulk and the drop interfaces can be eliminated.

5. There is a need for film thinning models, in which the interface mobility is calculated and not preset.

1.3. Scope and outline of the thesis

This thesis is a study of the effect of surfactant on the film thinning behaviour of single drop coalescence in oil/water systems. It is

confined to isothermal systems with no chemical reaction or mass transfer taking place between the oil and the water, and where the effect of electrical double layer is suppressed by the addition of an electrolyte in the water.

In the theoretical part, various film thinning models, in which the interface mobility is calculated and not arbitrarily assumed, are developed. The aims in developing these models are:

(i) to gain a better understanding of film thinning behaviour, and

(ii) to obtain a simple expression for the rate of thinning for the film thinning behaviour that is most likely to occur in practice.

The models for (i) are those for describing the change in film thickness with time and location in the film, and for explaining why even or uneven thinning occurs. The model for (ii) is the extended parallel disc model.

In the experimental part, the effect of additions of palmitic acid (an oil soluble surfactant) and the effect of drop size and bulk interface age on the film thinning behaviour of toluene drops are investigated. A novel drop forming tecnique is developed, whereby one nozzle can be used to form drops of different sizes without piercing the bulk interface; hence the possibility of surfactant transfer between the bulk and the drop interfaces is eliminated.

The outline of the thesis is as follows. In Chapter 2, the general equations for the fluid flow in the film are formulated and simplified by an order of magnitude analysis for the film thinning in oil/water systems. The boundary and initial conditions are carefully specified, and a postulate is put forward for the conditions for even and uneven thinning.

The experimental studies are described in Chapter 3. In Chapter 4

the numerical solution of the film thinning model is described, and its predictions compared with experimental observations. The extension of the parallel disc model by allowing the interfaces to have varying degrees of partial mobility is described in Chapter 5. This is the simple model which can be used to describe the thinning at the barrier ring for uneven thinning behaviour. Chapter 6 describes an algebraic analysis of a postulate for the conditions for even and uneven thinning, and an evaluation of this postulate based on experimental observations.

Literature cited

1. de Vries, A. J., Rec.Trav.Chim., 77(1958):81,209,283,383.

2. Overbeek, J. Th. G., Proc. IV Int.Congr.Surf.Act.Subst., Brussels, Sept. 1964, Vol. II, Sect. B, Gordon and Breach, London(1967):19.

3. Vrij, A., Disc.Far.Soc., 42(1966):23.

4. Vrij, A and Overbeek, J. Th. G., J.Am.Chem.Soc., 90(1968):3074.

5. Derjaguin, B. V., and Abricosova, I. I., Disc.Far.Soc., 18(1954):33.

6. Kitchener, J. A. and Prosser, A. P., Proc.Roy.Soc., A242(1967):403.

7. Black, W., et al, Trans.Far.Soc., 56(1960):1597.

8. Tabor, D., J.Coll.Intf.Sci., 31(1969):364, Nature, 219(1968):1120.

9. Verwey, E. J. W. and Overbeek, J. Th. G., "Theory of the stability of lyophobic colloids", Elsevier, Amsterdam (1948).

10. Overbeek, J. Th. G., in "Colloid science", H. R. Kruyt (Ed), Vol. I, Elsevier, Amsterdam (1952):Ch. 2,6 and 7.

11. Derjaguin, B. V., Trans.Far.Soc., 36(1940):203.

12. Kanner, B. and Glass, J. E. "Chemistry and physics of interfaces" Vol. II, Am.Chem.Soc., Washington, D.C. (1971): 49.

13. Cockbain, E. G. and MacRoberts, T. S., J.Coll.Sci., 8(1953):440

14. Elton, G. A. H. and Picknett, R. G., Proc. II Int.Congr.Surf.Act., Butterworths, London(1957):Vol. I,287.

15. Gillespie, T. and Rideal, E. K., Trans.Far.Soc., 52(1956):173.

16. Nielson, L. E. et al, J.Coll.Sci., 13(1958):441.

17. Hawksley, J. L. and Jeffereys, G. V., A.I.Ch.E.J., 11(1965):413.

18. Jeffereys, G. V. and Lawson, G., referred to by Jeffereys, G. V. and Davies, G. A., in "Recent advances in liquid/liquid extraction", Hanson, C.(Ed), Pergamon Press(1971):Ch. 14.

19. Hodgson, T. D. and Lee, J. C., J.Coll.Intf.Sci., 30(1969):94.

20. Mackay, G. D. M. and Mason, S. G., Can.J.Chem.Engng., 41(1963):203.

21. Hartland, S., Trans.Inst.Chem.Engrs.(London) 45(1967):T97.

22. Hodgson, T. D. and Woods, D. R., J.Coll.Intf.Sci., 30(1969):429.

23. Burrill, K. A. and Woods, D. R., J.Coll.Intf.Sci., 42(1973):15.

24. Hartland, S. Chem.Engng.Sci., 24(1969):611.

25. Hartland, S. Trans.Inst.Chem.Engrs.(London) 45(1967):T102.

26. Lawrence, A. C. S., "Soap films" Bell&Sons Ltd, London (1929).

28. Harkins, W. D. "The physical chemistry of surface films" Reinhold, N. Y. (1952):76.

29. Levich, V. G. "Physicochemical Hydrodynamics" Prentice Hall, N. J. (1962):Ch. VII.

30. Reynolds, O., Phil.Trans., A177(1866):157.

31. Stefan, J., Sitzber.Akad.Wiss.Wien.Math-naturw.Kl., 69(1874):713.

32. Charles, G. E. and Mason, S. G., J.Coll.Sci., 15(1960):235.

33. Hodgson, T. D., Ph.D. Thesis, Univ. Wales, Swansea, U.K. (1966)

34. Princen, H. M., J.Coll.Sci., 18(1963):178.

35. Chappelear, D. C., J.Coll.Sci., 16(1961):186.

36. Hartland, S. and Robinson, J. D., Can.J.Chem.Engng., 51(1973):647.

37. Hartland, S. and Wood, S. M., A.I.Ch.E.J., 19(1973):810,871.

38. Woods, D. R. and Burrill, K. A., J. Elct.Chem., 37(1972):191.

39. Hartland, S., J.Coll.Intf.Sci., 26(1968):383, Chem.Engng.Sci., 24 (1969):987.

40. Feuerstein, I. and Chappelear, D. C., Can.J.Chem.Engng., 50(1972):569.

41. Hartland, S., Chem.Engng.J., 1(1970):67.

42. Burrill, K. A., Ph.D. Thesis, McMaster Univ., Hamilton, Canada (1970)

43. Murdoch, P. G. and Leng, D. E., Chem.Engng.Sci., 26(1971):1881.

44. Marrucci, G., Chem.Engng.Sci., 24(1969):975.

Figure captions

1. Different types of coalescence: (a) gas/liquid, (b) water/air and (c) liquid/liquid, where Phase1/Phase2 denotes that Phase1 is the coalescing or dispersed fluid, and Phase2 is the continuous fluid.

2. Description of single drop coalscence: (i) rapid approach, (ii) drop arrest (film thinning), (iii) film rupture and drop contents inflow, and (iv) formation of a satellite drop.

3. The geometry and terminology of film thinning.

4. The mechanism of the retardation of interface movement by surfactant.

5. Hodgson's interface cleaning technique: both phases near the interface are withdrawn simultaneously because of the wetting properties of the interface cleaning probe and the thread.

6. Hodgson's drop forming technique: the drop size is not determined by the balance between the buoyancy and surface forces; but note the possibility of surfactant transfer between the bulk and the drop interfaces because of the piercing of the bulk interface.

a

Break up of foams

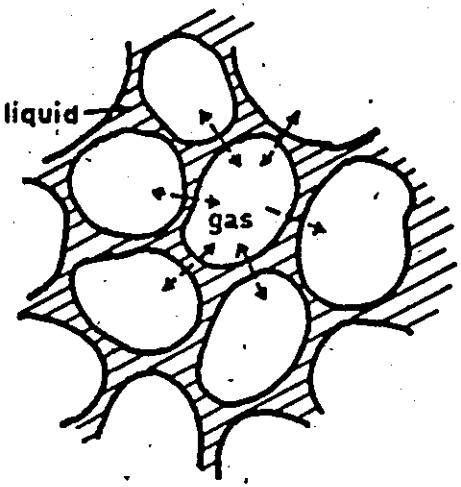

b

Formation of rain drops

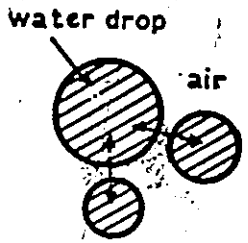

c

Coalescence in a settling tank

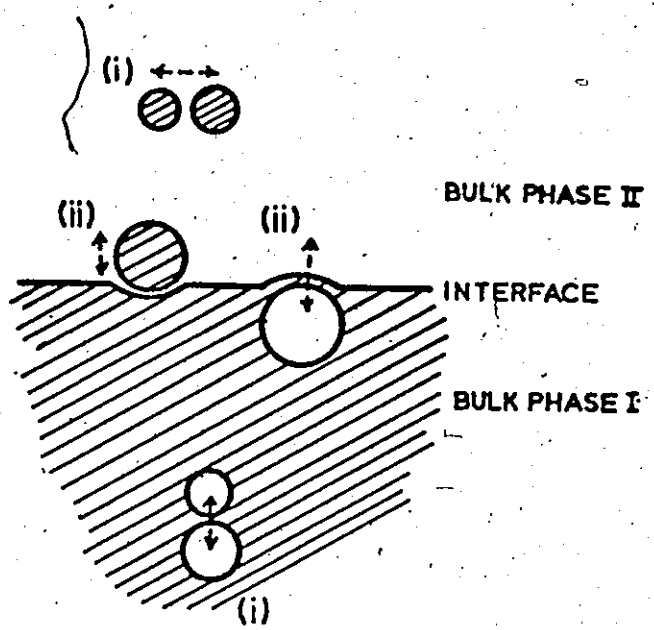

(i) Drop-drop coalescence

(ii) Drop-bulk phase coalescence

Figure 1

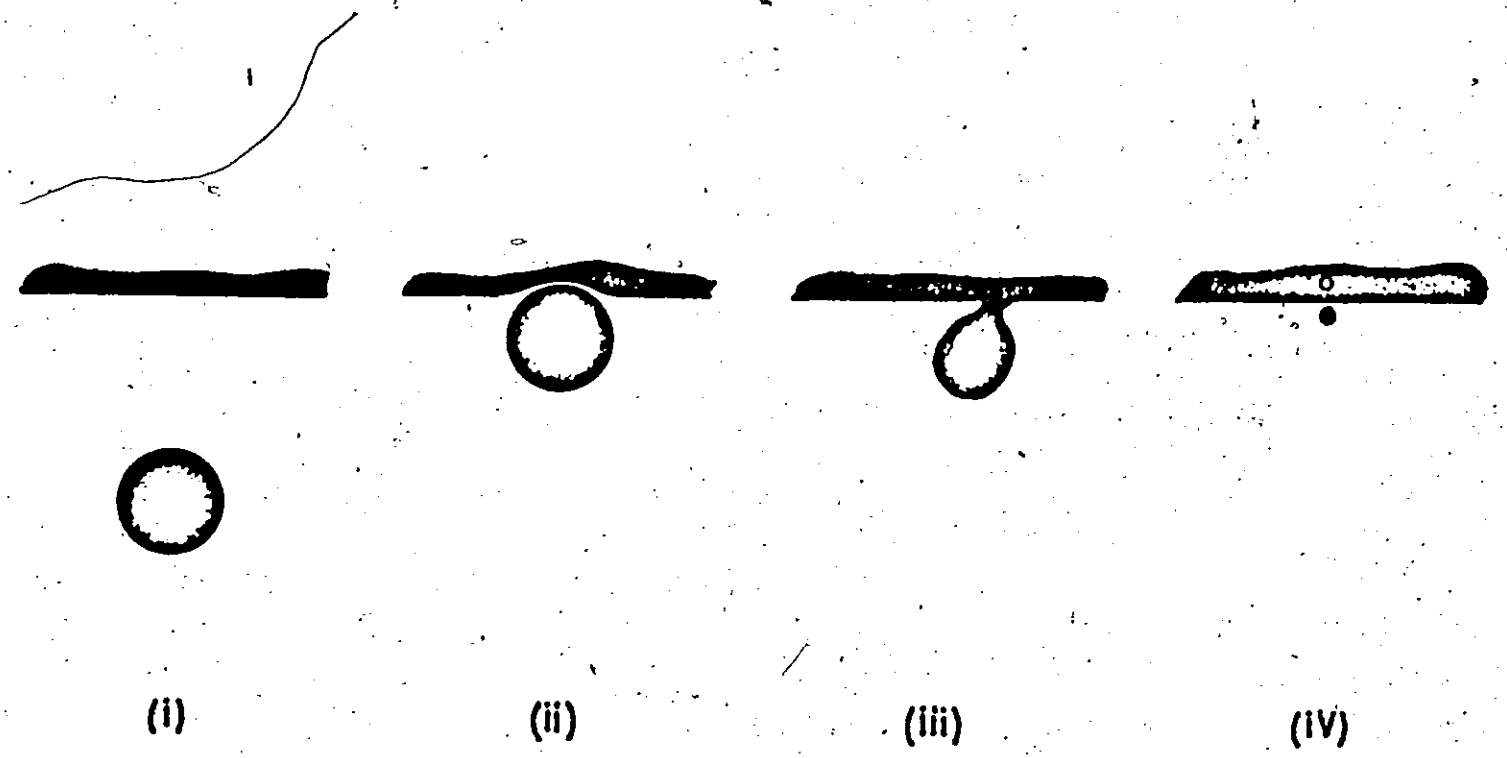

Figure 2

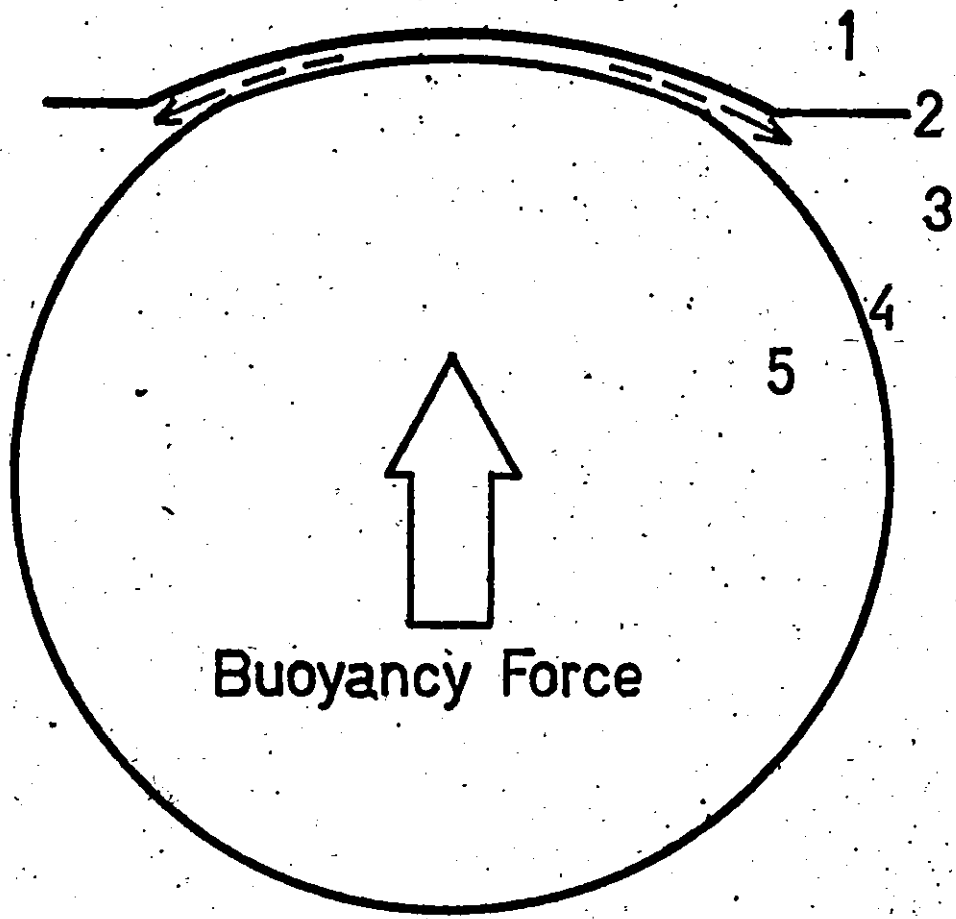

1	Bulk Phase
2	Bulk Interface
3	Continuous Phase
4	Drop Interface
5	Drop

——→ Fluid Flow in the Film

Figure 3

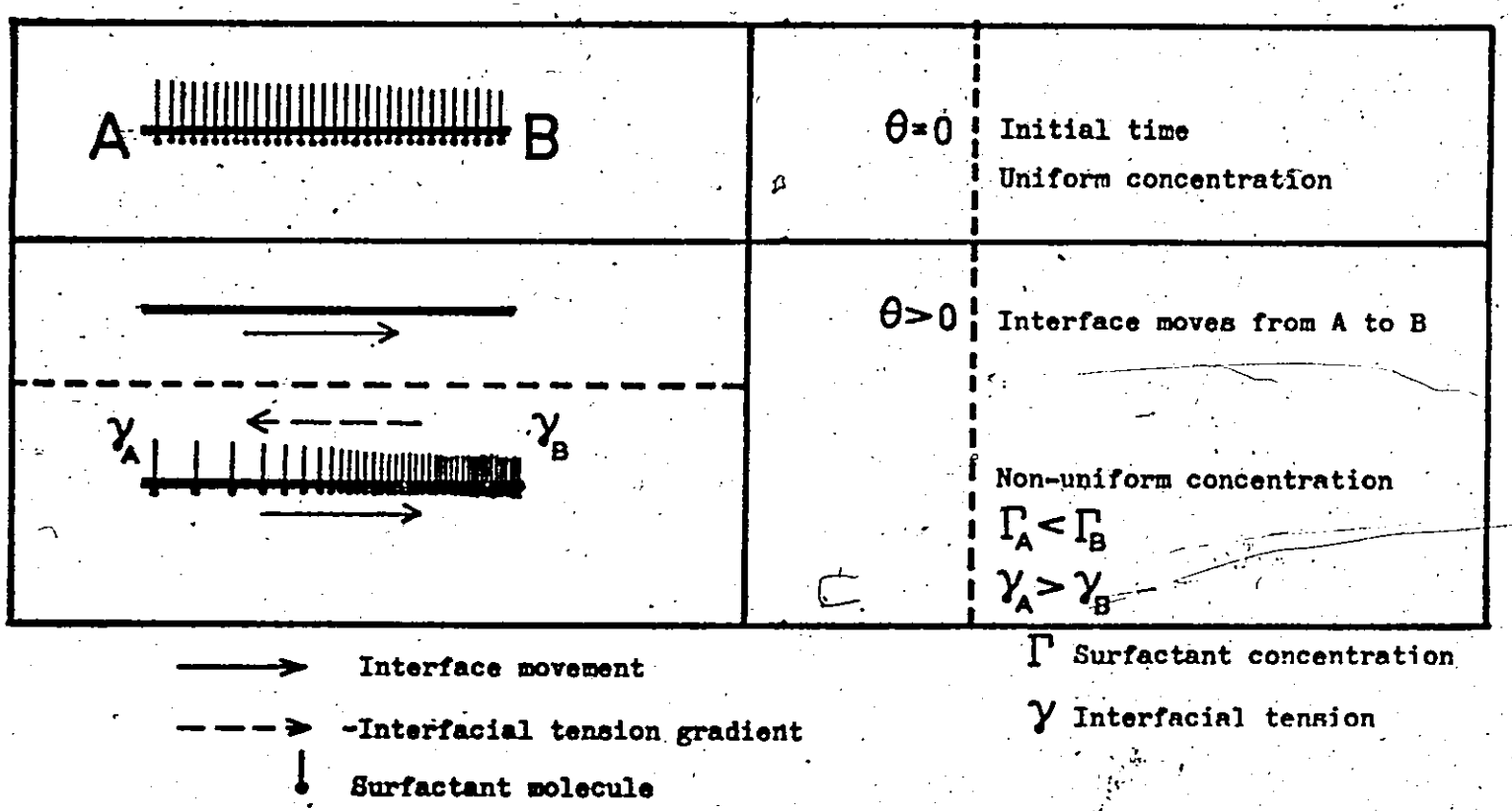
A
B
θ=0
Initial time
Uniform concentration
θ>0
Interface moves from A to B
γ_A
γ_B
Non-uniform concentration
$\Gamma_A < \Gamma_B$
$\gamma_A > \gamma_B$
Interface movement
-Interfacial tension gradient
Surfactant molecule
Γ Surfactant concentration
γ Interfacial tension

Figure 4

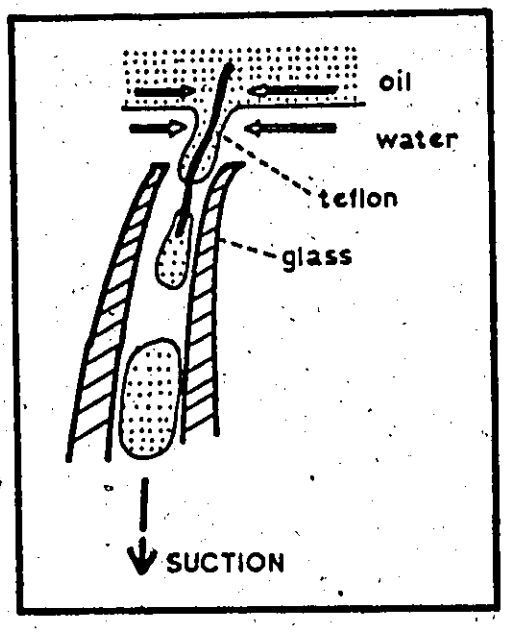

Figure 5

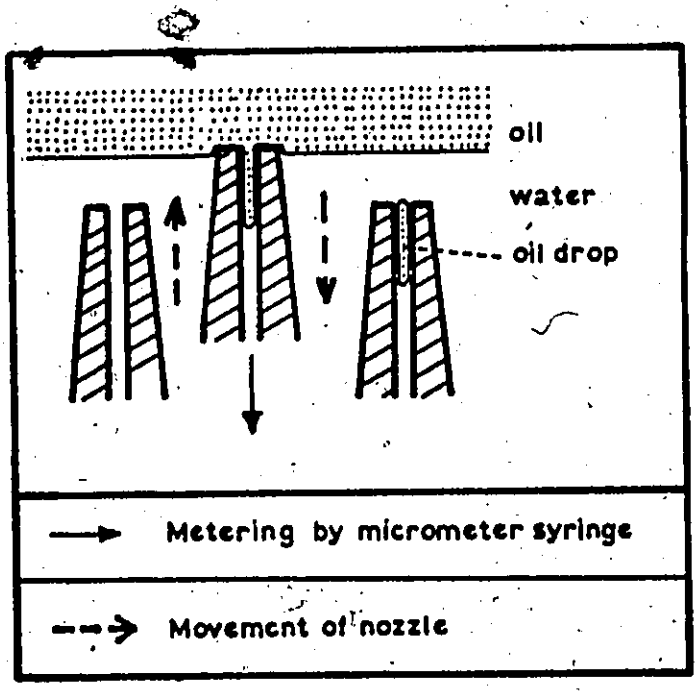

Figure 6

CHAPTER 2

MATHEMATICAL FORMULATION OF FILM THINNING

The basis for developing a film thinning model is the description of the fluid mechanics of the flow in the film. In this chapter, the film thinning equations are derived from first principles. The derivation shows how the force and mass balance equations are related, and clarifies the justification of the various assumptions which are needed to render the equations solvable.

First, the general equations are described and simplified (in this case for oil/water systems) via an order of magnitude analysis. The film thinning equations, their boundary and initial conditions are then carefully formulated. The suitability and the implications of the resulting film thinning model, and a method for obtaining the relevant dimensionless groups are discussed.

2.1. The general equations

For a fluid with constant density and viscosity, the isothermal equations of change in the film, the bulk phase and inside the drop are - in vector notation[1]:

(i) Equation of continuity

For the total fluid:

$$\nabla . \underline{V} = 0 \qquad (1)$$

and for the surfactant:

$$\frac{\partial c}{\partial \theta} = -\underline{V} \cdot \nabla c + \mathcal{D} \nabla^2 c \qquad (2)$$

where $\mathcal{D}$ is the bulk diffusion coefficient of the surfactant.

(ii) Equation of motion

$$\rho \frac{\partial \underline{V}}{\partial \theta} = -\rho \nabla \cdot \underline{V}\,\underline{V} - \nabla p + \mu \nabla^2 \underline{V} + \rho \underline{g} \qquad (3)$$

At each interface, the boundary conditions that must be satisfied are[2]:

$$\underline{V}^{(1)} = \underline{V}^{(2)} \qquad (4)$$

$$\tau_n^{(1)} - \tau_n^{(2)} = -\gamma\left(\frac{1}{\beta_1} + \frac{1}{\beta_2}\right) \qquad (5)$$

$$\tau_t^{(1)} - \tau_t^{(2)} = -\nabla \gamma \qquad (6)$$

where the supercripts 1 and 2 denote the two phases that are separated by the interface being considered, τ_n and τ_t are the normal and tangential components of the viscous shear tensor, and β_1 and β_2 are the principal radii of curvature. The RHS of Eqs. (5) and (6) are the normal pressure due to interface curvature and the interfacial tension gradient, respectively.

The values of τ_n and τ_t are calculated from the stress tensor $\underline{\underline{\tau}}$ and the interface curvature, where $\underline{\underline{\tau}}$ is related to $\underline{V}$ by the Newtonian stress-strain relationship[1]. The interfacial tension γ, which varies along the interface, is related to the surfactant concentration Γ by the surface equation of state, given by

$$\gamma = \gamma(\Gamma) \qquad (7)$$

The variation of Γ with time is given by the surfactant mass balance at the interface:

$$\frac{\partial \Gamma}{\partial \theta} = j_n + \mathcal{D} \nabla^2 \Gamma - \underline{U} \cdot \nabla \Gamma \qquad (8)$$

where j_n is the rate of bulk/interface transfer of surfactant molecules, $\mathcal{D}$ is the surface diffusion coefficient of the surfactant, and $\underline{U}$ is the interface velocity.

Eqs. (1) to (8) are the general equations that describe the flow of two fluids separated by an interface that contains surfactants. In film thinning, there are three bulk fluids - the drop, the film and the bulk phase - and two interfaces - the drop and the bulk interfaces. Therefore, Eqs. (1) to (3) must be solved for the three bulk fluids, and these solutions must satisfy Eqs. (4) to (8) at the two interfaces.

One of the difficulties in solving Eqs. (1) to (8) lies in the coupling of the equations, as can be seen by examining Eqs. (6) to (8). To obtain the velocity profiles, the distribution of the surfactant concentration at the interface (or the interfacial tension) must be known, as given by Eqs. (6) and (7). However, this distribution in turn depends on the interface velocity (hence the velocity profile), as shown by Eq. (8). In general, the solution of the film thinning equations by analytical methods is not possible; even numerical solutions still present a time consuming task. Therefore, the general film thinning equations must first be simplified, and yet the resulting simplified equations should be capable of describing the observed film thinning behaviour.

This chapter describes the simplification of the general equations and the specification of the boundary and initial conditions.

2.2. Simplification of the general equations

2.2.1. Equations of motion in the film

The geometry of the problem in axi-symmetrical cylindical coordinates is shown in Fig. 1. The z-axis passes through the centre of the drop and the r-axis coincides with the undeformed portion of the bulk interface.

With the following dimensionless variables

$r^\bullet = \frac{r}{R}$	$z^\bullet = \frac{z}{\sqrt{\frac{R\nu}{U}}}$	$\theta^\bullet = \frac{\theta}{R/U}$
$p^\bullet = \frac{p}{\rho U^2}$	$V_r^\bullet = \frac{V_r}{U}$	$V_z^\bullet = \frac{V_z}{\sqrt{\frac{U\nu}{R}}}$

(9)

the equations of motion[1] become

$$\frac{\partial V_r^\bullet}{\partial \theta^\bullet} = -\left(V_r^\bullet \frac{\partial V_r^\bullet}{\partial r^\bullet} + V_z^\bullet \frac{\partial V_r^\bullet}{\partial z^\bullet}\right) - \frac{\partial p^\bullet}{\partial r^\bullet} + \frac{1}{Re}\left(\frac{\partial^2 V_r^\bullet}{\partial r^{\bullet 2}} + \frac{1}{r^\bullet}\frac{\partial V_r^\bullet}{\partial r^\bullet} - \frac{V_r^{\bullet 2}}{r^{\bullet 2}}\right) + \frac{\partial^2 V_r^\bullet}{\partial z^{\bullet 2}} \tag{10}$$

$$\frac{\partial V_z^\bullet}{\partial \theta^\bullet} = -\left(V_r^\bullet \frac{\partial V_z^\bullet}{\partial r^\bullet} + V_z^\bullet \frac{\partial V_z^\bullet}{\partial z^\bullet}\right) - Re\frac{\partial p^\bullet}{\partial z^\bullet} + \frac{1}{Re}\left(\frac{\partial^2 V_z^\bullet}{\partial r^{\bullet 2}} + \frac{1}{r^\bullet}\frac{\partial V_z^\bullet}{\partial r^\bullet}\right) + \frac{\partial^2 V_z^\bullet}{\partial z^{\bullet 2}} + \left[\frac{\rho g^2 R^3}{\mu U^3}\right]^{\frac{1}{2}} \tag{11}$$

where

$$Re = \frac{\rho U R}{\mu} \tag{12}$$

The orders of magnitude of oil/water physical properties are

γ	ρ	μ	ν	g
dn/cm	gm/cc	poise	cm^2/sec	cm/sec^2
10	1	10^{-2}	10^{-2}	10^3

Based on previous film thinning observations, the orders of magnitude of the variables in film thinning are

r	z	θ	V_r	V_z	p
cm	cm	sec	cm/sec	cm/sec	dn/cm^2
10^{-2}	10^{-5}	1	10^{-3}	10^{-5}	10^2

Therefore, the orders of magnitude of the dimensionless variables are - for $U = 10^{-3}$ cm/sec and $R = 10^{-2}$ cm:

$r^\bullet$	$z^\bullet$	$\theta^\bullet$	$V_r^\bullet$	$V_z^\bullet$	$p^\bullet$	Re
1	10^{-4}	10^{-1}	1	10^{-4}	10^{8}	10^{-3}

The orders of magnitude of the terms in Eqs. (10) and (11) can be calculated by assuming that $d^n X / d\xi^n$ can be approximated by X/ξ^n. The results are:

$\frac{\partial V_r^\bullet}{\partial \theta^\bullet}$	$V_r^\bullet \frac{\partial V_r^\bullet}{\partial r^\bullet}$	$V_z^\bullet \frac{\partial V_r^\bullet}{\partial z^\bullet}$	$\frac{\partial p^\bullet}{\partial r^\bullet}$	$\frac{1}{Re} \nabla_r^2 V_r^\bullet$	$\frac{\partial^2 V_r^\bullet}{\partial z^{\bullet 2}}$
10	1	1	10^{8}	10^{3}	10^{8}

$\frac{\partial V_z^\bullet}{\partial \theta^\bullet}$	$V_r^\bullet \frac{\partial V_z^\bullet}{\partial r^\bullet}$	$V_z^\bullet \frac{\partial V_z^\bullet}{\partial z^\bullet}$	$Re \frac{\partial p^\bullet}{\partial z^\bullet}$	$\frac{1}{Re} \nabla_r^2 V_z^\bullet$	$\frac{\partial^2 V_z^\bullet}{\partial z^{\bullet 2}}$	$\left[\frac{\rho g^2 R^3}{\mu U^3}\right]^{1/2}$
10^{-3}	10^{-4}	10^{-4}	10^{9}	10^{-1}	10^{4}	10^{5}

Therefore the equations of motion can be simplified into

$$\frac{\partial p}{\partial r} = \mu \frac{\partial^2 V_r}{\partial z^2} \qquad (13)$$

$$\frac{\partial p}{\partial z} = 0 \qquad (14)$$

which are consistent with the assumptions of pseudo steady state, creeping flow and negligible hydrostatic effects.

2.2.2. The tangential and normal stresses

The tangential and normal stresses at a curved interface can be expressed in terms of the cylindrical coordinates stress tensor and the interface curvature by carrying out force balances in the r and z directions. (This process is often referred to as a tensor transformation.) The results are

$$\tau_n = \frac{1}{\left[1+\frac{\partial y}{\partial r}^2\right]}\left\{\frac{\partial y}{\partial r}^2 \tau_{rr} - 2\frac{\partial y}{\partial r}\tau_{rz} + \tau_{zz}\right\} \quad (15)$$

$$\tau_t = \frac{1}{\left[1+\frac{\partial y}{\partial r}^2\right]}\left\{\frac{\partial y}{\partial r}\left(\tau_{zz}-\tau_{rr}\right)+\left(1-\frac{\partial y}{\partial r}^2\right)\tau_{rz}\right\} \quad (16)$$

where y(r) denotes the shape of the interface (Fig. 2). The stress tensor components are given by

$$\tau_{rr} = p - 2\mu\frac{\partial V_r}{\partial r} \quad (17)$$

$$\tau_{zz} = p - 2\mu\frac{\partial V_z}{\partial z} \quad (18)$$

$$\tau_{rz} = \tau_{zr} = -\mu\left(\frac{\partial V_r}{\partial z} + \frac{\partial V_z}{\partial r}\right) \quad (19)$$

In the region of interest in the film, which is inside $r < 0.3\ b$ (where b is the drop radius), the interface curvature is small, that is $(dy/dr)^2 \ll 1$ [3]. By using an order of magnitude analysis similar to that used in the previous section, it can be shown that

$$\tau_{rr} = \tau_{zz} = p \quad (20)$$

$$\tau_{rz} = \tau_{zr} = -\mu\frac{\partial V_r}{\partial z} \quad (21)$$

$$\tau_{zz} \gg \tau_{rz} \quad (22)$$

Therefore the normal and shear stresses are given by

$$\tau_n = \frac{1}{1+\frac{\partial y}{\partial r}^2}\left\{\frac{\partial y}{\partial r}^2 \tau_{rr} + \tau_{zz}\right\} = p \quad (23)$$

$$\tau_t = \frac{1}{1+\frac{\partial y}{\partial r}^2}\left\{\left(1-\frac{\partial y}{\partial r}^2\right)\tau_{rz}\right\} = -\mu\frac{\partial V_r}{\partial z} \quad (24)$$

Eqs. (23) and (24) are the simplified expressions for the normal and shear stresses, needed on the LHS of Eqs. (5) and (6).

The normal stress due to interface curvature

For an axi-symmetrical interface, the principal radii of curvature are given by[4]

$$\frac{1}{\beta_1} = \frac{1}{\left\{1+\left(\frac{\partial y}{\partial r}\right)^2\right\}^{3/2}} \frac{\partial^2 y}{\partial r^2} \tag{25}$$

$$\frac{1}{\beta_2} = \frac{1}{\left\{1+\left(\frac{\partial y}{\partial r}\right)^2\right\}^{1/2}} \frac{1}{r} \frac{\partial y}{\partial r} \tag{26}$$

The expressions for the radii of curvature can be simplified because the interface curvature is small, that is $(\partial y/\partial r)^2 << 1$. Therefore the RHS of Eq. (5) is given by

$$\gamma\left(\frac{1}{\beta_1} + \frac{1}{\beta_2}\right) = \gamma \frac{1}{r}\frac{\partial}{\partial r}\left(r\frac{\partial y}{\partial r}\right) \tag{27}$$

2.2.3. The flow in the bulk phase and inside the drop

The flow in the bulk phase is caused by the movement of the bulk interface. The description of this flow is needed to calculate the normal and shear stresses exerted by the bulk phase to the bulk interface (cf. Eqs. (5) and (6)), and to complete the surfactant mass balance equations in the bulk phase and at the bulk interface (cf. Eqs. (2) and (8)). In Appendix A, an approximate analysis of the flow in the bulk phase is described. This analysis is not used in this thesis for computational reasons. Instead, to simplify the solution of the film thinning equations, the bulk phase is assumed to be inviscid; hence no shear stress is

exerted to the bulk interface. The corresponding normal stress is also assumed to be zero because the curvature of the bulk interface is small.

The same inviscid assumption is also made for the flow inside the drop. For the normal stress exerted by the drop at the drop interface, it is assumed that the pressure in the drop is given by that in an undeformed drop, thus

$$\tau_{n,drop} = \frac{2\gamma}{b} \qquad (28)$$

The rate of transfer of surfactant to an interface j_n

A number of models for the transfer of surfactant to an aging stationary interface have been proposed[5,6]; in Appendix B, a new model is also proposed. However, there is so far no expression for j_n that has been universally accepted. Furthermore, since the description of the flow in the bulk phase and inside the drop has been neglected, only a simple expression for j_n is needed. Hence, for simplicity assume that

$$j_n = k_3 (\Gamma_s - \Gamma) \qquad (29)$$

where Γ_s is the corresponding surface concentration of a stationary interface; that is, the concentration at large radial distances where there is no interface movement. The expression given by Eq. (29) can account for the desorption of surfactant from the interface, indicated by a negative value for j_n.

2.2.4. Surface equation of state

As a first approximation, the ideal surface equation of state can be used; that is,

$$\gamma_o - \gamma = k^* \Gamma \tag{30}$$

where γ_o is the interfacial tension of an uncontaminated interface.

2.3. The equations governing film thinning

Fig. 3 shows schematically the derivation of the film thinning equations. The derivation is based on the combination of the equations of change in the fidm and the force and surfactant mass balance equations at the drop and bulk interfaces. The resulting equations describe the variation with elapsed time of film thickness, pressure and radial velocity in the film, and the distribution of surfactant concentration at the interfaces. The details of the derivation are as follows.

2.3.1. The rate of film thinning

Integration of the equation of motion Eq. (13) with respect to z with these boundary conditions

$$V_r\,(z=z_1) = U_1 \tag{31}$$

$$V_r\,(z=z_2) = U_2 \tag{32}$$

gives

$$V_r = (z-z_2)\left\{\frac{1}{2\mu}\frac{\partial p}{\partial r}(z-z_1) + \frac{U_1-U_2}{h}\right\} + U_2 \tag{33}$$

where the interface velocities U_1 and U_2 are still to be determined.

The continuity equation is[1]

$$\frac{1}{r}\frac{\partial}{\partial r}(rV_r) + \frac{\partial V_z}{\partial z} = 0 \qquad (34)$$

Integration of Eq. (34) with respect to z, from $z = z_2$ to $z = z_1$ gives

$$\frac{\partial h}{\partial \theta} = V_z(z=z_1) - V_z(z=z_2) = -\int_{z_2}^{z_1} \frac{1}{r}\frac{\partial}{\partial r}(rV_r)\,dz \qquad (35)$$

where h is the film thickness, given by

$$h = z_1 - z_2 \qquad (36)$$

Substitution of Eq. (33) into Eq. (35) gives the expression for the rate of film thinning:

$$\boxed{\frac{\partial h}{\partial \theta} = \frac{1}{r}\frac{\partial}{\partial r}\left[r\left\{\frac{1}{12\mu}\frac{\partial p}{\partial r}h^3 - \frac{1}{2}(U_1+U_2)h\right\}\right]} \qquad (37)$$

2.3.2. Normal force balance

At the bulk interface

Substitution of Eqs. (23) and (27) into Eq. (5) gives

$$p - 0 = -\gamma_1 \frac{1}{r}\frac{\partial}{\partial r}\left(r\frac{\partial z_1}{\partial r}\right) \qquad (38)$$

At the drop interface

Substitution of Eqs. (23), (27) and (28) into Eq. (5) gives

$$\frac{2\gamma_2}{b} - p = -\gamma_2 \frac{1}{r}\frac{\partial}{\partial r}\left(r\frac{\partial z_2}{\partial r}\right) \qquad (39)$$

Since the surfactant concentration is low, the following applies

$$\gamma_o - \gamma_1 \ll \gamma_o \text{ , or } \gamma_1 = \gamma_o \qquad (40)$$

$$\gamma_o - \gamma_2 \ll \gamma_o \text{ , or } \gamma_2 = \gamma_o$$

Hence, Eq. (39) can be subtracted from Eq. (38) to give the relationship between pressure in the film and film curvature:

$$\boxed{p = \gamma\left(\frac{1}{b} - \frac{1}{2r}\frac{\partial}{\partial r}\left[r\frac{\partial h}{\partial r}\right]\right)} \qquad (41)$$

2.3.3. Tangential force balance

The shear stress exerted by the flow in the film at the bulk interface is given by Eq. (24):

$$\tau_{t1} = -\mu\frac{\partial V_r}{\partial z} \qquad z = z_1 \qquad (42)$$

which can be calculated from Eq. (33). The result is

$$\tau_{t1} = -\mu\frac{U_1 - U_2}{h} - \frac{1}{2}h\frac{\partial p}{\partial r} \qquad (43)$$

similarly, for the drop interface

$$\tau_{t2} = \mu\frac{\partial V_r}{\partial z} \qquad z = z_2 \qquad (44)$$

$$\tau_{t2} = \mu\frac{U_1 - U_2}{h} - \frac{1}{2}h\frac{\partial p}{\partial r} \qquad (45)$$

Substitution of Eq. (43) into Eq. (6), and Eq. (45) into Eq. (6) gives the equations for the tangential force balance:

At the bulk interface

$$-\mu\frac{U_1 - U_2}{h} - \frac{1}{2}h\frac{\partial p}{\partial r} - 0 = -\frac{\partial \gamma_1}{\partial r} \qquad (46)$$

At the drop interface

$$\mu \frac{U_1 - U_2}{h} - \frac{1}{2} h \frac{\partial p}{\partial r} - 0 = -\frac{\partial \gamma_2}{\partial r} \qquad (47)$$

The tangential force balance equations can be written in terms of the surfactant concentration distribution by using the differentiated form of the surface equation of state, that is

$$-\frac{\partial \gamma}{\partial r} = k^* \frac{\partial \Gamma}{\partial r} \qquad (48)$$

The results are

$$\boxed{k^* \frac{\partial \Gamma_1}{\partial r} + \mu \frac{U_1 - U_2}{h} + \frac{1}{2} h \frac{\partial p}{\partial r} = 0} \qquad (49)$$

$$\boxed{k^* \frac{\partial \Gamma_2}{\partial r} - \mu \frac{U_1 - U_2}{h} + \frac{1}{2} h \frac{\partial p}{\partial r} = 0} \qquad (50)$$

2.3.4. Surfactant mass balance

At the bulk interface

The surfactant mass balance equation Eq. (8) in axi-symmetrical cylindrical coordinates is

$$\boxed{\frac{\partial \Gamma_1}{\partial \theta} = k_3(\Gamma_{s1} - \Gamma_1) + D_s \frac{1}{r} \frac{\partial}{\partial r}\left(r \frac{\partial \Gamma_1}{\partial r}\right) - \frac{1}{r} \frac{\partial}{\partial r}\left(r U_1 \Gamma_1\right)} \qquad (51)$$

where the terms on the RHS of Eq. (51) represent, respectively, the bulk/interface transfer of surfactant (cf. Eq. (29)), surface diffusion and the convective transfer due to interface movement.

At the drop interface

For a spherical interface, Eq. (8) becomes

$$\frac{\partial \Gamma_2}{\partial \theta} = k_3(\Gamma_{s2} - \Gamma_2) + \frac{1}{r}\phi_r \frac{\partial}{\partial r}\left(r\phi_r \frac{\partial \Gamma_2}{\partial r}\right) - \frac{1}{r}\phi_r \frac{\partial}{\partial r}\left(r\phi_r^{-1} U_2 \Gamma_2\right) \qquad (52)$$

where

$$\phi_r = \left(1 - \left(\frac{r}{b}\right)^2\right)^{\frac{1}{2}}$$

However, in the region of interest, $r < 0.3\,b$, $\phi_r > 0.95$; hence, Eq. (52) can be simplified into

$$\boxed{\frac{\partial \Gamma_2}{\partial \theta} = k_3(\Gamma_{s2} - \Gamma_2) + \frac{1}{r}\frac{\partial}{\partial r}\left(r\frac{\partial \Gamma_2}{\partial r}\right) - \frac{1}{r}\frac{\partial}{\partial r}\left(r U_2 \Gamma_2\right)} \qquad (53)$$

This completes the derivation of the film thinning equations, given by Eqs. (37),(41),(49),(50),(51) and (53).

2.3.5. Boundary conditions

The highest order of derivative in Eqs. (37) and (41) is d^4h/dr^4 and in Eqs. (51) and (53), $d^2\Gamma_1/dr^2$ and $d^2\Gamma_2/dr^2$; hence four boundary conditions must be specified for the pressure or the film thickness, and two for each surfactant concentration at the interface. These are:

(i) Total force balance in the z direction

Because the flow in the film is very slow, the force acting on the film is balanced by the pressure in the film:

$$F = \int_0^\infty 2\pi r\, p\, dr \qquad (54)$$

Since only the drop buoyancy force is considered, hence

$$F = \frac{4}{3}\pi b^3 \Delta\rho\, g \qquad (55)$$

(ii) Far away from the centre, there is no flow

The pressure at r = ∞ can be set as the reference pressure, hence

$$p = 0 \quad \text{at } r = \infty \tag{56}$$

(iii) At the film centre, the pressure is finite

The second term on the RHS of Eq. (41) contains $1/r \cdot dh/dr$; hence to maintain a finite pressure at r = 0:

$$\frac{dh}{dr} = 0 \text{ at } r = 0 \tag{57}$$

(iv) At the film centre, the rate of thinning is finite

The first term on the RHS of Eq. (37) contains $1/r \; dp/dr$; hence

$$\frac{dp}{dr} = 0 \text{ at } r = 0 \tag{58}$$

The boundary conditions for the surface concentration are(omitting the subscripts 1 and 2) :

(i) At the film centre, the rate of change of Γ with time is finite

The RHS of Eq. (51) and (53) contain $1/r \; d\Gamma/dr$; hence

$$\frac{d\Gamma}{dr} = 0 \text{ at } r = 0 \tag{59}$$

(ii) Far away from the film centre, there is no interface movement

Since there is no interface movement, the concentration at r = ∞ is the stationary interface concentration:

$$\Gamma = \Gamma_s \text{ at } r = \infty \tag{60}$$

Note that Γ_s is a function of time if the interface is still aging.

Approximations for the boundary conditions that involve conditions at infinity

These boundary conditions, Eqs. (54),(56) and (60) are difficult to incorporate in the numerical solution. It is therefore necessary to replace the infinite radial distance by some finite radial distances.

For the pressure in the film, the boundary conditions are replaced by

$$F = \int_0^{R_p} 2\pi\, r\, p\, dr \qquad (54a)$$

and

$$p = 0 \quad \text{at} \quad r = R_p \qquad (56a)$$

where R_p is specified by

$$\frac{dp}{dr} = 0 \quad \text{at} \quad r = R_p \qquad (61)$$

Similarly, for the surface concentration:

$$\Gamma = \Gamma_s \quad \text{at} \quad r = R' \qquad (60a)$$

where R' is specified by

$$\frac{d\Gamma}{dr} = 0 \quad \text{at} \quad r = R' \qquad (62)$$

These approximations are shown diagramatically in Fig. 4.

2.3.6. Initial conditions

There are three time derivatives in the film thinning equations; therefore, three initial conditions must be specified to start the integration of the film thinning equations. These initial conditions are:

$$h(r, \theta = \theta_o) = h_o(r) \tag{63}$$

$$\Gamma_1(r, \theta = \theta_o) = \Gamma_{1o}(r) \tag{64}$$

$$\Gamma_2(r, \theta = \theta_o) = \Gamma_{2o}(r) \tag{65}$$

The selection of a suitable initial time is not straightforward because the film thinning equations are valid only in the region of small film thicknesses. If the initial time is chosen to coincide with the actual experimental initial time, another model must be developed to describe the initial motion of the drop during the period that the film thinning equations are not yet applicable. On the other hand, if the initial time is chosen such that the film thickness is in the region where the film thinning equations are applicable, the values of $\Gamma_{1o}(r)$ and $\Gamma_{2o}(r)$ are not readily known because the interfaces have moved prior to the selected initial time. Consider now the different choices of initial time, and the implications in terms of the values of the initial conditions and the need of developing an additional model to describe the initial motion of the drop, as summarized in Fig. 5.

Fig. 5a shows an experiment in which the drop is released from a location close to the interface (a typical distance is between 0.5 to 1 cm). The initial time selected is the instant just before the drop is released to the bulk interface. Thus the distributions of surface concentration at the initial time are uniform, $\Gamma_{1o}(r) = \Gamma_{s1}$ and $\Gamma_{2o}(r) = \Gamma_{s2}$. The initial film thickness profile $h_o(r)$ can be measured experimentally by using, for example the side photography method[7]. The additional model is one to describe the initial motion of the drop after it is released and the corresponding flow in the thick film and at the bulk interface. This model is difficult to develop because the manner by which

the drop is released from the capillary tube must be quantitatively accounted for.

In Fig. 5b, the drop is released from a location quite far from the bulk interface. Thus the drop will travel at its terminal velocity (after the initial accelaration period) until the bulk interface begins to retard its motion. This instant can be chosen as the initial time. Thus the initial distribution of surface concentration at the bulk interface is uniform, $\Gamma_{1o}(r) = \Gamma_{s1}$, and at the drop interface, the initial distribution is given by that at the interface of a drop travelling at its terminal velocity. The initial film thickness profile cannot be easily determined. The additional model is one which describes the retarded motion of the drop.

The initial time chosen in Fig. 5a or 5b is not suitable because of the difficulties in developing the additional model. Fig. 5c shows a selection of an initial time which does not require the development of an additional model. This initial time corresponds to the instant when the film begins to produce measurable interference colours; that is for film thicknesses less than 20,000 A^o. Thus the initial film thickness profile can be measured experimentally. The initial distributions of surface concentration are not uniform because the interfaces have moved prior to the initial time. These initial distributions can be calculated from the experimentally measurable rate of thinning at the selected initial time. In this thesis, the initial time shown in Fig. 5c is used.

Consider now the calculation of the initial distributions of surface concentration as outlined in Fig. 6. The calculation of surface concentrations and interface velocities are related because these variables

must satisfy the tangential force balance equations at the interfaces. Hence this calculation can be reduced into the calculation of one unknown, for example the bulk interface velocity U_1, as selected in Fig. 6.

Since the tangential force balance must always be satisfied, the value of U_1 which is consistent with the observed rate of thinning and the film thickness profile, must satisfy Eqs. (49) and (50), not only at the initial time θ_o, but also at some time later $\theta_o + \Delta\theta$. Combination of Eqs. (49) and (50) gives

$$k^*\left(\frac{\partial \Gamma_1}{\partial r} + \frac{\partial \Gamma_2}{\partial r}\right) + h\frac{\partial p}{\partial r} = 0 \qquad (66)$$

Since Eq. (66) must still be satisfied at $\theta_o + \Delta\theta$, the time derivative must also be satisfied:

$$k^*\frac{\partial}{\partial \theta}\left(\frac{\partial \Gamma_1}{\partial r} + \frac{\partial \Gamma_2}{\partial r}\right) + \frac{\partial}{\partial \theta}\left(h\frac{\partial p}{\partial r}\right) = 0 \qquad (67)$$

Because the order of differentiation is immaterial, Eq. (67) can be written as

$$k^*\frac{\partial}{\partial r}\left(\frac{\partial \Gamma_1}{\partial \theta} + \frac{\partial \Gamma_2}{\partial \theta}\right) + \frac{\partial}{\partial \theta}\left(h\frac{\partial p}{\partial r}\right) = 0 \qquad (68)$$

Eq. (68) is the equation for calculating U_1. The first term on the LHS of Eq. (68) can be calculated from the surfactant mass balance equations Eqs. (51) and (53); hence this term is a function of the unknown U_1. The second term can be calculated from the experimentally measured film thickness profile and rate of thinning at the initial time since h and p are related by the normal force balance equation Eq. (41).

Therefore, the value of U_1 calculated from Eq. (68) satisfies

the film thinning equations and agrees with the observed film thickness and rate of thinning. After U_1 is calculated, the other variables U_2, and $\Gamma_{1o}(r)$ and $\Gamma_{2o}(r)$ - the initial conditions - can be readily calculated from Eqs. (37),(49) and (50), respectively.

2.4. Discussion

2.4.1. Interface mobility

The main difference between the film thinning equations developed in this thesis and those previously developed lies in the description of the interface mobility. In this thesis, the interface mobility is not arbitrarily assumed, whereas previously it was assumed constant regardless of the surfactant concentration at the interface. Because the solution of the film thinning equations is much simpler when the interface mobility is assumed constant, it is important to examine whether the relaxation of this assumption is justifiable.

Consider first the dependence of the rate of thinning on interface velocity. Eq. (37) shows that the rate of thinning consists of the pressure and the interface velocity terms. The relative importance of these terms is a function of the film thickness h. Since the pressure gradient term contains h^3 and the interface velocity term, h^1, as the thinning proceeds and h decreases, the latter term will dominate the rate of thinning expression. In addition, the pressure gradient in the central region of the film is small (This will be confirmed in Chapter 4); therefore, since thinning or dimple formation occurs despite of the small pressure gradient, the interface velocity term is even more dominant in the central region of the film.

More important, however, is the fundamental consequence of assuming arbitrarily the interface mobility. As a result of this assumption, the equations for surfactant mass balance and tangential force balance need not be considered, and consequently the interface velocities U_1 and U_2 - and hence the interface velocity term in the rate of thinning expression - are essentially fixed. Therefore, the rate of thinning depends only on the pressure gradient and the film thickness profile. This implies that the rate of thinning for a given system (liquids and drop size) is uniquely determined by the film thickness since the pressure and film thickness are related by the normal force balance Eq. (42). Such a conclusion is not supported by experimental observations; different types of film thinning behaviour have been observed for the same liquids and drop size. Hence the interface mobility must be calculated and not preset.

The reason why it is incorrect to assume arbitrarily the interface mobility can also be seen by examining the calculation of the initial conditions. When this assumption is made, the initial distributions of surface concentration are not needed, hence there is only one initial condition that must be specified, namely the initial film thickness profile. Thus the initial rate of thinning is also not needed. This means that a model with constant mobility can predict the film thickness profiles at subsequent elapsed times based only on an initial film thickness profile. Such a prediction is in general incorrect since there can be different film thinning behaviour even though the initial film thickness profile is the same.

In summary, the constant mobility assumption is neither accurate nor correct fundamentally.

2.4.2. A postulate for the conditions for even and uneven thinning

The explanation of why thinning occurs evenly or unevenly is important in the understanding of coalescence; there is also a practical need to be able to estimate whether thinning will occur evenly or unevenly. If the thinning pattern is known, in certain cases a simple model can be used to describe the rate of thinning at a particular location in the film, for example the barrier ring. Unfortunately, different simple models are needed for different thinning patterns, such as even and uneven thinning. Therefore, the thinning pattern must be known if a simple model is to be used.

All the film thinning models so far developed are axi-symmetrical models. These models cannot describe uneven thinning. However, it may be possible to use an axi-symmetrical model to indicate the conditions under which thinning occurs evenly or unevenly.

Given a model which is capable of describing even thinning, consider the physical interpretation of the following possibilities that may arise in the calculation described in Fig. 6, Section 2.3.6:

(i) no real values for the interface velocities which satisfy the tangential force balance equations can be found, and

(ii) the surface concentration which would satisfy the tangential force balance equations is negative.

Because the model is axi-symmetrical, the interface velocity which is sought for is also an axi-symmetrical interface velocity. Therefore, the absence of a real value may indicate that the interface velocity which would satisfy the tangential force balance equations is a non-symmetrical quantity; that is, uneven thinning.

When the calculated surface concentration is negative, it indicates that there is insufficient surfactant at the interface to supply the necessary interfacial tension gradient to balance the applied shear stress exerted by the flow in the film. This also may lead to uneven thinning, as suggested by Burrill and Woods[8].

Therefore, one can suggest a postulate for the conditions for uneven thinning, namely when the tangential force balance equations cannot be satisfied under axi-symmetrical conditions. Conversely, one can postulate the conditions for even thinning:

(i) Real values for the interface velocities exist, AND

(ii) The surface concentrations are everywhere positive.

The interface velocities and surface concentrations can be calculated by the method described in Section 2.3.6 from experimental data on film thickness and rate of thinning. Therefore the validity of the postulate can be tested from the experimental data for both the even and uneven thinning behaviour.

Note that such a postulate cannot be formulated from a model in which the interface mobility is assumed constant because the problem of calculating interface velocities and surface concentrations does not arise.

2.4.3. The dimensionless groups in film thinning

The similarity analysis[9] is a useful method for determining the dimensionless groups in a system that has been modelled. The method is based on a linear transformation of all the variables that appear in the model. For example, for the variable x, a dimensionless variable x^+ is defined by

$$x^+ = \frac{x - x_A}{x_B}$$

where x_A and x_B are unknowns with the same units as x.

These dimensionless variables are substituted into the equations, the boundary and initial conditions of the model. The resulting dimensionless equations will contain dimensionless groups in terms of x_A's and x_B's. These unknowns are calculated such that a maximum reduction in the number of the dimensionless groups is obtained. The 'non-reducible' dimensionless groups are the dimensionless groups for the system being considered.

The application of the similarity analysis to the film thinning equations developed in this thesis gives the following results:

The dimensionless variables are

$h^* = \frac{h}{b}$	$p^* = \frac{p}{\gamma/b}$	$U_1^* = \frac{U_1}{\gamma/(\mu\sqrt{\phi})}$	$U_2^* = \frac{U_2}{\gamma/(\mu\sqrt{\phi})}$
$\Gamma_1^* = \frac{\Gamma_1}{\Gamma_{s1}}$	$\Gamma_2^* = \frac{\Gamma_2}{\Gamma_{s1}}$	$r^* = \frac{r}{2b^2\sqrt{\frac{\Delta\rho g}{3\gamma}}}$	$\theta^* = \frac{\theta}{\phi\mu b/\gamma}$

(69)

The dimensionless film thinning equations become

$$\frac{\partial H^*}{\partial \theta^*} = \frac{1}{r^*}\frac{\partial}{\partial r^*}\left[r^*\left\{\frac{1}{12}\frac{\partial p^*}{\partial r^*}h^{*3} - \frac{1}{2}(U_1^* + U_2^*)h^*\right\}\right] \tag{70}$$

$$p^* = 1 - \frac{1}{2\phi}\,\frac{1}{r^*}\frac{\partial}{\partial r^*}\left(r^*\frac{\partial H^*}{\partial r^*}\right) \tag{71}$$

$$\phi_3\, h^*\frac{\partial \Gamma_1^*}{\partial r^*} + (U_1^* - U_2^*) + \frac{1}{2}h^{*2}\frac{\partial p^*}{\partial r^*} = 0 \tag{72}$$

$$\phi_3\, h^*\frac{\partial \Gamma_2^*}{\partial r^*} - (U_1^* - U_2^*) + \frac{1}{2}h^{*2}\frac{\partial p^*}{\partial r^*} = 0 \tag{73}$$

$$\frac{\partial \Gamma_1^*}{\partial \theta^*} = \Phi_{12}\left(1 - \Gamma_1^*\right) + \Phi_6 \frac{1}{r^*}\frac{\partial}{\partial r^*}\left(r^* \frac{\partial \Gamma_1^*}{\partial r^*}\right) - \frac{1}{r^*}\frac{\partial}{\partial r^*}\left(r^* U_1^* \Gamma_1^*\right) \tag{74}$$

$$\frac{\partial \Gamma_2^*}{\partial \theta^*} = \Phi_{12}\left(\Phi_7 - \Gamma_2^*\right) + \Phi_6 \frac{1}{r^*}\frac{\partial}{\partial r^*}\left(r^* \frac{\partial \Gamma_2^*}{\partial r^*}\right) - \frac{1}{r^*}\frac{\partial}{\partial r^*}\left(r^* U_2^* \Gamma_2^*\right) \tag{75}$$

where the dimensionless groups are,

$$\Phi = \frac{4 b^2 \Delta\rho g}{3\gamma} \qquad \Phi_6 = \frac{\mu_p D}{\gamma b} \qquad \Phi_7 = \frac{\Gamma_{s2}}{\Gamma_{s1}} \qquad \Phi_9 = \frac{k^* \Gamma_{s1}}{\gamma} \qquad \Phi_{12} = \frac{\Phi \mu b k_3}{\gamma}$$

(76)

The boundary conditions become

$$\int_0^\infty 2\pi r^* p^* dr^* = 1 \tag{77}$$

$$p^* = 0 \quad r^* = \infty \tag{78}$$

$$\frac{\partial p^*}{\partial r^*} = 0 \quad r^* = 0 \tag{79}$$

$$\frac{\partial H^*}{\partial r^*} = 0 \quad r^* = 0 \tag{80}$$

$$\frac{\partial \Gamma_i^*}{\partial r^*} = 0 \quad r^* = 0\,, \; i = 1,2 \tag{81}$$

$$\Gamma_1^* = 1 \quad r^* = \infty \tag{82}$$

$$\Gamma_2^* = \Phi_7 \quad r^* = \infty \tag{83}$$

The dimensionless initial conditions are given by the same form as that shown in Eqs. (63) to (65); hence they need not be rewritten.

The results of the analysis show that only five parameters - the dimensionless groups defined in Eq. (76) - appear in the film thinning equations. These dimensionless groups show how the physical properties of the liquids $\Delta\rho$, μ and γ, the drop size b and the surface concentrations Γ_{s1} and Γ_{s2} are combined in their effects on film thinning behaviour. The physical interpretation of the dimensionless groups given in Eq. (76) is:

(i) ϕ is the ratio of buoyancy to surface forces,

(ii) ϕ_6 is a measure of the relative importance of surfactant mass transfer by surface diffusion and by convection, and ϕ_{12}, by adsorption and convection,

(iii) ϕ_7 is the ratio of Γ_{s2} to Γ_{s1}, and

(iv) ϕ_9 is the ratio of the lowering of interfacial tension to the uncontaminated interfacial tension.

An equivalent set of dimensionless equations would be obtained by defining

$$\Gamma_1^+ = \frac{\Gamma_1}{\Gamma_{s2}} \quad \text{and} \quad \Gamma_2^+ = \frac{\Gamma_2}{\Gamma_{s2}}$$

The values of ϕ_9 and ϕ_7 would then become

$$\phi_9 = \frac{k^* \Gamma_{s2}}{\gamma} \quad \text{and} \quad \phi_7 = \frac{\Gamma_{s1}}{\Gamma_{s2}}$$

Therefore ϕ_9 can represent the surface concentration at the bulk or the drop interface. It is convenient, however, to adopt a convention in which ϕ_9 represents the larger surface concentration so that

the value of ϕ_7 lies between zero and one. With this convention, interface 1 always refers to the interface which contains the larger surface concentration Γ_s. Hence, interface 1 may refer to the bulk or drop interface depending on the values of Γ_s at these interfaces.

2.4.4. Methods for measuring or estimating the system physical properties

The system physical properties that are needed in the solution of the film thinning equations developed in this thesis are:

(i) the liquid/liquid physical properties: density difference $\Delta\rho$, film viscosity μ and interfacial tension γ,

(ii) the drop radius b,

(iii) the surfactant physical properties: surface diffusion coefficient $\mathcal{D}$ and the rate constant for adsorption/desorption k_3, and

(iv) the stationary surface concentration at the bulk and drop interfaces Γ_{s1} and Γ_{s2}.

Consider now the methods for measuring these properties. The liquid/liquid physical properties can be readily measured by standard methods. In general data for $\Delta\rho$, μ and γ are available in standard handbooks.

The method for measuring drop size - unless a photograhic method is used - depends on the technique used for forming the drop. If the conventional drop-volume method is used, the drop size is calculated from the balance between buoyancy force and interfacial tension. If a method similar to that of Hodgson[15] is used, the drop size can be directly measured using a micrometer syringe.

The measurement of surface diffusion coefficient is difficult, especially for surfactants that are soluble in one or both the bulk fluids

because of the difficulties in measuring the surface concentration and also because of the effect of adsorption to or desorption from the interface, which cannot be isolated. Sakata and Berg[10] used a radioactive tracer technique to measure the surface diffusion coefficient of myristic acid at an air/water interface. They confirmed the validity of Fick's law and found the value of $\mathcal{D}$ to be between 3×10^{-5} and 3×10^{-4} cm^2/sec. The value of $\mathcal{D}$ for a complex protein of molecular weight of 70,000 at an air/water interface has also been measured[11]; it was found to be of the order of 10^{-6} cm^2/sec.

The adsorption/desorption constant k_3 is an empirical constant. An estimate for k_3 can be made from the simplified Ward-Tordai equation[5]. Assuming that k_3 is the equivalent rate of adsorption when the surface concentration reaches half of its eqilibrium value, the estimation can be made as follows.

The Ward-Tordai equation is

$$\Gamma_s = 2\left(\frac{\mathcal{D}\theta}{\pi}\right)^{\frac{1}{2}} c \qquad (84)$$

Differentiation of Eq. (84) with respect to time gives

$$\frac{d\Gamma_s}{d\theta} = \left(\frac{\mathcal{D}}{\pi\theta}\right)^{\frac{1}{2}} c \qquad (85)$$

Assuming a linear relationship between the bulk and surface concentration:

$$\Gamma_{eq} = K c \qquad (86)$$

then the substitution of Eq. (86) into Eq. (85) gives

$$\frac{d\Gamma_s}{d\theta} = \frac{1}{K}\left(\frac{\mathcal{D}}{\pi\theta}\right)^{\frac{1}{2}} \Gamma_{eq} \qquad (87)$$

The time taken to reach half of the equilibrium surface concentration $\theta_{1/2}$ can be calculated from Eqs. (86) and (84):

$$\theta_{1/2} = \frac{K^2}{16}\,\frac{\pi}{\mathcal{D}} \qquad (88)$$

Therefore, the estimate for k_3 can be obtained from Eqs. (88) and (87):

$$k_3 = \frac{4}{\pi}\,\frac{\mathcal{D}}{K^2} \qquad (89)$$

The value of K is about 1.6×10^{-3} cm[12] and $\mathcal{D}$ is of the order of 10^{-6} cm^2/sec; therefore k_3 is about 0.5 sec^{-1}.

The surface concentration Γ_s can be specified by the lowering of the interfacial tension $k^* \Gamma_s$ since a linear surface equation of state is used. In principle, $k^* \Gamma_s$ can be measured experimentally by, for example the pendant drop method[13], or estimated theoretically from, for example the Ward-Tordai equation[5]. (In the latter, the surfactant bulk diffusion $\mathcal{D}$ must be measured; cf. Ref. 14 for methods for measuring $\mathcal{D}$). However, the applicability of such measurements or estimations is doubtful because of the presence of surface active contaminants of unknown concentration in the coalescence cell[15-17]. While there is no doubt as to the existence of these surface active contaminants, their nature and concentration can only be speculated. Therefore, unless the measurement of Γ_s is carried out in the coalescence cell, the values of Γ_s independently measured can only be regarded as estimates.

2.5. Summary and conclusions

1. The general equations for the flow in two bulk fluids separated by an interface containing surfactants have been described and simplified for the film thinning in single drop coalescence in oil/water systems. The interface mobility, however, was not arbitrarily assumed in the simplification.

2. The major assumptions that have been made were:

(i) pseudo steady state, creeping flow and negligible hydrostatic effects for the flow in the film, which were justified by an order of magnitude analysis, and

(ii) inviscid flow in the bulk phase and inside the drop, and the use of a simple expression for the bulk/interface transfer of surfactant, which should be justified a posteriori.

3. The interface mobility must be calculated and not preset. The constant interface mobility assumption is neither accurate nor correct fundamentally.

4. All the boundary conditions can be specified from physical arguments:

(i) the pressure in the film balances the drop buoyancy force,

(ii) there is no fluid flow far from the film centre, and

(iii) all the variables remain finite at the film centre.

5. The initial conditions must be calculated from experimentally measured film thickness profile and rate of thinning at the selected initial time.

6. It is possible to use an axi-symmetrical model to postulate the conditions for even and uneven thinning, provided the interface mobility

is not arbitrarily assumed. A postulate has been put forward for the conditions for even and uneven thinning. Even thinning occurs if and only if:

(i) real values for the interface velocities exist, and

(ii) the surface concentrations are positive everywhere at the bulk and drop interfaces.

Otherwise, the thinning is uneven.

7. The dimensionless groups in film thinning are - based on the equations developed in this thesis:

$\phi = \frac{4}{3}\frac{b^2 \Delta\rho g}{\gamma}$	$\phi_6 = \frac{\mu \mathcal{D}}{\gamma b}$	$\phi_7 = \frac{\Gamma_{s2}}{\Gamma_{s1}}$	$\phi_9 = \frac{k^* \Gamma_{s1}}{\gamma}$	$\phi_{12} = \frac{\phi \mu b k_3}{\gamma}$

Literature cited

1. Bird, R. B. et al, "Transport phenomena" Wiley, N. Y. (1962).

2. Levich, V. G., "Physicochemical hydrodynamics" Prentice Hall, N. J. (1962):Ch. VII.

3. Burrill, K. A. and Woods, D. R., J.Coll.Intf.Sci., 30(1969):511.

4. Princen, H. M., "Surface and colloid science" , Matijevic, E. (Ed) Wiley-Interscience, N. Y. (1969):1.

5. Ward, A. F. H. and Tordai, L., J.Chem.Phys., 14(1946):453.

6. Hansen, R. S., J.Coll.Sci., 16(1961):549.

7. Hartland, S., Trans.Inst.Chem.Engrs. (London) 45(1967):T97.

8. Burrill, K. A. and Woods, D. R., J.Coll.Intf.Sci., 42(1973):15.

9. Hellums, J. D. and Churchill, S. W., Chem.Engng.Prog., Symp. Ser. #32,57(1961):75.

10. Sakata, E. K. and Berg, J. C., I&EC Fund., 8(1969):570.

11. Imahori, K., Bull.Chem.Soc.Japan, 25(1952):13.

12. Davies, J. T. and Rideal, E. K. "Interfacial phenomena" Ac. Press, N. Y. (1963).

13. Ward, A. F. H. in "Surface chemistry" Papers presented at a joint meeting of Societe Chimie Physique and the Faraday Society, (1947), Butterworths, London (1949):55.

14. Jost, W. "Diffusion in solids, liquids and gases" Ac. Press, N.Y. (1960).

15. Hodgson, T. D. and Lee, J. C., J.Coll.Intf.Sci., 30(1969):94.

16. Hodgson, T. D. and Woods, D. R., J.Coll.Intf.Sci., 30(1969):429.

17. Burrill, K. A. and Woods, D. R., J.Coll.Intf.Sci., 42(1973):15, 35.

Figure captions

1. Film geometry, showing the shear stresses and the interfacial tension gradients, the radial velocity profile and the pressure.

2. Stresses at a curved interface. The normal and tangential shear stresses can be expressed in terms of coordinate components of the stress tensor by carrying out a tensor transformation.

3. Outline of the derivation of the film thinning equations.

4. Approximations for the boundary conditions which involve an infinite number.

5. The selection of the initial time, showing the different values of the initial conditions, and the additional model which may need to be developed depending on the selection.

6. Outline of the calculation of the interface velocities and the distributions of surface concentration, given the film thickness and the rate of thinning. The calculation can be reduced into that of one variable, for example U_1 as shown in the diagram.

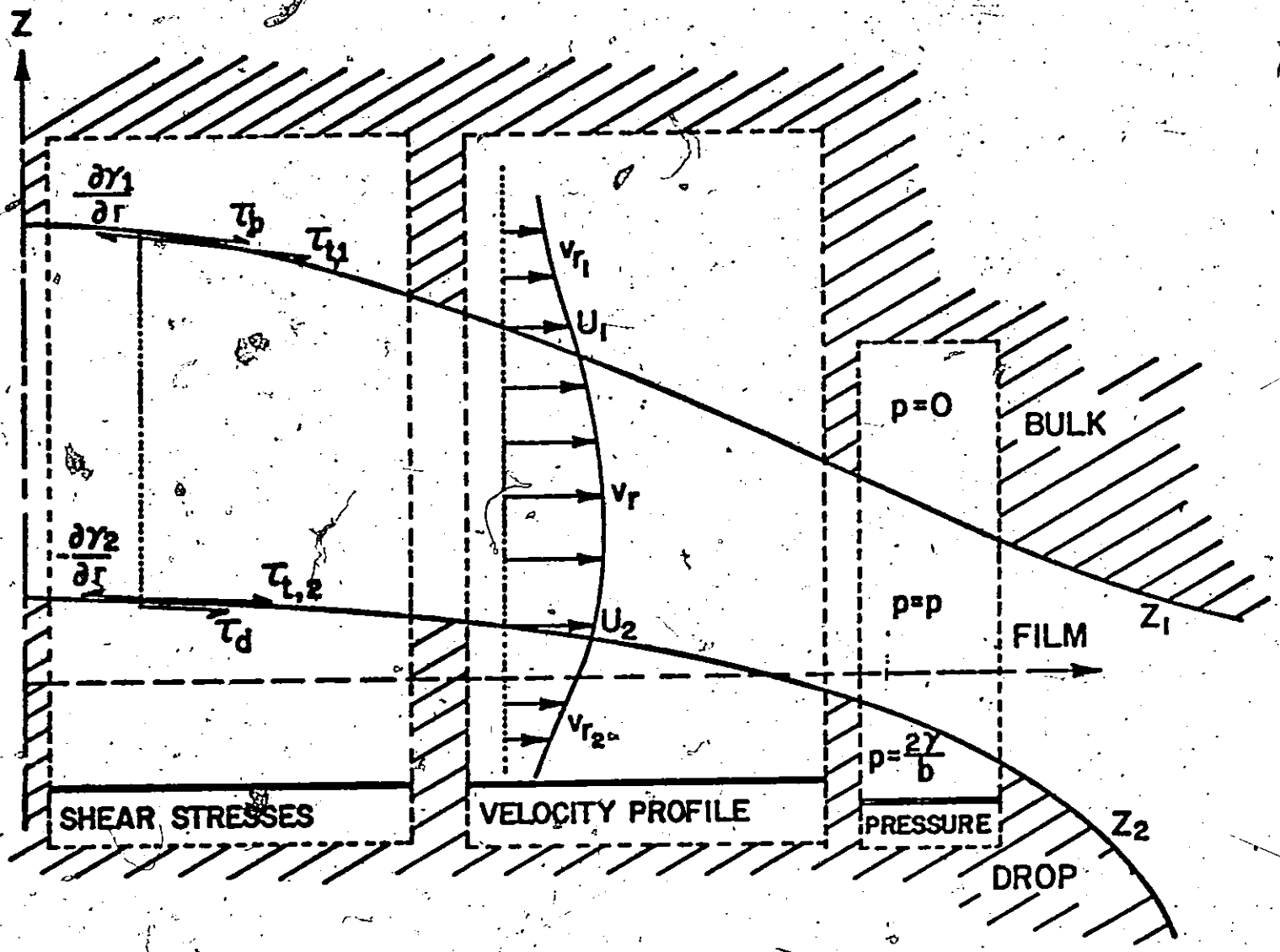
Z
$\frac{\partial \gamma_1}{\partial r}$
τ_b
$\tau_{t,1}$
v_{r_1}
U_1
p=0
BULK
v_r
$\frac{\partial \gamma_2}{\partial r}$
$\tau_{t,2}$
τ_d
U_2
p=p
FILM
Z_1
$v_{r_{2^*}}$
$p=\frac{2\gamma}{b}$
SHEAR STRESSES
VELOCITY PROFILE
PRESSURE
Z_2
DROP

Figure 1

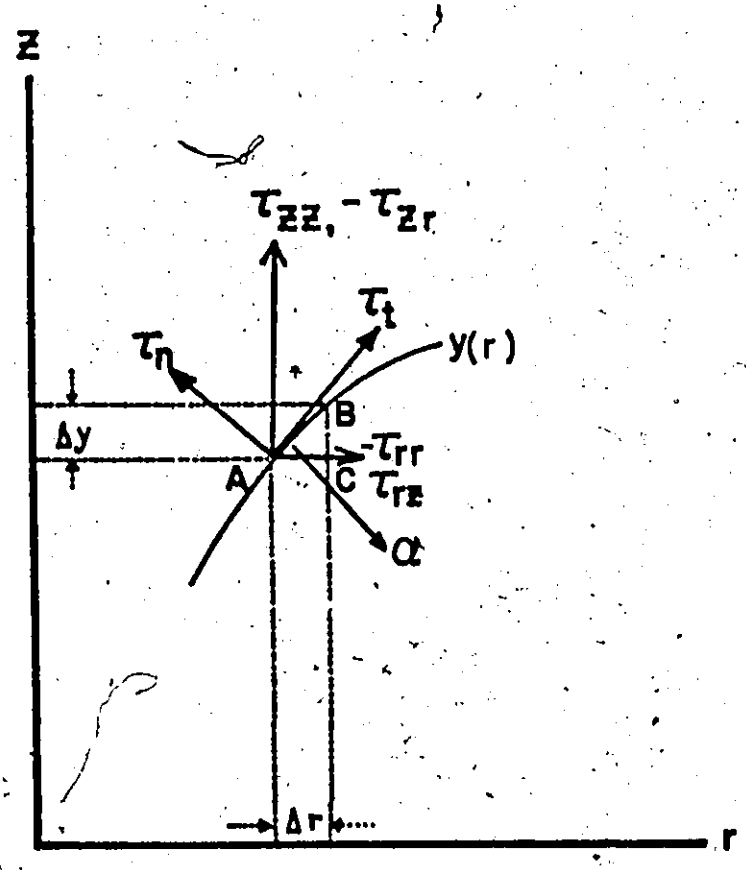
z
$\tau_{zz}, -\tau_{zr}$
τ_t
τ_n
y(r)
B
Δy
$-\tau_{rr}$
A
C
τ_{rz}
α
Δr
r

Figure 2

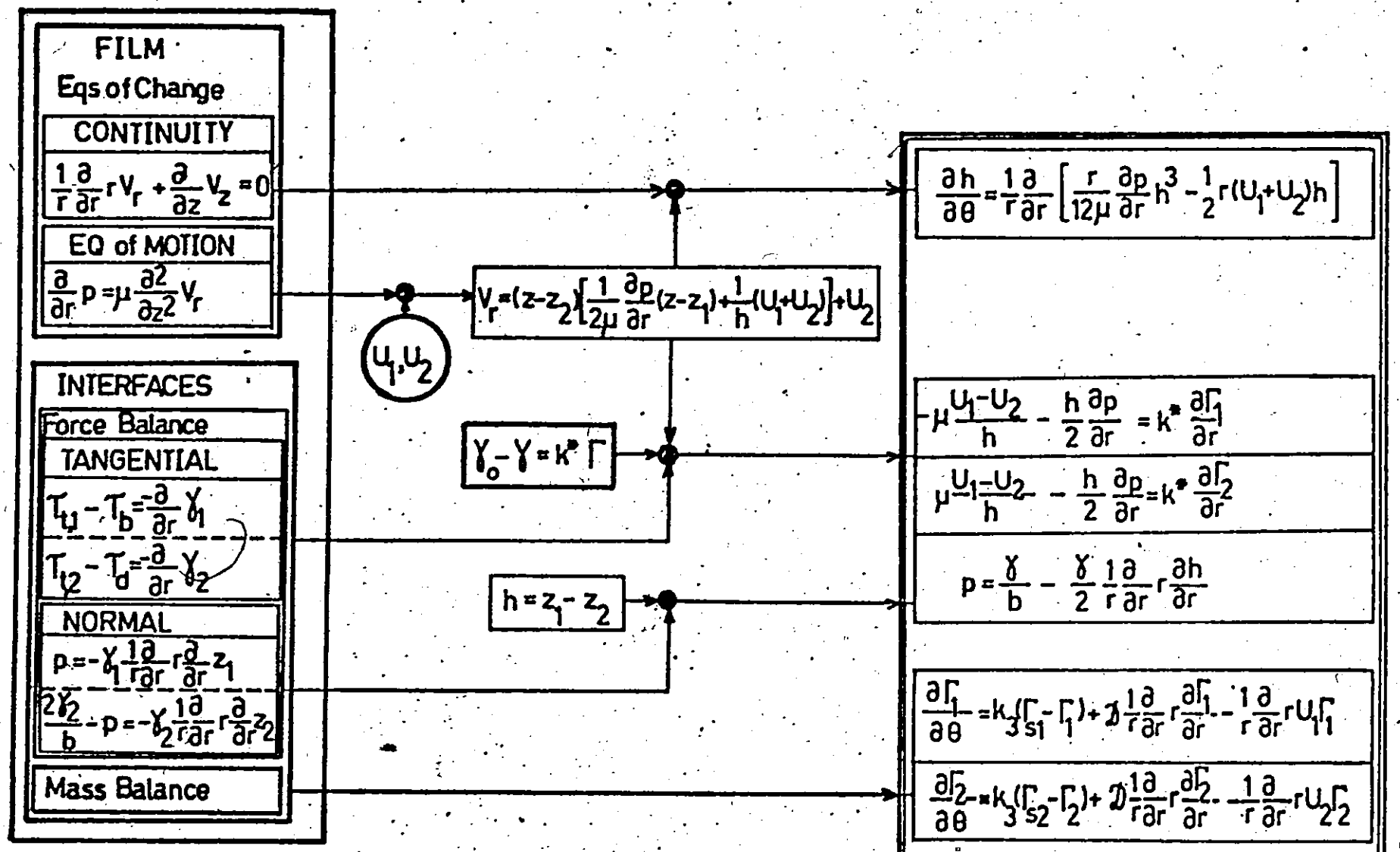
FILM
Eqs of Change
CONTINUITY
$\frac{1}{r}\frac{\partial}{\partial r}rV_r + \frac{\partial}{\partial z}V_z = 0$
EQ of MOTION
$\frac{\partial}{\partial r}p = \mu\frac{\partial^2}{\partial z^2}V_r$
INTERFACES
Force Balance
TANGENTIAL
$\tau_{t1} - \tau_b = \frac{\partial}{\partial r}\gamma_1$
$\tau_{t2} - \tau_d = \frac{\partial}{\partial r}\gamma_2$
NORMAL
$p = -\gamma_1\frac{1}{r}\frac{\partial}{\partial r}r\frac{\partial}{\partial r}z_1$
$\frac{2\gamma_2}{b} - p = -\gamma_2\frac{1}{r}\frac{\partial}{\partial r}r\frac{\partial}{\partial r}z_2$
Mass Balance
U_1, U_2
$V_r = (z-z_2)\left[\frac{1}{2\mu}\frac{\partial p}{\partial r}(z-z_1) + \frac{1}{h}(U_1+U_2)\right] + U_2$
$\gamma_o - \gamma = k^*\Gamma$
$h = z_1 - z_2$
$\frac{\partial h}{\partial \theta} = \frac{1}{r}\frac{\partial}{\partial r}\left[\frac{r}{12\mu}\frac{\partial p}{\partial r}h^3 - \frac{1}{2}r(U_1+U_2)h\right]$
$-\mu\frac{U_1-U_2}{h} - \frac{h}{2}\frac{\partial p}{\partial r} = k^*\frac{\partial \Gamma_1}{\partial r}$
$\mu\frac{U_1-U_2}{h} - \frac{h}{2}\frac{\partial p}{\partial r} = k^*\frac{\partial \Gamma_2}{\partial r}$
$p = \frac{\gamma}{b} - \frac{\gamma}{2}\frac{1}{r}\frac{\partial}{\partial r}r\frac{\partial h}{\partial r}$
$\frac{\partial \Gamma_1}{\partial \theta} = k_3(\Gamma_{s1} - \Gamma_1) + \mathcal{D}\frac{1}{r}\frac{\partial}{\partial r}r\frac{\partial \Gamma_1}{\partial r} - \frac{1}{r}\frac{\partial}{\partial r}rU_1\Gamma_1$
$\frac{\partial \Gamma_2}{\partial \theta} = k_3(\Gamma_{s2} - \Gamma_2) + \mathcal{D}\frac{1}{r}\frac{\partial}{\partial r}r\frac{\partial \Gamma_2}{\partial r} - \frac{1}{r}\frac{\partial}{\partial r}rU_2\Gamma_2$

Figure 3

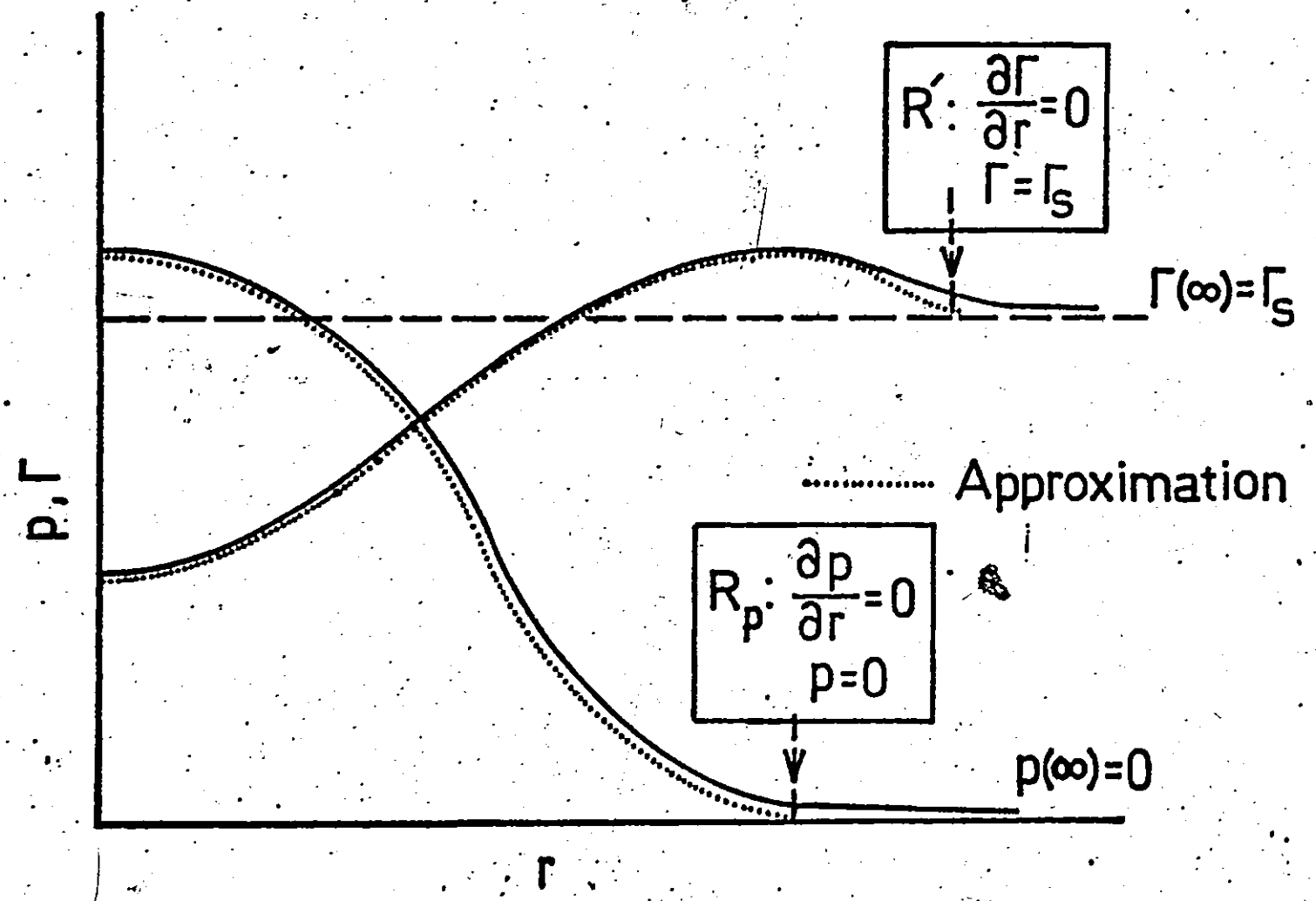

Figure 4

Selected initial time θ_o / Initial conditions	a	b	c
	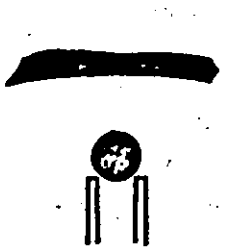		
Film thickness	? Difficult to estimate	? Difficult to estimate	Measured
Bulk interface concentration	$\Gamma_{10}(r) = \Gamma_{s1}$	$\Gamma_{10}(r) = \Gamma_{s1}$	Calculated *
Drop interface concentration	$\Gamma_{20}(r) = \Gamma_{s2}$	$\Gamma_{20}(r) = \Gamma_{v}(r)$	Calculated *
Additional model is required to describe	Initial motion of the drop after its release	Retarded motion of the drop	None

Figure 5

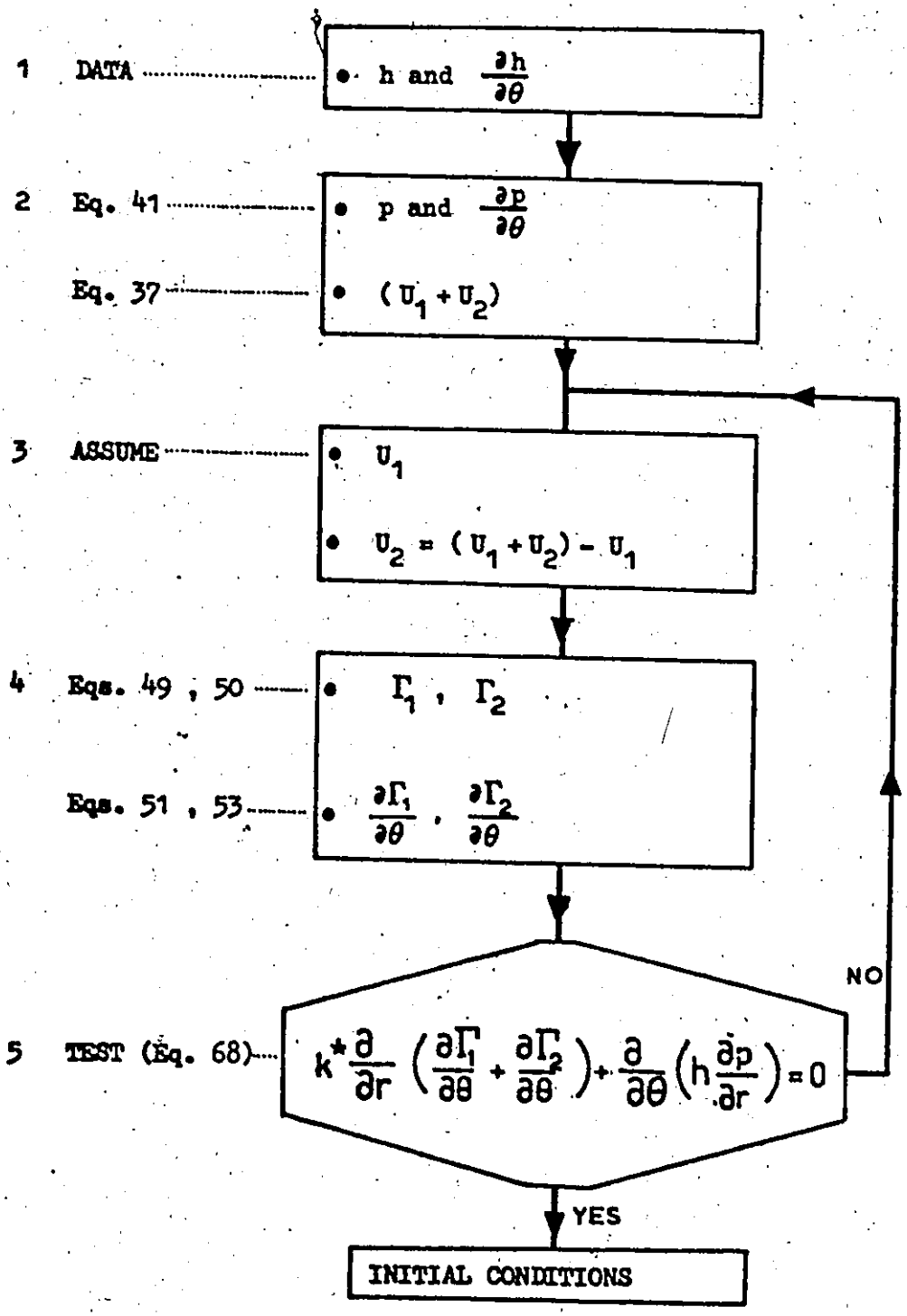
1 DATA
• h and $\frac{\partial h}{\partial \theta}$
2 Eq. 41
• p and $\frac{\partial p}{\partial \theta}$
Eq. 37
• $(U_1 + U_2)$
3 ASSUME
• U_1
• $U_2 = (U_1 + U_2) - U_1$
4 Eqs. 49 , 50
• Γ_1 , Γ_2
Eqs. 51 , 53
• $\frac{\partial \Gamma_1}{\partial \theta}$, $\frac{\partial \Gamma_2}{\partial \theta}$
5 TEST (Eq. 68)
$k^* \frac{\partial}{\partial r}\left(\frac{\partial \Gamma_1}{\partial \theta} + \frac{\partial \Gamma_2}{\partial \theta}\right) + \frac{\partial}{\partial \theta}\left(h \frac{\partial p}{\partial r}\right) = 0$
NO
YES
INITIAL CONDITIONS

Figure 6

CHAPTER 3

EXPERIMENTAL STUDIES

The effect of an oil soluble surfactant on the film thinning behaviour of toluene drops is studied. A brief discussion is first given of the methods of controlling the variables which affect film thinning. This is followed by the description of the apparatus used and the procedure for data gathering.

The observed film thinning behaviour and the methods of data analysis are described. A comparison is given between this work and previous work to evaluate the various experimental techniques used.

3.1. Methods of controlling the variables

The variables that must be controlled in a coalescence experiment are:

(i) the physical properties of the liquids and the drop size,

(ii) the physical properties of the surfactant, and

(iii) the surfactant concentration Γ_s at the bulk and drop interfaces.

Variables (i) and (ii) can be controlled by selecting suitable liquids and surfactants and by forming the drops accurately. The control of the surface concentration Γ_s is not easy because of the difficulties in removing completely surface active contaminants from the apparatus. Ideally the control can be achieved by first removing all the contaminants, and then adding deliberately known amounts of surfactant. In practice, however,

this is not possible. Therefore, the control of surface concentration can only be achieved indirectly.

For the bulk interface, interface cleaning is a form of an indirect control. The surface concentration thus starts from zero - at the completion of the cleaning - and gradually increases as the interface age increases because of surfactant adsorption. Interface cleaning is therefore a useful method of control for studying the effect of very low surface concentrations.

For the drop interface, interface cleaning cannot be applied. As a further complication, the drop interface age cannot be determined accurately because of its dependence on the manner by which the drop is formed. Therefore, it is desirable to eliminate the dependence of surface concentration Γ_s on interface age. This can be achieved by aging the drop interface for a sufficiently long period of time; hence the initial effect of surfactant adsorption is minimized. By this means, the surface concentration Γ_s can be maintained constant throughout an experiment with the same bulk surfactant concentration. To vary this surface concentration, different bulk surfactant concentrations are used.

3.2. Description of the apparatus

A coalescence apparatus consists essentially of:

(i) a drop forming device,

(ii) a coalescence cell, and

(iii) a film thickness measuring device.

The schematic diagram of the apparatus and a photograph are shown in Figs. 1 and 2, respectively. Drops were formed in the drop forming nozzle '2', loaded in the connecting tube '9', and then released to the

bulk interface in the coalescence cell '1'. The film thinning behaviour was observed by using the white light interference technique and recorded by a cine camera '11'.

All the parts of the apparatus that came into contact with the oil and the water were made of glass or teflon to permit thorough cleaning. The experiments were conducted in an enclosed, temperature-controlled room to minimize the possible contamination from dust in the surrounding air.

The drop forming device is shown diagramatically in the insert in Fig. 1, and a photograph is shown in Fig. 3. To form a drop, the desired volume was metered into the capillary tube 'C' by using a micrometer syringe. The oil slug was then cut by slowly injecting water through tube 'A'. This procedure was repeated until the desired number of drops was obtained. The accuracy and the reproducibility of the method were first checked by attaching a calibrated capillary tube to the end of the drop forming nozzle. The method was found accurate, reproducible and insensitive to the physical properties of the two liquids.

The range of drop sizes that can be formed in one drop forming nozzle is determined by the inside diameter of the capillary tube 'C'. The lower limit is reached when the drop begins to float in this tube and the upper limit, when the drop begins to break up. For the present apparatus, these limits were 0.002 and 0.008 ml for the toluene/water system.

The schematic diagram of the coalescence cell is shown in Fig.4. A number of previously developed techniques have been adopted: the interface cleaning technique and the use of a teflon ring to reverse the bulk interface curvature[1]. Three interface cleaning probes were used to clean the bulk interface which had an area of about 20 cm^2. The effectiveness of

the present cleaning method, in terms of the area to be cleaned and the number of interface cleaning probes, should be comparable to that used previously, where one probe was used to clean an area of about 12.5 cm^2.

The teflon ring was used to prevent the drop from rolling at the bulk interface. Because the bulk interface was slightly concave on the oil phase side, the drop could be released to the highest point at the bulk interface and 'held' in one position. This was necessary since the area of the microscope field of view was only about 1 mm^2.

The coalescence cell was to be used with oil soluble surfactants, so it was necessary to minimize the depletion of the bulk surfactant concentration in the bulk phase due to repeated interface cleanings. This required that the volume of the bulk phase be sufficiently large. However, the light interference technique imposed a restriction on the maximum depth of the bulk phase at the location where the interference colours were observed; this depth was about 1 cm. Therefore, the shape of the cell cover, shown in Fig. 4, had been designed such that these conditions were met: the bulk phase was shallow in the regions where the interference colours were measured, and yet its volume was sufficiently large to minimize the depletion due to interface cleanings. (The volume of the bulk phase was about 100 ml; see Eq. 3 of Ref.2).

The make-up reservoirs shown in Fig. 1 were used to replace the liquids lost due to interface cleanings. The make-up water reservoir was also used to adjust the bulk interface level in the coalescence cell. This adjustment was accomplished by the addition or the removal of the water in the coalescence cell. This was necessary because for a proper interface cleaning, the tip of the interface cleaning probe (which was

fixed to the coalescence cell) had to be positioned at the bulk interface. Otherwise the oil and the water could not be simultaneously removed.

The optical arrangements for observing and recording the interference colours are shown diagramatically in Fig. 5. In Fig. 5, the working mechanism of the light interference technique is also shown. The details of the optical equipment are tabulated in Table I. To observe the interference colours the microscope was focussed at the bulk interface; therefore, the media that existed between the microscope objective and the bulk interface should be optically homogeneous. This condition was met by selecting an oil for the bulk phase that had a refractive index close to that of the cell cover, and by placing an immersion oil between the microscope objective and the cell cover.

3.3. Purification and cleaning procedures.

The two liquids were mutually saturated water containing an electrolyte KCl and toluene containing a surfactant, palmitic acid. The water was distilled, at least once in a potassium permanganate solution, until its conductivity was less than one micromho. Three or four distillations of tap water were usually required to reach this level of purity.

The oil, which was of reagent grade purity, was distilled once in a glass packed bed distillation column. The water and oil were then stored in stoppered glass containers.

The electrolyte and the surfactant, which were also of reagent grade purity, were not further purified. The largest surfactant concentration was prepared by dissolving the required amount of palmitic acid in a volumetric flask. Lower concentrations were prepared volumetrically.

All the apparatus components that came into contact with the oil

and the water were cleaned by the following procedure:

(i) wash in boiling soap water and rinse thoroughly,

(ii) soak in acetone for at least 12 hours and then drain,

(iii) soak in freshly prepared chromic acid for at least 24 hours,

(iv) drain and rinse with phosphoric acid and the one micromho water, and

(v) dry in an oven.

In steps (ii) and (iii), an ultra-sonic bath was used to promote agitation. This was especially necessary for cleaning the capillary tubes. In step (iv), the rinsing was considered thorough when the spent water had a conductivity of less than one micromho.

3.4. Data gathering procedure

The procedure for assembling the apparatus is described in Appendix C. The bulk concentration of the oil used to form the drops was the same as that of the bulk phase; hence dilution or enrichment of the bulk surfactant concentration in the bulk phase, resulting from coalescence, was minimized.

The drops were formed and loaded in the connecting tube '9' (Fig. 1). Before they were released to the bulk interface, about 20 minutes were allowed to elapse to allow the drop interface to sufficiently age. A drop was released at least five seconds after the completion of the coalescence of the previously released drop. This was done to minimize the possible interaction between two successively released drops.

The bulk interface was cleaned, and a stop watch was started to time the bulk interface age. The drops in the connecting tube could now be released to the bulk interface at any desired bulk interface age. The variation of film thickness with elapsed time was observed through the

microscope and recorded by the cine camera. The details of the data gathering procedure are described in Appendix C.

An experimental run with the same drop size and bulk surfactant concentration was terminated when no appreciable change in the film thinning behaviour was observed; that is, when the bulk interface had sufficiently aged. Because the drop interface was aged and because the same surfactant concentration was used in the bulk phase and in the drop, during this experimental run, the surface concentration Γ_s at the drop interface remained constant, and at the bulk interface, increased from zero (at the completion of the interface cleaning) to a value equal to that at the drop interface.

The procedure for data gathering was repeated for duplicate runs and for experiments with different drop sizes and bulk surfactant concentrations. The order in which the experiments were carried out was to start with the lowest bulk surfactant concentration and then proceed with increasing concentrations. By this means, it was not necessary to repeat the apparatus cleaning procedure every time a different bulk surfactant concentration was used because the contamination from the previous experiments should be insignificant.

3.5. Observations and discussion

The bulk concentration of palmitic acid was varied from zero to 10^{-4} M, and the range of drop sizes was from 0.0025 to 0.005 ml. The experiments were conducted at 22 °C ± 1 °C.

The variation of film thickness with elapsed time was measured from the interference colours by using the table for the relationship between interference colour and film thickness[3,4].

The film thinning observations can be described by one of these patterns:

(i) Rapid thinning to about 600 Å, dimple formation, even thinning and film rupture,

(ii) The same as in (i) except that even thinning is followed by uneven thinning prior to film rupture, or

(iii) There is no rapid thinning; the film thins unevenly until rupture occurs.

Sample photographs of the interference colours for the different film thinning behaviour are shown in Figs. 6 to 8. To distinguish the different uneven thinning patterns in (ii) and (iii), these patterns are referred to as Type B and Type A, respectively.

The occurrence of dimple formation was always preceded by rapid thinning. During the rapid thinning, surfactant molecules at the bulk interface were swept towards the film periphery. Therefore, if the rapid thinning was arrested, the consequent interface contraction could cause a dimple formation. This explains the occurrence of dimple formation at small bulk interface ages because the bulk interface should be relatively mobile to allow the rapid thinning to occur.

The shift of even to uneven thinning is so far not fully understood. In Chapter 6, a postulate for the conditions for even and uneven thinning is analysed to explain this behaviour.

The absence of rapid thinning and the subsequent dimple formation at large bulk interface ages was the result of the adsorption of surfactant, which in turn caused the bulk interface to be less mobile.

A more detailed explanation of the mechanisms that lead to the

different film thinning behaviour has been given elsewhere[5].

The uneven thinning Type A, which occurred when the bulk interface age was large, was also observed when the bulk interface was not cleaned. This suggests that the condition for the occurrence of uneven thinning Type A is that both interfaces contain a 'large' surfactant concentration. Therefore, this behaviour of film thinning should be the one most likely to occur in practice. Fig. 9 shows an example of the variation of film thickness at the barrier ring with elapsed time for uneven thinning Type A.

Additional observations

As a preliminary investigation of the effect neighbouring drops have on the film thinning behaviour of single drop coalescence, film thickness measurements were carried out for the case when a drop was released to the bulk interface immediately after the previously released drop had just completed its first stage of coalescence. In all the measurements, the bulk interface was either old or not cleaned.

When no surfactant was added, the satellite drop of the previously released drop coalesced almost instantaneously. The film thinning behaviour of the 'second' drop was highly irregular, as shown in Fig. 10. The rest time of the second drop was always short - about one second.

When surfactant was added, the satellite drop of the previously released drop did not coalesce instantaneously. This satellite drop was still at the bulk interface by the time the second drop arrived at the bulk interface. Because of the deformation of the bulk interface due to this satellite drop, the second drop rolled towards this satellite drop. No irregular film thinning behaviour was observed except at the instant when the satellite drop joined the bulk phase. At this instant, there

was an abrupt change in the interference colour pattern, as shown in Fig. 11.

These observations are difficult to explain quantitatively. Nevertheless they appear to confirm the important role of surface concentration and the consequent interface movements in determining the film thinning behaviour. To show this, a qualitative explanation of these observations will be attempted.

As a result of the film rupture and the subsequent inflow of the drop contents to the bulk phase, surface waves at the bulk interface might be generated. These waves would not be readily damped in the absence of surfactant molecules. Therefore, when the second drop arrived at the bulk interface, these waves still persisted which might cause the occurrence of the observed irregular film thinning behaviour.

When more surfactant molecules were present at the bulk interface, these surface waves would be more readily damped. The absence of these surface waves when the second drop arrived at the bulk interface could explain the observed regular film thinning behaviour. However, when the satellite drop of the previously released drop joined the bulk phase, the resulting surface waves could still cause the observed abrupt change in the interference colour pattern. This abrupt change was immediately followed by a regular pattern because of the rapid damping of the surface waves.

3.6. Outline of the data analysis

The analysis of the experimental observations can be divided into three groups; these are the measurement of:

(i) the variation of the symmetrical film thickness profile with elapsed time, for testing the film thinning equations developed in Chapter 2,

(ii) the film thickness and the rate of thinning for both the symmetrical and unsymmetrical behaviour, for testing the postulate for the conditions for even and uneven thinning proposed in Chapter 2.4.2, and

(iii) the variation of film thickness at the barrier ring with elapsed time, for developing an empirical film thinning model - the extended parallel disc model.

The first is described in Chapter 4, the second in Chaper 6, and the third in Chapter 5.

3.7. Comparison with previous work

In this section, a comparison is given between this work and the work of Hodgson and Woods[1] and Burrill and Woods[5] to evaluate the various experimental techniques used.

Drop forming technique

The drop forming technique developed in this work has been designed to improve Hodgson's technique in the control of the surface concentration Γ_s at the drop interface. Because of the piercing of the bulk interface by the drop forming nozzle tip every time a drop is formed, there is a possibility of surfactant transfer between the bulk interface and the nozzle tip, and hence the drop interface (cf. Fig. 1-6). This transfer might be responsible for the observed sawtooth effect on some rest time data[2]. In addition, because the drop is released immediately after it is formed to the bulk interface, it is very difficult to estimate the drop interface age. In Burrill's analysis[3], the drop interface was assumed to be fully mobile based on the argument that it was exposed to the continuous phase for a short period of time. This assumption is not supported by the rest

time data. When the bulk concentration of sodium lauryl sulphate was 10^{-5} gm/l or higher, instantaneous coalescence did not occur; this shows that a sufficient amount of surfactant to cause an interface to be at least partially immobile was adsorbed almost instantaneously. Hence, in general, although the drop interface is exposed only for a short period of time, it may not be fully mobile.

In summary, the use of Hodgson's drop forming technique presents difficulties in controlling the surface concentration Γ_s at the drop interface. With the present drop forming technique, the possibility of surfactant transfer between the bulk and the drop interfaces is eliminated. Furthermore, the drops can be conveniently aged for a sufficiently long period of time, so that the surface concentration Γ_s can be maintained constant throughout an experimental run with the same bulk surfactant concentration.

Interpretation of the effect of bulk interface age

Because of the different drop forming techniques used, the dependence of film thinning behaviour on bulk interface age (for the same bulk surfactant concentration) in this work was different from that in the previous work[1,5]. For example, when the bulk interface age was large, the observed film thinning behaviour was uneven thinning Type A; whereas in the previous work, it was the slow even thinning Pattern IV. This difference in the effect of the bulk interface age can be seen by examining the variation of the dimensionless parameters ϕ_9 and ϕ_7 (Chapter 2.4.3) with bulk interface age, as shown in Fig. 12.

With the convention adopted in Chapter 2.4.3, in this work ϕ_9 refers to the drop interface because it was aged; that is, because the surface concentration Γ_s at the drop interface was always greater than or

equal to that at the bulk interface. Conversely, in the previous work ϕ_9 refers to the bulk interface because the drop interface was 'fresh'. Consequently, in this work ϕ_7 refers to the bulk interface and in the previous work, the drop interface.

Consider now the variation of ϕ_9 and ϕ_7 with bulk interface age. In this work ϕ_9 remains constant because the drop interface has aged sufficiently. The value of ϕ_7 increases from zero - at the completion of the interface cleaning - to a value of one because the same bulk surfactant concentration was used in the bulk phase and in the drop.

In the previous work, ϕ_9 increases with bulk interface age because of surfactant adsorption at the bulk interface. The value of ϕ_7 decreases because the surface concentration Γ_s at the drop interface remained constant. (The implied assumptions here are that the drop interface was always exposed for exactly the same period of time, and that there was no surfactant transfer between the bulk and the drop interfaces.)

In summary, for the same bulk surfactant concentration and bulk interface age, the film thinning behaviour observed in this work should not be compared to that observed in the previous work because of the different drop forming techniques used.

The effect of water soluble and oil soluble surfactants

Because the volume of the film is small compared to that of the bulk phase and the drop, it might be argued that the surfactant adsorption to the interfaces during film thinning would depend on whether the surfactant is soluble in the oil or in the water. If the surfactant is present in the film, the bulk concentration in the film might be rapidly depleted as a result of this adsorption; whereas if the surfactant is present in the

bulk phase and in the drop, this depletion would be insignificant. Therefore, this difference would affect the surface concentration distribution during film thinning and hence the film thinning behaviour.

Ideally one could investigate this subject by conducting coalescence experiments with surfactants that have identical physical properties except their solubility in water and oil. This investigation would require that the surfactant physical properties - the rate of adsorption, the lowering of interfacial tension and the surface diffusivity - be measured accurately. Unfortunately accurate data on these surfactant physical properties are not available at present. Therefore, a quantitative comparison between the effect of oil soluble and water soluble surfactants is beyond the scope of this thesis. Nevertheless the film thinning behaviour observed in this work can be compared to that observed in the previous work in which a water soluble surfactant was used.

Based on the experimental observations, there is no evidence to suggest that there is a drastic difference in the effect of oil soluble and water soluble surfactants. All the film thinning behaviour observed in this work can be identified in terms of the thinning 'patterns' introduced by Hodgson and Woods[1]; there were no new thinning patterns observed.

The effect of apparatus size

The thoroughness of an apparatus cleaning procedure is affected by the size and configuration of the apparatus. In general the larger the apparatus, the more contaminants will remain in the apparatus. The amount of the unremoved contaminants can be inferred from the rest time observations.

If the apparatus is thoroughly cleaned, instantaneous coalescence should occur when the bulk and drop interfaces have just been cleaned or

formed. As the interface age of the bulk interface (or the drop interface) increases, the adsorption of the contaminants will cause the interface to be partially mobile; hence at some critical interface age, instantaneous coalescence no longer occurs. The magnitude of this critical age is an indirect measure of the amount of the unremoved contaminants.

In the work of Burrill and Woods[2], the critical bulk interface age was about 8 minutes for toluene drops. In the present apparatus, the obtaining of the critical age must be carried out in a different manner because the drops were transported to the coalescence cell via the connecting capillary tube. The scheme used was to clean the bulk interface and then release drops of different ages to the clean bulk interface; therefore, it was the critical drop interface age that was measured. The value was found to be between 30 seconds and 1 minute, as measured from the instant the drop was formed to that when it was released.

While these results show that the present cleaning procedure was adequate, they also show that the present experiment was less clean perhaps because of the larger size of apparatus used than that used by Burrill and Woods[2]. This in turn indicates the difficulties in controlling the surfactant concentration in a large scale apparatus.

3.8. Summary and conclusions

1. A coalescence apparatus has been built which features a novel drop forming technique and a coalescence cell which can be used with oil and water soluble surfactants. With this drop forming technique, drops of different sizes can be formed using one nozzle without piercing the bulk interface; hence the possibility of surfactant transfer between the bulk and drop interfaces is eliminated.

2. The effect of additions of palmitic acid (zero to 10^{-4} M) and the effect of drop size (0.0025 to 0.005 ml) and bulk interface age on the film thinning behaviour of toluene drops have been measured using the white light interference technique. Additional measurements were made when drops were released to the bulk interface in rapid succession.

3. The observations of the film thinning behaviour show that:

(i) The film thinning behaviour changed from a dimple formation pattern to uneven thinning Type A, as the surface concentration Γ_s at the bulk interface increased from a value of zero to that at the drop interface.

(ii) Uneven thinning always occurred when the bulk interface was old and when it was not cleaned. This suggests that this pattern is the most common thinning pattern in practice.

(iii) New irregular thinning patterns were observed when drops were released to the bulk interface in rapid succession.

(iv) There is insufficient evidence to show that there is a drastic difference in the effect of oil soluble and water soluble surfactants.

4. The present experiment was less clean than that of Burrill and Woods[2] perhaps because the size of the apparatus used was larger.

Literature cited

1. Hodgson, T. D. and Woods, D. R., J. Coll.Intf.Sci., 30(1969):429.

2. Burrill, K. A. and Woods, D. R., J.Coll.Intf.Sci., 42(1973):35.

3. Lawrence, A. C. S. "Soap films" Bell&Sons, London (1929).

4. Burrill, K. A., Ph.D. Thesis, McMaster Univ., Canada (1970).

5. Burrill, K. A. and Woods, D. R., J.Coll.Intf.Sci., 42(1973):15.

CINE CAMERA	BOLEX - H16 Reflex
Lens	Macro-switar 26 mm, f/1.1
Motor	BOLEX - MCE-17B 12 fps to 64 fps
Film	KODAK - EF 7242 Tungsten 3200°K
Filter	KODAK - 82A, 82C
MICROSCOPE	OLYMPUS - MR Metallurgical
Lenses	
Objective	M 10
Eyepiece	7 X
Light Source	OFFICINE GALILEO 2650°K *
MOVIE ANALYZER	LW - 900 B

* Measured experimentally at
110 V AC (input) and 7 V DC (output)

TABLE I. Details of Optical Equipment.

Figure captions

1. Schematic diagram of the apparatus; the insert shows the cross-section of the drop forming nozzle.

2. Photograph of the apparatus; the numbers shown in the photograph correspond to those given in Fig.1.

3. Photograph of the drop forming nozzle.

4. Schematic diagram of the coalescence cell.

5. Schematic diagram of the optical equipment (left) and the working mechanism of the light interference technique (right).

6. Photographs of the interference colours for rapid thinning (not shown), arrest, dimple formation and even thinning until film rupture: drop size 0.0025 ml, palmitic acid concentration 10^{-6} M, and bulk interface age 110 sec.

7. Photographs of the interference colours for rapid thinning (not shown), arrest, dimple formation, even thinning and uneven thinning until film rupture: drop size 0.0025 ml, palmitic acid concentration 10^{-6} M, and bulk interface age 10 min.

8. Photographs of the interference colours for uneven thinning Type A: drop size 0.0025 ml, palmitic acid concentration 10^{-6} M, and bulk interface greater than 20 min.

9. Variation of film thickness at the barrier ring with elapsed time for uneven thinning Type A. The different symbols show duplicate runs; R denotes the instant of film rupture.

10. Photographs of the interference colours for the film thinning behaviour of a drop released to the bulk interface soon after the previously released drop has just completed the first stage of coalescence: drop

size 0.0025 ml, zero concentration of palmitic acid, and uncleaned bulk interface.

11. Same as Fig. 10, except the concentration of palmitic acid: 10^{-6} M.

12. Variation of ϕ_9 and ϕ_7 with bulk interface age in this work (upper diagram) and previous work[1,5] (lower diagram).

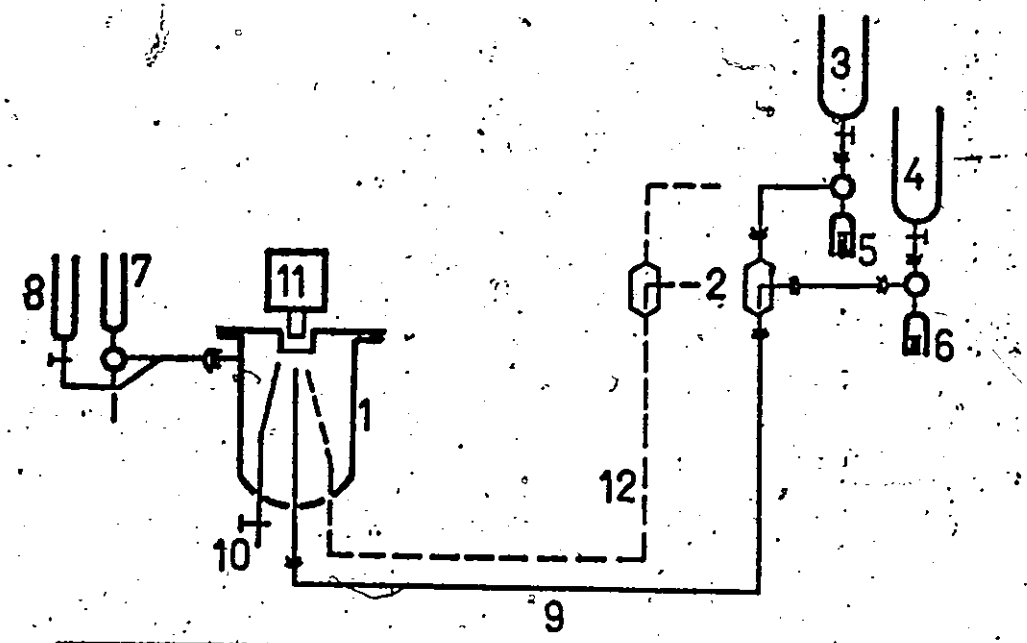

1	Coalescence Cell	9	Connecting Tube
2	Drop Forming Nozzle	10	Interface Cleaning Probe
3	Water Reservoir	11	Microscope and Camera
4	Oil Reservoir	12	Extension for Multi-drops
5,6	Agla syringe	—|	Two-way Stopcock
7	Make up Water Reservoir	—○—	Three-way Stopcock
8	Make up Oil Reservoir	—)(—	Ball&Socket Joint

Figure 1

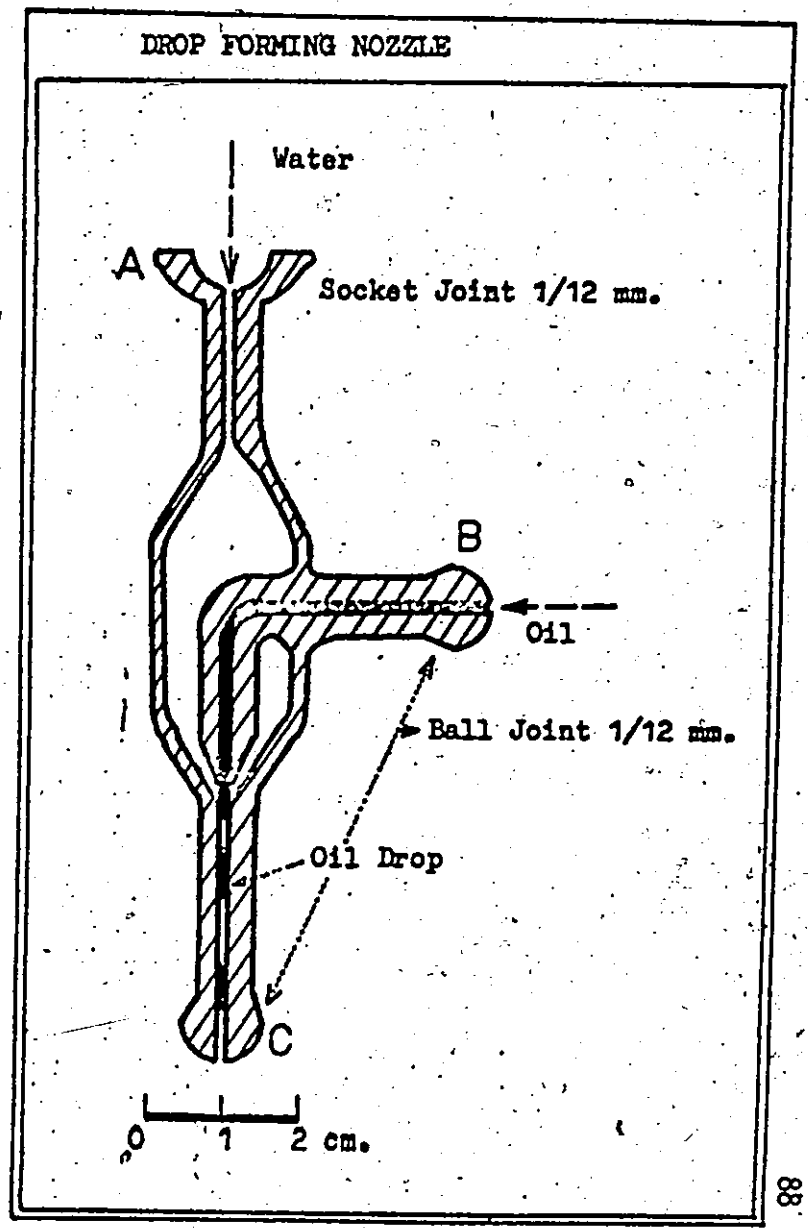

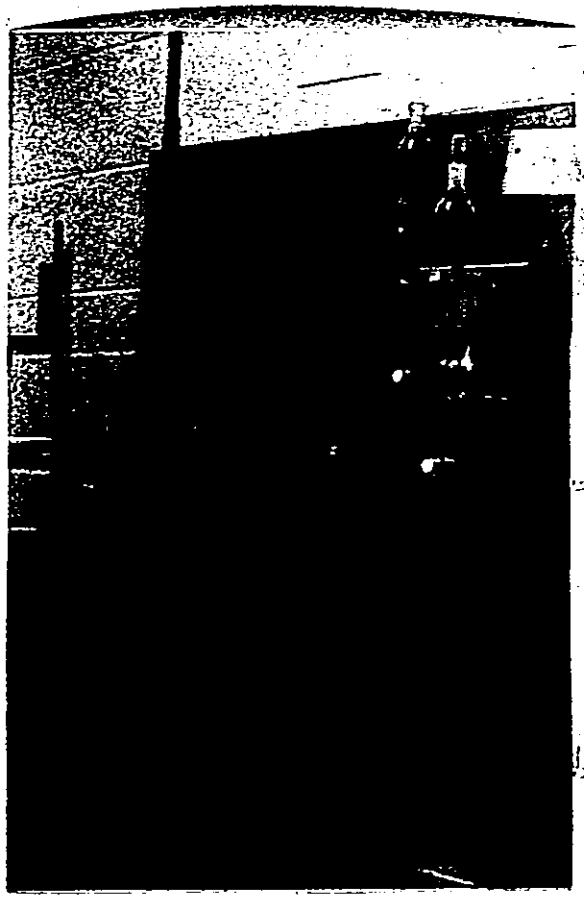

Figure 2

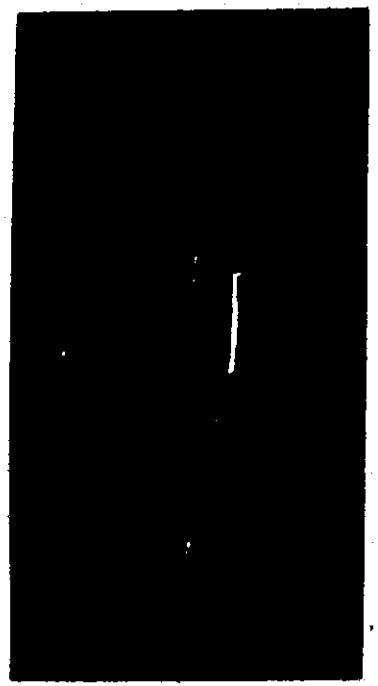

Figure 3

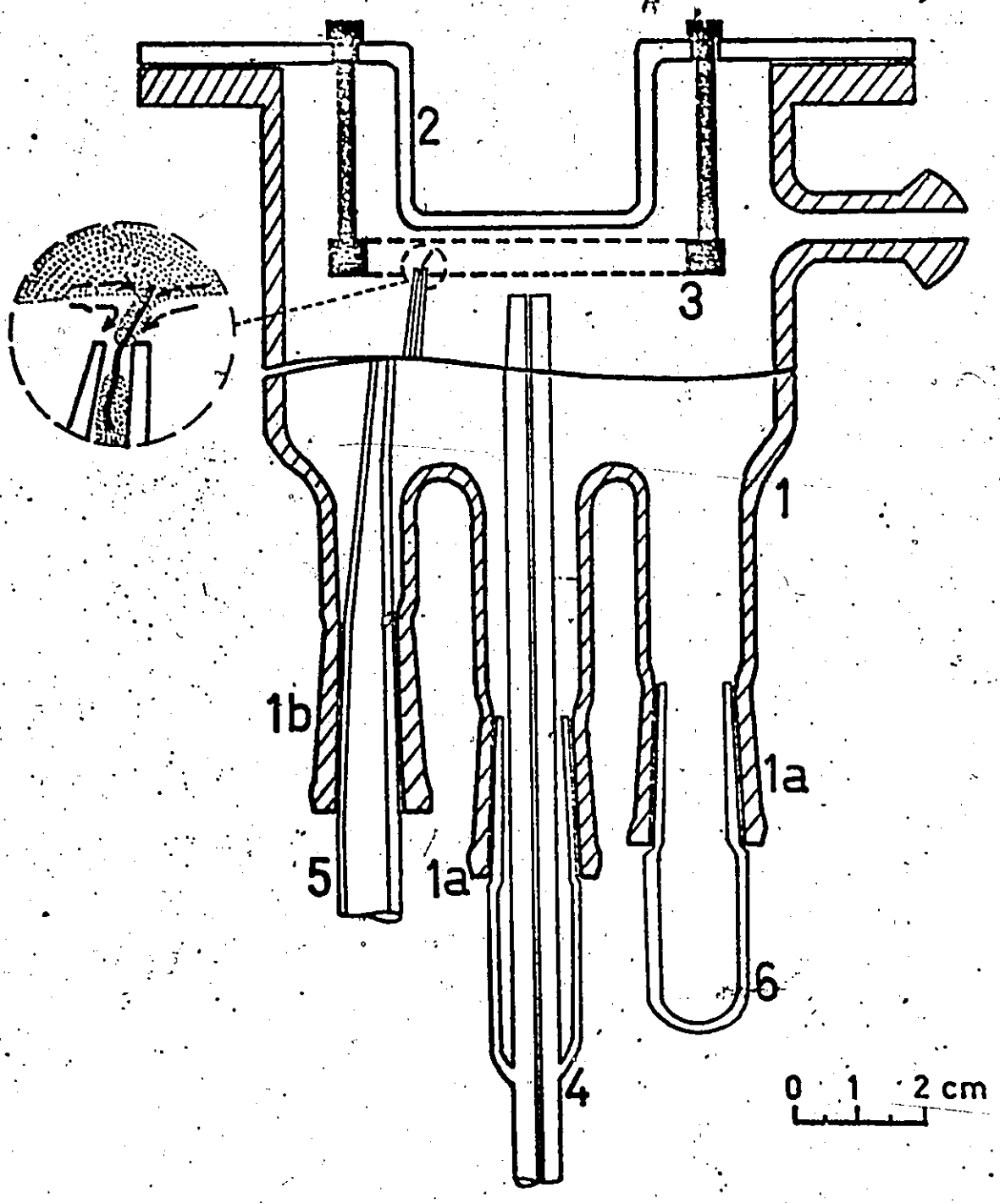

1	Coalescence Cell	4	Drop carrying tube
1a	Tapered Joint (4) 14/23 mm	5	Cleaning probe (3)
1b	(3) 10/30 mm	6	Plug (3)(x)
2	Cell Cover		
3	Teflon Ring		

(x) Provision for multiple drops experiment

Figure 4

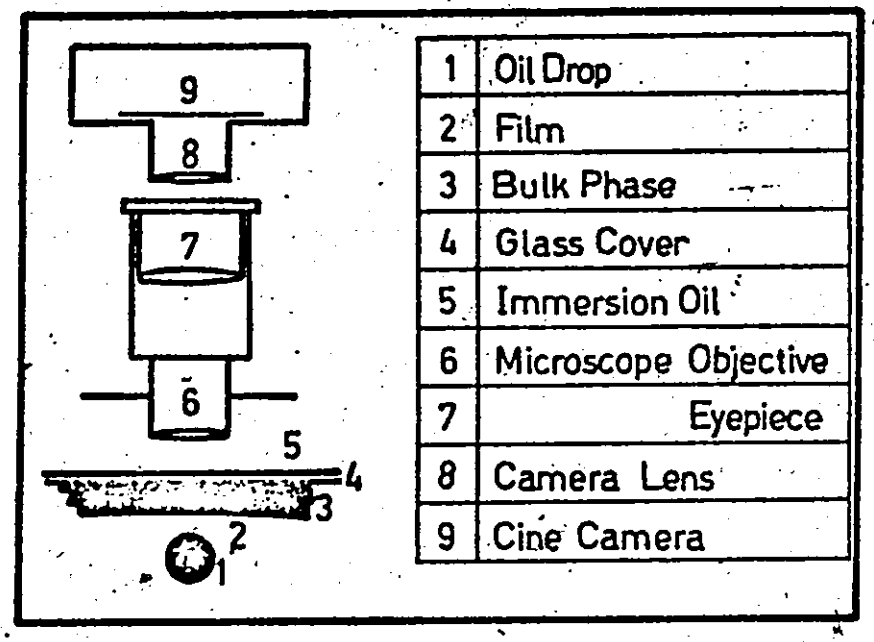

1	Oil Drop
2	Film
3	Bulk Phase
4	Glass Cover
5	Immersion Oil
6	Microscope Objective
7	Eyepiece
8	Camera Lens
9	Cine Camera

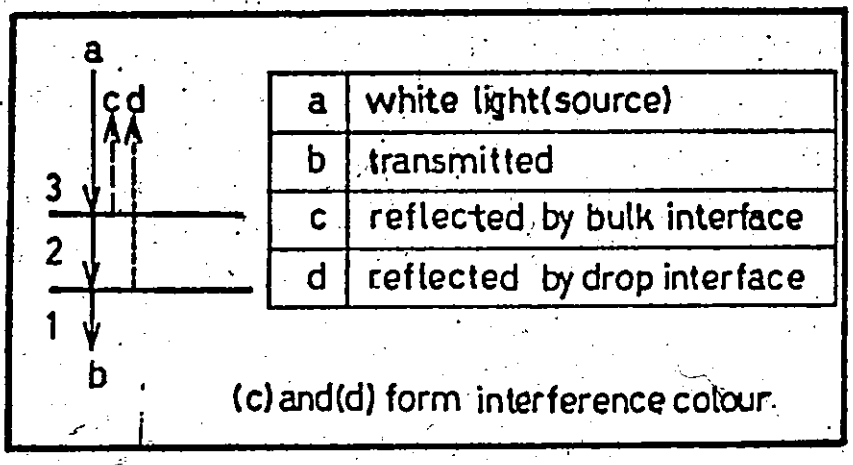

a	white light(source)
b	transmitted
c	reflected by bulk interface
d	reflected by drop interface

(c) and (d) form interference colour.

Figure 5

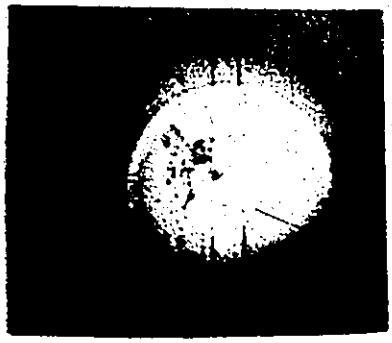

(a) Θ= 0 sec: Arrest after rapid thinning.

(b) Θ= 1.13 sec: Dimple formation.

(c) Θ= 4.86 sec: Arrest after dimple formation.

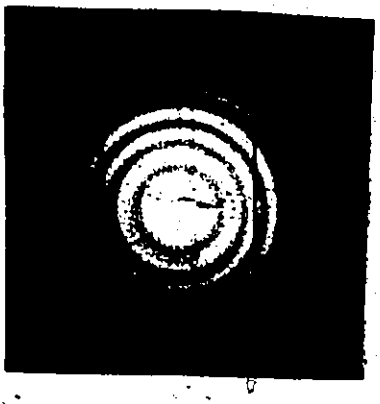

(d) Θ= 9.07 sec: Even thinning.

Figure 6

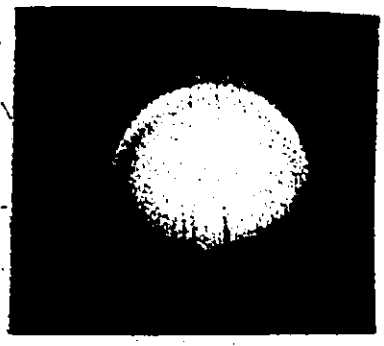

(a) θ= 0 sec: Arrest after rapid thinning.

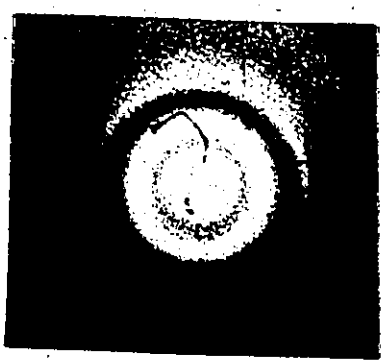

(b) θ= 0.32 sec: Dimple formation.

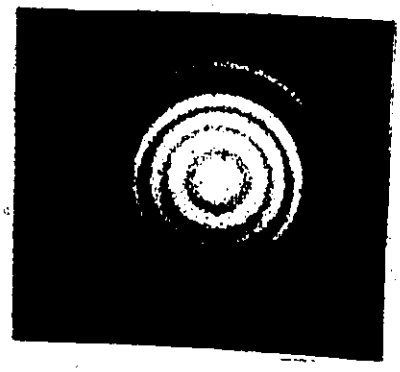

(c) θ= 1.78 sec: Dimple formation.

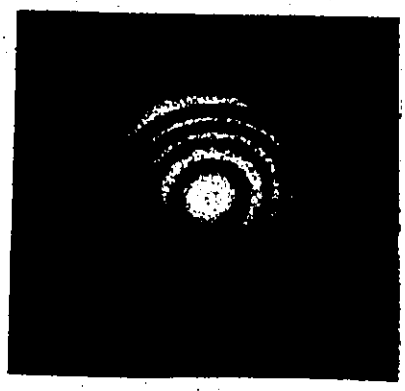

(d) θ= 3.65 sec: Onset of uneven thinning.

(e) θ= 3.97 sec: Uneven thinning Type B.

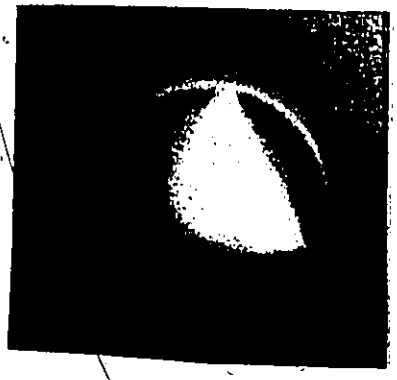

(f) θ= 16.52 sec: Just before film rupture.

Figure 7

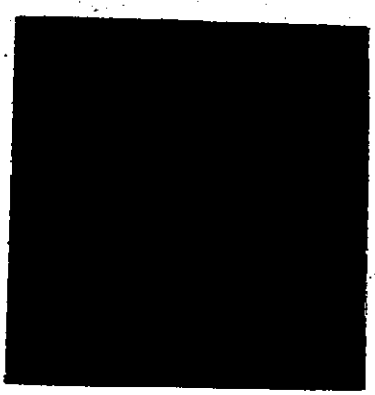

(a) θ= 0 sec: Uneven thinning Type A (No rapid thinning or dimple formation).

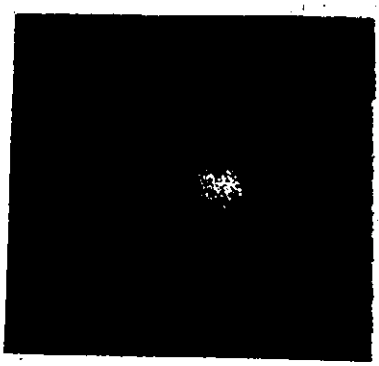

(b) θ= 2.35 sec

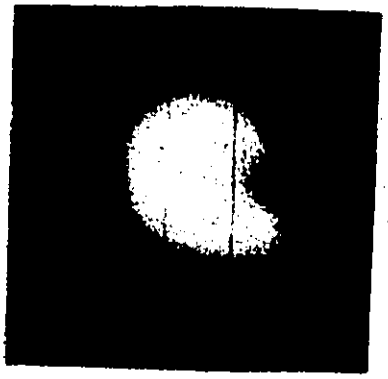

(c) θ= 7.86 sec: Just before film rupture.

Figure 8

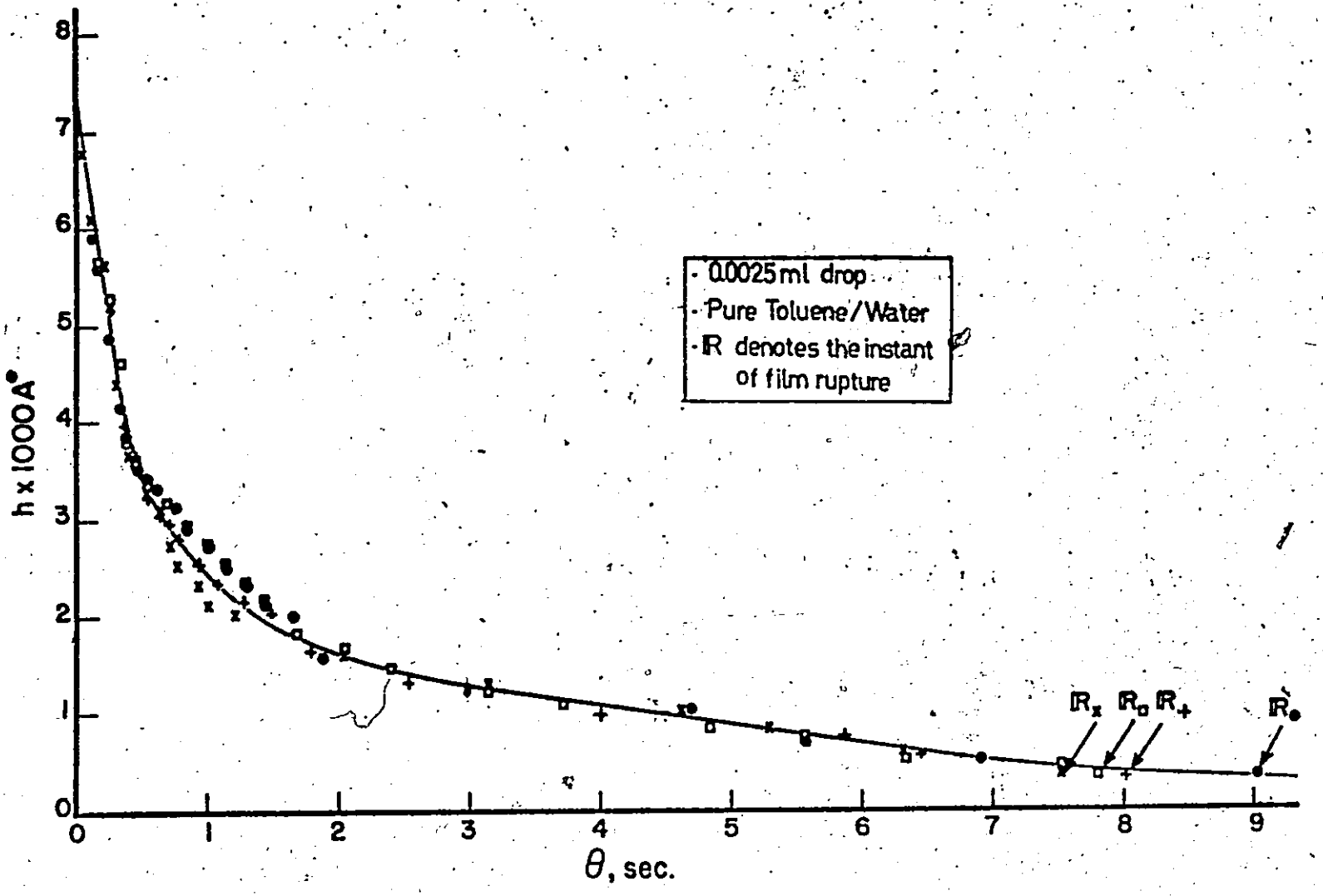
h x 1000A°
θ, sec.
0.0025 ml drop
Pure Toluene/Water
R denotes the instant of film rupture
R× R□ R+
R●

Figure 9

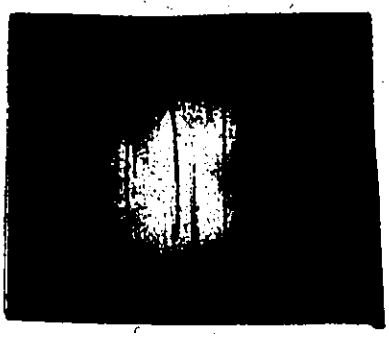

(a) θ= 0 sec: Irregular thinning pattern.

(b) θ= 0.41 sec

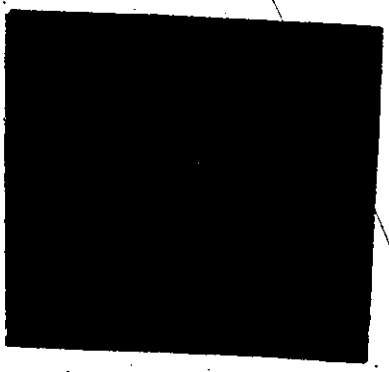

(c) θ= 0.81 sec: Just before film rupture.

Figure 10

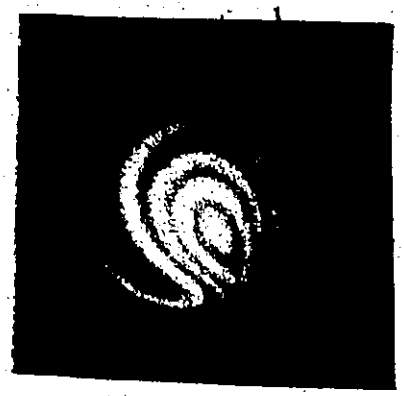

(a) Θ= 0 sec: 'Regular'

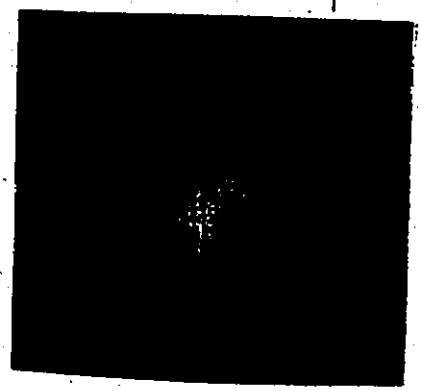

(b) Θ= 1.13 sec: The instant the satellite drop joined the bulk phase.

(c) Θ= 1.21 sec : The abrupt change in the film thinning behaviour

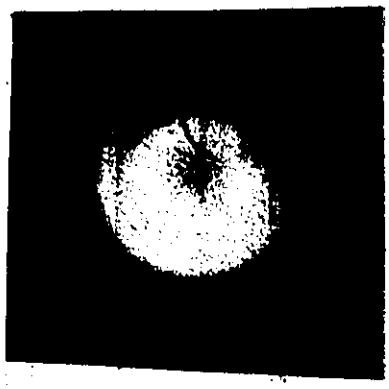

(d) Θ= 1.94 sec: The second satellite drop joined the bulk phase.

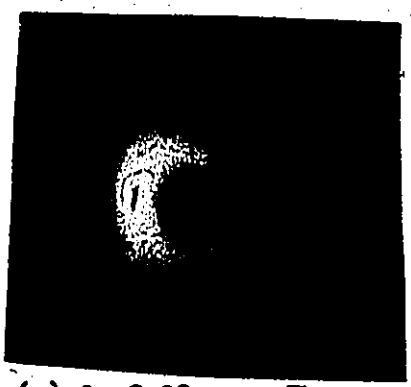

(e) Θ= 2.02 sec: The second abrupt change in the film thinning behaviour.

Figure 11

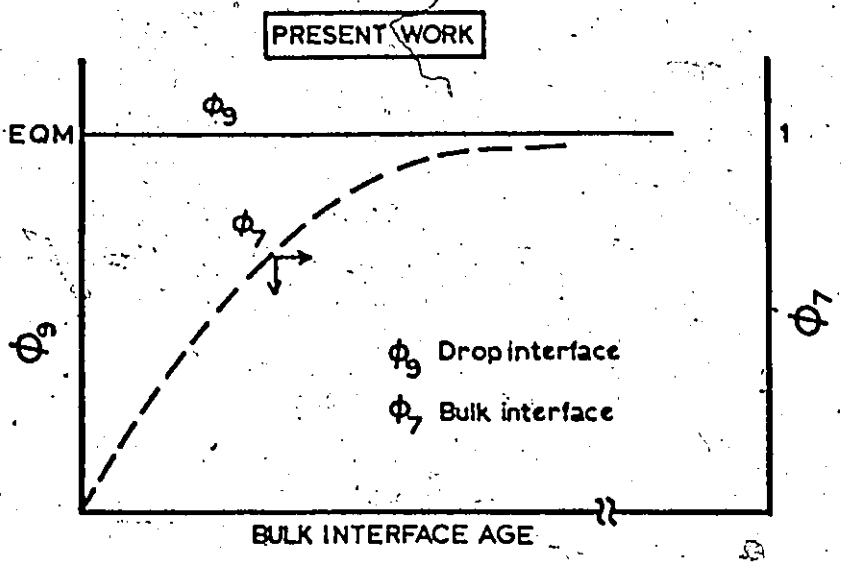

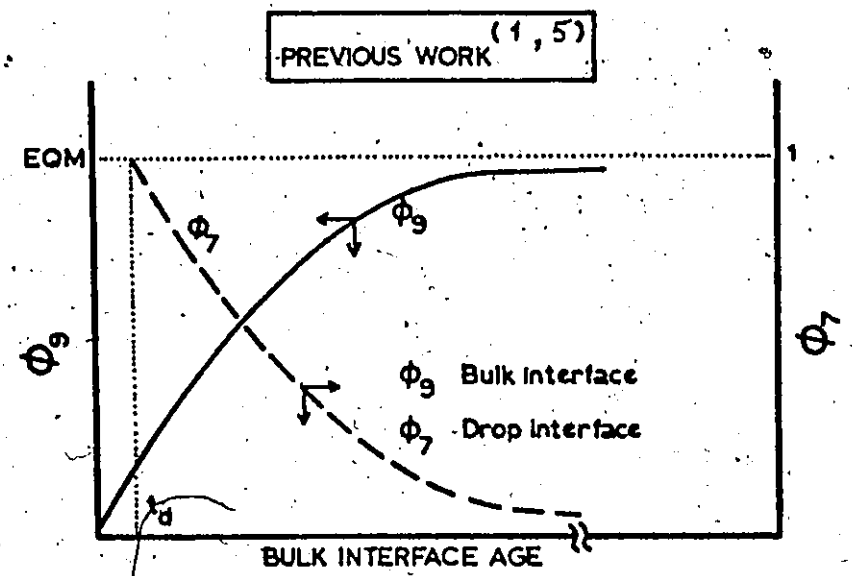

LEGEND • EQM Equilibrium surface concentration

• t_d Drop interface age

Figure 12

CHAPTER 4

THEORETICAL ANALYSIS OF SYMMETRICAL FILM THINNING BEHAVIOUR

This chapter describes the numerical solution of the film thinning equations developed in Chapter 2, and a comparison of the results with experimental observations of the variation of film thickness profile with time. The numerical solution is based on the representation of the pressure in the film by a polynomial function of the radial distance. The resulting model is referred to as the polynomial model.

4.1. Normalization of the film thinning equations

It is convenient to normalize the variables so that they all have numerical values that are of the same order of magnitude.

The normalized variables are defined by

$r^+ = \frac{r}{R}$	$\theta^+ = \frac{\theta}{T}$	$h^+ = \frac{h}{Y}$	$p^+ = \frac{p}{P}$	$U_1^+ = \frac{U_1}{U}$	$U_2^+ = \frac{U_2}{U}$	$\Gamma_1^+ = \frac{\Gamma_1}{\Gamma_{s1}}$	$\Gamma_2^+ = \frac{\Gamma_2}{\Gamma_{s1}}$

(1)

where the normalizing constants are

$Y = 10^{-5}$ cm	P = 100 dn/cm	U = 0.01 cm/sec	T = 1 sec

(2)

and R is the radius of the film area over which the interference colours are measured, and the surface concentration Γ_{s1} refers to the interface with the larger surface concentration.

The normalized film thinning equations are:

$$\frac{\partial h^*}{\partial \theta^*} = \frac{1}{r^*}\frac{\partial}{\partial r^*}\left[r^*\left\{\phi_4 \frac{\partial p^*}{\partial r^*} h^{*3} - \frac{1}{2}\phi_5 (U_1^* + U_2^*) h^*\right\}\right] \tag{3}$$

$$p^* \phi_1 = \phi - \frac{1}{2}\frac{1}{r^*}\frac{\partial}{\partial r^*}\left(r^* \frac{\partial h^*}{\partial r^*}\right) \tag{4}$$

$$\phi_9 \frac{\partial \Gamma^*}{\partial r^*} + \phi_{10} \frac{U_1^* - U_2^*}{h^*} + \frac{1}{2} h^* \frac{\partial p^*}{\partial r^*} = 0 \tag{5}$$

$$\phi_9 \frac{\partial \Gamma_2^*}{\partial r^*} - \phi_{10} \frac{U_1^* - U_2^*}{h^*} - \frac{1}{2} h^* \frac{\partial p^*}{\partial r^*} = 0 \tag{6}$$

$$\frac{\partial \Gamma_1^*}{\partial \theta^*} = \phi_{12}(1 - \Gamma_1^*) + \phi_6 \frac{1}{r^*}\frac{\partial}{\partial r^*}\left(r^* \frac{\partial \Gamma_1^*}{\partial r^*}\right) - \phi_5 \frac{1}{r^*}\frac{\partial}{\partial r^*}\left(r^* U_1^* \Gamma_1^*\right) \tag{7}$$

$$\frac{\partial \Gamma_2^*}{\partial \theta^*} = \phi_{12}(\phi_7 - \Gamma_2^*) + \phi_6 \frac{1}{r^*}\frac{\partial}{\partial r^*}\left(r^* \frac{\partial \Gamma_2^*}{\partial r^*}\right) - \phi_5 \frac{1}{r^*}\frac{\partial}{\partial r^*}\left(r^* U_2^* \Gamma_2^*\right) \tag{8}$$

The boundary conditions Eqs. (2-57), (2-58), (2-54a), (2-56a), (2-61), (2-59), (2-60a) and (2-62) become

$$\frac{\partial h^*}{\partial r^*} = 0 \qquad r^* = 0 \tag{9}$$

$$\frac{\partial p^*}{\partial r^*} = 0 \qquad r^* = 0 \tag{10}$$

$$\psi = \int_0^{R_p^*} 2 r^* p^* dr^* \tag{11}$$

$$p^* = 0 \qquad r^* = R_p^* \tag{12}$$

$$\frac{\partial p^*}{\partial r^*} = 0 \qquad r^* = R_p^* \tag{13}$$

$$\frac{\partial \Gamma_1^*}{\partial r^*} = 0 \qquad r^* = 0 \tag{14}$$

$$\Gamma_1^* = 1 \qquad r^* = R'^* \tag{15}$$

$$\frac{\partial \Gamma_1^*}{\partial r^*} = 0 \qquad r^* = R''^* \tag{16}$$

The boundary conditions for Γ_2^+ are the similar to those for Γ_1^+, except that the value of Γ_2^+ is equal to ϕ_7 in Eq. (15).

The normalizing dimensionless parameters are given by

$$\phi = \frac{R^2}{bY} \qquad \phi_1 = \frac{PR^2}{\gamma Y} \qquad \phi_4 = \frac{PY^2T}{12\mu R^2} \qquad \phi_5 = \frac{UT}{R} \qquad \phi_6 = \frac{\mathcal{D}T}{R^2}$$

(17)

$$\phi_7 = \frac{\Gamma_{s2}}{\Gamma_{s1}} \qquad \phi_9 = \frac{k^* \Gamma_{s1}}{PY} \qquad \phi_{10} = \frac{\mu U R}{PY^2} \qquad \phi_{12} = k_3 T \qquad \psi = \frac{F}{\pi R^2 P}$$

4.2. The polynomial model

As outlined in Chapter 2.3.6, there are three initial conditions that must be specified to start the solution of the film thinning equations: the film thickness profile and the surface concentration distributions at the bulk and drop interfaces. The initial film thickness profile is obtained experimentally, and the initial surface concentration distributions (and the corresponding interface velocities) are calculated from the experimentally measured rate of thinning.

Therefore, the solution of the film thinning equations can be conveniently divided into three stages:

(i) The description of the initial film thickness profile and rate of

thinning based on the polynomial pressure distribution.

(ii) The calculation of the initial surface concentration distributions and the interface velocities.

(iii) The integration of the film thinning equations to predict the variation with elapsed time of the film thickness profile.

The outline of the first two stages is shown in a flow chart diagram in Fig. 1. The method of calculating the surface concentration distributions and the interface velocities has already been described in Fig. 6 in Chapter 2.3.6; however, for computational reasons, the value of $(\Gamma_1 + \Gamma_2)$ is calculated instead of Γ_2. The integration of the film thinning equations is described in Section 4.2.3.

4.2.1. The description of the initial film thickness profile and rate of thinning

Assume that the pressure can be represented by a polynomial function of the radial distance r:

$$p^*(r^*, \theta^*) = \sum_{n=0}^{N}{}_e A_n(\theta^*) r^{*n} \qquad (18)$$

where the subscript e denotes that the summation is taken over even numbers of n because the pressure is a symmetrical function of r. Henceforth, for convenience, the superscript + which denotes normalized variables is omitted.

The film thickness can be written as

$$h = \sum_{n=0}^{N+2}{}_e L_n r^n \qquad (19)$$

where the coefficients L_n and A_n are related by the normal force balance equation Eq. (4). Substitution of Eqs. (18) and (19) into Eq. (4), and a term by term comparison of the resulting equation gives

$$L_n = \frac{2}{n^2}\left(\delta_{2n}\Phi - \Phi_1 A_n\right) \qquad n = 2,4\ldots N+2 \qquad (20)$$

where

$\delta_{m,n} = 1$ for m=n, and 0 otherwise.

The boundary conditions Eqs. (9) and (10) are automatically satisfied by the polynomial approximation; therefore only the boundary conditions Eqs. (11) to (13) must be satisfied by the coefficients A_n.

Since A_n and L_n are related by Eq. (20), the fitting of the initial film thickness profile can be formulated by:

$$\underset{A_n}{\text{Minimize}} \sum_i \left[h_i - \sum_{n=0}^{N+2} L_n r_i^n \right]^2 \qquad (21)$$

where h_i is the experimental film thickness at the radial location r_i, the summation is taken over the experimental points, and L_0 is given the value of the film thickness at the film centre.

For an N^{th} order polynomial for p, since only even terms are used, there are only ½(N+2) coefficients that can be chosen in the minimization of Eq. (21). However, of these coefficients, only ½(N+2) - 2 coefficients can be chosen independently because the boundary conditions Eqs. (11) to (13) must be satisfied.

The minimization of Eq. (21) was carried out using the Rosenbrock search technique[1], and the boundary conditions Eqs. (11) to (13) were solved using the Newton-Raphson method. The details are described in Appendix D.1.

Fig. 2 shows typical results of the fitting for N=6 and N=8; the value of N=8 is adequate to describe the film thickness profile.

The rate of thinning can also be expressed in a polynomial form by differentiating Eq. (19) with respect to time:

$$\frac{\partial h}{\partial \theta} = \sum_{n=0}^{N+2} \frac{dL_n}{d\theta} r^n \qquad (22)$$

where the coefficients $dL_n / d\theta$ can be calculated using the first order difference method:

$$\frac{dL_n(\theta_o)}{d\theta} = \frac{1}{\Delta\theta_o}\left(L_n(\theta_o+\Delta\theta_o) - L_n(\theta_o)\right) \qquad (23)$$

where $\Delta\theta_o$ is the time interval between two successively measured film thickness profiles. The value of L_n at $\theta + \Delta\theta_o$ can be calculated by the same method as that used to calculate the initial film thickness profile.

This completes the description of the initial film thickness profile and rate of thinning based on the polynomial pressure distribution.

4.2.2. Calculation of the initial interface velocities and surface concentration distributions

The outline of the calculation is given in Fig. 1. The calculations involved are as follows.

4.2.2.1. Sum of the interface velocities

Integration of the rate of thinning equation Eq. (3) with respect to r, from r=0 to r=r gives

$$rh\left\{\Phi_4 \frac{\partial p}{\partial r} h^2 - \frac{1}{2}\Phi_5 (U_1+U_2)\right\} - C_1 = \int_0^r r \frac{\partial h}{\partial \theta}\, dr \qquad (24)$$

where the integration constant C_1 is equal to zero because all the variables remain finite at r=0. The sum of the interface velocities is therefore given by

$$U_1+U_2 = \frac{2}{\phi_5}\left\{\phi_4 \frac{\partial p}{\partial r} h^2 - \frac{1}{r\,h}\int_o^r r \frac{\partial h}{\partial \theta}\, dr\right\} \qquad (25)$$

where the integral term is calculated from Eq. (22):

$$\frac{1}{r}\int_o^r r \frac{\partial h}{\partial \theta}\, dr = \sum_{n=0}^{N+2} \frac{1}{n+2} \frac{dL_n}{d\theta} r^{n+1} \qquad (26)$$

The sum of the interface velocities can therefore be calculated at any radial location since all the terms on the RHS of Eq. (25) are known from the initial film thickness and rate of thinning.

4.2.2.2. Sum of the surface concentrations

The combined equation of Eqs. (5) and (6):

$$\phi_9\left(\frac{\partial \Gamma_1}{\partial r} + \frac{\partial \Gamma_2}{\partial r}\right) = -h\frac{\partial p}{\partial r} \qquad (27)$$

can be integrated with respect to r from r=0 to r=r to give

$$\Gamma_1 + \Gamma_2 - (\Gamma_1 + \Gamma_2)_{r=o} = -\frac{1}{\phi_9}\int_o^r h \frac{\partial p}{\partial r}\, dr \qquad (28)$$

The integral term can be calculated from Eqs. (18) and (19):

$$\int_o^r h \frac{\partial p}{\partial r}\, dr = \sum_{n=2}^{2N+2} \frac{1}{n}\left(\sum_{j=o}^{n-2} (n-j)\, L_j\, A_{n-j}\right) r^n \qquad (29)$$

where it is defined that $A_n = 0$ for $n > N$, and $L_n = 0$ for $n > N+2$.

At r=0 the boundary condition Eq. (14) is automatically satisfied. The value of $(\Gamma_1 + \Gamma_2)$ at r=0 must be calculated from the boundary

conditions of the kind given by Eqs. (15) and (16). These boundary conditions extend beyond r=1, that is, beyond the region of measurable film thickness; therefore, it is necessary to make an assumption as to the variation with r of some variables in the region $r > 1$. Computationally, the simplest method is to choose the surface concentration as the assumed variable. The variation with r in the region $r > 1$ has been assumed to be parabolic starting from r=1, with a concentration and a slope that are equal to those of the distribution inside $r \ll 1$. This method is referred to as a parabolic extrapolation. To avoid an unnecessary distraction due to the lengthy algebra, the calculation of $(\Gamma_1 + \Gamma_2)$ at r=0 is given in Appendix D.2.3.

In the calculation of the interface velocities and the surface concentration distributions, it convenient to calculate first the rate of change of the sum of the surface concentrations. The calculations involved are as follows.

Differentiation of Eq. (28) with respect to time gives

$$\frac{\partial}{\partial\theta}\left(\Gamma_1+\Gamma_2\right)-\frac{\partial}{\partial\theta}\left(\Gamma_1+\Gamma_2\right)_{r=0}=-\frac{1}{\phi_9}\int_0^r \frac{\partial}{\partial\theta}\left(h\frac{\partial p}{\partial r}\right)dr \qquad (30)$$

The integral term can be calculated from the following relationship:

$$\frac{\partial}{\partial\theta}\left(h\frac{\partial p}{\partial r}\right)=h\frac{\partial}{\partial\theta}\frac{\partial p}{\partial r}+\frac{\partial h}{\partial\theta}\frac{\partial p}{\partial r} \qquad (31)$$

Hence by using Eqs. (18) and (19), the following is obtained:

$$\int_0^r \frac{\partial}{\partial\theta}\left(h\frac{\partial p}{\partial r}\right)dr=\sum_{n=2}^{2N-2}\frac{1}{n}\left\{\sum_{j=0}^{n-2}(n-j)\left(L_j\frac{dA_{n-j}}{d\theta}+\frac{dL_j}{d\theta}A_{n-j}\right)\right\}r^n \qquad (32)$$

The time derivative of the pressure coefficients can be calculated by differentiating the normal force balance equation Eq. (20) with respect to time:

$$\frac{dL_n}{d\theta} = -\frac{2}{n^2}\,\Phi_1\,\frac{dA_{n-2}}{d\theta} \qquad n = 2,4..\ N+2 \tag{33}$$

Therefore, all the terms on the RHS of Eq. (32) can be calculated from the known initial film thickness and rate of thinning. To complete the calculation of the rate of change of the sum of the surface concentrations, the value at r=0 is calculated by the same method as that used for calculating $(\Gamma_1 + \Gamma_2)$ at r=0. This is described in Appendix D.3.4.

4.2.2.3. Calculation of the interface velocity U_1

The surfactant mass balance equations Eqs. (7) and (8) can be combined to give

$$\frac{\partial}{\partial\theta}(\Gamma_1+\Gamma_2) - \Phi_{12}\left\{1+\Phi_7(\Gamma_1+\Gamma_2)\right\} - \Phi_6\,\frac{1}{r}\frac{\partial}{\partial r}\left\{r\frac{\partial}{\partial r}(\Gamma_1+\Gamma_2)\right\} = -\Phi_5\,\frac{1}{r}\frac{\partial}{\partial r}\left\{r(U_1\Gamma_1 + U_2\Gamma_2)\right\} \tag{34}$$

The LHS of Eq. (34) can be readily calculated from the known initial film thickness and rate of thinning by using Eqs. (28) and (30). The RHS of Eq. (34) can be calculated after a value for U_1 has been tentatively assumed; hence Eq. (34) is the equation for calculating U_1. The procedure for solving Eq. (34) for U_1 is as follows:

(i) assume a value for U_1,

(ii) calculate U_2 from the assumed value of U_1 and $(U_1 + U_2)$, given

by Eq. (25),

(iii) calculate Γ_1 from Eq. (5) , as described in Appendix D.2.3.5,

(iv) calculate Γ_2 from the already calculated Γ_1 and ($\Gamma_1 + \Gamma_2$), given by Eq. (28), and

(v) test if Eq. (34) is satisfied.

The calculation of U_1 from Eq. (34) was carried out using the repetitive substitution method as decribed in Appendix D.2.4. A typical convergence of this iterative method is shown in Fig. 3: an accuracy better than 0.001 was obtained in less than ten iterations using the value of $U_1 = 0$ everywhere at the interface as the first assumption.

The value of U_1 which satisfies Eq. (34) is consistent with the initial film thickness and rate of thinning. After U_1 has been calculated, U_2, Γ_1 and Γ_2 can be readily calculated, as shown in steps (ii), (iii) and (iv) respectively. This then completes the calculation of all the variables at the initial time.

4.2.3. Integration of the film thinning equations

The method for integrating the film thinning equations is shown schematically in Fig. 4; it is essentially a predictor-corrector method[2] in which the arithmetic average of the derivatives is used to progress to the next time interval. For example, for L_n:

$$L_n(\theta_o + \Delta\theta) = L_n(\theta_o) + \tfrac{1}{2}\left[\frac{dL_n}{d\theta}\bigg|_{\theta_o} + \frac{dL_n}{d\theta}\bigg|_{\theta+\Delta\theta}\right]\Delta\theta \qquad (35)$$

This integration method requires an iterative solution for each integration step. The scheme of iterative solution adopted was to assume tentatively the rate of thinning at time $\theta_o + \Delta\theta$. After this rate of

thinning had been assumed, the film thickness profile at $\theta_o+\Delta\theta$ could be calculated from Eq. (35). Therefore, at $\theta_o+\Delta\theta$ the film thickness profile and the rate of thinning were known. Hence the other variables - pressure, interface velocities and surface concentration distributions - could be calculated by the method used to solve the initial condition problem.

The value for the rate of thinning at $\theta_o+\Delta\theta$ was chosen such that the surfactant mass balance equation for Γ_1 was satisfied: the value of Γ_1 calculated by integration (cf. Eq. (35)) should be equal to that calculated from the initial condition problem at $\theta_o+\Delta\theta$.

As shown in Fig. 4, the iterative solution does not involve the last two coefficients of the rate of thinning polynomial. The reason is the boundary conditions Eqs. (11) to (13) must always be satisfied. To calculate the film thickness profile at $\theta_o+\Delta\theta$, L_0, L_2 ... L_{N-2} are calculated from Eq. (35), and then A_0, A_2 ... A_{N-4} from Eq. (20). The values of A_{N-2}, A_N and R_p can now be calculated fron Eqs. (11) to (13), and hence L_N and L_{N+2} can be calculated from Eq. (20). Therefore, the values of $dL_N/d\Theta$ and $dL_{N+2}/d\Theta$ are not needed in Eq. (35).

The problem of calculating the rate of thinning at $\theta_o+\Delta\theta$ was solved as a minimization problem. The 'independent variables' were the coefficients $dL_n/d\Theta$, and the objective function was the sum of squares of the difference between the value of Γ_1 calculated by integration and that calculated from the initial condition problem at $\theta_o+\Delta\theta$.

The minimization technique used is illustrated in Fig. 5 for two independent variables. From the starting point M_1, a better value M_2 is searched along the principal axes by the path M_1-M_1'-M_2, where M_1' is the

minimum along the x_1-axis. This is referred to as the first stage. The second stage is the search for a minimum along the newly found direction M_1-M_3. This two-stage minimization process is repeated using M_3 as the starting point. The search for a minimum along the principal axis or along the direction M_1-M_3 was carried out by using the method of Davies et al[1], described in Appendix D.3.2.

The minimization was terminated when:

(i) the difference in Γ_1 calculated by integration and that calculated from the initial condition problem at $\theta_o + \Delta\theta$ was less than 0.002, or

(ii) the search failed to progress further than 0.01 which corresponded to an accuracy of 10 Å/sec. in the rate of thinning.

The maximum integration step size was determined by testing that the integration results were not significantly affected when this step size was reduced. The actual step size was chosen so as to yield a compromise between the number of integration steps required to cover a time interval and the computational time required to calculate the coefficients $dL_n/d\theta$ at each integration step. The value used was 0.004 sec as determined by preliminary tests.

4.3. Results and discussion

There are essentially two types of symmetrical film thinning behaviour: dimple formation, which is followed by arrest and even thinning, and the slow even thinning Pattern IV[3], in which the film is arrested at a large film thickness and thinning occurs mainly in the barrier ring region. These observations have not been successfully described by previously developed models. In this thesis, it has been suggested that the main

cause of failure is the incorrect assumption of constant interface mobility. The polynomial model has been developed to test this supposition.

Comparison of the polynomial model predictions with experimental observations

The comparison was carried out by measuring the film thickness profile and the rate of thinning at some instant during dimple formation or thinning, and then comparing the model predictions of the subsequent film thickness profiles with those experimentally observed. This comparison was made for the necessary elapsed time to show that the model could follow the trends of the observed film thinning behaviour.

The results are shown in Figs. 6 to 10, and the systems used and the corresponding physical properties are shown in Tables Ia to Ic. (More data on dimple formation have been used because this behaviour in particular is strongly dependent on interface movement.) The methods for estimating the values of the physical properties used will be discussed later.

In each comparison, the initial film thickness profile at $\theta = 0$ was obtained from the data by using the method described in Section 2.1, and the initial rate of thinning was calculated from Eq. (23). The subsequent film thickness profiles were calculated by using the methods described in Sections 2.2 and 2.3.

Fig. 6 shows a comparison for dimple formation. The data are shown as rectangulars which represent the interference colours at different radial locations in the film. The observed film thickness in the central region is slightly overestimated and in the barrier ring region, underestimated. The trends of behaviour are, however, correctly predicted: the film thickness increases in the central region and decreases in the

barrier ring region. This is consistent with the observed dimple formation and simultaneous thinning in the barrier ring region.

A better agreement could have been obtained by refining further the selection of the values for the surfactant physical properties and the model parameter β (cf. Eq. (D-31) of Appendix D). However, such an effort would not contribute significantly to the purpose of the comparison. The results in Fig. 6 have already shown that the polynomial model is capable of describing the observed behaviour.

The results of the comparison for dimple formation for different systems are shown in Figs. 7 to 9. These results further confirm the validity of the polynomial model.

In Fig. 7a, the model is used to describe the even thinning that occurs after dimple formation is arrested. The observed slow rate of thinning and barrier ring expansion are correctly predicted by the polynomial model.

The comparison for an anisole/water system which exhibited the slow even thinning Pattern IV[3] is shown in Fig. 10. The observed behaviour is correctly predicted: the film thickness at the centre is practically constant and thinning occurs only in the barrier ring region.

So far, the trends of these observed film thinning behaviour have not been correctly predicted by the models reported in literature. Burrill[12] was the first to develop a model which could indicate dimple formation; all the other models could not even show that dimple formation might occur. In Burrill's model, the predicted rate of dimple formation was much too fast - in the order of ten times than that observed. Furthermore, his model predicted an increase in the film thickness in the barrier ring

region; that is, the model predicted an approach to a uniform film thickness as the dimple formation progressed. Burrill's model also predicted incorrectly the trends of the slow even thinning Pattern IV. The rate of thinning at the film centre was highly overestimated, and as a result an approach to a uniform film thickness (instead of the 'deepening' of the 'pocket' as observed) was predicted.

Figs. 6 to 10 show that the polynomial model is capable of following the observed trends of the different film thinning behaviour. The predictions agree with the experimental observations to within 10 to 20% in most locations in the film, except in the barrier ring region where the error can be as high as 70%. The reasons for this large error are that the film thickness in the barrier ring is small (hence large relative errors), and that the polynomial approximation becomes less accurate with increasing radial distance.

Figs. 6 to 10 show snap-shot views of the different aspects of film thinning behaviour. This method of comparison, which ensures that the model is capable of describing the different types of film thinning behaviour, has been adopted because of the large computation time required to solve the polynomial model. It would be interesting to use the polynomial model to describe film thinning over a longer period of elapsed time so that one can visualize, for example the behaviour of dimple formation gradually becoming arrested and then followed by even thinning. However, the computation time would be prohibitively large. In addition, in all the snap-shot calculations, constant values for the parameter β and the surface concentrations $k^*\Gamma_{s1}$ and ϕ_7 were used. These approximations are reasonable only for a short period of elapsed time. The para-

meter β - which represents the location where the interfaces are not influenced by the flow in the film - should be related to the radial velocity profile in the film. The values of $k^* \Gamma_{s1}$ and ϕ_7 vary with elapsed time if the interfaces are still aging. Therefore, the use of the polynomial model for a long period of elapsed time would have required a very large computation time because of the necessary adjustments of β, ϕ_7 and $k^* \Gamma_{s1}$. Even when these values were assumed constant, the computation time required for one second of actual elapsed time was about ten minutes in a CDC 6400 digital computer.

Sensitivity of the polynomial model predictions to physical properties

The values of the surface diffusion coefficient $\mathcal{D}$, the adsorption rate constant k_3 and the surface concentrations expressed in terms of $k^* \Gamma_{s1}$ and ϕ_7 that were used in the solution of the polynomial model were estimates because accurate data on these values were not available. It is therefore necessary to investigate the effect of changes in these estimates on the polynomial model predictions. This investigation is necessary to ensure that the characteristics of the model predictions are not drastically altered by small changes in the values of these estimates. Furthermore, this investigation should show whether the polynomial model predicts correctly (based on qualitative physical arguments) the effect of these estimates.

The effect of the model parameter β was also included in this investigation because its value was an estimate.

Figs. 11 to 14 show the effect of $\mathcal{D}$ and k_3, $k^* \Gamma_{s1}$, ϕ_7 and β on the predicted film thickness profiles for the dimple formation shown in Fig. 6. These profiles were calculated using the same initial film

thickness profile and rate of thinning as those used in Fig. 6.

The results in Figs. 11 to 14 show that despite the changes in the predicted film thickness profiles, the same trends of film thinning behaviour were obtained; that is, dimple formation which is accompanied simultaneously by thinning at the barrier ring. This indicates that the use of estimates for the surfactant physical properties and the surface concentrations $k^* \Gamma_{s1}$ and Φ_7 is acceptable for the purpose of testing if the polynomial model is capable of describing the different film thinning observations.

Consider now the variation of the rate of dimple formation with these estimates. The rate of dimple formation decreases with increasing β and k_3, $k^* \Gamma_{s1}$ and Φ_7, and with decreasing β, as shown in Figs. 11 to 14, respectively.

The effect of β and k_3 can be explained in terms of their effect on surface concentration distribution. These surfactant physical properties are a measure of how fast a uniform concentration is restored. As β and k_3 increase, the surface concentration distribution becomes closer to a uniform value. This means a smaller concentration gradient, a smaller interfacial tension gradient and consequently a smaller interface velocity. Because the rate of dimple formation is determined by the magnitude of the interface velocity, the increase in β and k_3 will cause a decrease in the rate of dimple formation.

The effect of $k^* \Gamma_{s1}$ and Φ_7 shown in Figs. 12 and 13 is as expected because as these concentrations increase, the interfaces become less mobile. This in turn causes a decrease in the interface velocity, and consequently a decrease in the rate of dimple formation.

The decrease in the rate of dimple formation with decreasing β

can be explained by examining the physical meaning of β. The value of β is a measure of the radial location where the interfaces are not influenced by the flow in the film. It can be expected therefore, that the larger the interface velocity, the larger is the value of β. Conversely, the smaller the value of β, the smaller is the interface velocity; hence the slower is the rate of dimple formation.

Figs. 11 to 14 also show that the decrease in the rate of dimple formation is accompanied by an increase in the rate of thinning in the barrier ring region. This behaviour can be explained in terms of the effect of $\mathcal{P}$, k_3, $k^*\Gamma_{s1}$, ϕ_7 and β on the rate of dimple formation. In the barrier ring region, thinning occurs because the outward flow due to the pressure gradient is larger than the inward flow due to interface movement. Therefore, the smaller the interface velocity, as shown by the slower rate of dimple formation, the faster is the rate of thinning in the barrier ring region.

The radial velocity, pressure, interface velocities and surfactant concentration distributions

These variables have not so far been measured directly; they can only be calculated - with the aid of a film thinning model - from the film thickness measurements. Because these variables are related to the film thinning behaviour, a better understanding of film thinning behaviour should be gained by calculating these variables.

Figs. 15a to 15d show the values of the radial velocity profile, the pressure, the interface velocities and the surface concentration distributions for the dimple formation shown in Fig. 6. The radial velocity profile was calculated from Eq. (2-13). Fig. 15a shows that the inward

flow due to movement of the bulk interface is larger than the outward flow due to movement of the drop interface and the pressure gradient; thus it is consistent with the observed dimple formation.

The variation of the pressure in the film with elapsed time is shown in Fig. 15b. In the central region , the pressure is practically uniform and constant, and changes in pressure occur only in the barrier ring region. The constancy of the pressure in the central region is consistent with the observation of constant film curvature in this region, reported also elsewhere[3]. Despite the small pressure gradient in the central region, changes in film thickness (that is, dimple formation) occur; hence the flow in the film in this region is controlled mainly by interface movement. This is a further confirmation of this thesis' supposition that the interface mobility should not be arbitrarily assumed.

Neither the pressure nor its gradient is equal to zero at the barrier ring. In fact, it is in the barrier ring region that changes in pressure with elapsed time occur. The increase in the negative pressure gradient with elapsed time, coupled with the decrease in the interface velocities (Fig. 15c) show why the dimple formation is accompanied simultaneously by thinning at the barrier ring. A negative pressure gradient causes the film to thin, whereas the interface movement in this case causes dimple formation; therefore, an increase in the former and a decrease in the latter will result in film thinning, as observed in the barrier ring region.

The point marked γ/b in Fig. 15b denotes the pressure in a uniform film where the pressure in the bulk phase is zero and the drop is undeformable. The calculated pressure at the centre is higher than γ/b, which is consitent with the condition for the existence of a 'pocket' and

a barrier ring suggested by Burrill and Woods[5].

The variation with elapsed time of the interface velocities and the surface concentration distributions are shown in Figs. 15c and 15d. The features of these results are the following:

(i) The decrease in the magnitude of the interface velocities with elapsed time, and the corresponding approach of the surface concentrations to uniform distributions are consistent with the observed decrease in the rate of dimple formation.

(ii) The surface concentration at the drop interface in the central region decreases with elapsed time because of the convective transfer due to the outward movement of the drop interface (that is, positive drop interface velocity). Similarly, the increase in surface concentration at the bulk interface in the central region is due to the negative bulk interface velocity.

(iii) The interface velocities at the bulk and drop interfaces are in the opposite direction. These results are in agreement with the observations of Hartland[6], who photographed the motion of tracer particles in the film, in the bulk phase and inside the drop.

(iv) The change in direction of the interface velocity in the film periphery at θ=1.215 sec can be explained in terms of the surface concentration distribution. Th initial outward movement of the drop interface causes the surface concentration in the film periphery to be less than that outside the film, as shown in Fig. 15d. As a result, the interfacial tension at the drop interface in the film periphery will be higher than that outside the film. This will cause the drop interface to move from the outside of the film to the film periphery; hence the interface velo-

city is negative. The explanation of the behaviour at the bulk interface is similar to that at the drop interface.

The results in Figs. 15a to 15d show that the calculated values of the radial velocity, the pressure, the interface velocities and the surface concentration distributions are consistent with experimental observations and the values expected from qualitative physical arguments. This can be interpreted as a further confirmation of the polynomial model.

Similar calculations as those used in Figs. 15a to 15d have been carried out at the instant the dimple formation is arrested. The results shown in Figs. 16a and 16b were obtained using the experimental film thickness profile and zero rate of thinning everywhere in the film. (The use of zero rate of thinning everywhere in the film was not strictly correct because thinning always occurred in the barrier ring region. This assumption was used to simplify the calculations. The consequence of this is seen later in the calculated values of the interface velocities.)

The interface velocities are low, and the surface concentration distributions are practically uniform, as shown in Fig. 16b. However, the fluid in the film is not stagnant, as shown in Fig. 16a: there are inward and outward flows which are exactly balanced. This is expected because of the negative pressure gradient that exists in the film; therefore, to maintain zero rate of thinning, the interfaces must move to balance the outward flow due to the negative pressure gradient.

The increase in the magnitude of the interface velocities in the barrier ring is the consequence of the incorrect use of zero rate of thinning in this region. Because the pressure gradient is relatively large in this region, the interface velocities must also be large to maintain

the imposed condition of zero rate of thinning. In the actual case, since thinning occurred in the barrier ring region, there might not be any increase in the magnitude of the interface velocities in this region.

The estimation of the surfactant physical properties and the surface concentrations $k^*\Gamma_{s1}$ and ϕ_7

The results in Figs. 11 to 14 show that for the purpose of determining whether the polynomial model is capable of describing film thinning observations, it is not critical to obtain accurate values for the surface diffusion coefficient $\mathcal{D}$, the rate constant for adsorption k_3, the surface concentrations $k^*\Gamma_{s1}$ and ϕ_7, and the parameter β. Nevertheless, the estimates used must be reasonable and within the expected values.

The method for estimating k_3 has already been described in Chapter 2.4.4. The estimate used for $\mathcal{D}$ was between the values for myristic acid, 3×10^{-5} to 30×10^{-5} cm^2/sec [7] and for a complex protein, 0.1×10^{-5} cm^2/sec [9] at an air/water interface. The estimate for β used corresponded to radial locations - where the interfaces were not influenced by the flow in the film - that were approximately equal to the drop radius. The value of β used in the thinning shown in Figs. 7a and 10, $\beta=1.5$, was smaller than that used in the dimple formation in Figs. 6 to 9, $\beta=2$, because of the smaller magnitude of the rate of thinning.

To estimate the values of $k^*\Gamma_{s1}$ and ϕ_7 the concentration of the unremoved contaminants in the coalescence cell must be known. Unless this concentration is known, $k^*\Gamma_{s1}$ and ϕ_7 can be obtained only by directly measuring the interfacial tensions of the bulk and drop interfaces in the cell. This requires a technique which would not interfere with the film thickness measurements. Until such a technique is developed, the estima-

tion of $k^* \Gamma_{s1}$ and ϕ_7 will always involve a speculation as to the concentration of the unremoved contaminants in the cell. For reasons to be discussed later, the estimation of this contaminant concentration based on experimental evidence so far available yields inconclusive results.

The values for $k^* \Gamma_{s1}$ and ϕ_7 shown in Table Ic were estimates which yielded film thickness predictions that agreed well with those experimentally observed. These estimates were surprisingly not unreasonable. The lowering of interfacial tension caused by the contaminants was $\sim$ 0.2 dn/cm for the present experiment, and for the 'cleaner' experiment of Hodgson and Woods[3], 0.1 dn/cm. The variation of Γ_s with interface age was approximately proportional to $t^{0.4}$ (cf. the Ward-Tordai equation[11], which overestimates Γ_s, with a proportionality of $t^{0.5}$).

The experimental evidence showing the existence of contaminants in the coalescence cell was given by the observed variation of rest time with bulk interface age even though no surfactant was deliberately added[3,4,8]. This variation is shown schematically in Fig. 17. There are two critical interface ages: t_c, when instantaneous coalescence no longer occurs, and t_a, when no further interface aging effect is observed. The value of t_a could be as high as 20 minutes.

Let us now consider whether it is possible to obtain an estimate of the contaminant concentration based on Fig. 17. Ward[10] showed that the bulk surfactant concentration was related to the time taken for the interface to age sufficiently. He measured the variation of γ of hexane/water with interface age for different bulk concentrations of palmitic acid. The results are shown schematically in Fig. 18: the equilibrium interfacial tension γ_e is reached after a finite time t_e which

increases with increasing bulk surfactant concentration. Therefore, t_e is an indirect measure of the bulk surfactant concentration. Some values of t_e were: for $c=10^{-2}$ M, $t_e = 30$ sec and $\gamma_o - \gamma_e = 9$ dn/cm; and for $c=4\times10^{-2}$ M, $t_e=20$ min and $\gamma_o - \gamma_e = 18$ dn/cm.

The results of Ward confirm the suggestion that the observed interface aging effect on rest time was due to contaminants because the deliberately added surfactant should be adsorbed to the interface almost instantaneously because of its low concentration.

The large value of t_a in Fig. 17 suggests at first that the contaminant concentration in the coalesecence cell is very large. However, this suggestion is not consistent with the thorough cleaning and purification procedures that have been used. Furthermore, the effect of the deliberately added surfactant would not have been noticeable. (The curve shown in Fig. 17 is shifted to the left with increasing bulk concentration of the deliberately added surfacatnt.) A plausible explanation of this discrepancy is that the bulk diffusivity of the contaminants is very low; this would cause a large value of t_e despite the low contaminant concentration (cf. the Ward-Tordai equation[11]).

If the contaminants have a low bulk diffusivity, they may be composed of large molecules. This means that their effect on an interface will be different from that of a smaller sized surfactant. For example, the ideal surface equation of state may not apply even at low concentrations. Moreover, these contaminants may affect the surface viscosity such that the apparent lowering of interfacial tension for a flow system is different from that for a stationary system; therefore, it may not be appropriate to use a static experiment, such as the pendant drop method, to

obtain estimates for the values of $k^* \Gamma_{s1}$ and ϕ_7.

There is a further complication in attempting to estimate the contaminant concentration from Fig. 17. The value of t_a varied - from 6 to 20 min with no apparent trends - with different bulk concentrations of the deliberately added surfactant ranging from zero to 10^{-5} M[4]. This variation might be caused by the variation in the contaminant concentration and/or interaction between the surfactant and the contaminants. Whatever the cause might be, it appears that the surface concentration Γ_s in the coalescence cell is not simply related to the bulk concentration of the deliberately added surfactant.

The preceding discussion shows the difficulties in obtaining estimates for $k^* \Gamma_{s1}$ and ϕ_7 and establishing a sound quantitative method for relating these estimates to the bulk concentration of the deliberately added surfactant.

The role of a film thinning model in the prediction of rest times

To predict the rest time for a given system - liquids, drop size, surfactant and its concentration - one must be able to determine the rate of film thinning and the critical film thickness at rupture. Because the subject of film rupture is beyond the scope of this thesis, this discussion is restricted to cases in which the critical thickness can be assumed constant. Therefore, the rest time prediction requires only the calculation of the rate of thinning.

One of the difficulties in predicting the rate of thinning for a given system lies in the dependence of the rate of thinning on the type of film thinning behaviour. A film thinning model, such as the polynomial model, can only describe the rate of thinning after the film is formed.

Although the time taken to form the film is in general negligible compared to the total coalescence time, this does not mean that the manner by which the film is formed can be neglected; how the film is formed determines the subsequent film thinning behaviour. This is shown mathematically by the need to specify the initial rate of thinning as well as the initial film thickness profile in the solution of a film thinning model.

The initial film thickness profile and rate of thinning, which reflect the manner by which the film is formed, are dependent on the system physical properties. This dependence need not be known provided these initial values can be measured experimentally. However, for an a priori prediction of the rate of thinning, these initial values must be calculated from the system physical properties because by definition, an a priori prediction requires no other experimental measurements but the system physical properties.

It is therefore important to recognize the scope of a film thinning model. The model is useful for explaining why certain behaviour occurs, thereby increasing our understanding of film thinning behaviour; however, it cannot be used to predict rest times unless the initial film thickness profile and rate of thinning can be calculated a priori from the system physical properties.

Consider now the use of a simple model for predicting rest times. A simple model is one that gives the rate of thinning in an algebraic form in terms of the system physical properties. The application of a simple model is restricted only to one type of film thinning behaviour, as shown by the model of Hodgson and Woods[3] and the extended parallel disc model developed in Chapter 5. This restriction has a fundamental basis, namely

a simple model should be applied only to films that are formed in the same manner, as shown by the same type of film thinning behaviour.

The application of a simple model for predicting rest times is more practical compared to that of a fundamental model: the rate of thinning equation is simpler, and it gives rest time predictions based only on the system physical properties. This simple model must, however, be applied only to one type of film thinning behaviour.

4.4. Summary and conclusions

1. The film thinning equations developed in Chapter 2 have been solved numerically based on a polynomial representation of the pressure in the film, and the results compared with experimental observations of the film thinning behaviour of toluene and anisole drops. The model is referred to as the polynomial model.

2. The polynomial model satisfactorily described the variation in film thickness profile with elapsed time for all types of symmetrical film thinning behaviour including dimple formation and thinning. In most locations in the film, the model predictions agreed within 10 to 20 %, except in the barrier ring region, where the film was thin, the error could be as high as 70 %.

3. The predicted effect of the surfactant physical properties and k_3, and the surface concentrations $k^* \Gamma_{s1}$ and ϕ_7 agreed with that expected from physical arguments. The rate of dimple formation (and hence the interface mobility) was shown to decrease with increasing β, k_3, $k^* \Gamma_{s1}$ and ϕ_7.

4. The agreement between the model predictions and experimental observations confirms this thesis' supposition that the interface mobility

must not be arbitrarily assumed.

5. The calculation of the film thinning variables shows that:

(i) The pressure in the film remains practically constant and uniform in the central region, and falls rapidly in the barrier ring region; at the barrier ring, neither the pressure nor its gradient is equal to zero.

(ii) Thinning occurs in the barrier ring region during dimple formation because of the increase in the negative pressure gradient with elapsed time and the decrease in the rate of dimple formation.

(iii) When dimple formation is arrested, the fluid in the film is not stagnant; there are inward and outward flows which are exactly balanced.

Literature cited

1. Box, M. J. et al "Non-linear optimization techniques" I.C.I. Monograph No. 5, Oliver&Boyd, Edinburgh(1969).

2. James, M. L. "Applied numerical methods for digital computation with Fortran" Int.Textbook, Pa. (1967):326.

3. Hodgson, T. D. and Woods, D. R., J.Coll.Intf.Sci., 30(1969):429.

4. Burrill, K. A. and Woods, D. R., J.Coll.Intf.Sci., 42(1973):35

5. Ibid:15.

6. Hartland, S., Chem.Engng.Sci., 24(1969):611.

7. Sakata, E. K. and Berg, J. C., I&EC Fund., 8(1969):570.

8. Hodgson, T. D. and Lee, J. C., J.Coll.Intf.Sci., 30(1969):94.

9. Imahori, K., Bull.Chem.Soc.Japan, 25(1952):13.

10. Ward, A. F. H. in "Surface chemistry" Papers presented at a joint meeting of Societe Chimie Physique andthe Faraday Society (1947) Butterworths, London (1949):55.

11. Ward, A. F. H. and Tordai, L., J.Chem.Phys., 14(1946):453.

Table Ia. The systems used for testing the polynomial model

I	II	III	IV	V	VI
Toluene	0.0025	Palmitic acid	10^{-6}	110	Fig. 6
Toluene	0.0025	Palmitic acid	10^{-6}	600	Figs. 7, 7a
Toluene	0.0025	Palmitic acid	10^{-5}	90	Fig. 8
Toluene	0.004	Palmitic acid	0	60	Fig. 9
Anisole*	0.005	Sodium lauryl sulphate	10^{-6}	600	Fig. 10

Legend

I Oil

II Drop size, ml

III Surfactant

IV Bulk surfactant concentration, M

V Bulk interface age, sec

VI Results

* Hodgson and Woods[3], Fig. 10a

Table Ib. The liquid/liquid physical properties

	Interfacial tension	Density difference
	dn / cm	gm / ml
Toluene/Water	33.5	0.133
Anisole/Water *	20.5	0.0097

* Burrill[12], p. 428; see also Appendix D.4.

Table Ic. The surfactant physical properties, surface concentrations and model parameter β used in the film thinning predictions

- Surface diffusion coefficient, $\mathcal{D}$ = 0.8×10^{-5} cm^2/sec
- Adsorption rate constant, k_3 = 0.5 sec^{-1}
- Model parameter, β = 2, for Figs. 6 to 9; and β = 1.5 for Figs. 7a and 10

	$k^* \Gamma_{s1}$	Φ_7
	dn/cm	—
Fig. 6	0.275	0.40
Fig. 7, 7a	0.275	0.60
Figs. 8	0.325	0.35
Fig. 9	0.225	0.45
Fig. 10	0.10	0.15

Figure captions

1. Outline of the calculation (at the initial time) of pressure, interface velocities and surfactant concentration distributions from the data on film thickness profile and rate of thinning. The numbered (i) triangles are the sections in this chapter and Appendix D, in which the calculation is carried out, (ii) solid circles show that the results obtained in the corresponding sections are needed in the calculation, and (iii) broken circles show that the values of the variables have already been calculated or can be readily calculated from the corresponding sections.

2. The effect of different number of terms in the pressure polynomial on the accuracy of the film thickness fitting. The value of N=8 corresponds to a 5-term polynomial since only even terms are used.

3. Typical convergence of the repetitive substitution method for calculating U_1. In the diagram, the first assumption is zero velocity every where in the film.

4. Flow chart of the solution of the film thinning equations after the initial conditions have been calculated.

5. Schematic diagram of the minimization method used to calculate the rate of thinning at $\theta + \Delta\theta$. The diagram shows the method for two variables.

6 to 10. Comparison of the model predictions with the data. The film thickness profile at $\theta = 0$ is a curve fit of the data, and the subsequent profiles are the polynomial model predictions.

11. The effect of surface diffusivity β and the adsorption constant k_3 on the solution of the polynomial model. The initial film thickness profile and rate of thinning used are those for the dimple formation shown in Fig. 6.

12 to 14. The effect of surface concentrations $k^* \Gamma_{s1}$ and ϕ_7, and parameter β (cf. Eq. D-31) on the solution of the polynomial model for the dimple formation shown in Fig. 6.

15. The film thinning variables for the dimple formation shown in Fig. 6. : (a) The radial velocity profile at $\theta = 0$, showing that the inward flow is larger than the outward flow for dimple formation.

(b) Variation of pressure in the film with elapsed time. The pressure is practically uniform and constant in the central region, and changes occur only in the barrier ring region. Neither the pressure nor its gradient are zero at the barrier ring. The point marked γ/b shows the pressure in a uniform film.

(c) Variation of the interface velocities with elapsed time. The interface velocities decrease with elapsed time.

(d) Variation of surface concentration distributions in the film with elapsed time. The concentrations approach uniform distributions as the dimple formation proceeds.

16. The film thinning variables at the instant dimple formation is arrested.

(a) Film thickness profile, pressure and radial velocity profile. The radial velocity profile shows that the inward and the outward flows are exactly balanced; thus the fluid in the film is not stagnant.

(b) The surface concentration distributions and interface velocities. The distributions are practically uniform and the velocities are very small. The increase in the magnitude of the interface velocity in the barrier ring region is caused by the inaccurate assumption that the rate of thinning everywhere in the film is zero. (In reality, thinning always occurs in the barrier ring region.)

17. Schematic diagram of the variation of rest time with bulk interface age[3,4,8]. The interface ages t_c and t_a are those when instantaneous coalescence no longer occurs, and when no further aging effect is observed, respectively.

18. Schematic diagram of the variation of interfacial tension with interface age and bulk surfactant concentration. The equilibrium interfacial tension is reached sooner for a smaller bulk surfactant concentration.

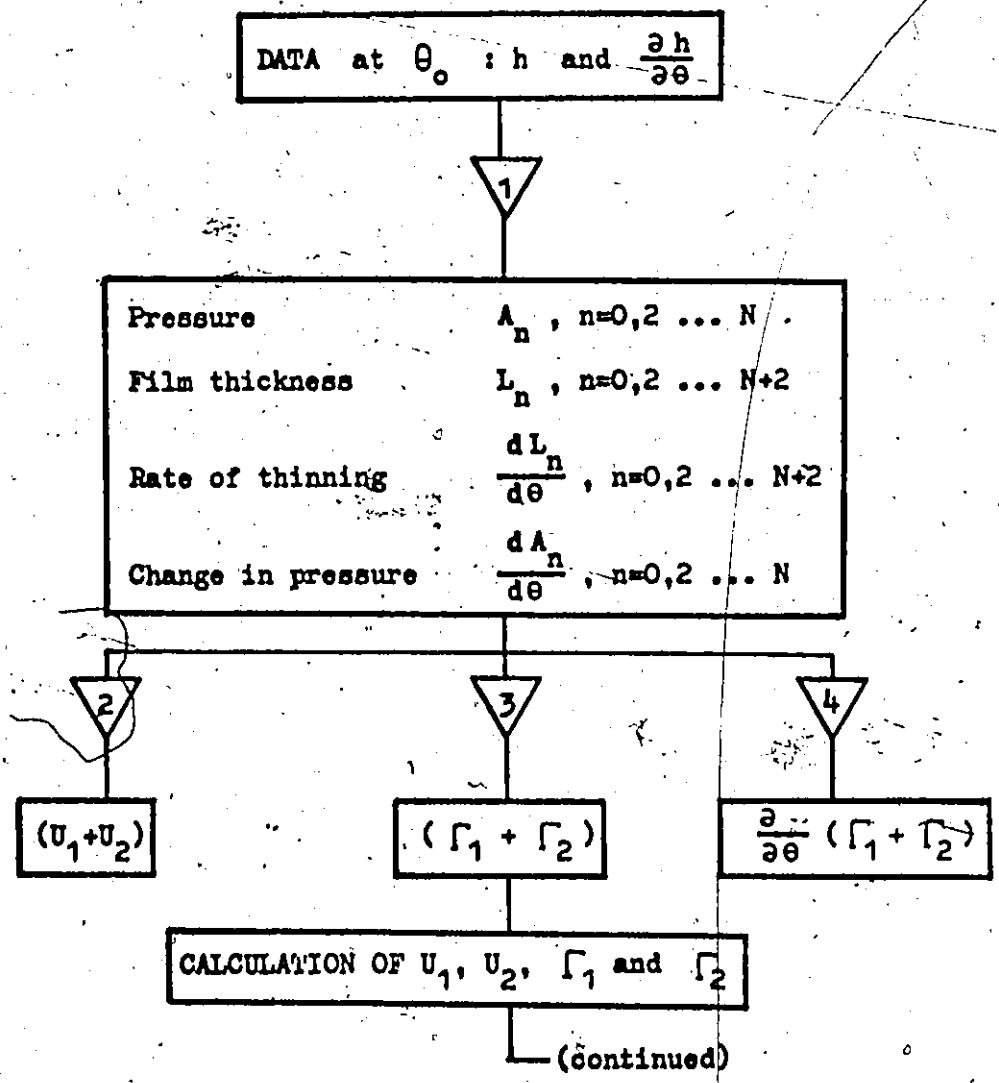

Legend - 1. Section 4.2.1 and Appendix D-1.
2. Section 4.2.2 and Appendix D- 2.2.
3. Section 4.2.2.2 and Appendix D-2.1, D-2.3.1, D-2.3.2 and D-2.3.3.
4. Section 4.2.2.3 and Appendix D-2.1, D-2.3.1, D-2.3.2, D-2.3.3 and D-2.3.4.
5. Appendix D-2.1, D-2.3.1, D-2.3.2, D-2.3.3 and D-2.3.5.
6. Appendix D-2.4.

Figure 1

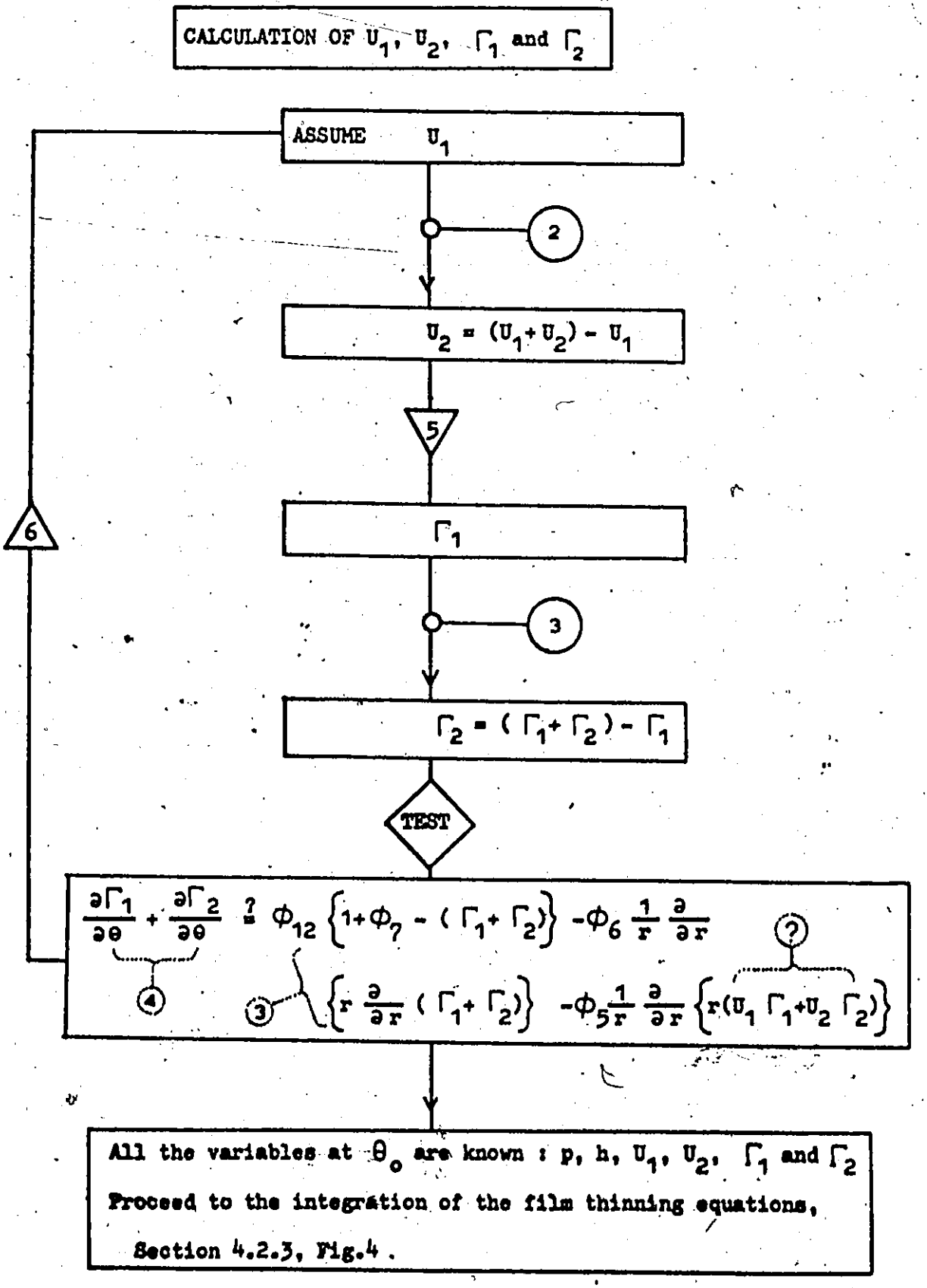

Figure 1 (continued)

Figure 2

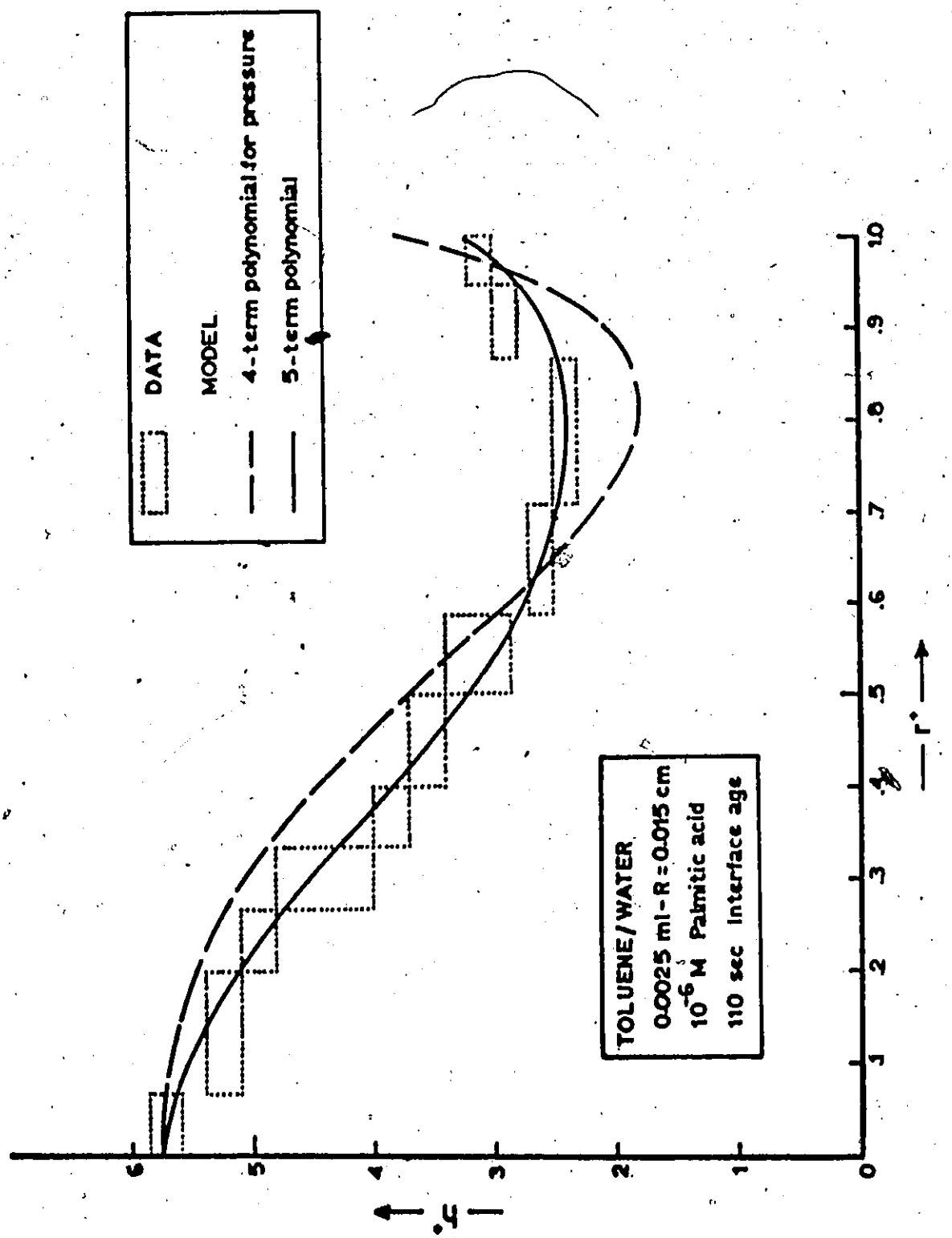
DATA
MODEL
4-term polynomial for pressure
5-term polynomial
TOLUENE/WATER
0.0025 ml-R = 0.015 cm
10^{-6} M Palmitic acid
110 sec Interface age
— r' —
— P —
0
1
2
3
4
5
6
.1
.2
.3
.4
.5
.6
.7
.8
.9
1.0

Figure 3

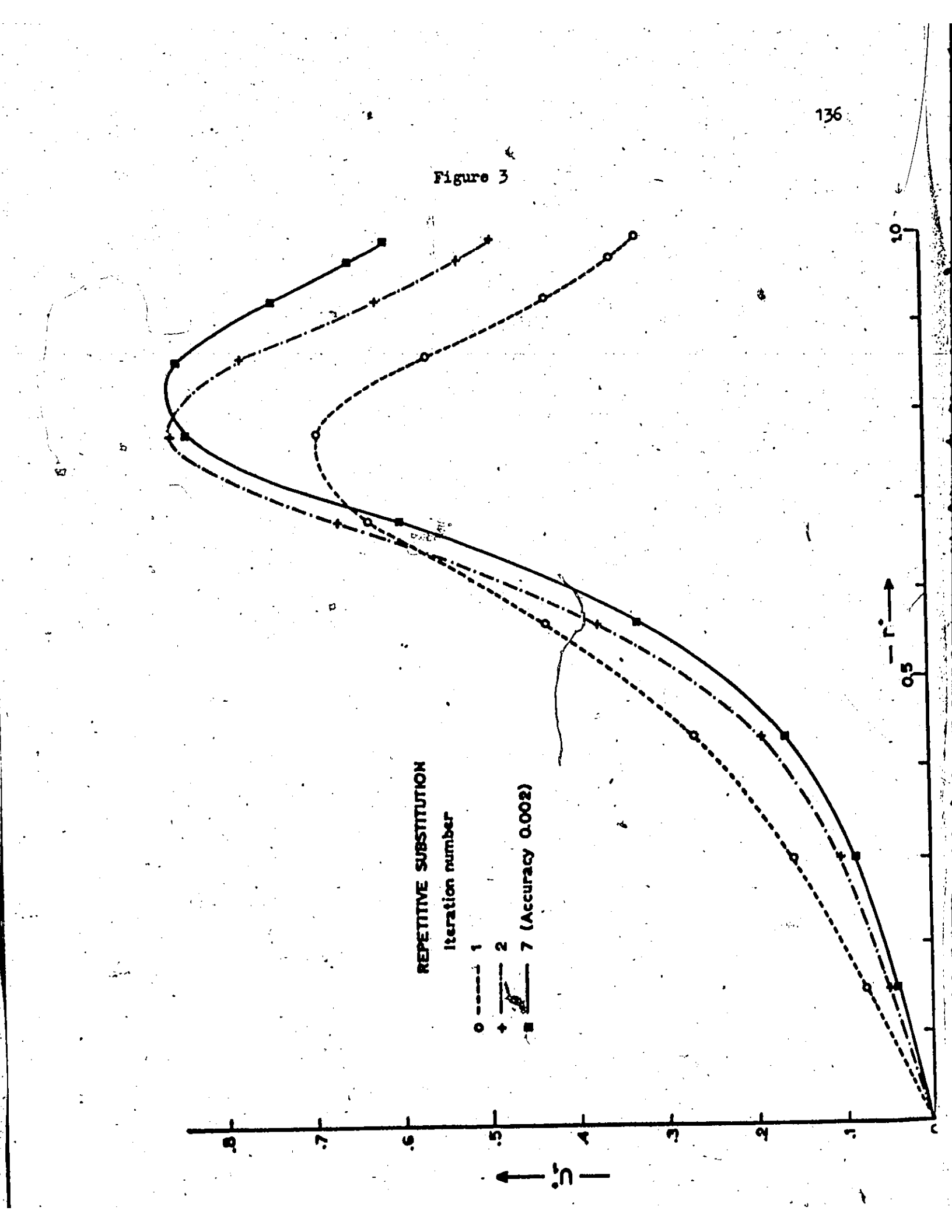
REPETITIVE SUBSTITUTION
Iteration number
o 1
+ 2
■ 7 (Accuracy 0.002)
— u_i' →
— r_i' →
.8
.7
.6
.5
.4
.3
.2
.1
0
0.5
1.0

Figure 4

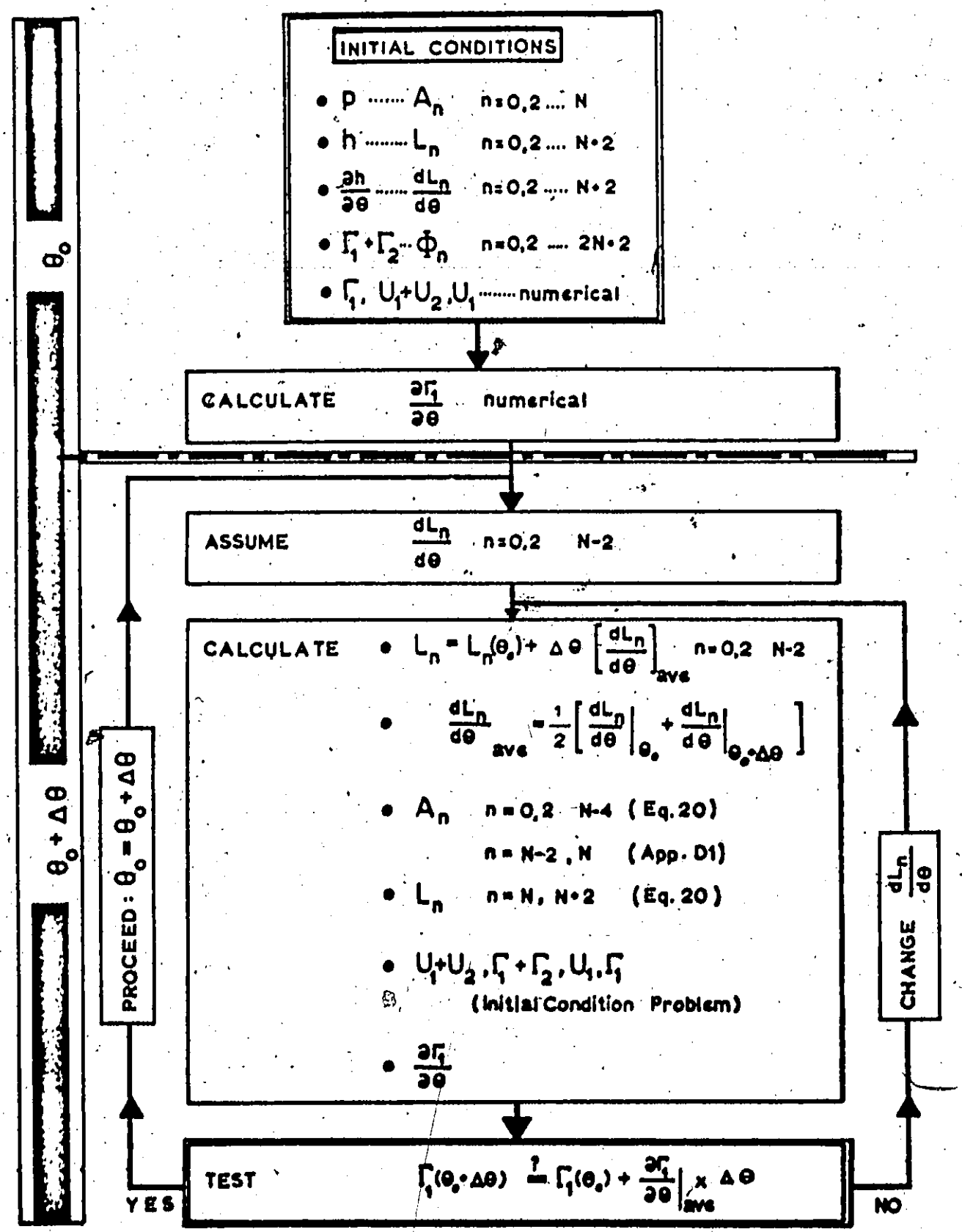
INITIAL CONDITIONS
• p ..... A_n n=0,2 .... N
• h ..... L_n n=0,2 .... N+2
• $\frac{\partial h}{\partial \theta}$ ..... $\frac{dL_n}{d\theta}$ n=0,2 .... N+2
• $\Gamma_1+\Gamma_2 \cdots \Phi_n$ n=0,2 .... 2N+2
• Γ_1, U_1+U_2, U_1 ..... numerical
CALCULATE $\frac{\partial \Gamma_1}{\partial \theta}$ numerical
ASSUME $\frac{dL_n}{d\theta}$ n=0,2 N-2
CALCULATE
• $L_n = L_n(\theta_o) + \Delta\theta \left[\frac{dL_n}{d\theta}\right]_{ave}$ n=0,2 N-2
• $\frac{dL_n}{d\theta}_{ave} = \frac{1}{2}\left[\frac{dL_n}{d\theta}\Big|_{\theta_o} + \frac{dL_n}{d\theta}\Big|_{\theta_o+\Delta\theta}\right]$
• A_n n=0,2 N-4 (Eq.20)
n=N-2, N (App. D1)
• L_n n=N, N+2 (Eq.20)
• U_1+U_2, $\Gamma_1+\Gamma_2$, U_1, Γ_1
(Initial Condition Problem)
• $\frac{\partial \Gamma_1}{\partial \theta}$
TEST $\Gamma_1(\theta_o+\Delta\theta) \stackrel{?}{=} \Gamma_1(\theta_o) + \frac{\partial \Gamma_1}{\partial \theta}\Big|_{ave} \times \Delta\theta$
YES
NO
PROCEED: $\theta_o = \theta_o + \Delta\theta$
CHANGE $\frac{dL_n}{d\theta}$
θ_o
$\theta_o + \Delta\theta$

Figure 5

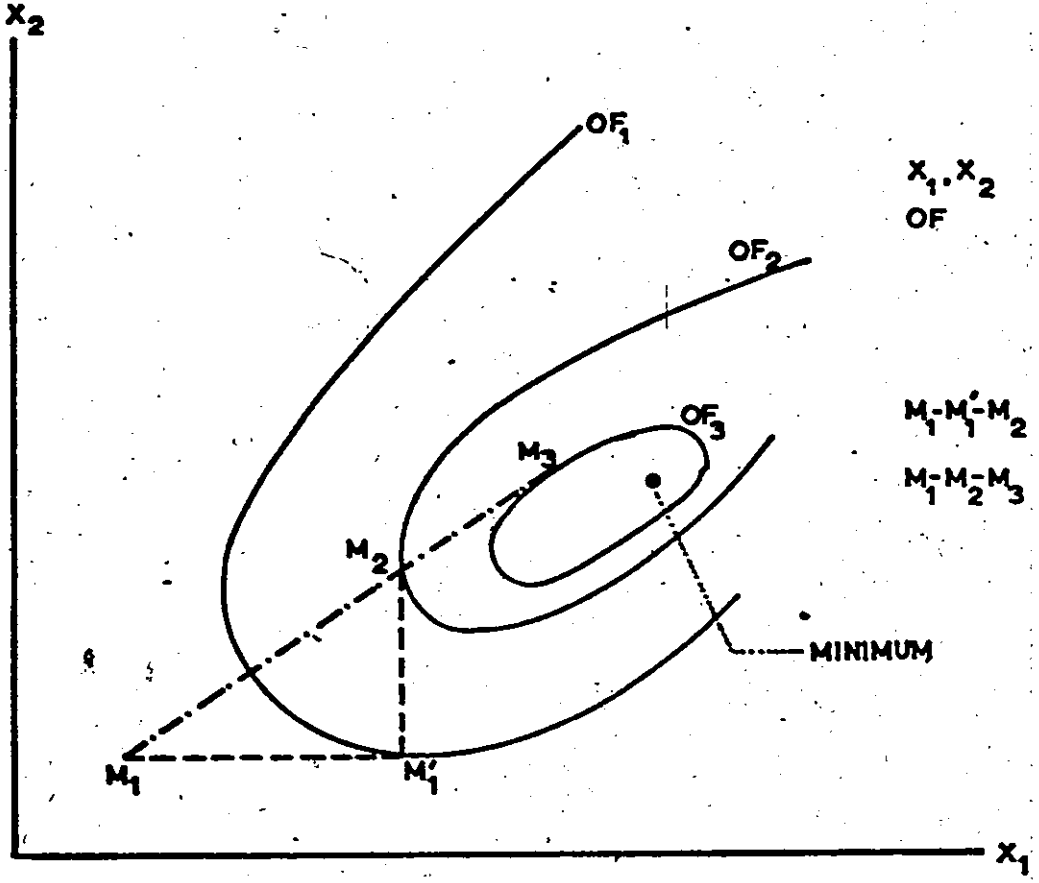

X_1, X_2 Independent variables

OF Contour of equal objective function

$OF_1 > OF_2 > OF_3$

M_1-M'_1-M_2 STAGE I

M_1-M_2-M_3 STAGE II

Figure 6

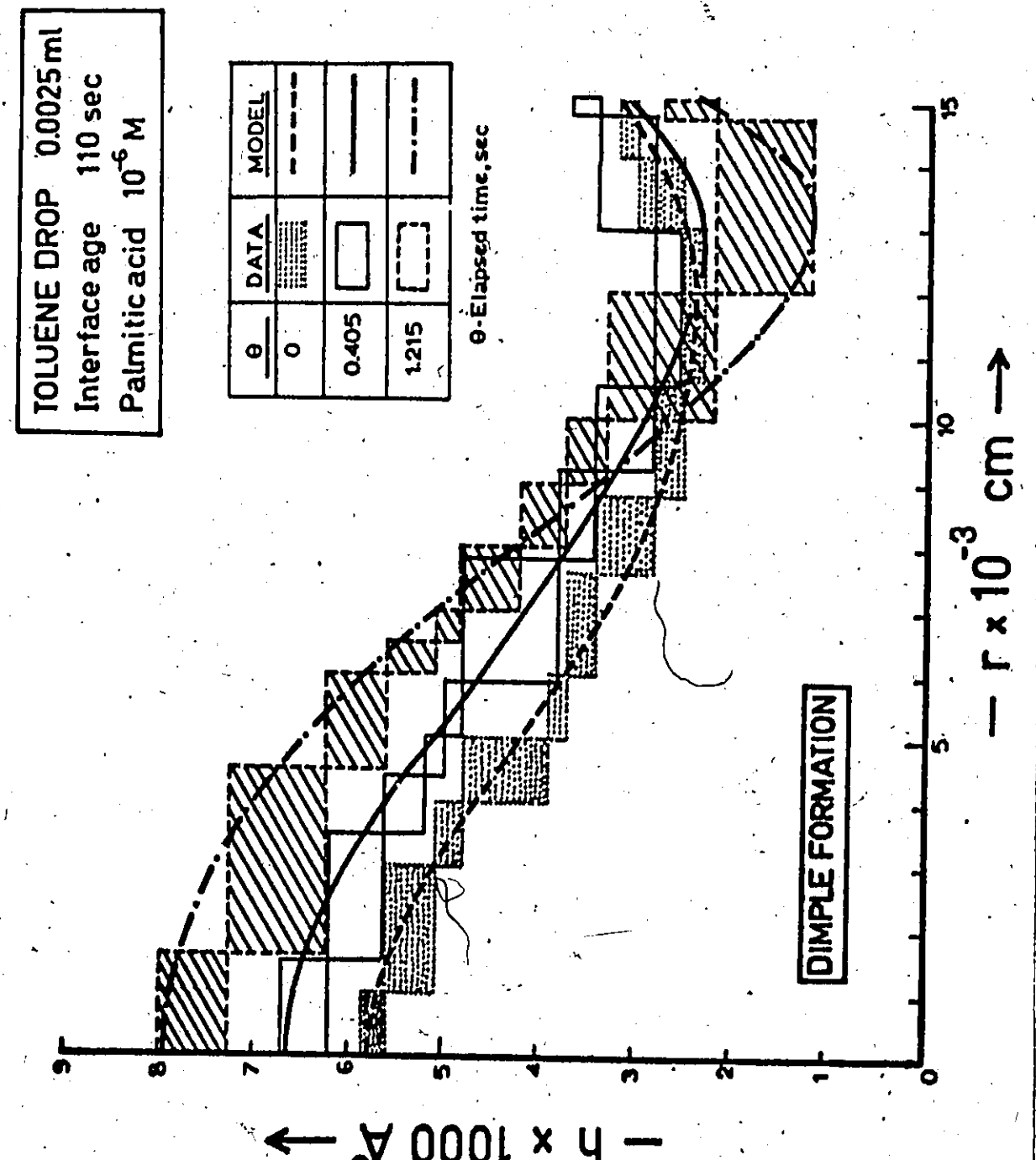
TOLUENE DROP 0.0025 ml
Interface age 110 sec
Palmitic acid 10^{-6} M
θ
DATA
MODEL
0
0.405
1.215
θ-Elapsed time, sec
DIMPLE FORMATION
— h x 1000 A° →
— r x 10^{-3} cm →

Figure 7.

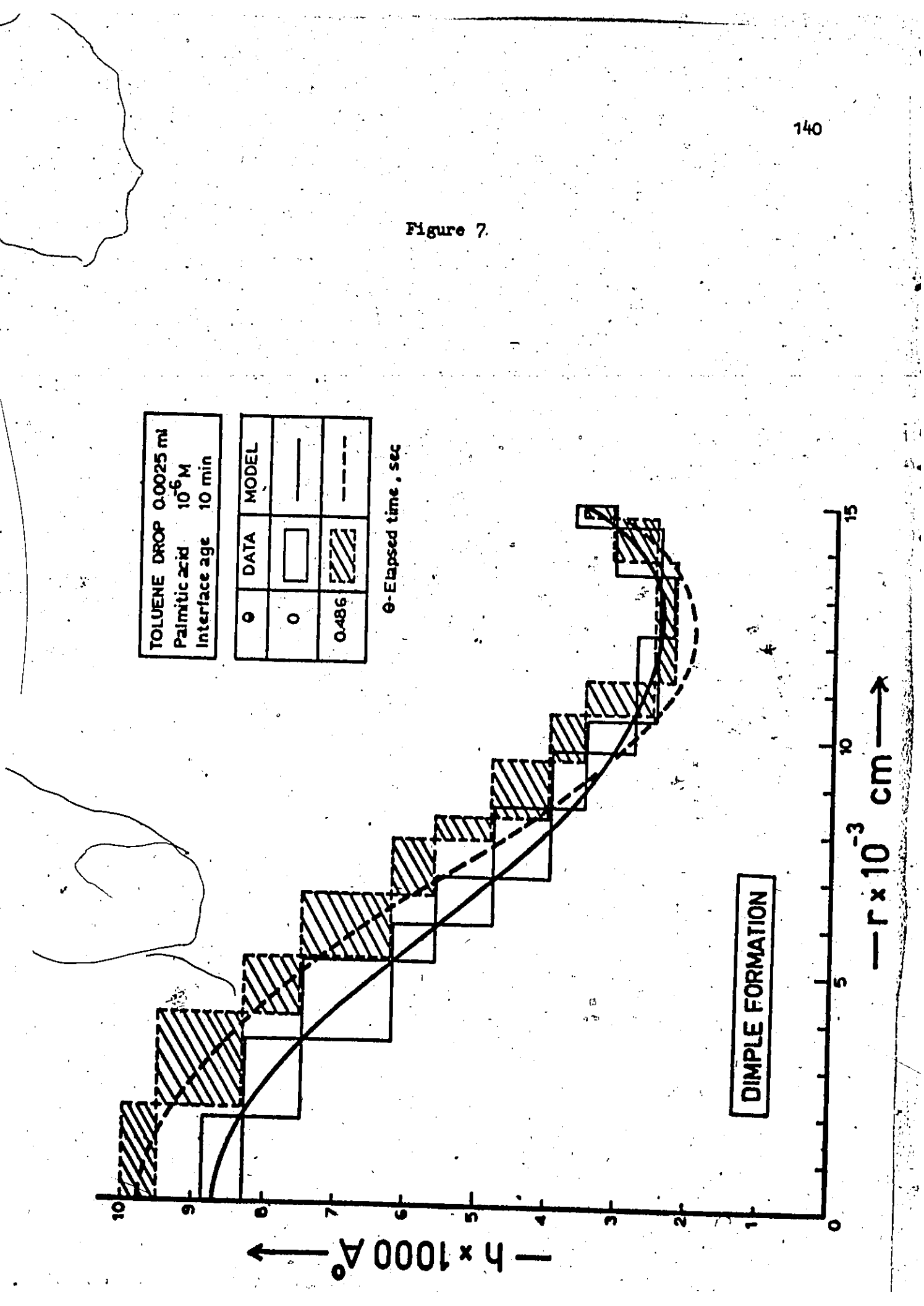
TOLUENE DROP 0.0025 ml
Palmitic acid 10^{-6} M
Interface age 10 min
θ DATA MODEL
0
0.486
θ-Elapsed time, sec
h x 1000 A°
r x 10^{-3} cm
DIMPLE FORMATION
0
1
2
3
4
5
6
7
8
9
10
5
10
15

Figure 7a

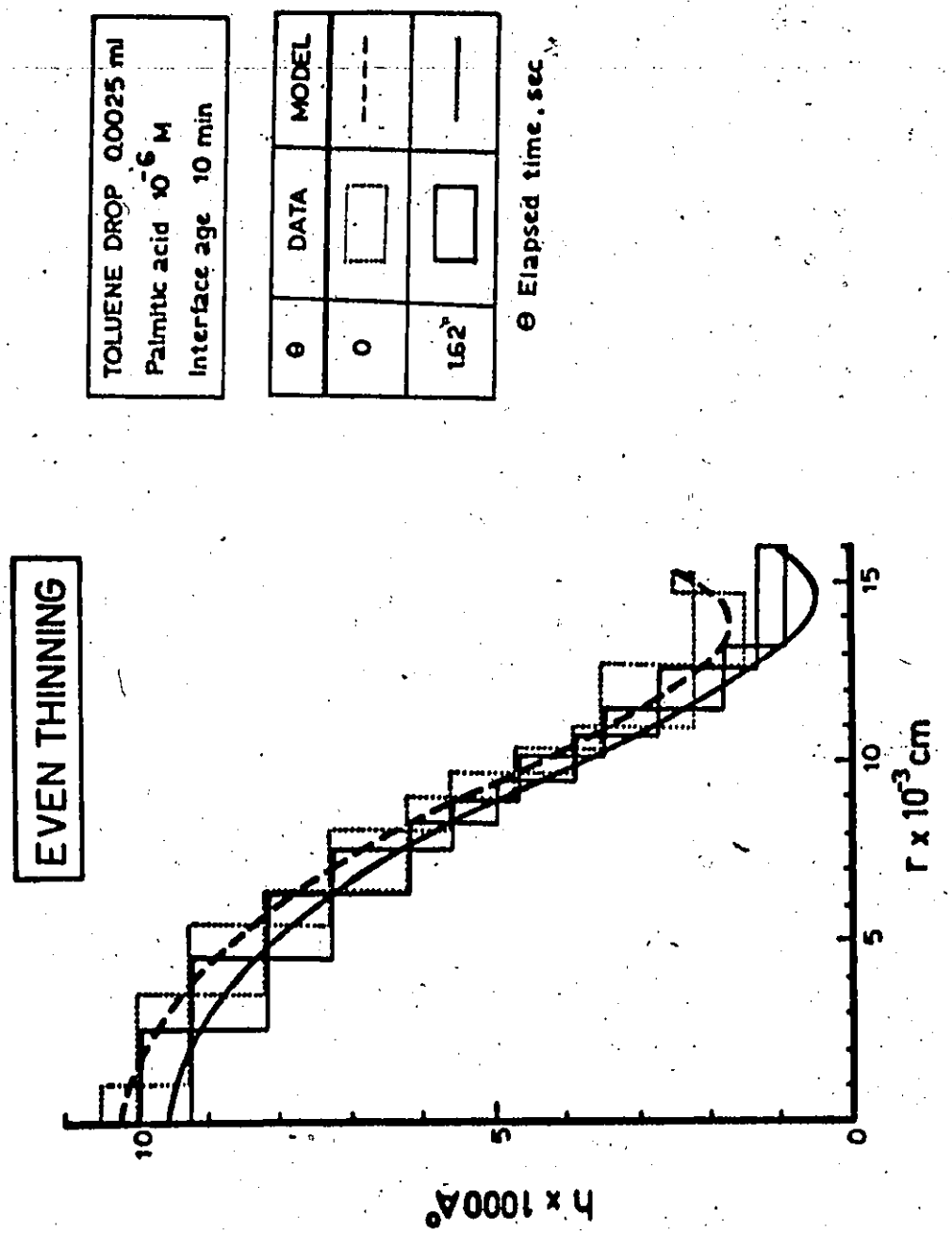
TOLUENE DROP 0.0025 ml
Palmitic acid 10^{-6} M
Interface age 10 min
θ
DATA
MODEL
0
162°
θ Elapsed time, sec
EVEN THINNING
h x 1000A°
10
5
0
15
10
5
Γ x 10^{-3} cm

Figure 8

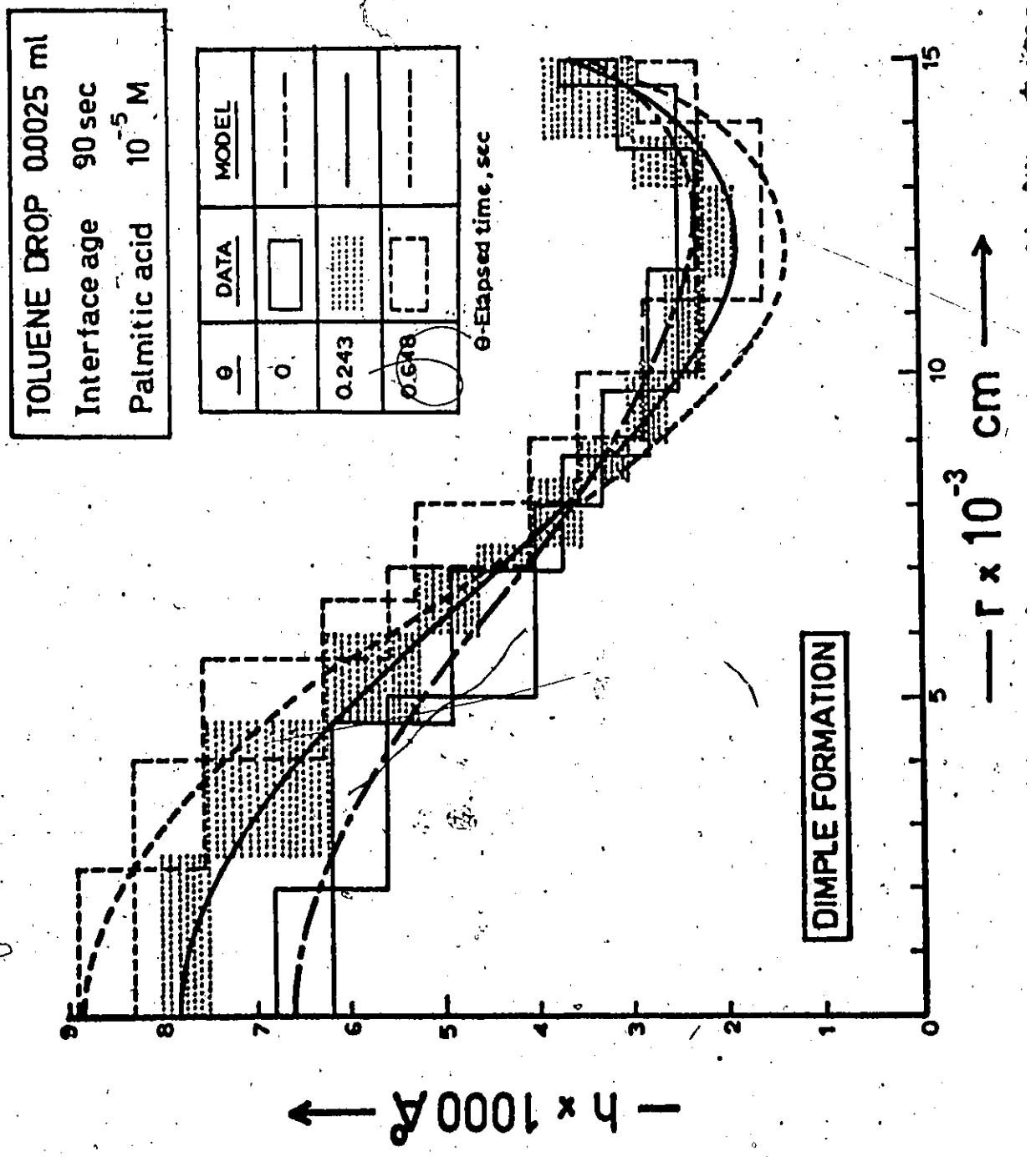
TOLUENE DROP 0.0025 ml
Interface age 90 sec
Palmitic acid 10^{-5} M
θ
DATA
MODEL
0
0.243
0.648
θ-Elapsed time, sec
DIMPLE FORMATION
h x 1000 Å
r x 10^{-3} cm

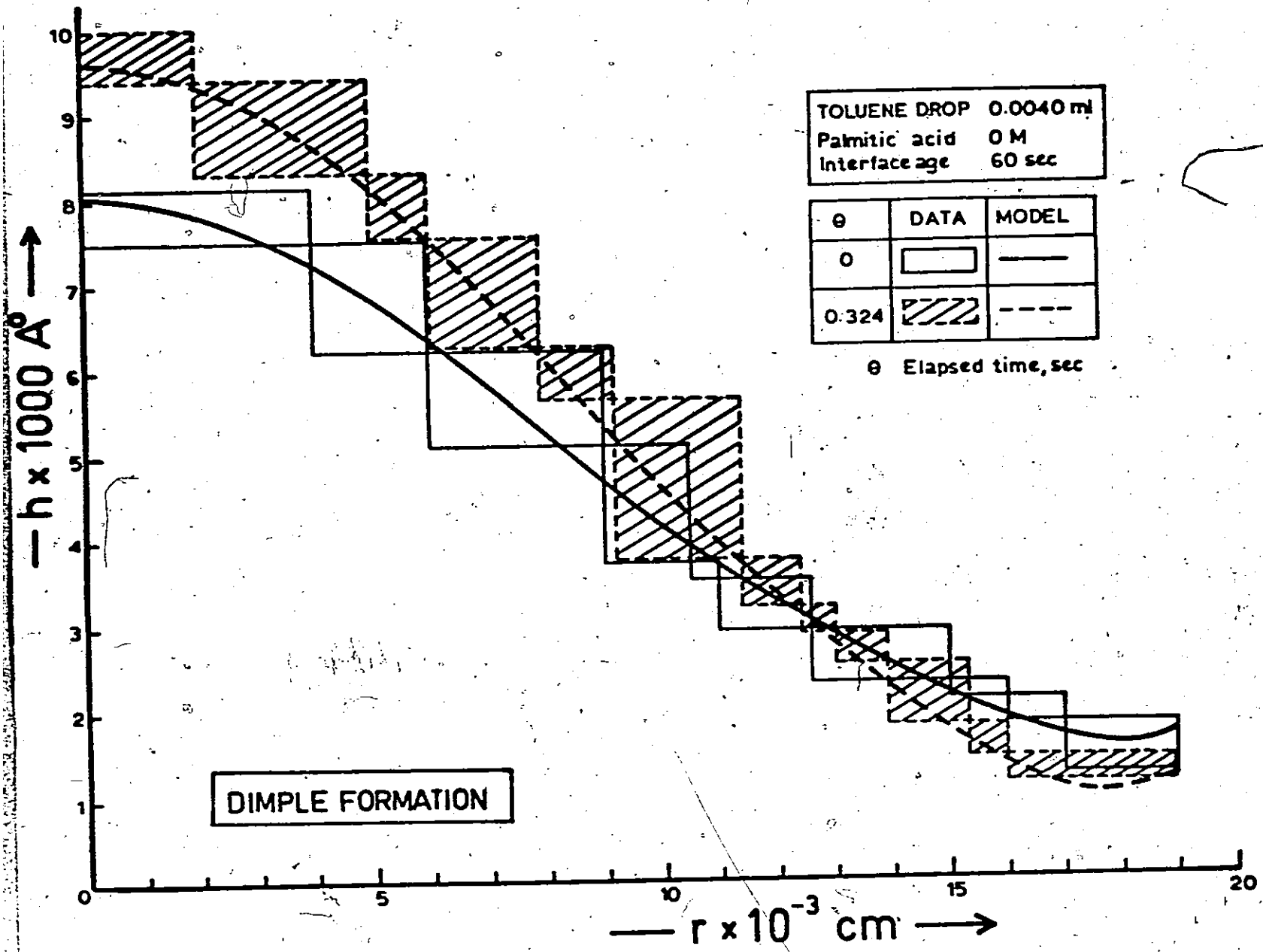
TOLUENE DROP 0.0040 ml
Palmitic acid 0 M
Interface age 60 sec
θ DATA MODEL
0
0.324
θ Elapsed time, sec
— h x 1000 A° —
— r x 10⁻³ cm —
DIMPLE FORMATION
0
5
10
15
20
1
2
3
4
5
6
7
8
9
10

Figure 9

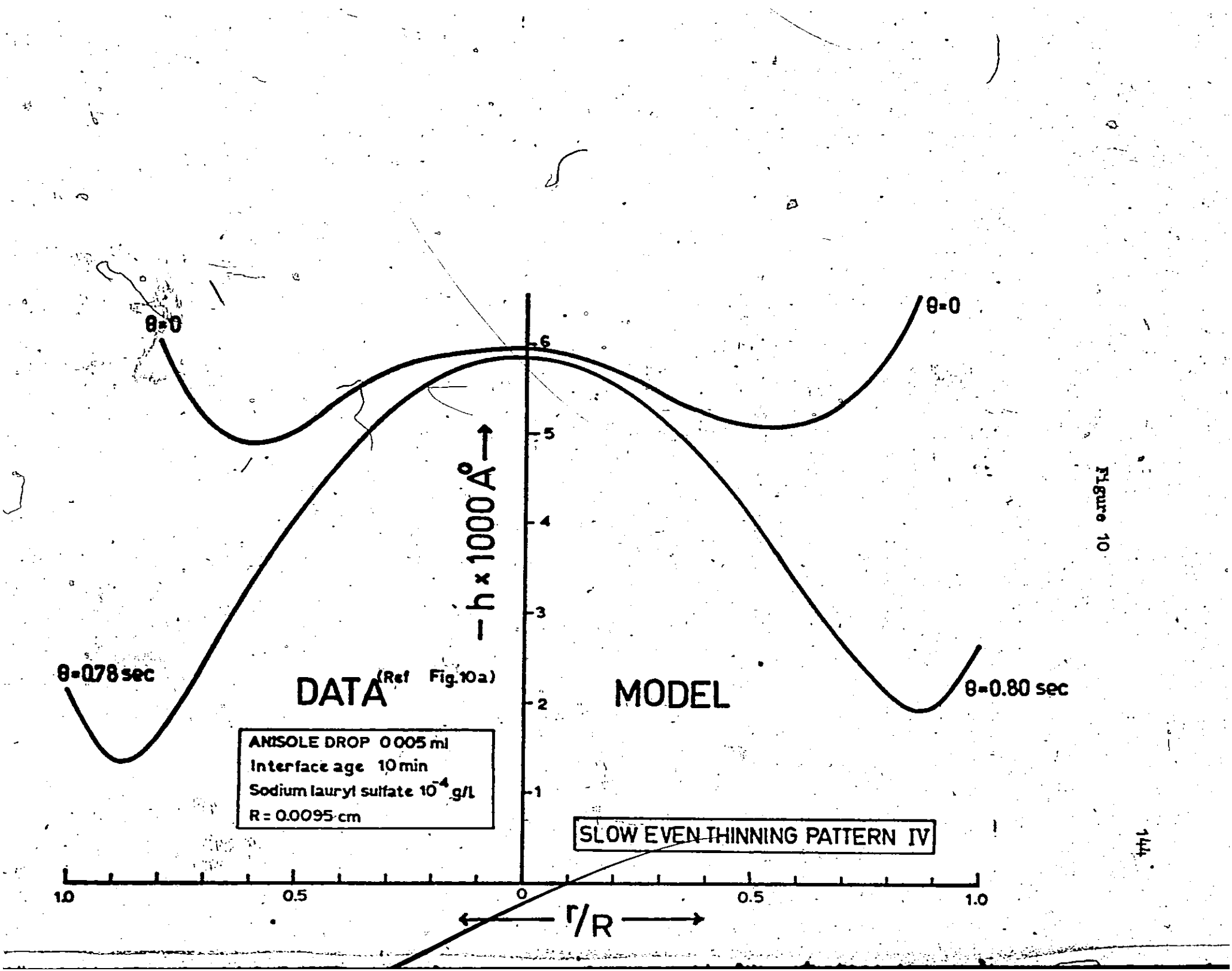
θ=0
θ=0
6
5
4
3
2
1
−h×1000 A°
θ=0.78 sec
DATA (Ref Fig.10a)
MODEL
θ=0.80 sec
ANISOLE DROP 0.005 ml
Interface age 10 min
Sodium lauryl sulfate 10^{-4} g/l
R = 0.0095 cm
SLOW EVEN THINNING PATTERN IV
1.0
0.5
0
0.5
1.0
r/R

Figure 10

Figure 11

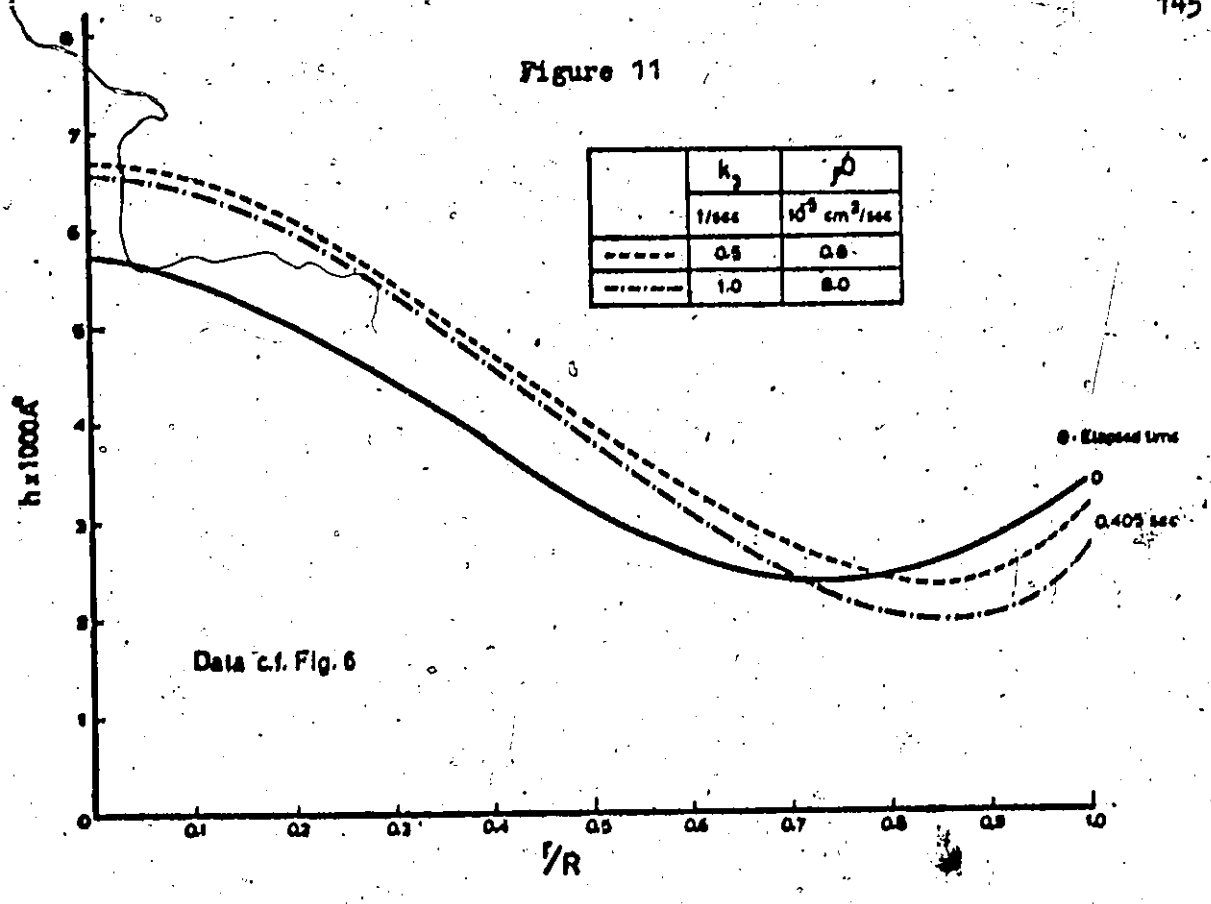

Figure 12

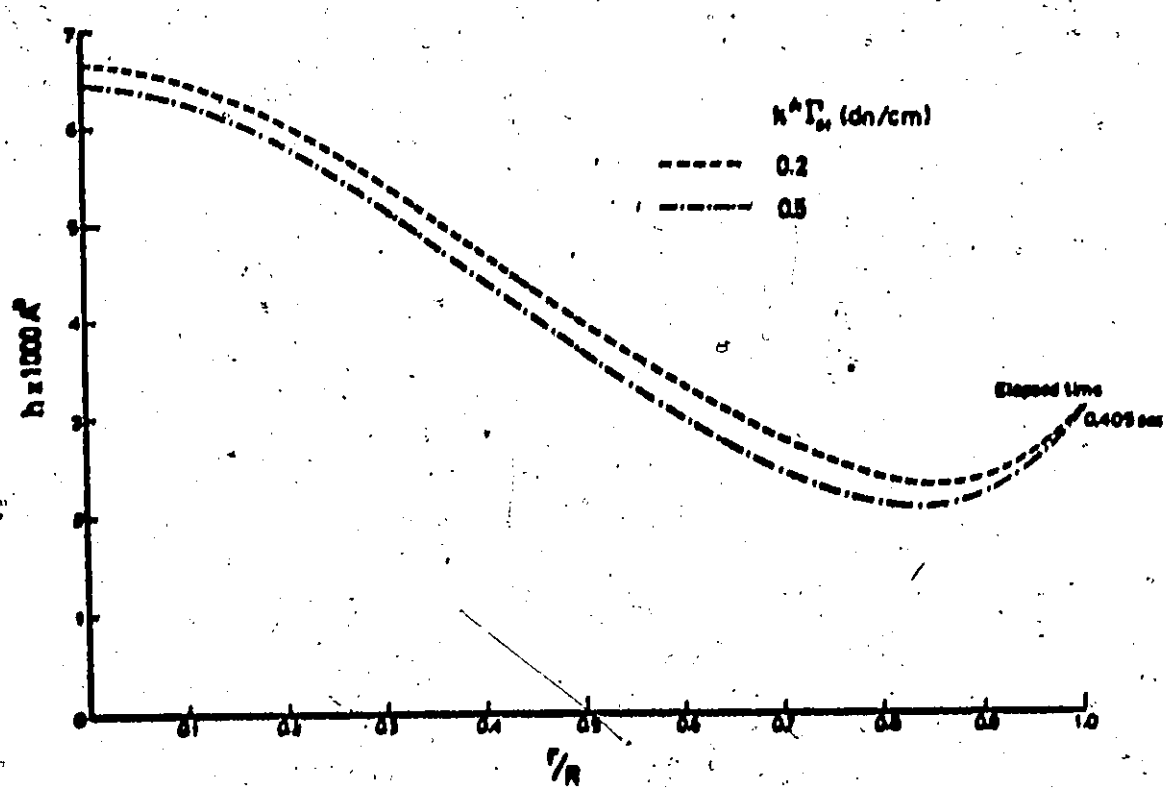

Figure 13

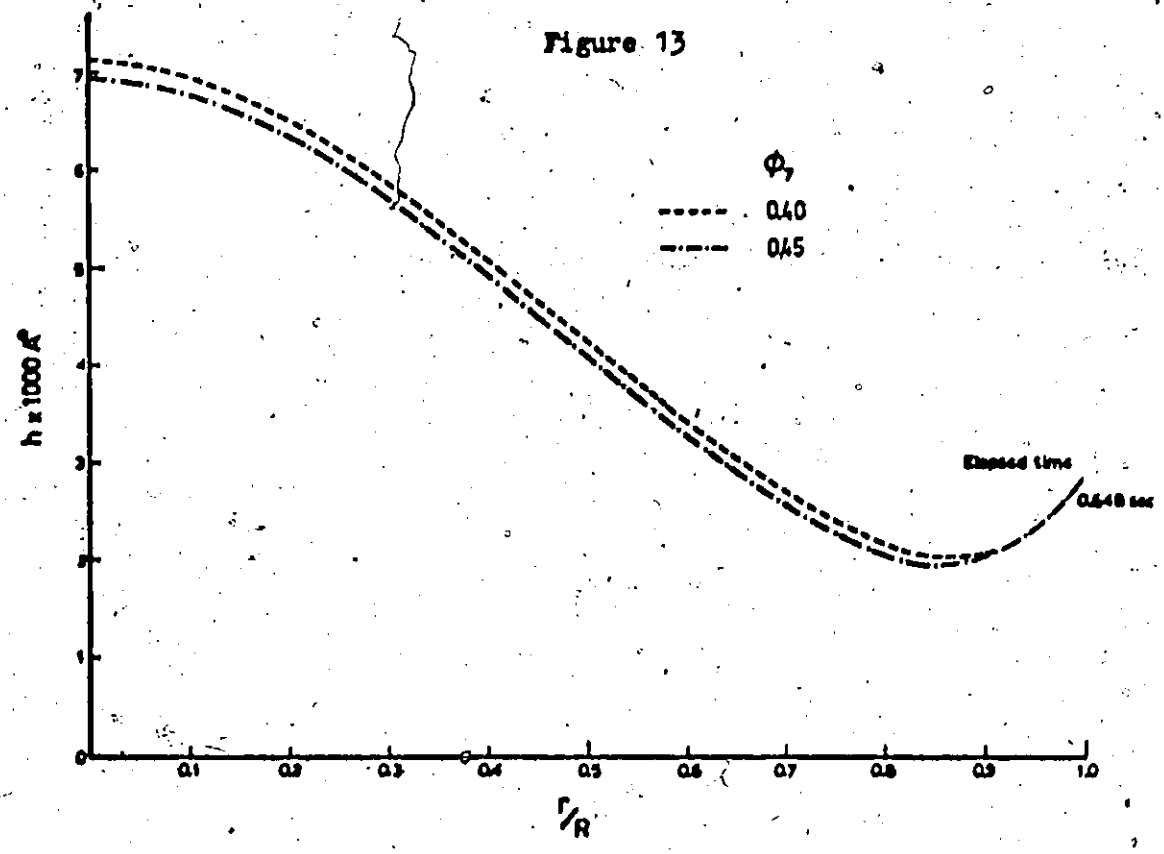

Figure 14

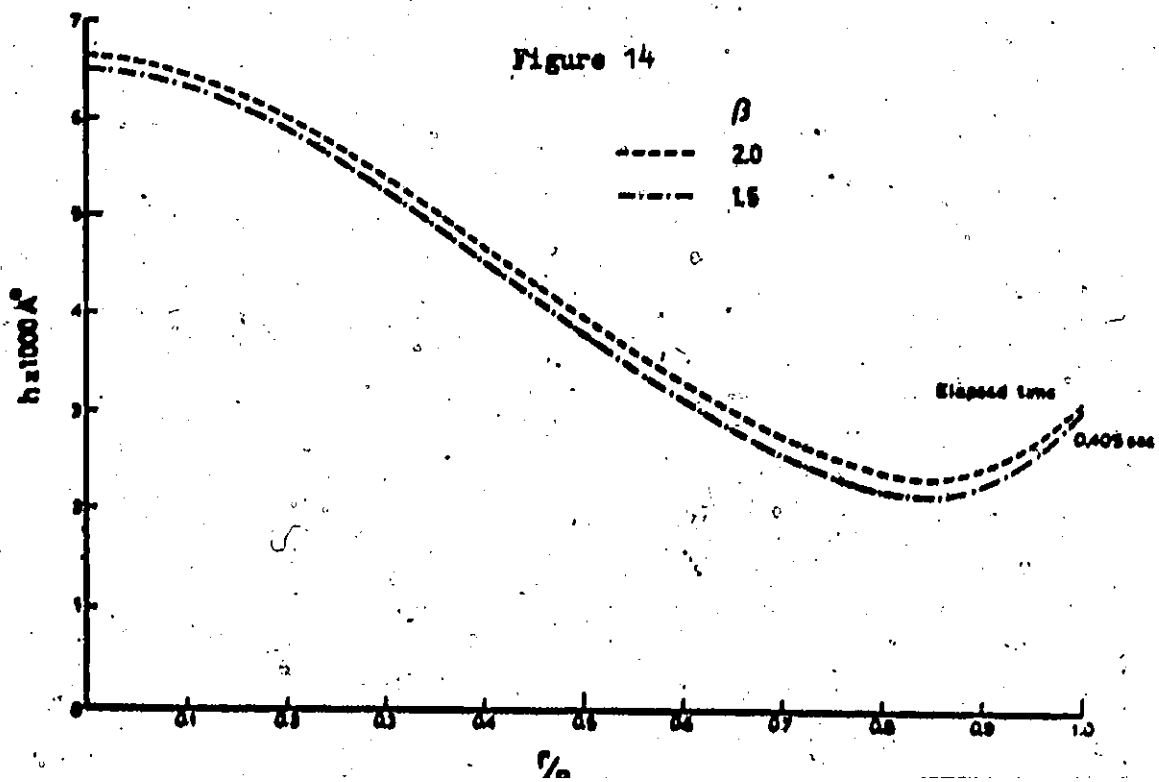

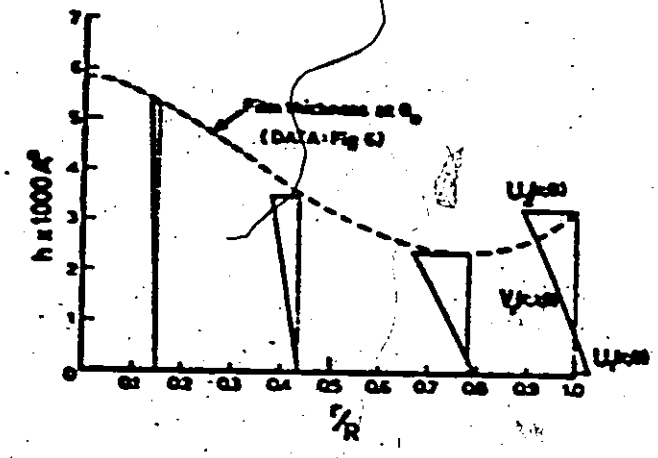

(a) Radial velocity profile at θ_2

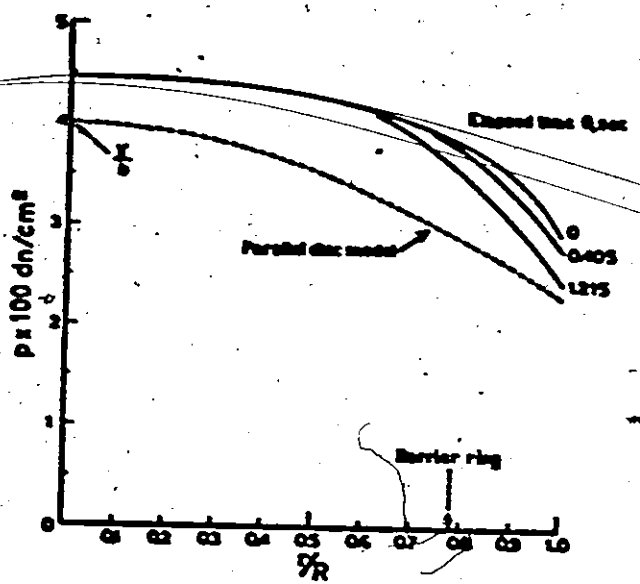

(b) Variation of pressure with elapsed time

(c) Variation of interface velocity

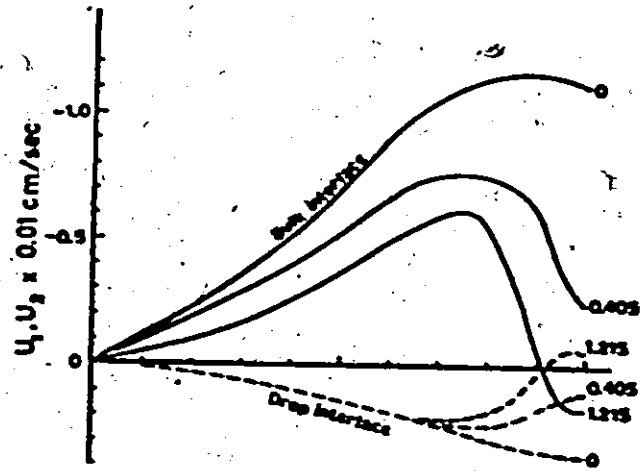

(d) Variation of surface concentration

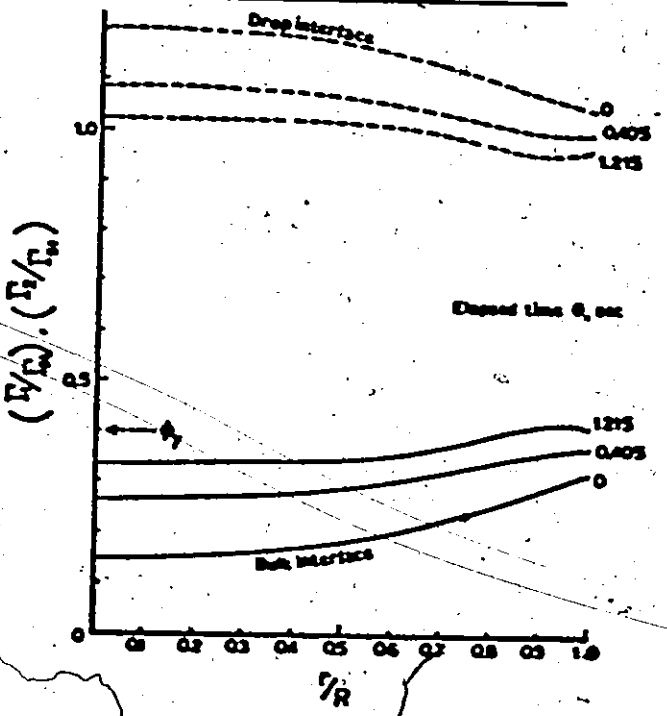

Figure 15

Figure 16

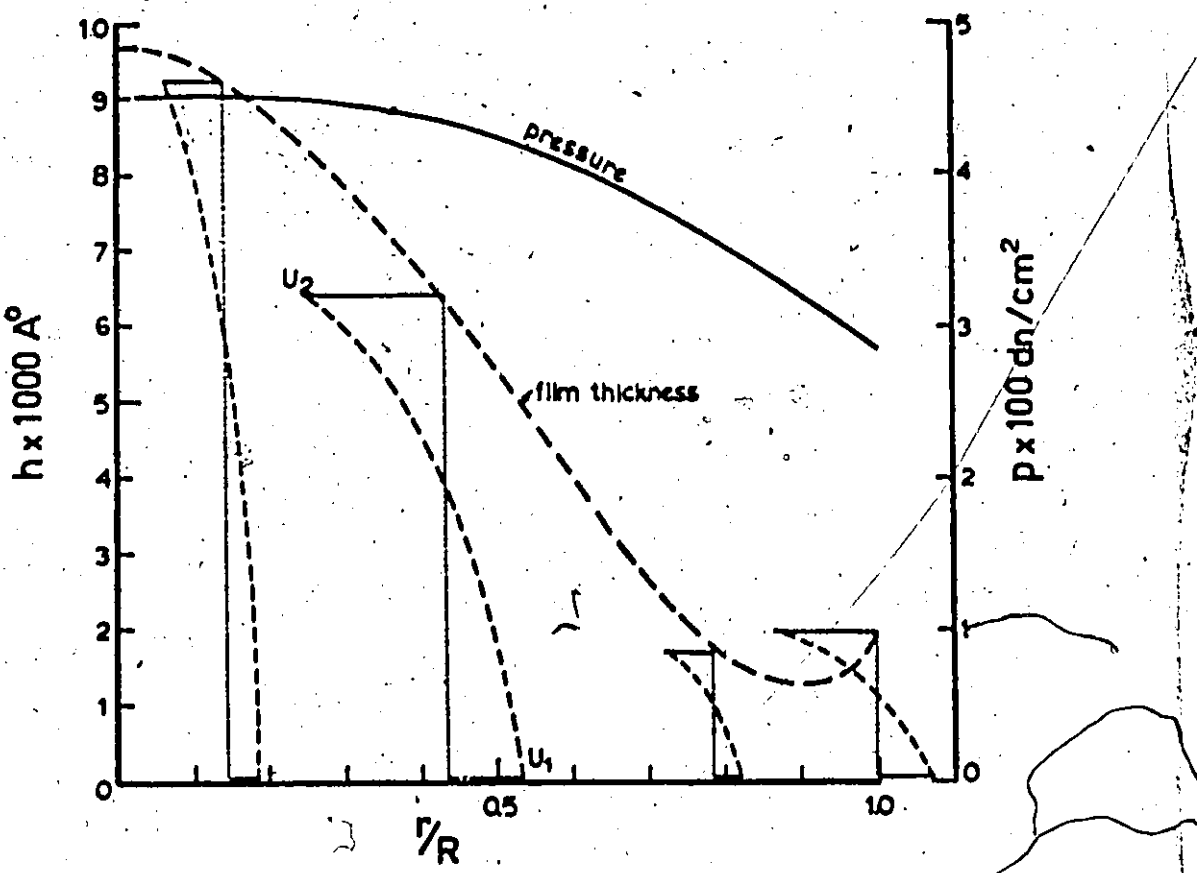

FILM THICKNESS, PRESSURE and RADIAL VELOCITY

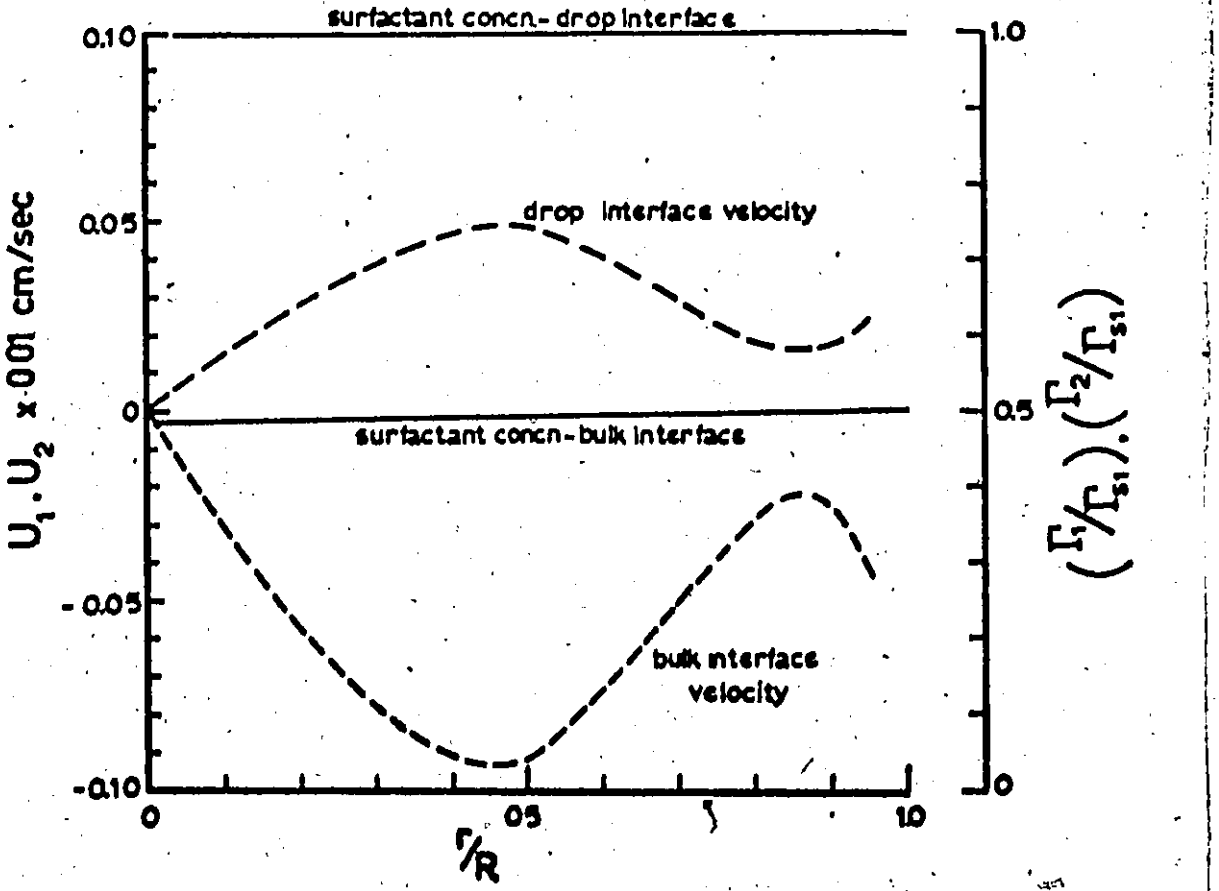

SURFACE CONCENTRATION and INTERFACE VELOCITY

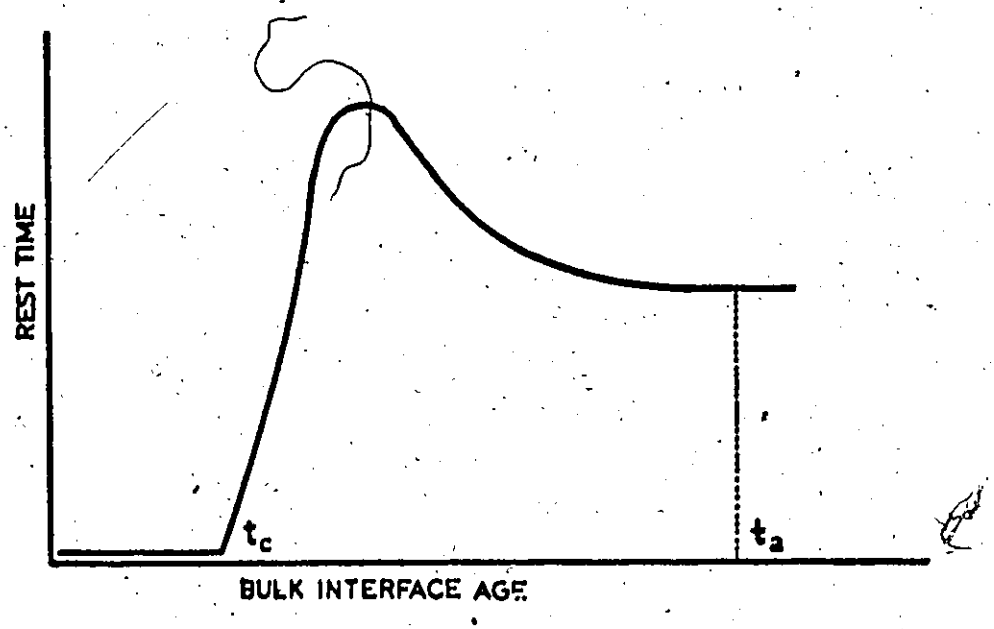

Fig. 17 Variation of rest time with bulk interface age

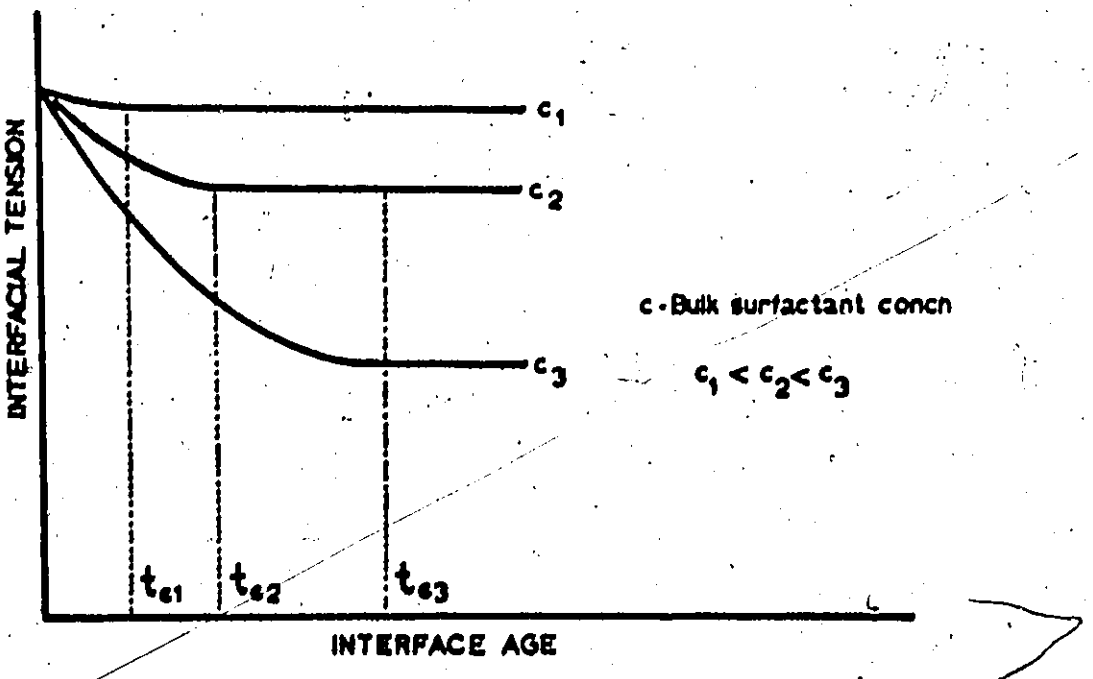

Fig.18 Interfacial tension of an aging interface

CHAPTER 5

APPLICATION OF THE PARALLEL DISC MODEL FOR UNEVEN THINNING

Uneven thinning is the pattern that is most likely to occur in practice; hence it is important to be able to predict the rate of thinning for this pattern. The prediction by mathematical modelling for the entire film area is difficult because of the lack of symmetry in the film. Thus a reasonable and practical approach is to use an empirical model to describe the thinning at the barrier ring since it is the location of film rupture.

In this chapter, the extension of the parallel disc model is studied. The extension is to allow the interfaces to have partial mobility which may vary as the film thinning proceeds.

5.1. Review of the parallel disc model

The parallel disc model was developed by Reynolds[1] and Stefan[2] to describe the rate of thinning of a film bounded by two parallel interfaces thatwere completely immobile. The rate of thinning is given by

$$-\frac{dh}{d\theta} = \frac{2\pi}{3}\frac{1}{\mu}\frac{F}{A^2}h^3 \qquad (1)$$

where F is the force which acts on the interfaces, A is the contact area of the interfaces and μ is the film viscosity.

The rest time Θ can be calculated by integrating Eq. (1) between the limits of $h = h_o$, the initial thickness at $\theta = 0$, and $h = h_1$, the critical thickness at $\theta = \Theta$. The result for $h_o = \infty$ is

$$\Theta = \frac{3}{4\pi} \mu \frac{A^2}{F} \frac{1}{h_1^2} \tag{2}$$

Because a liquid/liquid interface may not be completely immobile, a similar analysis[3] has been carried out which allowed one or both interfaces to be fully mobile. The results can be conveniently combined with the original parallel disc model by introducing a parameter Φ :

$$-\frac{dh}{d\theta} = \frac{8\pi}{3\Phi} \frac{1}{\mu} \frac{F}{A^2} h^3 \tag{3}$$

$$\Theta = \frac{3\Phi}{16\pi} \mu \frac{A^2}{F} \frac{1}{h_1^2} \tag{4}$$

where Φ is equal to 0, 1 or 4 for 0, 1 or 2 immobile interfaces. The value of $\Phi = 0$ corresponds to a trivial case of very rapid thinning and zero rest time; that is, the occurrence of instantaneous coalescence in extremely clean systems[4,5].

The application of the parallel disc model for describing film thinning in liquid/liquid systems should be regarded only as an empirical approach. Because of the existence of a pressure gradient in the film, the film thickness cannot be uniform. It is understood therefore that this model is to be applied only to a particular location in the film; the barrier ring is usually chosen since it is the location of film rupture.

The use of Eqs. (3) and (4) requires the specification of the

values for F and A. For a drop approaching a planar interface, F and A can be estimated as follows. The force F is the drop buoyancy force, that is,

$$F = \frac{4}{3}\pi b^3 \Delta\rho g \tag{5}$$

and the area A is

$$A = \pi r_c^2 \tag{6}$$

where r_c is the equilibrium barrier ring radius, which depends on the assumed interface geometry. For the most commonly used geometries shown in Fig. 1, r_c can be written as

$$r_c = b^2\sqrt{\frac{2 n_G \Delta\rho g}{3\gamma}} \tag{7}$$

where the geometrical factor n_G has a value of $n_G = 1$ for the geometries marked (a) and (b) in Fig. 1[6] or $n_G = 2$ for the geometry (c), the Chappelear's model[7].

Combination of Eqs. (5) to (7) gives

$$\frac{A^2}{F} = \frac{\pi n_G^2}{3}\,\frac{\Delta\rho g b^5}{\gamma^2} \tag{8}$$

Thus the substitution of Eq. (8) into Eqs. (3) and (4) gives the rate of thinning and the rest time of a drop approaching a planar interface. The result for the rate of thinning is

$$-\frac{dh}{d\theta} = \frac{8}{\Phi n_G^2}\,\frac{\gamma^2}{\mu\Delta\rho g b^5}\,h^3 \tag{3a}$$

The parallel disc model given by Eq. (3a) describes the observed thinning rates only over a narrow range of film thicknesses and

overestimates the rest times. Thus various modifications have been attempted. Most of the attempts have been to obtain values for A^2/F which are more accurate than that given by Eq. (8). In this chapter, the method of modifying the parallel disc model is to allow Φ to have fractional values. This has also been suggested by Hartland and Wood[8] in their work with viscous systems and large drops.

5.2. Extension of the parallel disc model

In the parallel disc model, the interface mobility is assumed to be extreme; that is, there can only be zero, one or two immobile interfaces. This may be the main reason why the parallel disc model fails because in general a liquid/liquid interface is neither completely immobile nor fully mobile. The mobility of an interface depends on the concentration of surfactant and the applied shear stress at the interface. Therefore, a logical extension of the parallel disc model is to allow Φ to have fractional values (interpreted as partial mobility) which may vary as the film thinning proceeds (to account for the variation in the applied shear stress).

The various expressions for Φ in terms of the number of immobile and mobile interfaces are[8,9]

$$\Phi = n_I^2 \tag{9}$$

$$\Phi = \frac{2n_I}{3-n_I} \tag{10}$$

$$\Phi = (2-n_M)^2 \tag{11}$$

$$\Phi = \frac{4-2n_M}{1+n_M} \tag{12}$$

where n_I and n_M are the number of immobile and mobile interfaces, respectively.

For integer values of n_I and n_M, it does not matter which of these expressions is used since $\Phi = 0$, 1 or 4 for $n_I = 0$, 1 or 2 and $n_M = 2$, 1 or 0 . However, since partially mobile interfaces are considered, hence fractional values of n_I and n_M, it is desirable to select an expression which gives numerical values of n_I or n_M that are consistent with the concept of interface mobility used in this thesis, namely the relationship between interface velocity and the applied shear stress at the interface.

Consider now the values of n_I and n_M for the various possible variation of film thickness with elapsed time as shown in Fig. 2. The slope of the curve, as given by Eq. (3), is proportional to $-(1/\Phi)$ at a given film thickness. Thus the value of Φ and the corresponding n_I and n_M given by Eqs. (9) to (12) can be calculated as shown in the accompanying table.

Curves (a), (b) and (c) represent the parallel disc model with $\Phi = 0$, 1 and 4 respectively. For these curves Eqs. (9) and (10) and Eqs. (11) and (12) produce identical numerical values for n_I and n_M.

In curve (d) the film thickness does not vary with elapsed time because the flows in the film - due to interface movements and pressure gradient - are exactly balanced. Thus Φ approaches infinity and so do n_I and n_M calculated from Eqs. (9) and (11). The values calculated from Eqs. (10) and (12) are finite: $n_I = 3$ and $n_M = -1$. A value of n_I greater than two is difficult to realize physically, since there are only two interfaces. On the other hand, a negative value for n_M can be interpreted

as the case where the interface velocity is in the opposite direction to the applied shear stress.

Curve (e) shows dimple formation where the film thickness increases with elapsed time. The value of Φ is negative, hence Eqs. (9) and (11) give imaginary values for n_I and n_M. Again Eqs. (10) and (12) give finite values for n_I and n_M.

In summary, Eq. (12) is the most versatile expression for describing partial mobility.

5.3. Results and discussion

The thinning pattern used in this analysis was the uneven thinning of Type A (Chapter 3.5). This pattern was always observed when the bulk interface was old or when it was not cleaned. Since the drop interface was also aged, this thinning pattern should be the one that is most likely to occur in practice.

Figs. 3a and 3b show the thinning at the barrier ring for 0.0025 ml toluene drops and the typical scatter of the data for duplicate runs. In Fig. 3b it is shown that for the same thinning pattern and thinning rate, the rest time may vary because of the variation in the critical film thickness. For this reason, an evaluation of film thinning models should be based on thinning rates and not on rest times.

Consider first the comparison between the thinning rate data and the parallel disc model predictions with constant values of Φ. The model prediction can be calculated by integrating Eq. (3a) from $h = h_o$ at $\theta = 0$ to $h = h$ at $\theta = \theta$ where the value of h_o is chosen to coincide with the initial film thickness of the data. Fig. 4 shows the experimental thinning rates for 0.0025 ml toluene drops with various bulk con-

centrations of palmitic acid, and the model predictions with Φ = 1 and 4 and n_G = 1 and 2. The agreement is not very good. This may be caused by the incorrect physical property dependence of the model and/or the incorrect assumption of constant Φ, that is, the extreme mobility assumption. To determine which is the more dominant cause, the thinning rate data can be plotted in a generalized form. The method is as follows:

Integration of Eq. (3a) from $h = h_o$ at $\theta = 0$ to $h = h$ at $\theta = \theta$ and rearrangement of the result gives

$$\frac{\mu \Delta\rho g b^5}{\gamma^2}\left\{\frac{1}{h^2}-\frac{1}{h_o^2}\right\} = \frac{16}{\Phi n_G^2}\theta \qquad (13)$$

Hence the plot of the LHS of Eq. (13) againt elapsed time θ is independent of system physical properties if the parallel disc model predicts correctly the physical property dependence. Furthermore, if Φ is constant the generalized plot is a straight line.

Fig. 5 shows the thinning rates of the data for various sizes of toluene drops and bulk concentrations of palmitic acid together with the model predictions with Φn_G^2 = 1, 4 and 16. (The interfacial tension γ of pure mutually saturated toluene/water was used. This is a reasonable assumption since the concentration of palmitic acid is low. The largest concentration should lower γ by not more than 1 dn/cm [10], less than 3% of the value of γ)

The following observations can be made from the results in Fig. 5:

(i) The parallel disc model predicts quite well the dependence of thinning rate on drop size. This is shown by the results that the generalized thinning rate data for different drop sizes but the same surfactant

concentration lie on one curve.

(ii) The value of Φ varies with elapsed time since the generalized thinning rate data do not lie on a straight line.

(iii) The value of Φ depends also on surfactant concentration as shown by the existence of different generalized thinning rate curves for different surfactant concentrations.

(iv) The constant values of $\Phi n_G^2 = 1$ and 16 represent the limiting cases since they bracket all the data.

The conclusion that can be drawn from Fig. 5 is that the parallel disc model can be used to describe the rate of thinning of the data provided that the variation of Φ with surfactant concentration and elapsed time is taken into account. This can be interpreted as a further support to the supposition that the interface mobility should not be arbitrarily assumed in film thinning modelling. Consider now the calculation of n_M as given by Eq. (12) and the physical interpretation of the results.

Eq. (3a) can be rearranged to yield

$$-\frac{dh}{d\theta}\frac{1}{h^3}\frac{\mu\Delta\rho g b^5}{\gamma^2} = \frac{8}{\Phi n_G^2} \qquad (14)$$

Therefore the value of Φ and hence n_M can be calculated from Eq. (14) by using the thinning rate data. The results are shown in Fig. 6 where the value of $n_G = 2$ was used.

Fig. 6 shows that the degree of partial mobility n_M

(i) decreases with increasing surfactant concentration and

(ii) increases with elapsed time and approaches a constant value regardless of the surfactant concentration.

The behaviour of n_M can be shown to be consistent with the expected behaviour of a liquid/liquid interface. The degree of mobility n_M can be defined in the simplest way by $n_M \alpha U/U_p$, where U is the actual interface velocity and U_p is the interface velocity if the interface was free of surfactant (upon application of the same shear stress).

As the surfactant concentration increases, a larger interfacial tension gradient can be set up to balance the applied shear stress. Thus U is smaller, n_M decreases and hence the interface becomes less mobile.

The effect of surfactant concentration on n_M is less pronounced with decreasing magnitude of the applied shear stress. The reason is the decreasing concentration that is needed to set up the necessary interfacial tension gradient to balance the shear stress. In the limit, as the shear stress approaches zero, the mobility is independent of the surfactant concentration since no interfacial tension gradient has to be set up. This also means that the mobility of a contaminated interface increases with decreasing magnitude of the applied shear stress since the mobility approaches that of an uncontaminated interface, which by definition is fully mobile.

The shear stress that is exerted by the flow in the film at the interfaces decreases with elapsed time because the rate of thinning decreases as the film thins. Therefore the explanation of the behaviour of n_M can be given as follows. The degree of mobility

(i) decreases with increasing surfactant concentration because the interfaces are less mobile,

(ii) increases with elapsed time because the shear stress decreases, and

(iii) approaches a constant value regardless of the surfactant con-

centration because the shear stress decreases.

Consider now a further test on the physical property dependence of the parallel disc model. For surfactants of the same properties and concentration, the generalized plot in Fig. 5 should apply to any system. Therefore the variation of film thickness with elapsed time of any system can be predicted from Fig. 5. If the generalized thinning rate curve in Fig. 5 is denoted by $w(\theta)$, the result can be written as

$$\frac{1}{h^2(\theta)} = \frac{1}{h_o^2} + \frac{\gamma^2}{\mu \Delta\rho g b^5} w(\theta) \qquad (15)$$

where the system physical properties refer to the system for which the variation of h with θ is to be predicted.

The variation of h with θ for a 0.015 ml anisole drop and zero surfactant concentration is shown in Fig. 7a. The solid curve represents the data[11] and the dotted curve is the variation calculated from Eq. (15). The agreement is within 15%, which is satisfactory considering the simplicity of the present model and the difference in the physical properties.

The test can also be performed in terms of the generalized plot, as shown in Fig. 7b. The curve marked (a) is the $w(\theta)$ used in Fig. 7a (reproduced from Fig. 5) and the points marked 'Data' are the calculated generalized plot of the data. Again, the agreement is satisfactory. (The seemingly large error at large values of θ is caused by the magnification of errors through the term $1/h^2$.)

It is important to note that the analysis was carried out for only one film thinning pattern. Thus the extended parallel disc model cannot be expected to apply to other thinning patterns. For example, for

slow even thinning Pattern IV[4] the dependence of the rate of thinning at the barrier ring on drop size is given by b^{-2} instead of b^{-5} as given by the parallel disc model. The discrepancy should not be interpreted as a contradiction because the film shape and the governing mechanism for the film thinning are different. In uneven thinning Type A the film thickness profile is almost parallel and the thinning occurs over the entire film area, whereas in slow even thinning Pattern IV there is a large pocket or dimple and the thinning occurs only in the region outside the barrier ring. The suggestion that there is a change in the dependence of the rate of thinning on drop size depending on the thinning mechanism has been confirmed by Burrill's analysis[9].

In summary, the use of a simple model is limited only to one thinning pattern.

5.4. Summary and conclusions

1. The parallel disc model with the use of varying partial mobility can describe satisfactorily the thinning at the barrier ring for uneven thinning Type A in toluene/water and anisole/water systems.

2. The variation of the degree of partial mobility with bulk surfactant concentration and elapsed time during thinning is consistent with the expected behaviour of a liquid/liquid interface. The degree of partial mobility increases with decreasing bulk surfactant concentration and increasing elapsed time, and approaches a constant value when the film is very thin and the rate of thinning is very low.

3. The parallel disc model with constant values of $\Phi n_G^2 = 1$ and $\Phi n_G^2 = 16$ could be used to bracket the observed variation of film thickness with elapsed time.

4. The use of a simple model to describe film thinning is limited to only one thinning pattern.

5. An evaluation of a film thinning model should be based on thinning rates and not on rest times unless the critical film thickness is constant.

Literature cited

1. Reynolds, O., Phil. Trans., A177 (1866):157

2. Stefan, J., Sitzber.Akad.Wiss.Wien.Math.-Kl., 69 (1874):713

3. Hodgson, T. D., Ph.D. Thesis, Univ. Coll. Swansea, U.K. (1966)

4. Hodgson, T. D. and D. R. Woods, J. Coll. Int. Sci., 30 (1969):429

5. Burrill, K. A. and D. R. Woods, J. Coll. Int. Sci., 42 (1973):15,35

6. Charles, G. E. and S. G. Mason, J. Coll. Sci., 15 (1960):235

7. Chappelear, D. C., J. Coll. Sci., 16 (1961):186

8. Hartland, S. and S. M. Wood, A.I.Ch.E. J., 19 (1973):810,871

9. Burrill, K. A., Ph.D. Thesis, McMaster Univ. Canada, (1970)

10. Ward, A. F. H., in "Surface Chemistry": papers presented at a joint meeting of Societe Chime Physique and Faraday Soc., 1947, Butterworths Sci. Pub., London (1949):55

11. Hodgson, T. D., Unpublished data, McMaster University, Canada (1967)

Table I Physical properties of Anisole/Water and Toluene/Water

Film viscosity 0.01 poise

Density difference and interfacial tension

	Anisole/Water	Toluene/Water
$\Delta\rho$ g/ml	0.0097	0.133
γ dn/cm	20.5	33.5

Figure captions

1. The different geometries that have been used to approximate the contact area of the interfaces. In (a) the drop is deformable and the bulk interface is rigid, (b) the drop is rigid and the bulk interface is deformable and (c) the drop and the bulk interface are deformable, the Chappelear's model[7]. The symbols r_{c1} and r_{c2} denote the barrier ring radii for the different geometries.

2. Various possible variation of film thickness with elapsed time depending on the interface mobility. In (a), (b) and (c) there are two, one and zero fully mobile interfaces, respectively, in (d) and (e) the mobility is negative , that is, one of the interfaces or both move toward the film centre. In (d) the film thickness is constant and (e) the film thickness increases with elapsed time, that is, dimple formation. The accompanying table shows the values of Φ and n_I and n_H given by Eqs. (9) to (12)

3. Variation of film thickness with elapsed time at the barrier ring for uneven thinning Type A. The different symbols denote duplicate runs and R denotes the instant of film rupture.

4. Comparison between the data and the parallel disc model predictions with constant interface mobility.

5. Comparison between the data and the parallel disc model predictions with constant mobility in terms of a generalized plot. The parallel disc model prediction is a straight line with a slope of $1/(\Phi\, n_0^2)$.

6. Variation of the degree of mobility with bulk surfactant concentration and elapsed time. The value of n_H is calculated from Eq. (12) with $n_0 = 2$.

7a. Comparison between the thinning rate data for an anisole drop and that predicted by the extended parallel disc model based on the thinning rate data for toluene drops. The dotted curve is calculated from Eq. (15) and the generalized curve obtained from toluene/water system in Fig. 5.

7b. Comparison as in Fig. 7a in terms of a generalized plot. The points marked 'Data' are calculated from the data and the curve (a) is reproduced from Fig. 5 for toluene/water system.

a

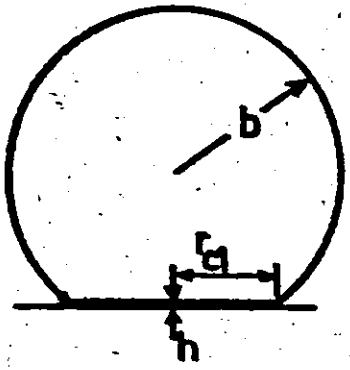

Deformable Drop

$$r_{c1} = b^2 \sqrt{\frac{2\Delta\rho g}{3\gamma}}$$

b

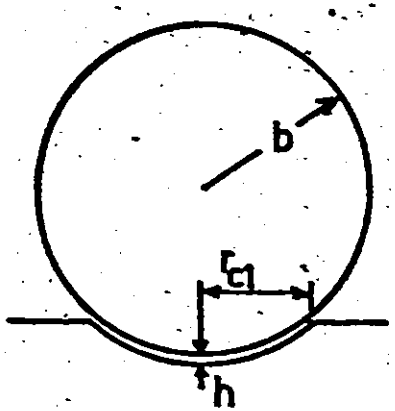

Deformable Bulk

c

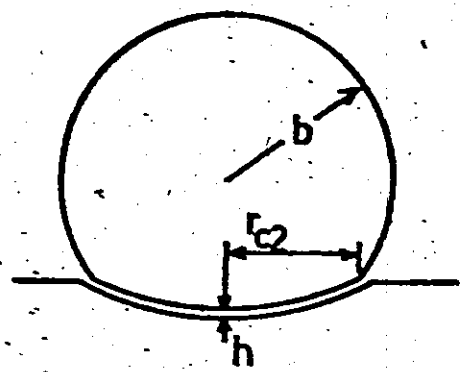

Both Deformable

$$r_{c2} = 2b^2 \sqrt{\frac{\Delta\rho g}{3\gamma}}$$

Figure 1

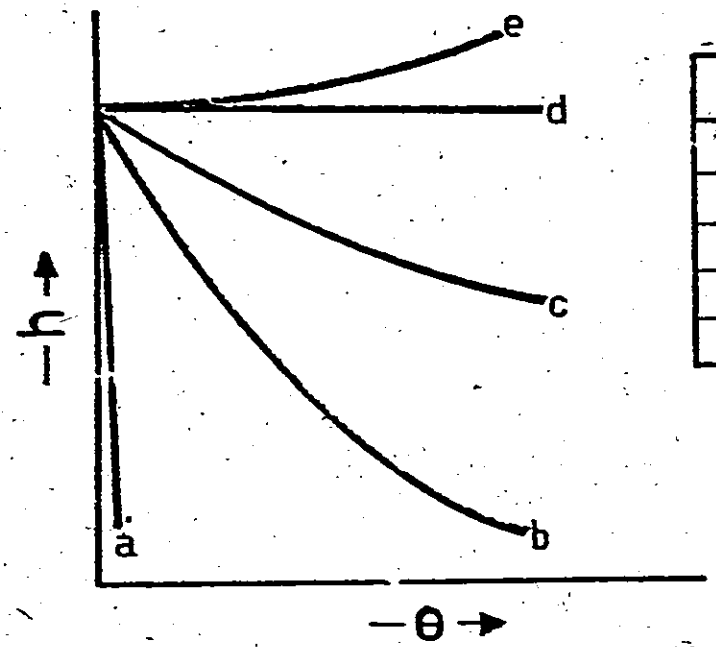

	Ø \ Eq	η_I 9	η_I 10	η_M 11	η_M 12
a	0	0	0	2	2
b	1	1	1	1	1
c	4	2	2	0	0
d	∞	$\sqrt{\infty}$	3	$+\sqrt{\infty}$	-1
e	<0	i	>3	i	<-1

i-complex number

Figure 2

Figure 3a

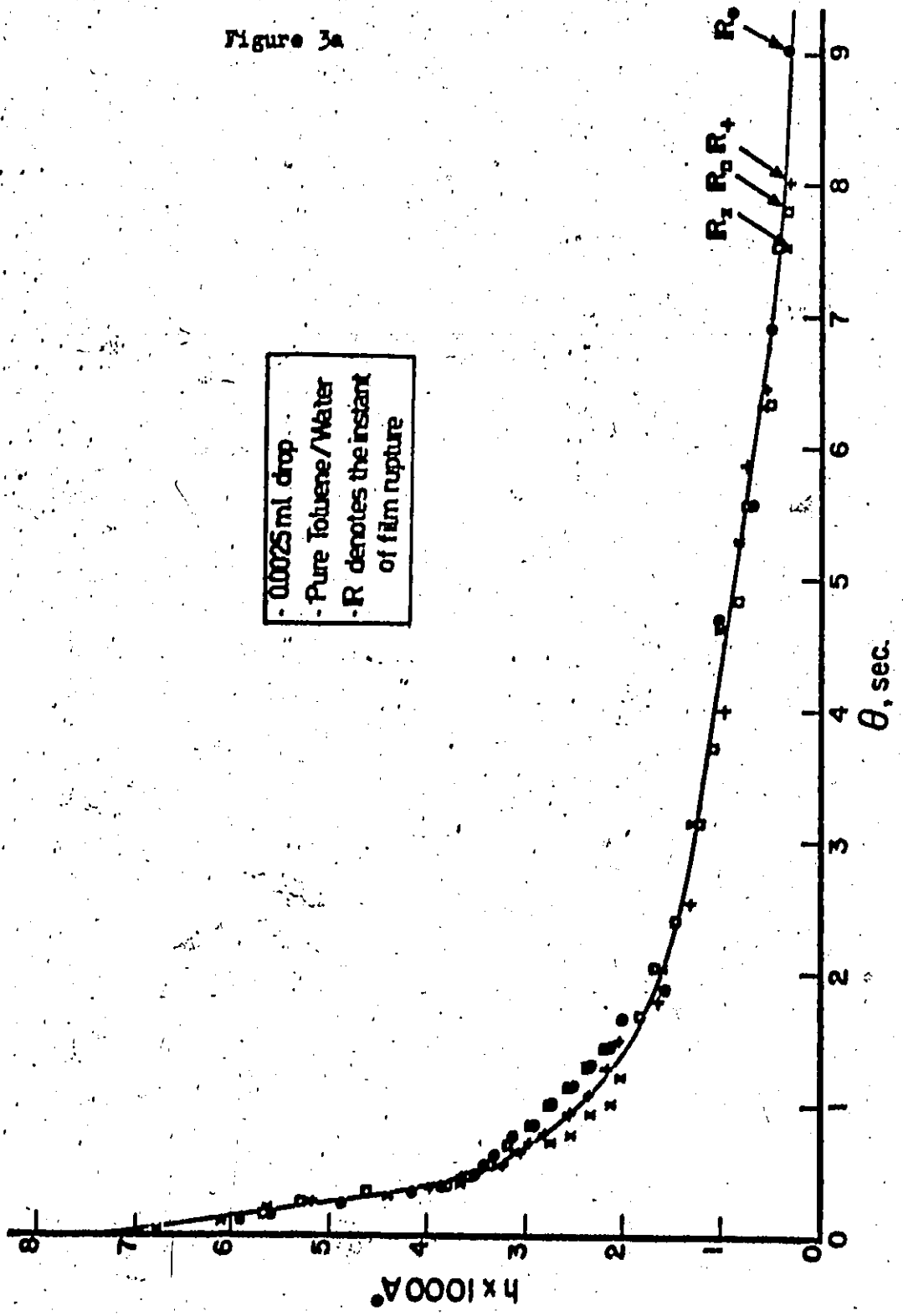
- 0.0025ml drop
- Pure Toluene/Water
-R denotes the instant of film rupture
R₀
R₁ R₂ R₃
h x 1000A°
θ, sec.

Figure 3b

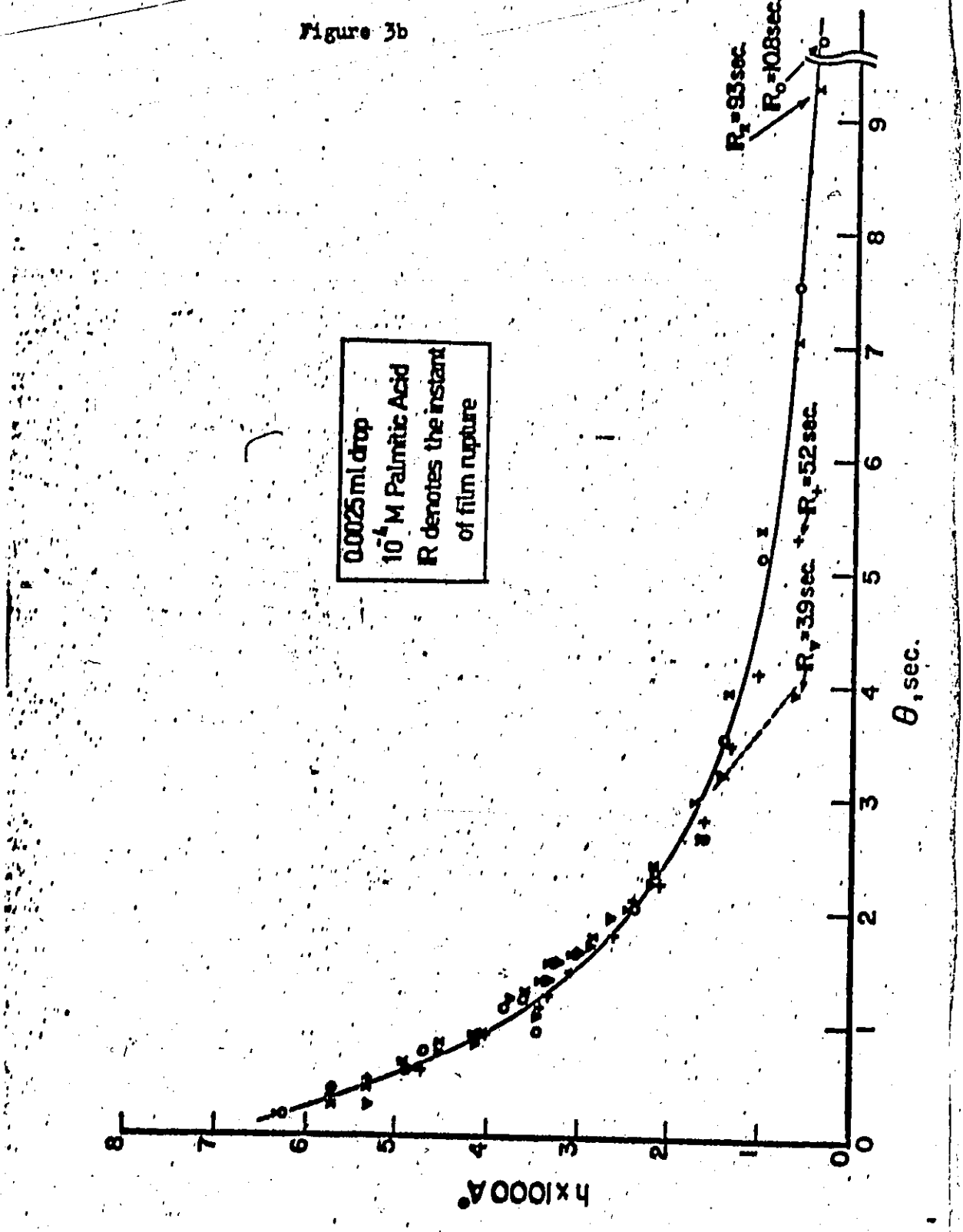
0.0025 ml drop
10^{-4} M Palmitic Acid
R denotes the instant of film rupture
R_4=93sec
R_0=108sec
R_7=39sec
R_4=52sec
h x 1000 A°
θ, sec.

Figure 4

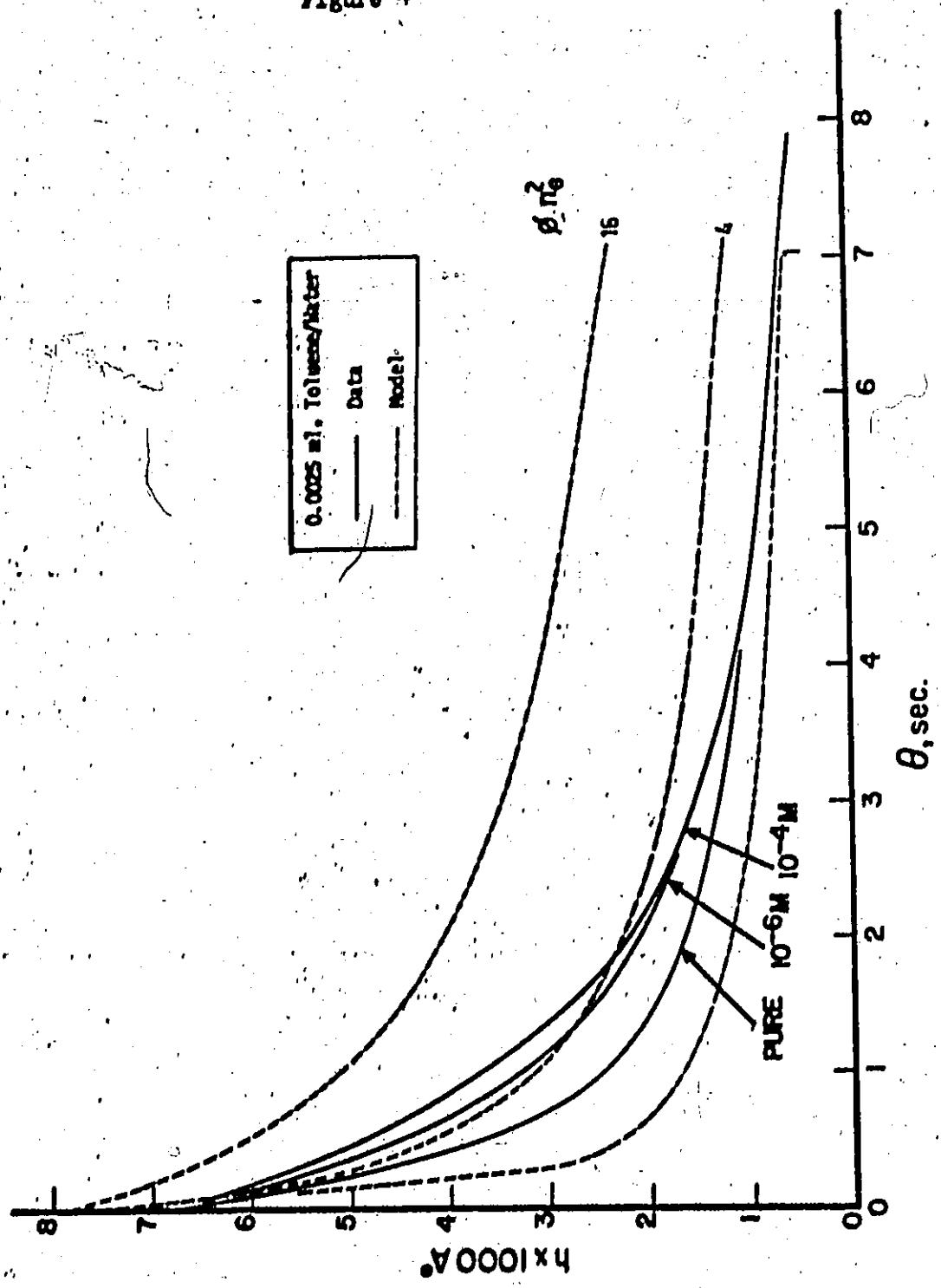
0.0025 ml. Tellacine/Water
Data
Model
$\beta.n_0^2$
16
4
PURE
10^{-6}M
10^{-4}M
h x 1000 A°
θ, sec.
0
1
2
3
4
5
6
7
8

Figure 5

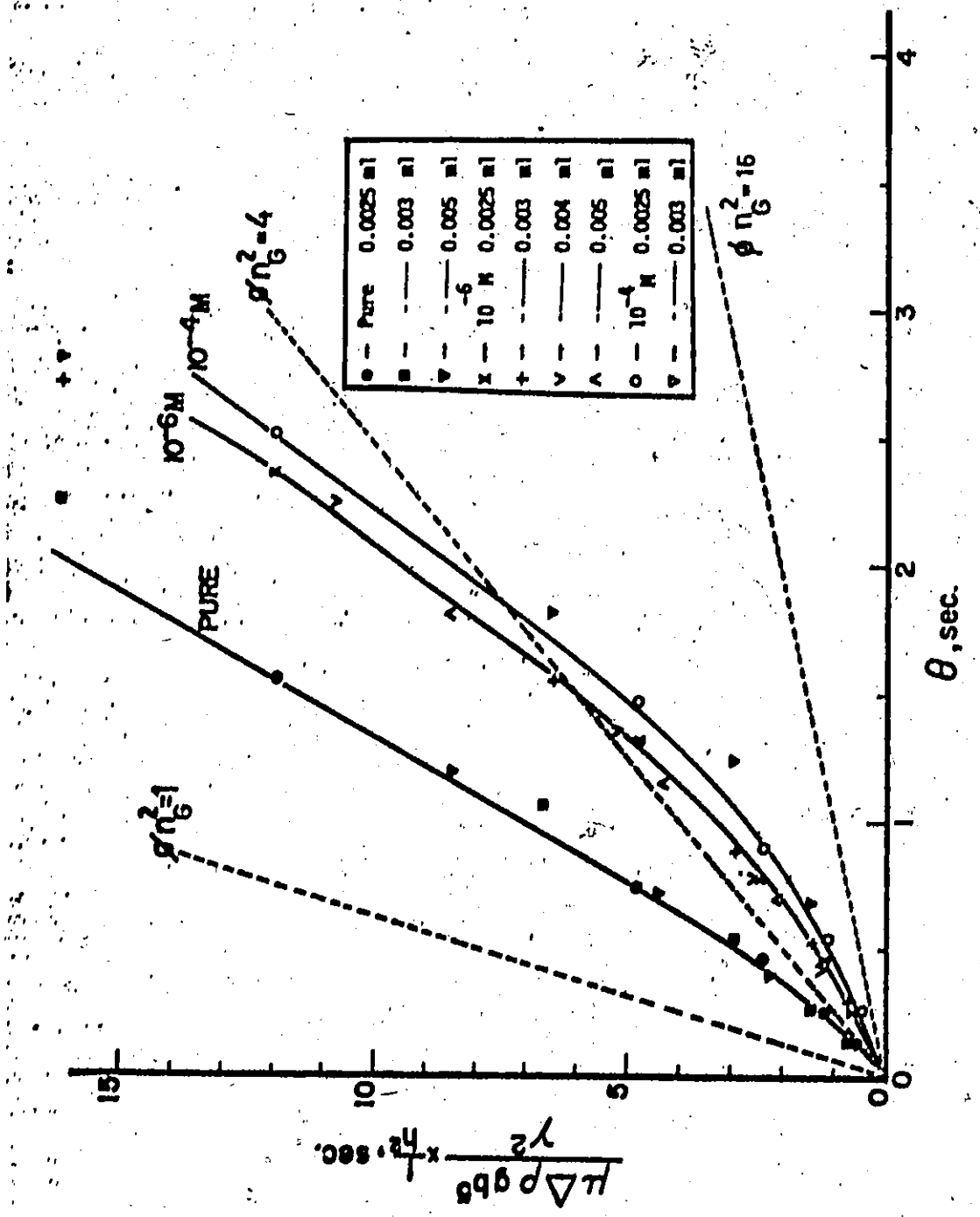
Pure 0.0025 ml
0.003 ml
0.005 ml
10⁻⁶ M 0.0025 ml
0.003 ml
0.004 ml
0.005 ml
10⁻⁴ M 0.0025 ml
0.003 ml
PURE
10⁻⁶M
10⁻⁴M
$\phi\eta_G^2$=16
$\phi\eta_G^2$=4
$\phi\eta_G^2$=1
θ, sec.
$\frac{\mu\Delta\rho\, g b^6}{\gamma^2} \times \frac{1}{h^2}$, sec.

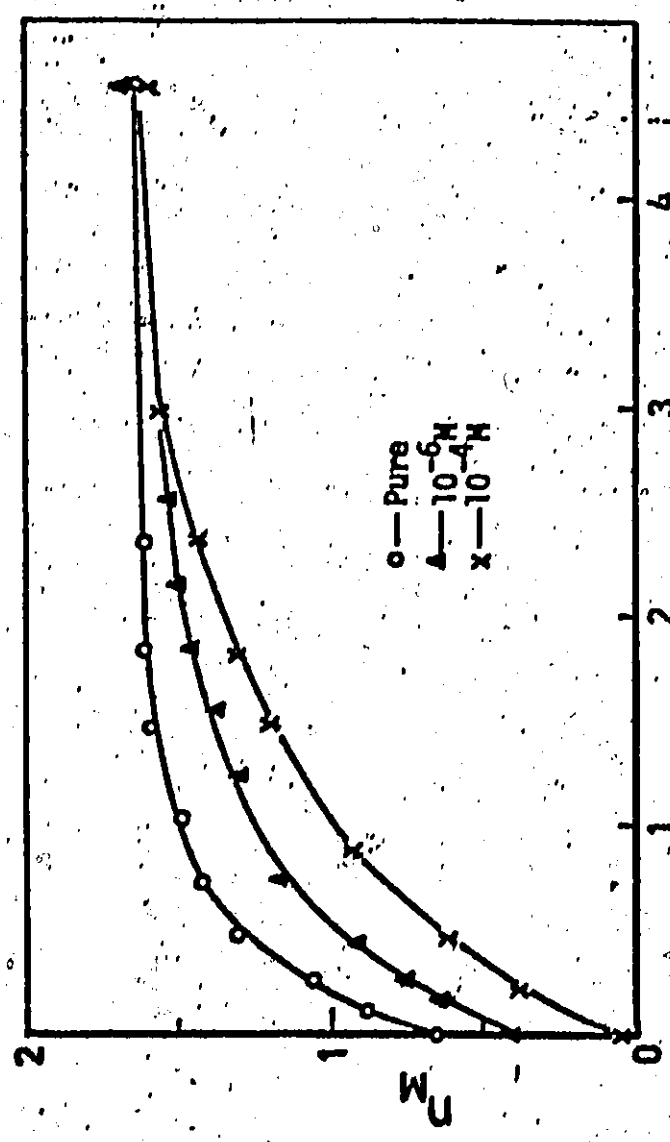

Figure 6

Figure 7a

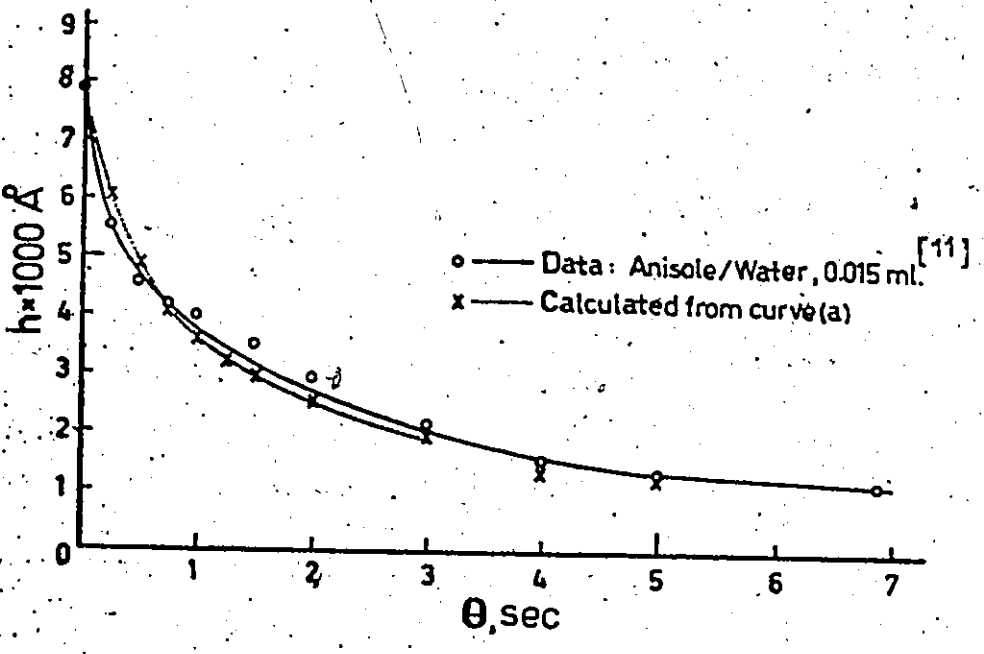

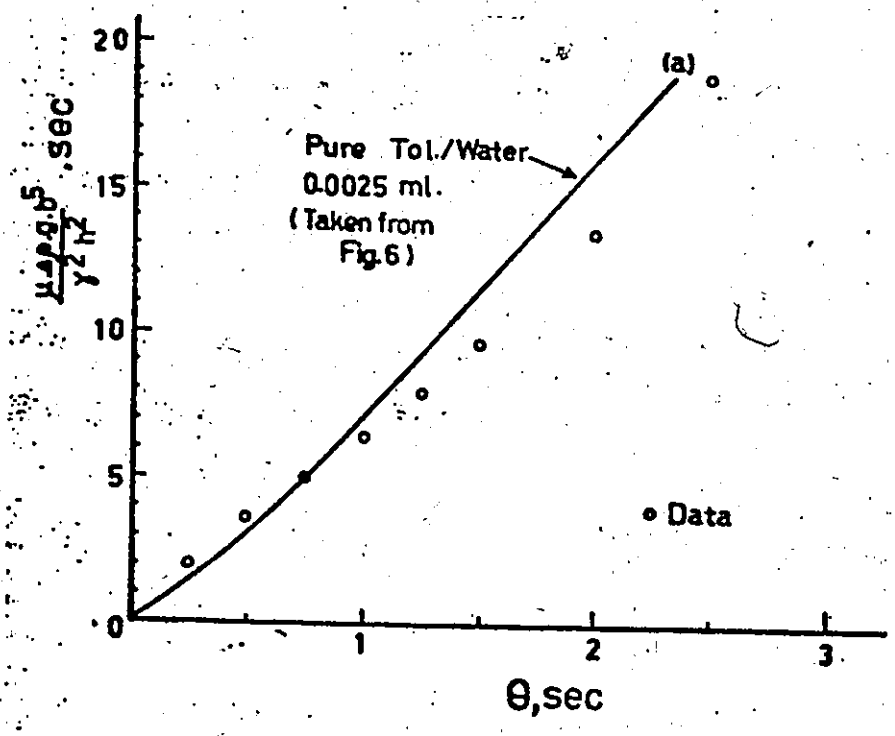

Figure 7b

CHAPTER 6

ALGEBRAIC ANALYSIS OF EVEN AND UNEVEN THINNING

As a result of not assuming arbitrarily the interface mobility, it is possible to put forward a postulate for the conditions under which thinning occurs evenly or unevenly, as shown in Chapter 2.4.2. In this chapter, the postulate is analysed algebraically and its predictions compared with experimental observations.

The analysis is based on the assumption that the pressure in the film can be represented by a parabolic function of the radial distance. The resulting model - referred to as the parabolic model - is therefore a truncated form of the polynomial model.

6.1. Film thinning equations for the parabolic model

Assume that the pressure is a parabolic function of the radial distance and, to simplify further the analysis, that the film is uniform in thickness; that is,

$$p^+ = A_0 + A_2 r^{+2} \qquad (1)$$

$$h^+ = L_0$$

where the superscript + denotes normalized variables, defined by Eq. (4-1), and A_0, A_2 and L_0 are the coefficients for the pressure and the film

thickness, respectively.

To maintain consistency in the film thinning equations, the other variables must be given by:

$U_1^+ = B_1\, r^+$	$U_2^+ = D_1\, r^+$
$\Gamma_1^+ = G_0 + G_2\, r^{+2}$	$\Gamma_2^+ = H_0 + H_2\, r^{+2}$

(2)

where B_1, D_1, G_0 and G_2, and H_0 and H_2 are the coefficients for the interface velocities and the surface concentration distributions, respectively.

The film thinning equations can thus be expressed in terms of these coefficients by substituting Eqs. (1) and (2) into Eqs. (4-3) to (4-8). The results are:

Rate of film thinning

$$\frac{dL_o}{d\theta^+} = 4\phi_4 A_2 L_o^3 - \phi_5 (B_1 + D_1) L_o \tag{3}$$

Tangential force balance

$$2\phi_9 L_o G_2 + \phi_{10}(B_1 - D_1) + L_o^2 A_2 = 0 \tag{4}$$

$$2\phi_9 L_o H_2 - \phi_{10}(B_1 - D_1) + L_o^2 A_2 = 0 \tag{5}$$

Surfactant mass balance

$$\frac{dG_o}{d\theta^+} = \phi_{12}[1 - G_o] + 4\phi_6 G_2 - 2\phi_5 G_o B_1 \tag{6}$$

$$\frac{dH_o}{d\theta^+} = \phi_{12}[\phi_7 - H_o] + 4\phi_6 H_2 - 2\phi_5 H_o D_1 \tag{7}$$

where the dimensionless parameters ϕ's are defined in Eq. (4-17).

The normal force balance equation is not included because the film is assumed to be uniform; hence the parabolic model has the same inconsistency at that found in the parallel disc model.

The boundary condition for pressure is the total force balance in the z-direction:

$$\int_0^{R_p} 2\pi r p \, dr = F \tag{8}$$

where R_p is the radial location where the pressure is zero; that is,

$$p^+ (r^+ = R_p^+) = 0 \tag{9}$$

For the surface concentrations, the total balance boundary condition Eq. (D-23); that is,

$$\int_0^{R'} 2\pi r \Gamma \, dr = \pi R'^2 \Gamma_s \tag{10}$$

These boundary conditions can be expressed in terms of the coefficients for the pressure and surface concentrations by substituting Eqs. (1) and (2) into Eqs. (8) to (10). The results are:

$$A_0^2 = -2\psi A_2 \tag{11}$$

$$R_p^{+2} = 2\psi / A_0 \tag{12}$$

$$G_0 + \tfrac{1}{2} R_p^{+2} G_2 = 1 \tag{13}$$

$$H_0 + \tfrac{1}{2} R_p^{+2} H_2 = \phi_7 \tag{14}$$

where ψ is the normalized buoyancy force defined by Eq. (4-17), and ϕ_7 is defined by $\phi_7 = \Gamma_{s2} / \Gamma_{s1}$.

The pressure at the film centre is assumed to be that in a

film of uniform thickness; that is,

$$A_0 = \frac{\gamma}{P\,b} \qquad (15)$$

where P is the normalizing constant for the pressure.

Eqs. (3) to (8) and (11) to (15) are the film thinning equations for the parabolic model.

6.2. Analysis of the postulate

The postulate put forward in Chapter 2.4.2 can be stated as follows. Given a set of system physical properties, film thickness and rate of thinning, even thinning (or dimple formation) occurs if and only if there exist:

(i) real values for the interface velocities, and

(ii) positive surface concentrations everywhere at the bulk and drop interfaces,

which satisfy the tangential force balance equations. Otherwise, the thinning is uneven.

Therefore, to analyse the postulate the interface velocities and the surface concentration distributions must be calculated from the given set of system physical properties, film thickness and rate of thinning. Consider first the calculation, then the algebraic formulation of the postulate.

Calculation of the interface velocities and the surface concentration distributions

The calculation is based on the condition that the tangential force balance equations Eqs. (4) and (5) must be satisfied at the time θ

and some later time $\theta+\Delta\theta$, where θ is the time when the film thickness and the rate of thinning are specified. Therefore the time derivatives of Eqs. (4) and (5) must also be satisfied.

The time derivatives of Eqs. (4) and (5) can be combined to give

$$\frac{dG_2}{d\theta^+} + \frac{dH_2}{d\theta^+} = -\frac{A_2}{\Phi_9}\frac{dL_o}{d\theta^+} \tag{16}$$

The RHS of Eq. (16) can be calculated from the given rate of thinning and the system physical properties, and the LHS can be expressed in terms of the interface velocities and the surface concentrations from the surfactant mass balance equations Eqs. (6) and (7) and the boundary conditions Eqs. (13) and (14). The procedure for the latter is as follows.

The time derivatives of Eqs. (13) and (14) can be combined to give

$$\frac{dG_2}{d\theta^+} + \frac{dH_2}{d\theta^+} = -\frac{2}{R_p^{+2}}\left[\frac{dG_o}{d\theta^+} + \frac{dH_o}{d\theta^+}\right] \tag{17}$$

Hence, equating the RHS of Eqs. (16) and (17) gives

$$\frac{dG_o}{d\theta^+} + \frac{dH_o}{d\theta^+} = \frac{R_p^{+2} A_2}{2\Phi_9}\frac{dL_o}{d\theta^+} \tag{18}$$

The LHS of Eq. (18) can be expressed in terms of the coefficients B_1, D_1, G_0, G_2, H_0 and H_2 by using the surfactant mass balance equations Eqs. (6) and (7). The result is

$$\Phi_{12}\left(1+\Phi_7-G_o-H_o\right)+4\Phi_6\left(G_2+H_2\right)-2\Phi_5\left(G_oB_1+H_oD_1\right) = \frac{R_p^{+2}A_2}{2\Phi_9}\frac{dL_o}{d\theta^+} \tag{19}$$

Eq. (19) is the equation used for calculating the interface velocities

and the surface concentration distributions.

The RHS of Eq. (19) can be readily calculated from the given rate of thinning and the system physical properties from Eqs. (11), (12) and (15), and the LHS can be expressed in terms of one unknown, for example the interface velocity B_1. The procedure for the latter is as follows:

(i) calculate the sum of the interface velocities ($B_1 + D_1$) from the rate of thinning equation Eq. (3),

(ii) express D_1 in terms of B_1 and ($B_1 + D_1$),

(iii) calculate G_2 and H_2 in terms of B_1 from Eqs. (4) and (5), and

(iv) calculate G_0 and H_0 in terms of B_1 from Eqs. (13) and (14).

Therefore, all the terms on the LHS of Eq. (19) can be expressed in terms of B_1. After B_1 has been calculated, then D_1 can be readily calculated from the known value of ($B_1 + D_1$), and G_0, G_2, H_0 and G_2 from Eqs. (4), (5), (13) and (14).

The details of the calculation of B_1 from Eq. (19) are given in Appendix E, where the calculation is carried out in terms of ζ, defined by

$$B_1 = \zeta (B_1 + D_1) \tag{20}$$

Algebraic formulation of the postulate for the conditions for even and uneven thinning

As shown in Appendix E, Eq. (19) can be written in terms of ζ by

$$A^* \zeta^2 + B^* \zeta + C^* = 0 \tag{21}$$

where A^*, B^* and C^* are given by the system physical properties, the film thickness and the rate of thinning.

Therefore, the conditions for even thinning are:

(i) Real values for the interface velocities exist, that is

$$B^{*2} - 4A^* C^* \geq 0 \qquad (22)$$

AND

(ii) The surface concentrations are positive in $0 \leq r^+ \leq R_p^+$, that is

$$G_0 \geq 0 \text{ and } G_0 + R_p^{+2} G_2 \geq 0 \qquad (23)$$

and $$H_0 \geq 0 \text{ and } H_0 + R_p^{+2} H_2 \geq 0 \qquad (24)$$

Otherwise, the thinning is uneven.

All the terms in inequalities (22) to (24) can be calculated from the system physical properties, the film thickness and the rate of thinning. Therefore, the validity of the postulate can be verified by experimental observations: if the observed behaviour is even, all the inequalities must be satisfied, and conversely if the observed behaviour is uneven one of the inequalities must be violated.

6.3. Results and discussion

The experimentally observed film thinning behaviour can be classified in terms of even and uneven thinning behaviour into three groups:

(i) Completely uneven behaviour, where the interference colours are unsymmetrical from the instant they are first observed until they disappear when the film ruptures. This group represents the uneven thinning Type A and the Pattern III of Hodgson and Woods[1].

(ii) Completely even behaviour, where the interference colours remain symmetrical for the entire period of film thinning. This group represents

the dimple formation and even thinning observed in Chapter 3, and the Patterns II and IV of Hodgson and Woods[1] for the cases where the dimple formation or thinning remains even.

(iii) Combination of even and uneven behaviour, where there is a shift from even to uneven behaviour or vice versa. (In some cases this shift occurred more than once.) This behaviour may happen during thinning or dimple formation.

The purpose of this chapter is to determine whether these experimental observations are predicted correctly by the postulate given by inequalities (22) to (24).

For a given system - that is, liquids, drop size, surfactant and surface concentrations Γ_{s1} and Γ_{s2} - whether thinning or dimple formation occurs evenly or unevenly depends only on the film thickness and the rate of film thinning. It is therefore convenient to first 'map' the predicted even and uneven thinning regions, and then to plot the 'thinning path' of the data (that is, the variation of the rate of thinning with film thickness). If the postulate is valid, the even or uneven thinning path of the data must lie in the correct region.

Consider first the postulate testing for the case of both the drop and bulk interfaces having the same Γ_s. For this case, the experimentally observed behaviour was the uneven thinning Type A, as shown in Chapter 3.5.

The predicted even and uneven thinning regions for 0.0025 and 0.005 ml toluene drops are shown in Fig. 1 by the curves marked A, B, C and D. These curves were calculated from inequalities (22) to (24) using the values of $k^* \Gamma_{s1} = k^* \Gamma_{s2} = 0.05$ dn/cm and 1.0 dn/cm, $\Phi_7 = 1$ and the surfactant physical properties given in Table 4-Ic.

The thinning paths of the data are superimposed on the map Fig. 1 for various drop sizes ranging from 0.0025 to 0.005 ml, and bulk concentrations of palmitic acid from zero to 10^{-4} M. The results show that all these thinning paths lie in the predicted uneven thinning region; thus the postulate predicts correctly the observed uneven behaviour.

The results in Fig. 1 can be extended to other oil/water systems. In Chapter 5, it was shown that the thinning path for uneven thinning Type A was given by the extended parallel disc model Eq. (5-3a):

$$-\frac{dh}{d\theta} = \frac{1+n_M}{2-n_M}\,\frac{\gamma^2}{\mu\Delta\rho g b^5}\,h^3 \qquad (25)$$

where in this chapter h is equivalent to L_0 because the film is assumed to be uniform in thickness. Eq. (25) can be written in a dimensionless form:

$$-\frac{dh^*}{d\theta^*} = \frac{4}{3}\,\frac{1+2n_M}{2-n_M}\,h^{*3} \qquad (26)$$

where the parameter Φ has been replaced by the degree of partial mobility n_M defined in Eq. (5-12), the value of $n_G=2$ has been used, and the dimensionless variables are defined by

$$h^* = \frac{h}{b} \quad \text{and} \quad \theta^* = \frac{3}{4}\,\frac{\theta}{(b^3\mu\Delta\rho g/\gamma^2)} \qquad (27)$$

Fig. 5-6 shows that the value of n_M varies from $n_M=0$ at large film thicknesses to $n_M=1.6$ as the thinning proceeds. The thinning paths given by Eq. (26) for these two limiting values of n_M are shown in Fig. 2 by the broken lines marked $n_M=0$ and $n_M=1.6$. These paths are straight lines with a slope of 1/3 because a logarithmic plot has been used. To show that $n_M=0$ and $n_M=1.6$ are the limiting values, the thinning paths of the

data for 0.0025 ml toluene drops are also plotted in Fig. 2.

The predicted regions of even and uneven thinning are shown in Fig. 2 by the curves marked A, B and C. These curves were calculated from inequalities (22) to (24) using the values of $\phi = 4\, b^2 \Delta\rho g / 3\gamma$ corresponding to 0.0025 and 0.005 ml toluene drops, and $k^* \Gamma_s$ =0.05 and 1.0 dn/cm at a toluene/water interface.

Fig. 2 again shows that the thinning paths of the data lie in the predicted region of uneven thinning. Furthermore, these results can be qualitatively extended to other oil/water systems. At large film thicknesses, the value of n_H is close to zero and hence the thinning path lies in the uneven thinning region, as shown in the top right hand corner of Fig. 2. As the thinning proceeds, n_H increases such that the thinning path will remain in the uneven thinning region. When n_H is equal to 1.6, the thinning is predicted to be uneven until the value of h^* is about 10^{-5} (the intersection of curve C and the thinning path n_H=1.6). This thickness corresponds to about 200 Å for a 0.035 ml drop. Therefore, the postulate predicts uneven behaviour for the entire period of film thinning because film rupture usually occurs at a thickness between 200 and 400 Å.

The results in Figs. 1 and 2 show that the predictions of the extended parallel disc model and the postulate are consistent. When both interfaces have the same Γ_s, the thinning pattern is uneven, as experimentally observed, and the thinning path is given by the extended parallel disc model Eq. (26), as shown in Chapter 5. These experimental observations are predicted correctly by the postulate: when both interfaces have the same Γ_s and the thinning path is given by Eq. (26), the thinning pattern is predicted to be uneven.

The thinning paths shown in Figs. 1 and 2 are those at the barrier ring. In the strictest sense, the paths at the film centre should have been used because the parabolic model is only applicable in the central region of the film. However, for this particular case of uneven thinning Type A the use of the thinning paths at the barrier ring is acceptable because the rate of thinning at the film centre is faster than that at the barrier ring. Therefore, the thinning paths shown in Figs. 1 and 2 would have been shifted to the right if the thinning paths at the film centre had been used; hence the outcome of the postulate testing would have been the same.

The results of the postulate testing for different types of film thinning behaviour are shown in Figs. 3 to 5. In each case, the thinning path was plotted using the film thickness and the rate of thinning at the film centre. The estimated range of surface concentrations $k^* \Gamma_{s1}$ and ϕ_7 used in the mapping of the even and uneven thinning regions are shown in each diagram; this range was estimated by the method described in Chapter 4.2.5.

In Figs. 3 and 4, the postulate is tested with anisole/water systems[1,2]. The uneven thinning paths a-b and a'-b'-c' in Fig. 3 lie in the predicted region of uneven thinning. Similarly, the even thinning path a'-b'-c'-d' in Fig. 4 lies in the predicted even thinning region marked by A'B'. The path a-b-c-d in Fig. 4, which undergoes changes from even (a-b) to uneven (c) and back to even behaviour again (d), is again correctly predicted.

The testing of the postulate for the case of dimple formation is shown in Fig. 5. The observed dimple formation paths a-b-... g and a'-b'-.. g' are correctly predicted. Initially, the dimple formation occurred

unevenly (b-c-d and b'-c'-d'), and then when the rate of dimple formation had decreased, the dimple formation occurred evenly (e-f-g and e'-f'-g').

The validity of the postulate is confirmed by experimental observations, as shown in Figs. 1 to 5. However, it is important to distinguish the application of the results for the uneven thinning Type A and those for the other types of thinning behaviour. In the former, it is possible to extend the results to the prediction of uneven thinning behaviour when both interfaces have the same surface concentration Γ_s because the thinning path given by Eq. (26) is known a priori. On the other hand, for the other types of thinning behaviour, the thinning paths can be determined only experimentally; therefore, the postulate can be used only to give an explanation of the observed behaviour and not to give an a priori prediction.

Interpretation of the four thinning 'patterns' of Hodgson and Woods[1]

The results in Figs. 1 to 5 show that uneven behaviour tends to occur with the combination of small film thicknesses and large rate of thinning (or dimple formation). This is intuitively expected since the shear stress inbalance[2] - which is essentially the basis for the postulate - can occur more readily with larger interface velocities. Consider now the application of this concept for the interpretation of the four thinning 'patterns' of Hodgson and Woods[1]. These four patterns are:

(i) Pattern I : rapid thinning and instantaneous coalescence,

(ii) Pattern II : rapid thinning, arrest, dimple formation and thinning,

(iii) Pattern III : uneven thinning, and

(iv) Pattern IV : slow even thinning.

The thinning paths for these four patterns are shown schematically

in Fig. 6 by the curves (a) to (d). The regions of even and uneven thinning are separated by the curves marked AOB; only one set of regions is shown for clarity of illustration.

Curve (a) is the thinning path for Pattern I; the rate of thinning is very large at all film thicknesses. This path lies in the uneven thinning because during rapid thinning there is insufficient surfactant to set up an interfacial tension gradient to balance the shear stresses at the interfaces.

Pattern II is described by curve (b). The rapid thinning is not followed by film rupture; it is arrested and then dimple formation begins, as indicated by the horizontal portion of curve (b). The initial dimple formation may occur evenly or unevenly depending on whether the path (b1) or (b2) is followed (cf. Fig. 5). Then the dimple formation becomes even because its rate decreases, and finally the dimple formation is arrested and thinning begins. The thinning may occur evenly or unevenly depending on whether the path (b3) or (b4) is followed.

Curve (c) corresponds to Pattern III. The rate of thinning is considerably smaller than that for rapid thinning; however, it is still sufficiently large to be in the uneven thinning region (cf. Fig. 3). If the thinning persists until the film is very thin, the pattern may become symmetrical. This has been observed experimentally; when the interference colour was grey to black, about 400 Å, the rate of thinning was very low and the film was practically uniform in thickness.

The rate of thinning for Pattern IV is very low; thus this path lies in the even thinning region, as shown by curve (d). If the rate of thinning remains low as the thinning proceeds, the even behaviour persists,

as shown by the path (d1) (cf. path a'-b'-c'-d' in Fig. 4). On the other hand, if the rate of thinning increases, as indicated by the path (d2), the behaviour may change to uneven (cf. path a-b-c in Fig. 4).

6.4. Summary and coclusions

1. A postulate for the conditions for even and uneven thinning has been put forward. This postulate states that even thinning occurs if and only if the tangential force balance equations at the interfaces can be satisfied under symmetrical conditions; that is,

(i) real values for the interface velocities exist, and

(ii) the surface concentrations are positive everywhere at the bulk and drop interfaces. Otherwise, the thinning is uneven.

2. The postulate has been analysed algebraically based on the parabolic representation of the pressure in the film. The experimental observations of even and uneven thinning (and dimple formation) for toluene and anisole drops were predicted correctly by the postulate. The four thinning patterns of Hodgson and Woods[1] can also be explained in terms of the postulate.

3. Uneven behaviour tends to occur with the combination of small film thicknesses and large rates of thinning or dimple formation.

Literature cited

1. Hodgson, T. D. and Woods, D. R., J.Coll.Intf.Sci., 30(1969):429.

2. Burrill, K. A. and Woods, D. R., J.Coll.Intf.Sci., 42(1973):15.

Figure captions

1. Postulate testing for the case of both interfaces having the same surface concentration, ϕ_7=1. The regions of even and uneven thinning are separated by the curves marked A, B, C and D for different drop sizes and surface concentrations expressed in terms of $k^* \Gamma_s$. The thinning paths of the data are shown by the dotted curves.

2. Generalization of the postulate testing for the case of ϕ_7=1. The regions of even and uneven thinning for different liquids and drop sizes (expressed in terms of the dimensionless group ϕ) and surface concentrations (expressed in terms of the dimensionless group $k^* \Gamma_s / \gamma$) are separated by the curves marked A, B and C. The broken lines marked n_M=0 and n_M=1.6 are the thinning paths given by the parallel disc model with constant interface mobility (Eq. 26); the thinning paths of the data are shown to be between these limits.

3. Postulate testing for the observed uneven thinning in anisole/water systems. The shaded area separate the even and uneven thinning regions for the expected range of surface concentrations. The thinning paths of the data are shown by the broken curves.

4. Postulate testing for the observed even thinning and change overs from even to uneven thinning. The shaded area bordered by AB separate the even and uneven thinning regions for the data marked ● , and A'B' for the data marked ▲ . The thinning paths are shown by the broken curves.

5. Postulate testing for dimple formation. The even and uneven thinning (dimple formation, in this case) are separated by the solid curves, and the thinning paths are shown by the broken curves.

6. Interpretation of the thinning paths of Hodgson and Woods[1]

in terms of the postulate. The regions of even and uneven thinning are separated by the solid curves marked AOB. The thinning paths (a) Pattern I: rapid thinning and instantaneous coalescence, (b) Pattern II: rapid thinning, arrest, dimple formation and thinning, (c) Pattern III: uneven thinning, and (d) Pattern IV: slow even thinning.

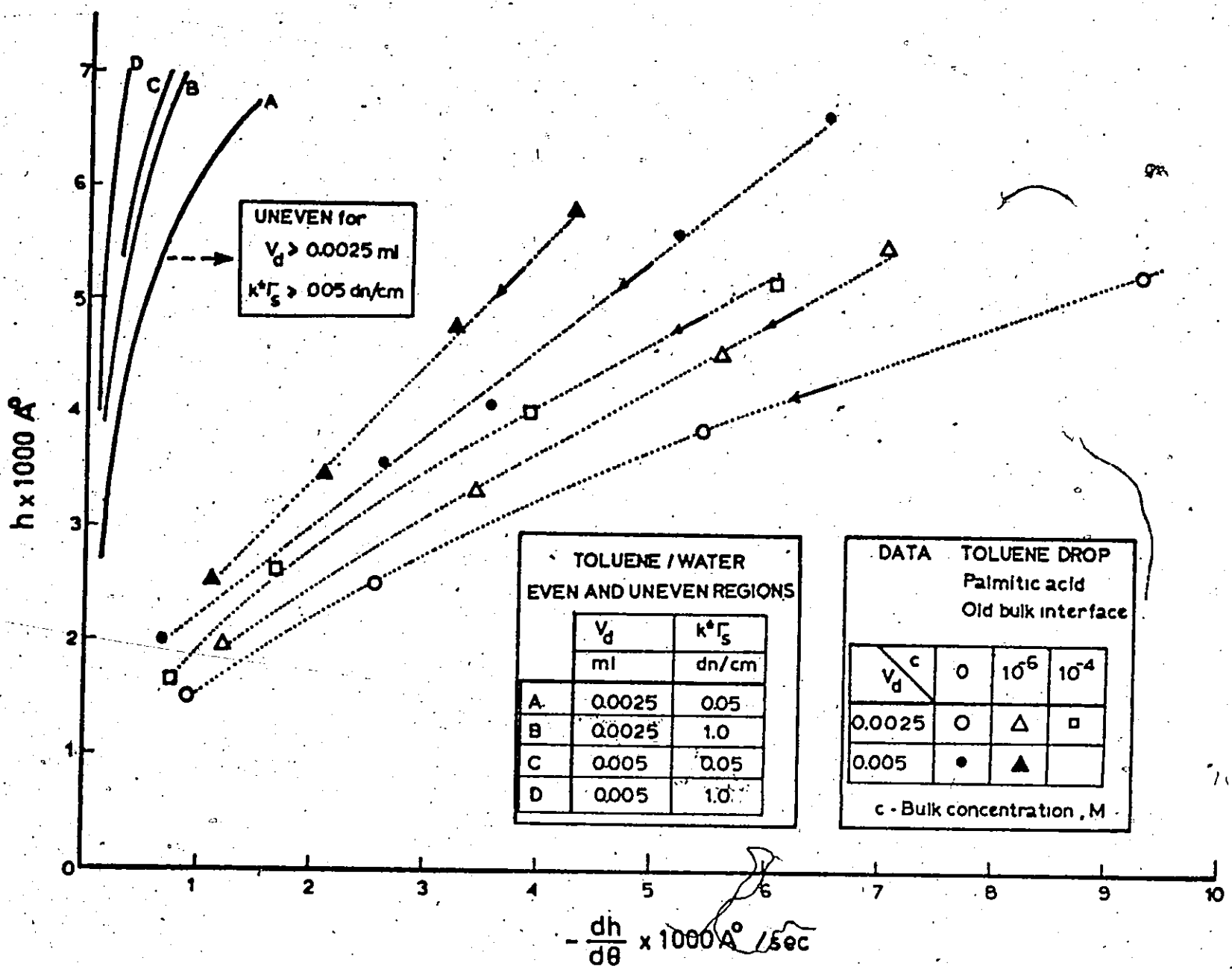
h x 1000 A°
- dh/dθ x 1000 A°/sec
A
B
C
D
UNEVEN for
V_d > 0.0025 ml
$k^*\Gamma_s$ > 005 dn/cm
TOLUENE / WATER
EVEN AND UNEVEN REGIONS
V_d ml
$k^*\Gamma_s$ dn/cm
A 0.0025 0.05
B 0.0025 1.0
C 0.005 0.05
D 0.005 1.0
DATA TOLUENE DROP
Palmitic acid
Old bulk interface
V_d \ c | 0 | 10^{-6} | 10^{-4}
0.0025 | O | Δ | □
0.005 | • | ▲ |
c - Bulk concentration, M

Figure 1

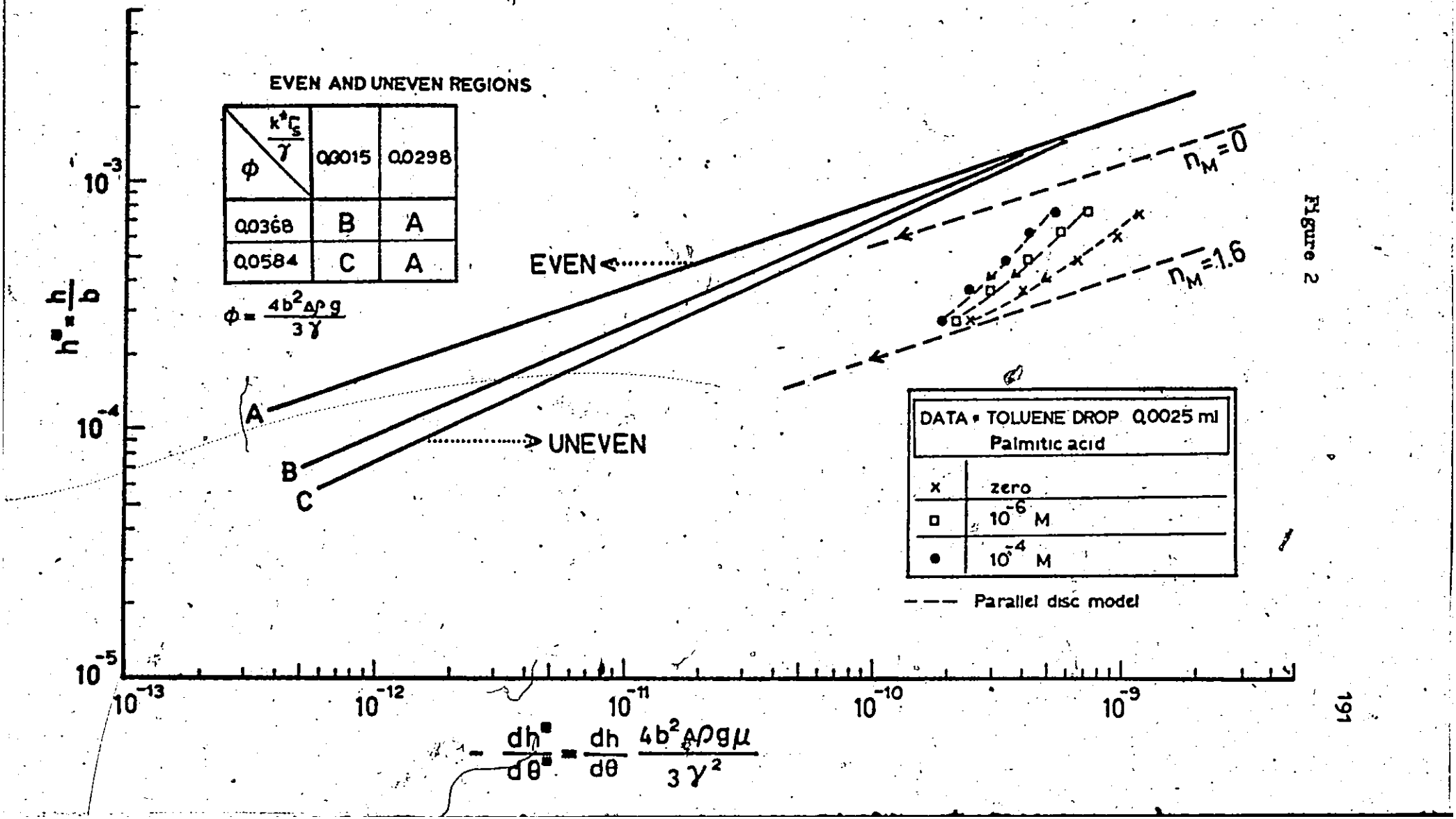
EVEN AND UNEVEN REGIONS
$\frac{k^*\Gamma_s}{\gamma}$ / ϕ
0.0015
0.0298
0.0368
B
A
0.0584
C
A
$\phi = \frac{4b^2\Delta\rho g}{3\gamma}$
EVEN
UNEVEN
A
B
C
$n_M = 0$
$n_M = 1.6$
DATA • TOLUENE DROP 0.0025 ml
Palmitic acid
x zero
□ 10^{-6} M
● 10^{-4} M
Parallel disc model
$h^* = \frac{h}{b}$
10^{-3}
10^{-4}
10^{-5}
10^{-13}
10^{-12}
10^{-11}
10^{-10}
10^{-9}
$-\frac{dh^*}{d\theta^*} = \frac{dh}{d\theta}\frac{4b^2\Delta\rho g\mu}{3\gamma^2}$

Figure 2

Figure 3

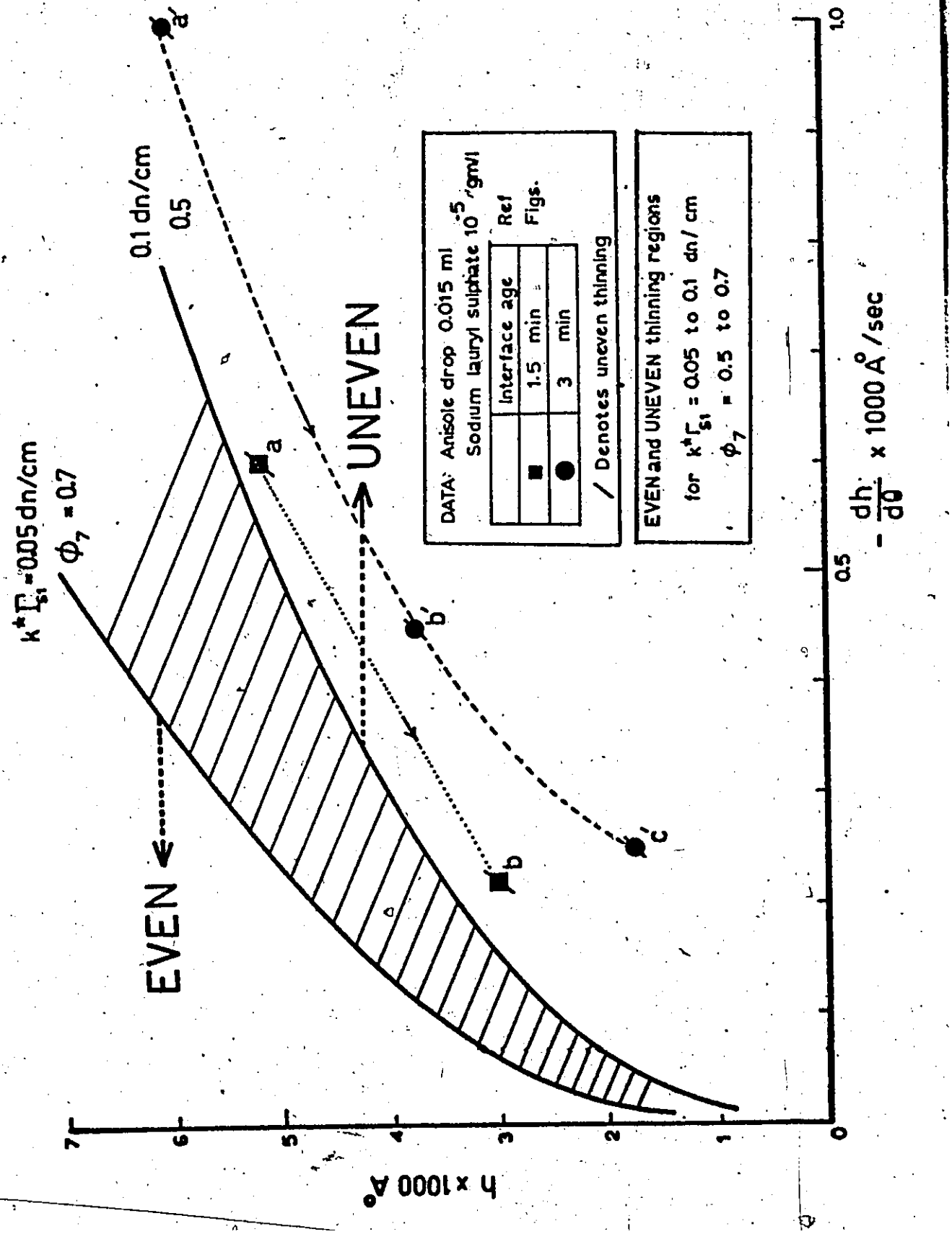
h x 1000 A°
7
6
5
4
3
2
1
0
0.5
1.0
$-\frac{dh}{d\theta}$ x 1000 A°/sec
EVEN
UNEVEN
0.1 dn/cm
0.5
$k^*\Gamma_{s1}$=0.05 dn/cm
ϕ_7 = 0.7
a
a'
b
b'
c'
DATA: Anisole drop 0.015 ml
Sodium lauryl sulphate 10^{-5} gm/l
Interface age
Ref Figs.
1.5 min
3 min
/ Denotes uneven thinning
EVEN and UNEVEN thinning regions
for $k^*\Gamma_{s1}$ = 0.05 to 0.1 dn/cm
ϕ_7 = 0.5 to 0.7

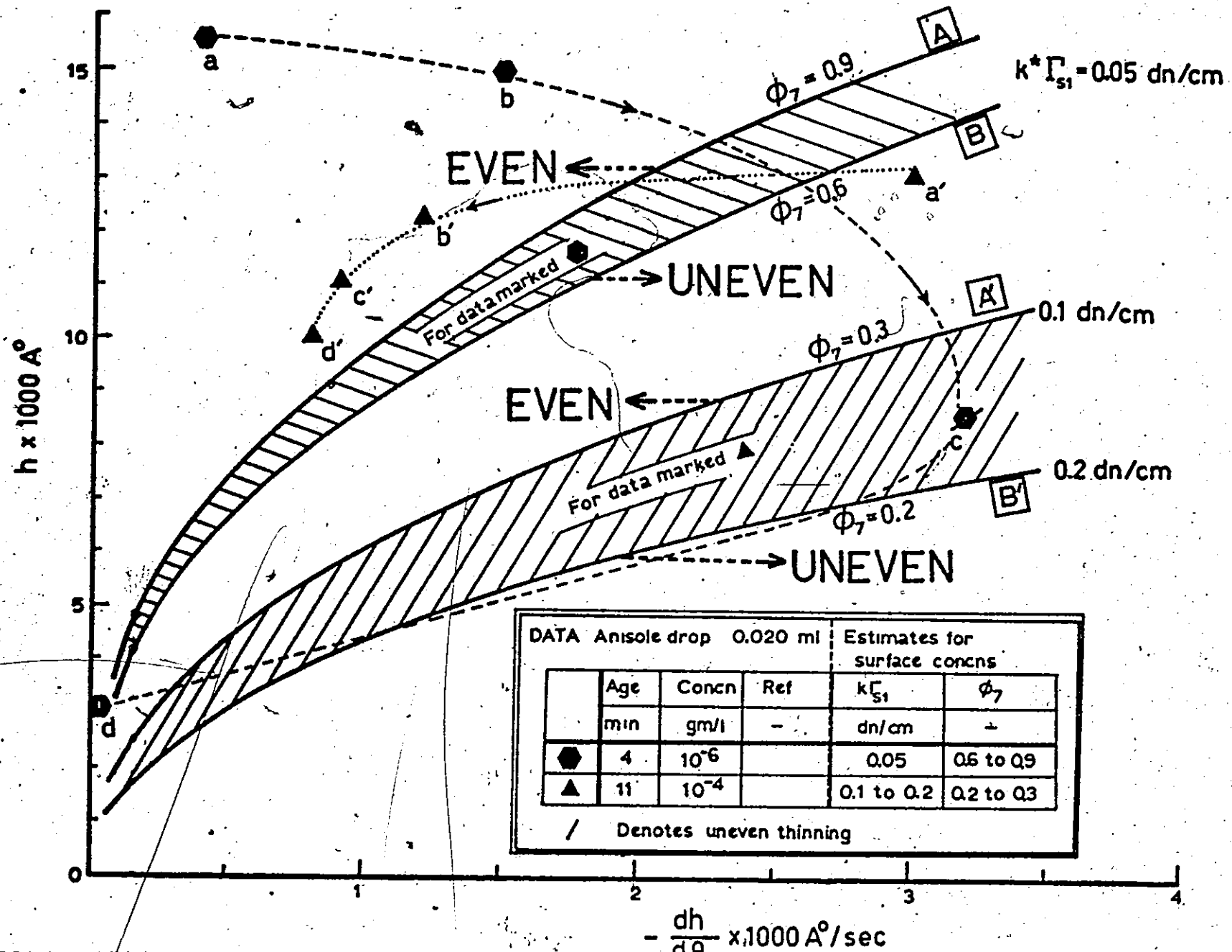

DATA Anisole drop 0.020 ml				Estimates for surface concns	
	Age	Concn	Ref	$k\Gamma_{s1}$	ϕ_7
	min	gm/l	–	dn/cm	–
●	4	10^{-6}		0.05	0.6 to 0.9
▲	11	10^{-4}		0.1 to 0.2	0.2 to 0.3

/ Denotes uneven thinning

Figure 4

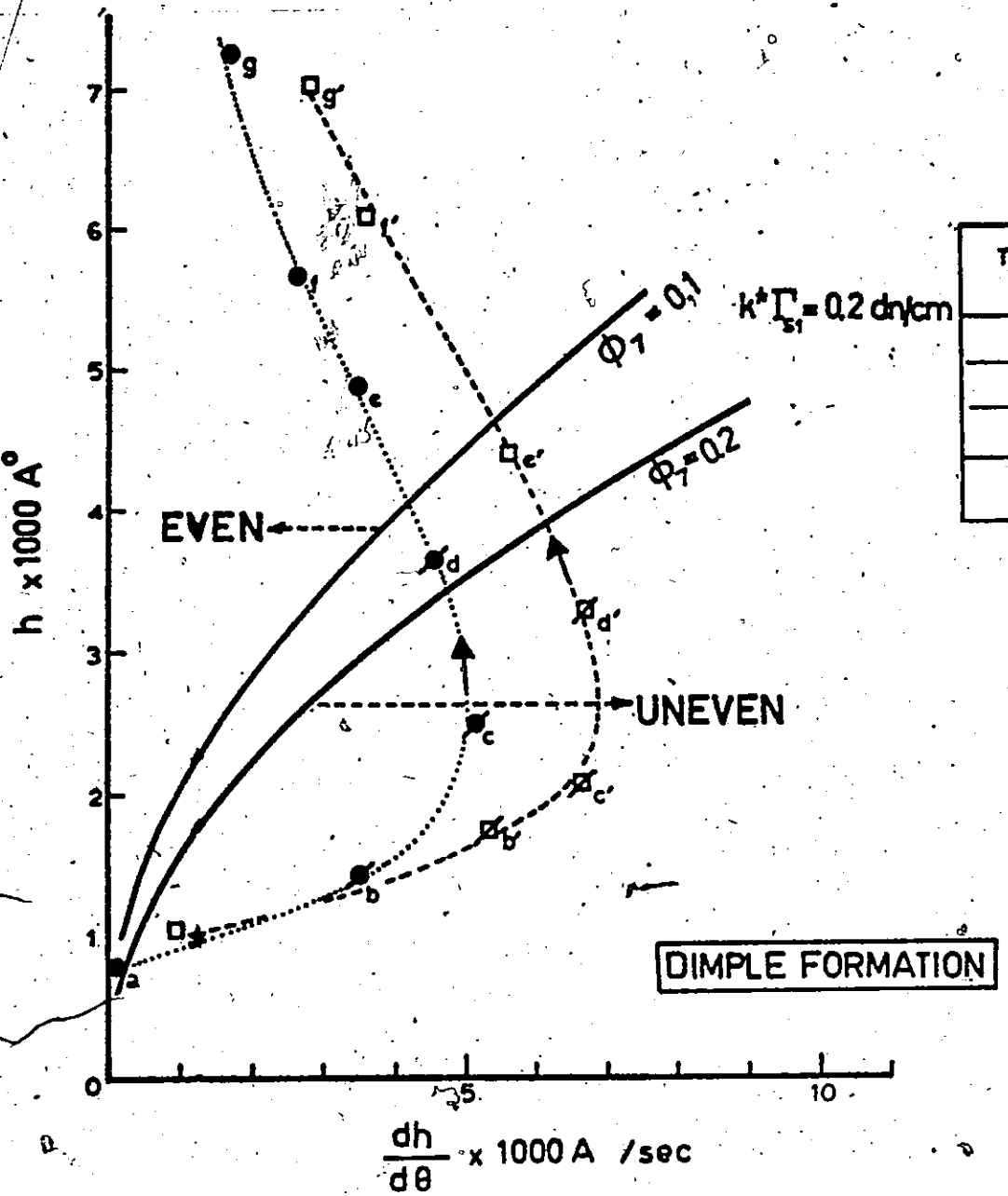
h x 1000 A°
$\frac{dh}{d\theta}$ x 1000 A /sec
EVEN
UNEVEN
$\Phi_1 = 0.1$
$\Phi_1 = 0.2$
$k^* \Gamma_{s_1} = 0.2$ dyn/cm
DIMPLE FORMATION
TOLUENE DROP 0.0025 ml
Zero surfactant concn
Bulk interface age
75 sec
450 sec
/ Denotes uneven behaviour

Figure 5

Figure 6

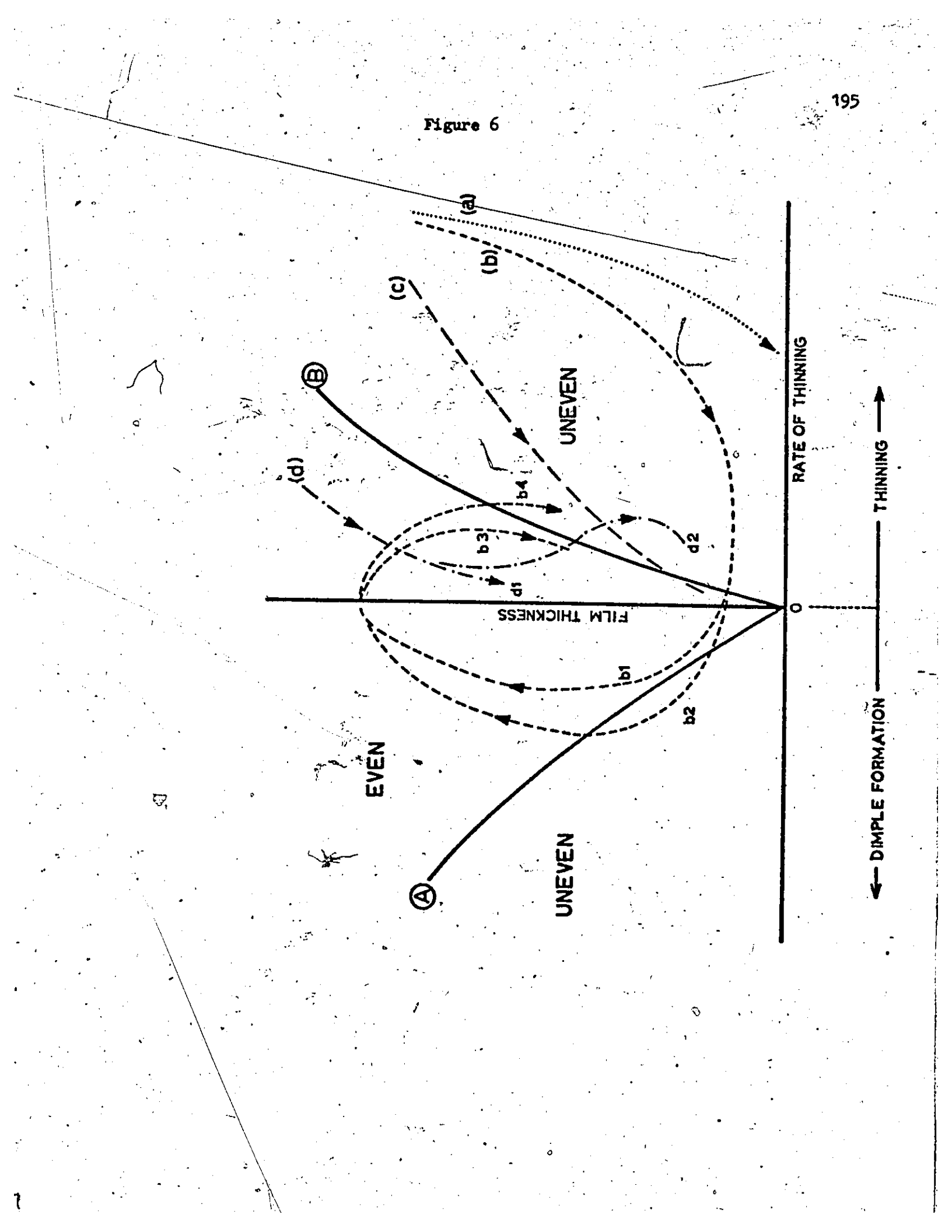
(a)
(b)
(c)
(d)
B
A
UNEVEN
UNEVEN
EVEN
b1
b2
b3
b4
d1
d2
FILM THICKNESS
O
RATE OF THINNING
THINNING
DIMPLE FORMATION

CHAPTER 7

SUMMARY AND CONCLUSIONS

The detailed conclusions have been given in Chapters 2 to 6. The general conclusions are now presented to give an overall view of this thesis and its major contributions.

Mathematical modelling of film thinning

1. In previously developed film thinning models, except in Burrill's model[1], the bulk and the drop interfaces were assumed to be completely immobile or fully mobile. This extreme mobility assumption neglected the effect of surfactant on the flow properties of an interface. Consequently, these models could not even account for the existence of different types of film thinning behaviour for the same liquids and drop size. Burrill's model, which assumed a fully mobile interface and calculated the mobility of the other interface, could show that different types of film thinning behaviour might occur. However, his model predicted film thinning behaviour that was opposite to what was observed.

In this thesis, a model has been developed in which the interface mobility of the bulk and drop interfaces is calculated. Because the interface mobility is not assumed arbitrarily, it is possible to put forward a postulate for the conditions for even and uneven thinning.

2. The numerical solution of this model, referred to as the polynomial model, has been obtained, and the results compared with experiment-

al observations. The polynomial model is capable of describing all types of film thinning behaviour including dimple formation and thinning. This result confirms this thesis' supposition that the main cause of failure of previously developed models is the incorrect assumption of extreme mobility.

By using the polynomial model, the variation with elapsed time of the pressure in the film, the interface velocities and the surface concentration distributions can be calculated. These calculations can increase our understanding of film thinning behaviour; for example, the calculations of the pressure in the film and the interface velocities during dimple formation show that thinning occurs in barrier ring because of the increase in the negative pressure gradient with elapsed time and the decrease in the interface velocities.

3. For the purpose of predicting rest times, an empirical model is more practical to use than a fundamental model. The extended parallel disc model has been developed to describe the rate of thinning at the barrier ring for uneven thinning. This type of film thinning behaviour has been chosen because the conditions for its occurrence are close to those found in practice. The extended parallel disc model satisfactorily describes the experimentally observed rate of thinning of toluene and anisole drops.

The extension of the parallel disc model by allowing the interfaces to have varying degrees of partial mobility has also been suggested by Hartland and Wood[2] for their work with large drops and viscous systems. However, in this thesis, the model has been applied to the film thickness at the barrier ring instead of the average thickness; hence, it is more directly applicable for predicting rest times. Furthermore, a different expression for partial mobility has been used which gives numerical values

that are consistent with the concept of interface mobility used in this thesis.

The results of the extended parallel disc model further show that the interface mobility should not be assumed constant.

4. The conditions under which thinning occurs evenly or unevenly have so far been unknown. A knowledge of these conditions is important, not only for a better understanding of film thinning behaviour, but also in the use of an empirical model because such a model can only be applied to one type of film thinning behaviour.

An algebraic analysis has been carried out of the postulate put forward in Chapter 2.4.2 for the conditions for even and uneven thinning. The analysis is based on a parabolic distribution of the pressure in the film. Despite the simplicity of the analysis, the occurrence of even or uneven thinning (or dimple formation) has been predicted correctly. The thinning patterns of Hodgson and Woods[3] can also be explained in terms of the postulate.

5. A similarity analysis[4] has been applied to obtain the dimensionless groups in the film thinning equations developed in Chapter 2. These dimensionless groups, which show how the system physical properties are combined in their effects on film thinning behaviour, are useful in the planning experiments with different liquids, surfactants and drop sizes so as to obtain a wide range of experimental conditions.

Experimental studies

6. A novel drop forming technique has been developed by which drops of different sizes can be formed using one drop forming nozzle without the need of piercing the bulk interface. This technique combines

the advantages of Hodgson's technique[3] (accurate and convenient) and those of the drop volume technique (no transfer of surfactant between the bulk and drop interfaces).

7. The film thickness measurements confirm the results of previous work - the sensitivity of film thinning behaviour to surfactant - and show observations that have not been previously reported. These are the occurrence of the uneven thinning Type A (Chapter 3.5) under the conditions that are close to those found in practice, and the new patterns which result when drops are released to the bulk interface in rapid succession. These observations suggest that an empirical approach should be adopted in the modelling of film thinning found in practice because of the difficulty in developing a fundamental non-symmetrical model, and indicate the complexity of the analysis of multiple drops coalescence.

Literature cited

1. Burrill, K. A., Ph.D. Thesis, McMaster University, Canada (1970).

2. Hartland, S. and Wood, S. M., A.I.Ch.E.J., 19(1973):810,871; see also Hartland, S. and Robinson, J. D., Can.J.Chem.Engng., 51(1973):647.

3. Hodgson, T. D. and Woods, D. R., J.Coll.Intf.Sci., 30(1969):429.

4. Hellums, J. D. and Churchill, S. W., Chem.Engng.Prog., Symp. Series #32, 57(1961):75.

APPENDIX A

THE SHEAR STRESS EXERTED BY THE BULK PHASE AT THE BULK INTERFACE

In the formulation of the film thinning equations given in Chapter 2, the bulk phase was assumed inviscid and hence the shear stress τ_b exerted by the bulk phase was neglected. While this assumption is valid for liquids with viscosity of the order of 0.01 poise, in general the shear stress must be calculated to solve the tangential force balance equation at the bulk interface.

This appendix presents a mathematical model for calculating the shear stress τ_b. The model is an extension of the problem of " Flow near a wall suddenly set into motion " [1].

1. The problem of " Flow near a wall suddenly set into motion "

The geometry of the problem is shown in Fig. 1. At time $\theta < 0$, the fluid is stationary and at $\theta = 0$ the wall is suddenly set into motion with a constant velocity U_1. The differential equation for the velocity profile $V_r(z, \theta)$ is (omitting the superscript which denotes the bulk phase)

$$\frac{\partial V_r}{\partial \theta} = \nu \frac{\partial^2 V_r}{\partial z^2} \qquad (1)$$

where ν is the kinematic viscosity. The boundary and initial conditions:

$$V_r = 0 \quad \theta \leqslant 0 \tag{2}$$

$$V_r = 0 \quad z = \infty \tag{3}$$

$$V_r = U_1 \quad z = 0 \tag{4}$$

2. Extension of the problem

During film thinning the flow in the bulk phase is caused by the movement of the bulk interface. It can be expected therefore that the differential equation governing the flow in the bulk phase is also given by Eq. (1); the difference lies in the boundary condition at z = 0, where the wall velocity (that is, the bulk interface velocity in this problem) varies with both position r and time θ .The boundary condition Eq. (4), which must be modified to account for the variation, becomes

$$V_r = U_1(r,\theta) \quad z = 0 \tag{5}$$

where $U_1(r, \theta)$ is the bulk interface velocity.

3. Solution of the extended problem

Define the Laplace transform of V_r by

$$\bar{V}_r(r,z,s) = L\left\{V_r(r,z,\theta)\right\} = \int_0^\infty V_r\, e^{-s\theta}\, d\theta \tag{6}$$

The differential equation Eq. (1) and the initial condition Eq. (2) can be transformed to give

$$s\,\bar{V}_r - 0 = \nu \frac{d^2\bar{V}_r}{dz^2} \tag{7}$$

which is an ordinary differential equation in z.

The solution of Eq. (7) is

$$\bar{V}_r = C_1(r,s)\exp\left(-\sqrt{\frac{s}{\nu}}\,z\right) + C_2(r,s)\exp\left(+\sqrt{\frac{s}{\nu}}\,z\right) \qquad (8)$$

Application of Eq. (3) gives $C_2 = 0$ and Eq. (5) gives

$$\bar{V}_r = \bar{U}_1 \exp\left(-\sqrt{\frac{s}{\nu}}\,z\right) \qquad (9)$$

where

$$\bar{U}_1 = L\{U_1\} \qquad (10)$$

The inverse transform of the exponential term in Eq. (9) is[2]

$$L^{-1}\left\{\exp\left(-\sqrt{\frac{s}{\nu}}\,z\right)\right\} = \frac{1}{2\sqrt{\pi\nu}}\,\frac{z}{\theta^{3/2}}\exp\left(-\frac{z^2}{4\nu\theta}\right) \qquad (11)$$

Therefore the inverse of $\bar{V}_r$ is given by the convolution theorem :

$$V_r = \frac{z}{2\sqrt{\pi\nu}}\int_0^\theta U_1(r,\zeta-\theta)\,\frac{1}{\zeta^{3/2}}\exp\left(-\frac{z^2}{4\nu\zeta}\right)d\zeta \qquad (12)$$

4. The shear stress at the bulk interface

The shear stress is given by

$$\tau_b = \mu\,\frac{\partial V_r}{\partial z} \quad \text{at } z=0 \qquad (13)$$

which can be calculated by differentiating Eq. (12) with respect to z and evaluating the result at z = 0. The final result is

$$\tau_b = \frac{1}{2}\sqrt{\frac{\rho\mu}{\pi}}\int_0^\theta U_1(r,\theta-\zeta)\,\frac{1}{\zeta^{3/2}}\exp\left(-\frac{z^2}{4\nu\zeta}\right)d\zeta\Bigg|_{z=0} \qquad (14)$$

which is the expression for the shear stress exerted by the bulk phase at the bulk interface which is moving with a velocity of U_1 (r,θ).

If the variation of U_1 with time is small, Eq. (14) can be simplified into

$$\tau_b = \sqrt{\frac{\rho\mu}{\pi\theta}}\ U_1 \qquad (15)$$

which is the same expression as that given by the original problem of " Flow near a wall suddenly set into motion".

Eq. (14) or the simplified form Eq. (15) is the expression needed to complete the tangential force balance at the bulk interface if the bulk phase cannot be assumed inviscid.

5. Literature cited

1. Bird, R. B. et al " Transport phenomena " John Wiley & Sons, New York (1960):124

2. Roberts, G. E. and H. Kaufman " Table of Laplace transforms " W. B. Saunders, Philadelphia (1966):246

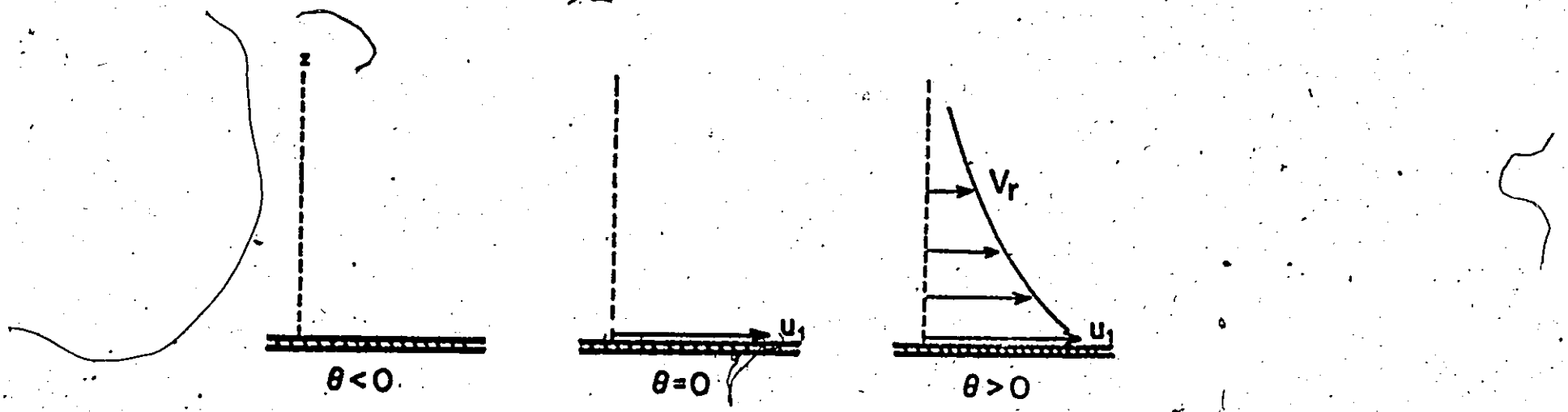

FIG. 1 : FLOW NEAR A WALL SUDDENLY SET INTO MOTION

APPENDIX B

ADSORPTION OF SURFACTANT MOLECULES AT AN AGING STATIONARY INTERFACE

The variation in interfacial tension with time after an interface has just been formed or cleaned shows that the adsorption of surfactant molecules at the interface is not accomplished instantaneously. The kinetics of the adsorption can be important in film thinning since it affects the surface concentration and therefore the interface movement.

This appendix describes a theory for the adsorption of surfactant at an interface, a method for testing the theory and the use of the theory in the modelling of film thinning. The theory was not used in the formulation of the film thinning equations in Chapter 2 because no experimental verification has been carried out. Attempts to measure the variation in interfacial tension using the pendant drop method failed because the required accuracy in the measurement of the pendant drop dimensions could not be obtained. Nevertheless, the theory is included in this thesis as a theoretical contribution to knowledge of the kinetics of adsorption of surfactant at an interface.

1. The adsorption mechanism

Fig. 1 shows the geometry of the interface and the bulk phase. The flat interface, set at coordinate $z = 0$, is infinitesimally thin and the bulk phase extends from a hypothetical sublayer at $z = 0$ to $z = \infty$.

At the initial time $\theta = 0$ when the interface has just been formed or cleaned, the interface and the sublayer do not contain surfactant, and as the interface ages, the transfer of surfactant from the bulk phase to the interface takes place by

(i) Fick's law bulk diffusion from the bulk phase to the sublayer and

(ii) Adsorption from the sublayer to the interface given by a first order reversible reaction mechanism.

2. Mathematical formulation

(i) The Fick's law bulk diffusion is given by

$$\frac{\partial c(z,\theta)}{\partial \theta} = \mathcal{D} \frac{\partial^2 c(z,\theta)}{\partial z^2} \qquad (1)$$

where $c(z,\theta)$ denotes the variation of bulk surfactant concentration with position z and interface age θ, and $\mathcal{D}$ is the bulk diffusion coefficient. The boundary conditions are specified at $z = \infty$ where the bulk concentration c_o is assumed constant, and at $z = 0$ where the bulk diffusional flux is equal to the increase in surface concentration. That is,

$$c(\infty,\theta) = c_o \qquad (2)$$

$$\mathcal{D}\frac{\partial c}{\partial z} = \frac{\partial \Gamma}{\partial \theta} \quad \text{at } z = 0 \qquad (3)$$

The initial condition is given by uniform bulk concentration, hence

$$c(z,0) = c_o \qquad z > 0 \qquad (4)$$

(ii) Adsorption from the sublayer to the interface:

$$\frac{\partial \Gamma}{\partial \theta} = -k_2 \Gamma + k_1 c_s \qquad (5)$$

where c_s is the sublayer concentration defined by

$$c_s(\theta) = c(0,\theta) \qquad (6)$$

and k_2 is the rate constant for desorption (in sec^{-1}) and k_1 is the rate constant for adsorption (in cm/sec). The initial condition is given by zero surface concentration, that is

$$\Gamma(0) = 0 \qquad (7)$$

The adsorption model contains two parameters k_1 and k_2 which are not independent. When the interface has sufficiently aged, the equilibrium condition is attained and hence the rate of adsorption is equal to zero. The surface concentration is given by the equilibrium concentration Γ_e, and the concentration at the sublayer is equal to that in the bulk phase; thus Eq. (5) becomes

$$\frac{d\Gamma}{d\theta} = 0 = k_1 c_0 - k_2 \Gamma_e$$

and hence

$$k_2 = \frac{k_1 c_0}{\Gamma_e}$$

where Γ_e and c_0 are related by the adsorption isotherm of the surfactant being considered. Therefore, the model contains only one independent parameter.

3. Transformation of the equations

Substitution of the following transformed variables

$c^* = \frac{c - c_o}{c_o}$	$\Gamma^* = \frac{k_1 \Gamma}{\mathcal{D} c_o}$	$\theta^* = \frac{k_1^2 \theta}{\mathcal{D}}$	$z^* = \frac{k_1 z}{\mathcal{D}}$

(8)

into Eqs. (1) to (7) gives

$$\frac{\partial c^*}{\partial \theta^*} = \frac{\partial^2 c^*}{\partial z^{*2}} \tag{1a}$$

$$\frac{\partial c^*}{\partial z^*} = \frac{\partial \Gamma^*}{\partial \theta^*} \quad \text{at } z^* = 0 \tag{2a}$$

$$c^*(z^*, o) = 0 \qquad z^* > 0 \tag{3a}$$

$$c^*(\infty, \theta^*) = 0 \tag{4a}$$

$$\frac{\partial \Gamma^*}{\partial \theta^*} = 1 + c_s^* - \gamma \Gamma^* \tag{5a}$$

$$\Gamma^*(o) = 0 \tag{7a}$$

where

$$\gamma = \frac{k_2 \mathcal{D}}{k_1^2} \tag{9}$$

4. Solution by Laplace transforms

Define the Laplace transforms of $c^*(z, \theta)$ and $\Gamma^*(\theta)$ by

$$\bar{c}(z^*, s) = \mathcal{L}\left\{c^*(z^*, \theta^*)\right\} = \int_0^\infty c^*(z^*, \theta)\, e^{-s\theta}\, d\theta \tag{10}$$

$$\bar{\Gamma}(s) = \mathcal{L}\left\{\Gamma^*(\theta)\right\} \tag{11}$$

Application of Laplace transformation to Eqs. (1a) to (7a) gives

$$\frac{d^2\bar{c}}{dz^{*2}} = s\,\bar{c} - 0 \tag{12}$$

$$\bar{c}(\infty, s) = 0 \tag{13}$$

$$\frac{d\bar{c}}{dz^*} = s\,\bar{\Gamma} - 0 \quad \text{at} \quad z^* = 0 \tag{14}$$

$$s\,\bar{\Gamma} = \frac{1}{s} + \bar{c}_s - \gamma\,\bar{\Gamma} \tag{15}$$

where

$$\bar{c}_s(s) = \bar{c}(0, s) \tag{16}$$

Integration of Eq. (12) gives

$$\bar{c} = C_1(s)\exp(-\sqrt{s}\ z^*) + C_2(s)\exp(\sqrt{s}\ z^*) \tag{17}$$

where $C_2 = 0$ by the application of the boundary condition Eq. (13). Hence Eq. (17) becomes

$$\bar{c} = C_1(s)\exp(-\sqrt{s}\ z^*) \tag{18}$$

The result of setting $z^+ = 0$ in Eq. (17) is

$$\bar{c}_s = \bar{c}(0, s) = C_1 \tag{19}$$

Differentiation of Eq. (17) with respect to z^+ and evaluation of the result at $z^+ = 0$ gives

$$\left.\frac{d\bar{c}}{dz^*}\right|_{z=0} = -\sqrt{s}\ \bar{C}_1(s) \tag{20}$$

Therefore, combination of Eqs. (19), (20), (14) and (15) gives

$$C_1(s) = \frac{1}{\sqrt{s}(s+\sqrt{s}+Y)} \tag{21}$$

$$\Gamma(s) = \frac{1}{s(s+\sqrt{s}+Y)} \tag{22}$$

Hence Eq. (18) becomes

$$\bar{c}(z^*,s) = \frac{1}{\sqrt{s}(s+\sqrt{s}+Y)} \exp(-\sqrt{s}\, z^*) \tag{23}$$

The bulk surfactant concentration $c^+(z,\theta)$ and the surface concentration $\Gamma^+(\theta)$ are calculated by inverting Eqs. (23) and (22) respectively. Consider now the inversion of Eq. (22).

The inversion is based on the following relationship[1]

$$L^{-1}\left\{\frac{1}{\sqrt{s}}\bar{\chi}(\sqrt{s})\right\} = \left[\frac{1}{\pi\theta}\right]^{\frac{1}{2}} \int_0^\infty \chi(\zeta) \exp\left(-\frac{\zeta^2}{4\theta}\right) d\zeta \tag{24}$$

where

$$L^{-1}\left\{\bar{\chi}(s)\right\} = \chi(\theta)$$

Eq. (22) can be written as

$$\bar{\Gamma}(s) = \frac{1}{\sqrt{s}\left[\sqrt{s}\left(\sqrt{s}^{\,2}+\sqrt{s}+Y\right)\right]} = \frac{1}{\sqrt{s}}\,\bar{\chi}(\sqrt{s}) \tag{22a}$$

where

$$\bar{\chi}(s) = \frac{1}{s(s^2+s+Y)} \tag{25}$$

Thus Eq. (22a) is now in the form given by Eq. (24). The inverse of Eq. (22a) depends on the numerical value of Y.

For convenience, let us define the following

$$L^{-1}\left\{\frac{1}{s^2+s+\gamma}\right\} = \eta(\theta) \qquad (26)$$

then the three possible cases and the corresponding inverses are:

Case 1 : $\gamma > 0.25$

$$\eta(\theta) = \frac{1}{\omega_1}\exp(-\tfrac{1}{2}\theta)\sin(\omega_1\theta)$$

$$\chi(\theta) = \int_0^\theta \eta(\zeta)\,d\zeta = \frac{1}{\gamma}\left\{1-\frac{1}{\omega_1}\exp(-\tfrac{1}{2}\theta)\left(\tfrac{1}{2}\sin\omega_1\theta+\omega_1\cos\omega_1\theta\right)\right\} \qquad (27)$$

$$\Gamma(\theta) = \frac{1}{\gamma}\left\{1-\frac{1}{\omega_1}\frac{1}{\sqrt{\pi\theta}}\int_0^\infty \exp(-\tfrac{1}{2}\zeta-\frac{\zeta^2}{4\theta})\left(\tfrac{1}{2}\sin\omega_1\zeta+\omega_1\cos\omega_1\zeta\right)d\zeta\right\}$$

where

$$\omega_1^2 = \gamma - 0.25 \qquad (28)$$

Case 2 : $\gamma = 0.25$

$$\eta(\theta) = \theta\exp(-\tfrac{1}{2}\theta)$$

$$\chi(\theta) = 2\left(2-(\theta+2)\exp(\tfrac{1}{2}\theta)\right) \qquad (29)$$

$$\Gamma(\theta) = 4-\frac{2}{\sqrt{\pi\theta}}\int_0^\infty (\zeta+2)\exp(-\tfrac{1}{2}\zeta-\frac{\zeta^2}{4\theta})\,d\zeta$$

Case 3 : $Y < 0.25$

$$\eta(\theta) = \frac{1}{2\omega_2}\left(\exp-(\tfrac{1}{2}-\omega_2)\theta - \exp-(\tfrac{1}{2}+\omega_2)\theta\right)$$

$$\chi(\theta) = \frac{1}{Y} - \frac{1}{2\omega_2}\left(\frac{1}{\frac{1}{2}-\omega_2}\exp-(\tfrac{1}{2}-\omega_2)\theta - \frac{1}{\frac{1}{2}+\omega_2}\exp-(\tfrac{1}{2}+\omega_2)\theta\right) \qquad (30)$$

$$\Gamma^*(\theta^*) = \frac{1}{Y} - \frac{1}{2\omega_2}\frac{1}{\sqrt{\pi\theta^*}}\int_0^\infty \left\{\frac{\exp-(\frac{1}{2}-\omega_2)\zeta}{\frac{1}{2}-\omega_2} - \frac{\exp-(\frac{1}{2}+\omega_2)\zeta}{\frac{1}{2}+\omega_2}\right\} \exp\left(-\frac{\zeta^2}{4\theta^*}\right) d\zeta$$

where

$$\omega_2^2 = 0.25 - Y \qquad (31)$$

Thus, given the parameter Y, the variation with interface age of Γ for a given bulk surfactant concentration c_o can be calculated from Eqs. (27), (29) or (30). It can be verified that at $\theta = 0$ the value of Γ^+ is equal to zero and as θ approaches ∞ the value of Γ^+ approaches $1/Y$, which is the dimensionless equilibrium surface concentration.

Fig. 3 shows the variation of Γ^+ with interface age for different values of k_1 but the same bulk surfactant concentration and bulk diffusion coefficient. As expected, the equilibrium surface concentration is reached sooner the larger the value of k_1.

5. Method of testing the model

To test the model, data as shown in Fig. 2a are required; that is, the variation of interfacial tension γ with interface age for different bulk surfactant concentrations. Also required are the equilibrium relationships between γ, Γ and c_o. For low bulk concentrations, the

equations are [2]

$$\Pi = \gamma_o - \gamma = RT\, A_1 \ln\left(\frac{x}{A_2} + 1\right) \tag{32}$$

$$\Gamma = A_1 \frac{x}{x + A_2} \tag{33}$$

$$\Pi = RT \ln \frac{A_1}{A_1 - \Gamma} \tag{34}$$

where A_1 and A_2 are the parameters and x is the bulk concentration in mole-fraction.

The outline of the model testing is as follows.

(i) Plot the equilibrium $\gamma_o - \gamma_e$ as a function of c_o as shown in Fig. 2b

(ii) Find the best values for A_1 and A_2 from Eq. (32) and Fig. 2b

(iii) For each bulk concentration calculate the variation of Γ with interface age from Fig. 2a and Eq. (34). (The implied assumption here is that the surface equation of state Eq. (34) applies at an aging interface) The results shown in Fig. 2c are now the 'experimental' variation of Γ with interface age and bulk surfactant concentration.

(iv) Calculate the best value of k_1 from Eq. (27), (29) or (30) and Fig. 2c.

If the model is valid, there should be a value of k_1 which gives a good fit between Fig. 2c and the predicted values given by Eq. (27), (29) or (30).

6. The use of the adsorption model in the modelling of film thinning

The expression for the rate of adsorption to the interface j_n,

needed in the surfactant mass balance equation at the interface Eq. (2-8), is given by

$$j_n = k_1 c_s - k_2 \Gamma \qquad (35)$$

where the values of k_1 and k_2 are known from the adsorption model.

To use Eq. (35) in a film thinning model, one must also solve the surfactant mass balance equation in the bulk phase, since the value of c_s is needed in Eq. (35). This value of c_s depends on the flow in the bulk phase, which in turn depends on the bulk interface velocity. Thus there exists a coupling between the equations for the surfactant mass balance (in the bulk phase and at the interface) and the tangential force balance at the interface.

An outline of the solution of this coupled set of equations is as follows:

(i) assume tentatively the bulk interface velocity,

(ii) solve the surfactant mass balance equations in the bulk phase and at the interface,

(iii) calculate the interfacial tension gradient, and

(iv) check the assumed value for the bulk interface velocity from the tangential force balance equation.

7. Literature cited

1. Roberts, G. E. and H. Kaufman " Table of Laplace Transforms" W. B. Saunders, Philadelphia (1966): 171

2. Lucassen-Rynders, E. H. and M. van den Temple, Proc. IV Cong. on Surface Active Agents, Sect. B, Vol. 2 (1964): 779

Figure captions

1. The geometry of the model. The bulk phase extends from $z = 0$ to $z = \infty$, the initial concentration is c_o and the variation in concentration is denoted by $c(z, \theta)$; the hypothetical sublayer is located next to the interface at $z = 0$, the initial concentration is zero and the variation in the sublayer concentration is denoted by $c_s(\theta)$, and the interface is located at $z = 0$, the initial surface concentration is zero and the variation in surface concentration is denoted by $\Gamma(\theta)$.

2. (a) Dynamic interfacial tension data, showing the variation in interfacial tension with interface age and bulk surfactant concentration, (b) Variation of surface pressure $\gamma_o - \gamma_e$ with bulk surfactant concentration, and (c) The calculated variation of surface concentration with interface age and bulk surfactant concentration.

3. Sample calculation of the model, showing the variation in surface concentration with interface age and the model parameter k_1.

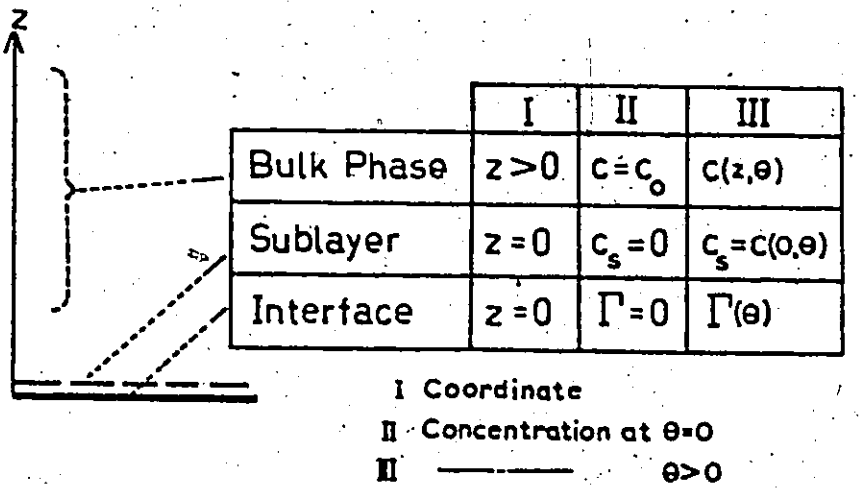

	I	II	III
Bulk Phase	$z>0$	$c=c_o$	$c(z,\theta)$
Sublayer	$z=0$	$c_s=0$	$c_s=c(0,\theta)$
Interface	$z=0$	$\Gamma=0$	$\Gamma(\theta)$

Figure 1.

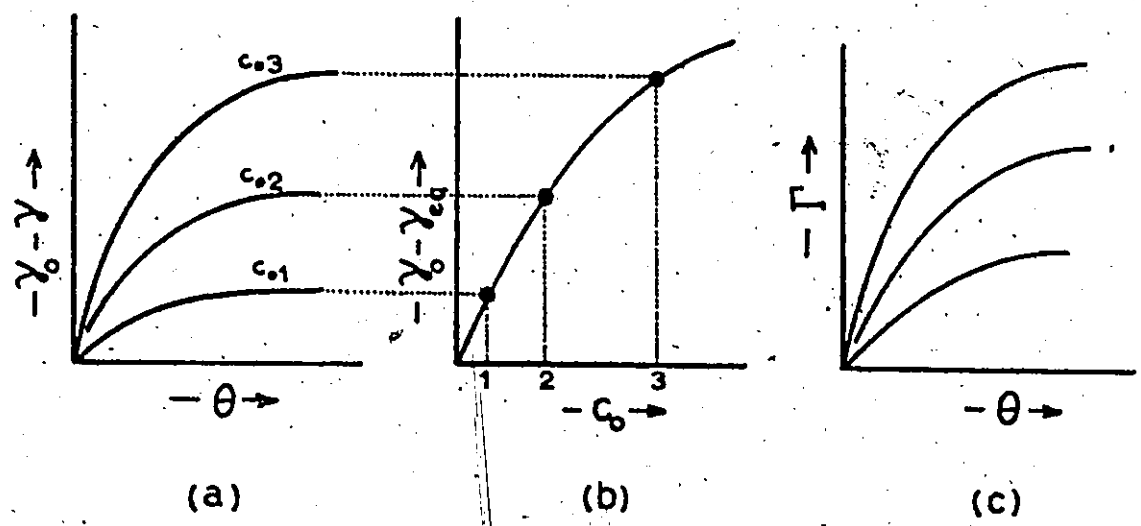

Figure 2

Figure 3

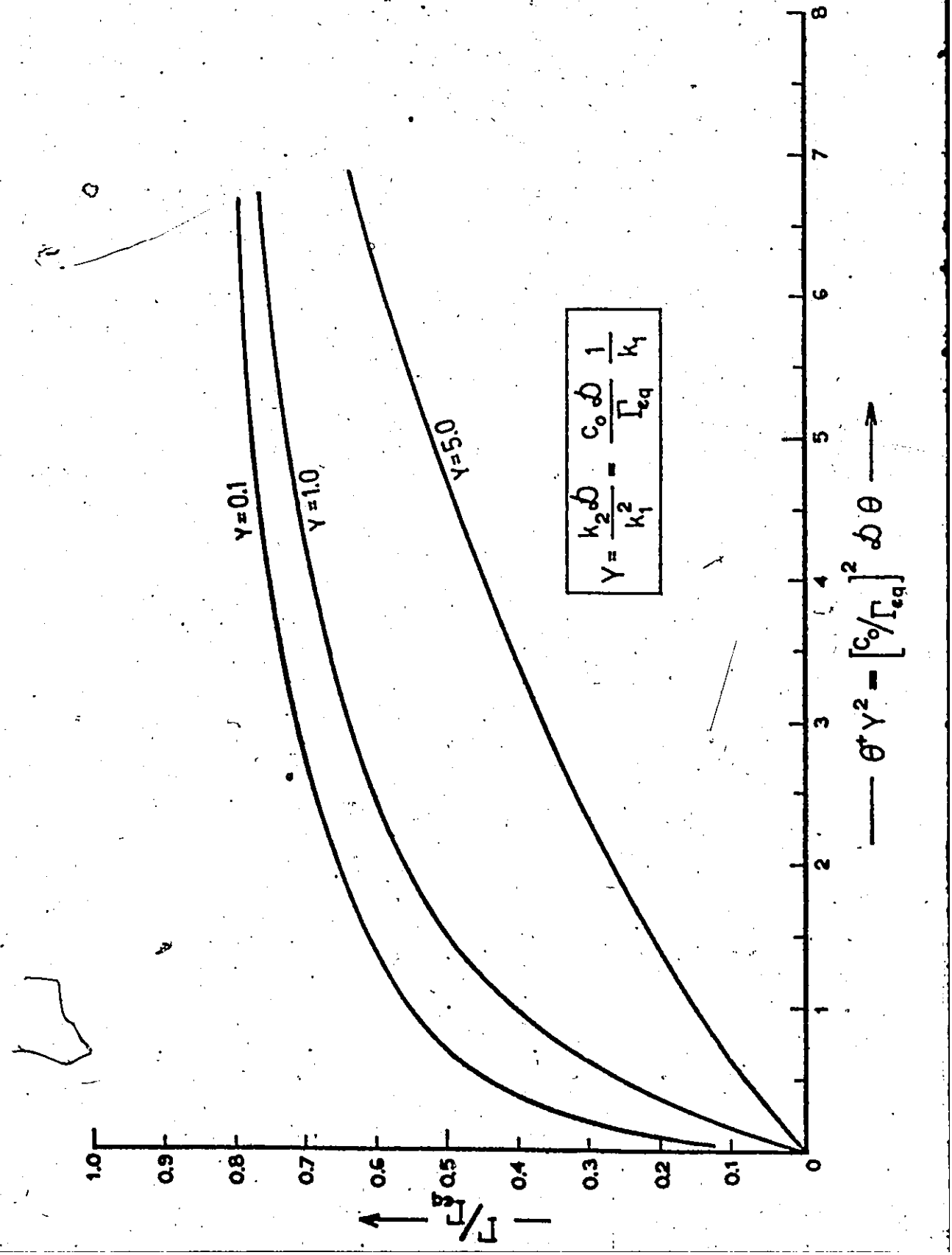
Γ/Γeq
1.0
0.9
0.8
0.7
0.6
0.5
0.4
0.3
0.2
0.1
0
1
2
3
4
5
6
7
8
θ*γ² = [c0/Γeq]² kd θ
γ=0.1
γ=1.0
γ=5.0
γ = k2d/k1² = c0 d/Γeq 1/k1

APPENDIX C

EXPERIMENTAL DETAILS

This appendix describes the procedures for assembling and operating the coalescence apparatus and the calibrations for photographing the interference patterns.

1. Assembly of the apparatus

The schematic diagram of the apparatus is shown in Fig. 1. The components of the apparatus were mounted on a frame by spring clamps or clamps, made of metal strips or woods, screwed to the frame. By this means the apparatus could be assembled quickly.

Prior to the assemby, the apparatus was cleaned according to the procedure described in Chapter 3.3. During the assembling of the apparatus polyethylene gloves were worn to prevent accidental touching with bare hands the parts that would come into contact with the oil and water. For assembling the teflon ring to the coalescence cell cover (cf Fig. 3-4) clean teflon coated tweezers were used.

The sequence of the assembly was as follows.

1. Assemble all the stop cocks
2. Mount the drop forming nozzle
3. Attach the tubes which connect the drop forming nozzle to the oil and water reservoirs '3' and '4' (Fig. 1)
4. Assemble the plungers and the micrometer screws to the Agla syringes '5' and '6'

5. Mount the oil and water reservoirs '3' and '5'

6. Assemble the coalescence cell (that is, teflon ring, interface cleaning probes, plugs, drop carrying tube and coalescence cell cover, cf Fig. 3-4)

7. Assemble the connecting tube '9'

8. Mount the make up oil and water reservoirs '7' and '8' and attach them to the coalescence cell.

2. Operation of the apparatus

2.1. Preliminary operation

The first step was to remove air from the drop forming nozzle and the connecting tubes. The procedure was as follows.

1. Fill the oil and water reservoirs '3', '4', '7' and '8'

2. Fill the coalescence cell with water to a level higher than the drop carrying tube but lower than the coalescence cell cover

3. Remove air from the drop forming nozzle

- withdraw water from the coalescence cell to the drop forming nozzle using Agla syringe '5'

- flush air to the water reservoir '3'

- repeat until all the air in the drop forming nozzle is removed (Note: at all times the water level in the coalescence cell must be maintained above the drop carrying tube)

4. Remove air from Agla syringe '6' to the oil reservoir '4' by moving the plunger up and down.

5. Let oil flow from the oil reservoir '4' to the tip of the capillary tube in the drop forming nozzle (this displaces air from the

tube connecting the drop forming nozzle and the oil reservoir '4' to the connecting tube '9')

6. Remove the air in the connecting tube '9' by letting water flow from the water reservoir '3' to the coalescence cell.

7. Fill the coalescence cell with oil from the make up oil reservoir '8'

8. Adjust the bulk interface level in the coalescence cell by draining or adding water (from reservoir '7') using the stop cock connected to the coalescence cell and the make up water reservoir '9'.

2.2. Drop formation

The procedure for drop formation was as follows.

1. Position the plungers in the Agla syringes in the bottom position

2. Raise the plunger in Agla syringe '6' until oil reaches the tip of the capillary tube in the drop forming nozzle

3. Meter the desired volume of drop using the micrometer screw

4. Inject slowly water from Agla syringe '5' to cut the oil slug and then inject more water to separate the oil drops

5. Repeat the last two steps to form more drops

(Note: during the metering of the oil slug, the three-way stop cock connected to Agla syringe '5' should be in closed position, and in the next step of cutting the oil slug, the three-way stop cock connected to Agla syringe '6' should be in closed position)

The micrometer was graduated such that the volume of oil delivered could be measured within 0.00005 ml[1].

2.3. Drop centering at the bulk interface

Because of the narrow field of view of the microscope for observing the interference colours , it was necessary to ensure that the drop did not roll at the bulk interface. The tip of the tube where the drops drops were released, therefore, had to be directly underneath the highest position at the bulk interface. The procedure was as follows.

1. Focus the microscope at the bulk interface directly above the tip of the drop carrying tube (cf Fig. 3-4)

2. Release a drop to the bulk interface and check if the drop rolls out of the microscope field of view. If not, the drop is properly centered

3. Adjust the position of the coalescence cell cover until the drop is centered. (The adjustments change the position of the teflon ring and therefore the bulk interface curvature relative to the drop carrying tube.)

2.4. Bulk interface cleaning

The procedure was as follows.

1. Adjust the level of the bulk interface in the coalescence cell (Section 2.1. step 8) so that the tip of the interface cleaning probe is just underneath the bulk interface

2. Open the stop cocks in the interface cleaning probes and withdraw about 5 ml of liquid from each interface cleaning probe. (If the bulk interface level is properly positioned the liquid withdrawn should be an equal mixture of oil and water)

3. Calibrations for photographing the interference colours

Filming speed

The actual filming speed of the cine camera was calibrated by

photographing a stop watch. Fig. 2 shows the calibration curve at 12 frames/sec setting. The actual speed was 12.35 frames/sec - corresponding to 0.081 sec between two successive frames.

Balancing filters

The camera film was specified for tungsten light 3200 ^{o}K colour temperature, whereas the colour temperature of the light source was measured at 2650 ^{o}K (set at 110 volts AC and 7 volts DC, cf Table 3-I). The balancing filters needed to obtain the true colour of the interference patterns were chosen from the table given by Feininger[2] (Table 3-I)

Aperture setting

The correct aperture setting was determined by trial and error. The result was full aperture opening at f/1.1 and the light source set at 110 volts AC and 7 volts DC.

Scale calibration

A microscope graticule was photographed in two mutually perpendicular directions under the same conditions as those for photographing the interference patterns. The photographs of the graticule served two purposes. The first was to measure radial distances in the film and the second was to allign the position of the movie analyser (projector) with respect to the screen where the interference patterns were projected and measured (when the proper allignment was obtained, there was no distortion of the projected image of the graticule in both directions).

Colour calibration

The relationship between interference colour and film thickness is

shown in Table I [3,4]. The measurement of film thickness is thus based on the identification of the interference colour and the order to which the colour belongs. Thus it is necessary to become familiar with the colours in the different orders. For this purpose an experiment as shown diagramatically in Fig. 3 was carried out. Two convex lenses were pressed against one another and the thickness of the air gap between the lenses was measured by the white light interference technique. By varying the position of the lower lens, it was then possible to photograph colours belonging to different orders and use them as standards. Some of the photographs are shown in Fig. 4.

The results of the experiments showed that the colours given in Table I were complete and that at large film thicknesses there was a tendency for one of the colours to be shifted. The green-pink sequence at large film thicknesses appeared in the photographs as blue-white sequence. This might be caused by the shift in one of the colours as a result of imperfection in the camera lens called chromatic abberation. (That is, because of the difference in wave lengths different colours are focussed at different locations in the camera film).

4. Notes on additional experimental observations

Several observations were noted during the process of cleaning the apparatus and storing the chemicals which could be important for obtaining reproducible data. These were:

(i) Electrostatic charge on the teflon components: After the cleaning procedure was completed, it was observed that the teflon components possessed an electrostatic charge. The source of the charge was unknown;

however, the charge could be neutralized by simply immersing the teflon components in a water containing an electrolyte.

(ii) Adsorption of gaseous contaminants at clean glass surfaces: One of the properties of clean glass surfaces is that they are wetted by water. It was observed that when a clean glass component was left to dry in the oven for two days or longer, the glass surface was no longer wetted by water (the appearance of droplets instead of film of water). The cause could be the adsorption of gaseous contaminants from the surrounding air. It is therefore important that the apparatus is assembled as soon as possible after the cleaning and drying processes are completed.

(iii) Contamination from containers: When distilled water was stored in a polyethylene container, it was observed that within one week the electrical conductivity of the water had increased two to three times the original value of about one micromho. The increase in conductivity was not observed when a glass container was used. Therefore a glass cotainer should be used for storage.

5. Literature cited

1. Calibration specification of Agla brand Micrometer Syringe Outfit, Burroughs Wellcome & Co, London, England.

2. Feininger, A. " Successful color photography " Prentice Hall Englewood Cliffs, N. J., 4th ed. (1966):137

3. Lawrence , A. C. S. "Soap films" Bell & Sons, London (1929)

4. Burrill, K. A., Ph. D. Thesis, McMaster University, Hamilton, Can. (1970):417

TABLE I. Interference colour - Film thickness relationship

(For films with a refractive index of 1.33)

COLOUR	THICKNESS*	COLOUR	THICKNESS
First order		Fourth order	
Black	0.2 - 0.4	Green (grass)	6.2 - 6.5
Grey	0.4 - 0.8	Green	6.5 - 7.0
White	0.8 - 1.2	Yellow (greenish)	7.0 - 7.5
Brown (light)	1.2 - 1.4	Red (carmine)	7.5 - 8.3
Brown (dark)	1.4 - 1.8		
Purple	1.8 - 2.2	Fifth order	
		Green	8.3 - 9.2
Second order		Pink	9.2 - 10.3
Purple	2.2 - 2.3		
Blue (dark)	2.3 - 2.5	Sixth order	
Blue	2.5 - 2.7	Green	10.3 - 11.3
Green (bluish)	2.7 - 2.9	Pink	11.3 - 12.4
Green	2.9 - 3.2		
Green (yellowish)	3.2 - 3.3	Seventh order	
Yellow	3.3 - 3.5		
Orange	3.5 - 3.7	Green	12.4 - 13.5
Red (crimson)	3.7 - 3.9	Pink	13.5 - 14.7
Third order			
Purple (deep)	3.9 - 4.1		
Purple	4.1 - 4.3		
Blue (dark)	4.3 - 4.4		
Blue	4.4 - 4.6		
Green (bluish)	4.6 - 4.8		
Green (emerald)	4.8 - 5.1		
Green (yellowish)	5.1 - 5.5		
Red (carmine)	5.5 - 5.9		
Red (bluish)	5.9 - 6.2		

* - In thousands of Angstroms

- To convert the table for films with a refractive index of n, multiply the thicknesses by (1.33/n).

Figure captions

1. Schematic diagram of the apparatus. The insert shows the cross-section of the drop forming nozzle.

2. Calibration curve of the cine camera set at 12 frames per second. The actual speed was 12.35 frames per second, corresponding to 0.081 sec between two frames.

3. Schematic diagram of the apparatus for 'colour calibration'. The diagram on the left shows the mechanism of the formation of interference colour.

4. Sample results of the colour calibration experiment: the interference colour at the centre (a) grey, 400 to 800 A^{o} (b) dark brown, 1400 to 1800 A^{o} (c) third order green, 4800 to 5100 A^{o} and (d) fourth order green, 6450 to 6950 A^{o}.

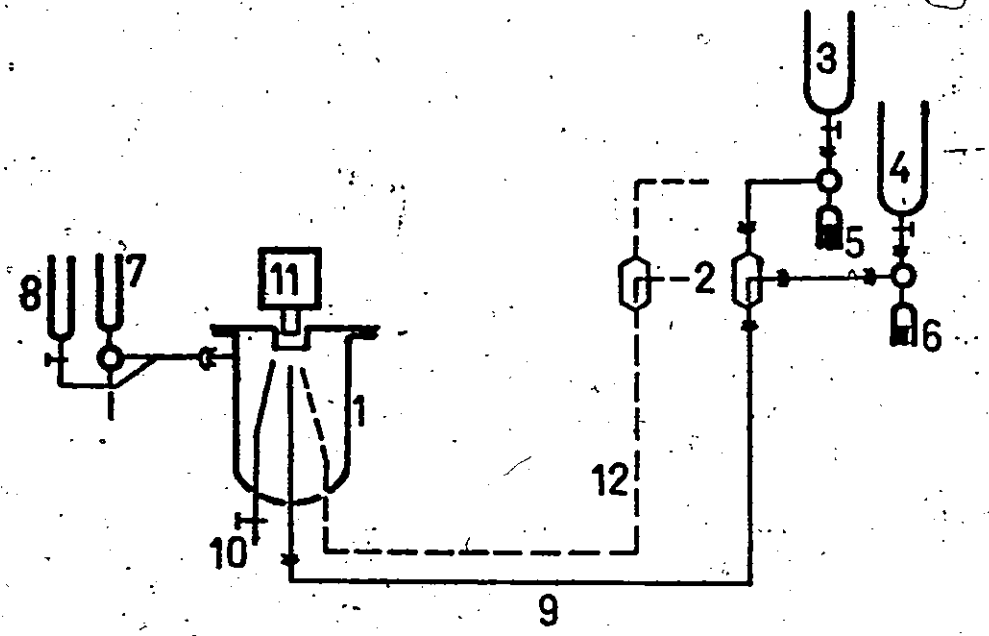

1	Coalescence Cell	9	Connecting Tube
2	Drop Forming Nozzle	10	Interface Cleaning Probe
3	Water Reservoir	11	Microscope and Camera
4	Oil Reservoir	12	Extension for Multi-drops
5,6	Agla syringe	—|	Two-way Stopcock
7	Make up Water Reservoir	—⊙—	Three-way Stopcock
8	Make up Oil Reservoir	—⊃—	Ball&Socket Joint

Figure 1

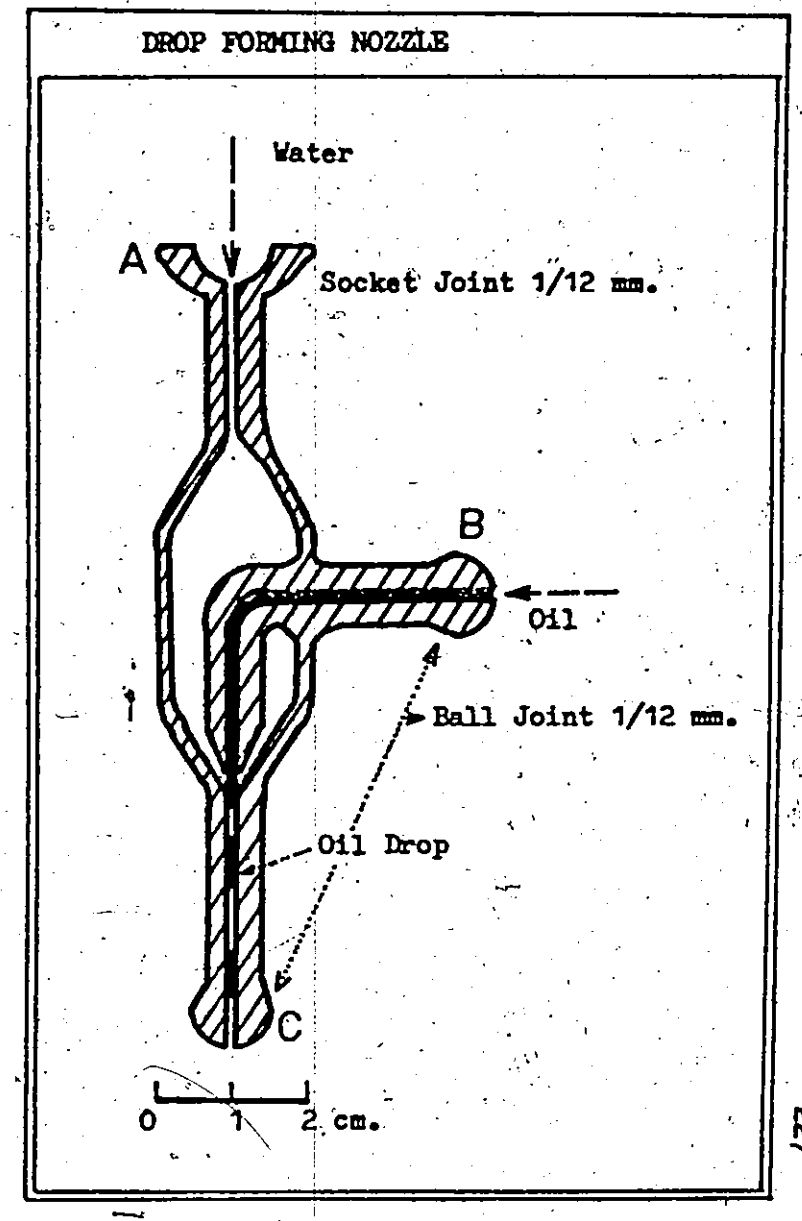

Figure 2

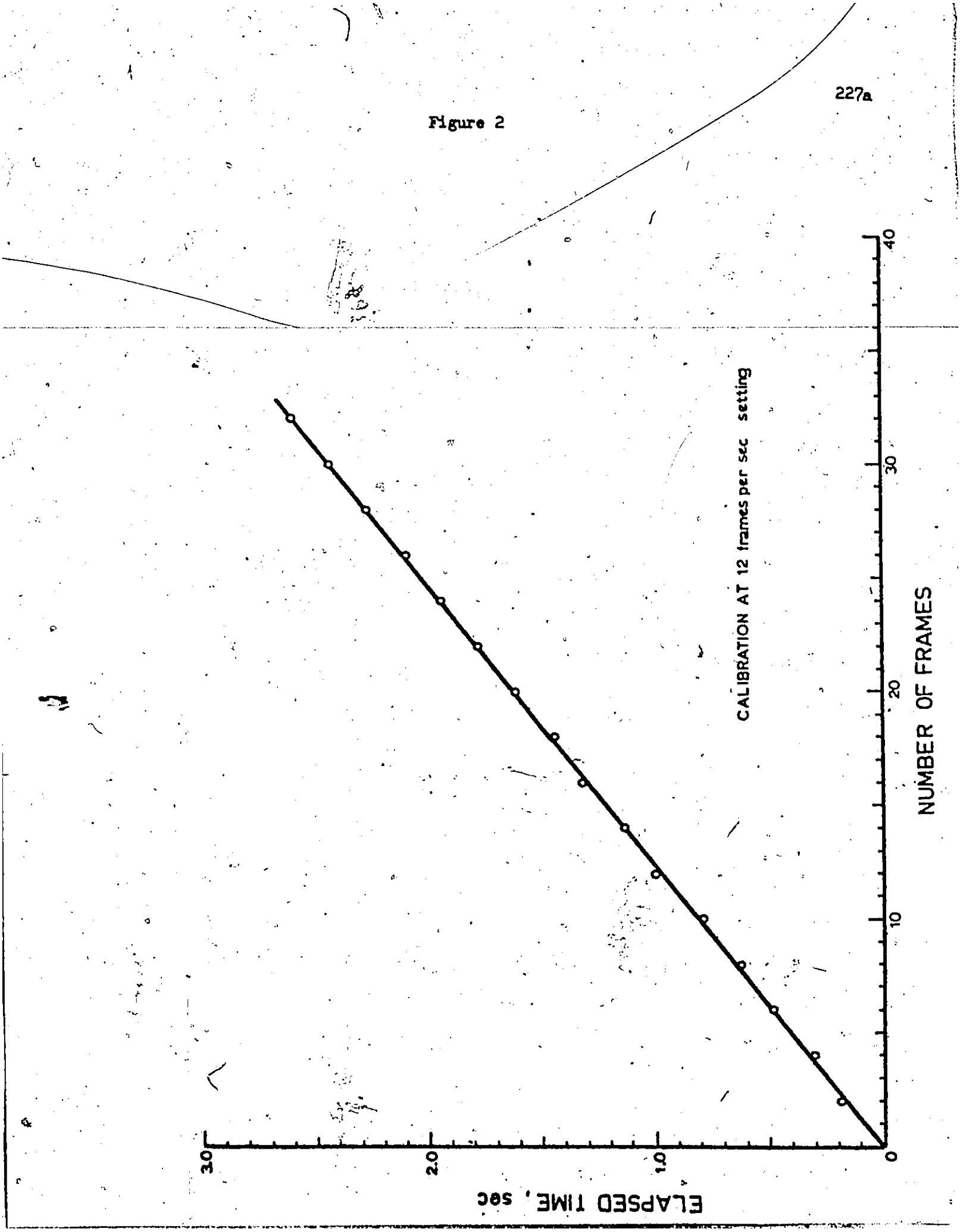
CALIBRATION AT 12 frames per sec setting
ELAPSED TIME, sec
NUMBER OF FRAMES
0
1.0
2.0
3.0
10
20
30
40

Figure 3

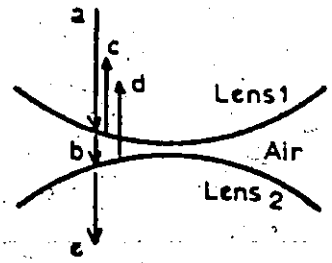

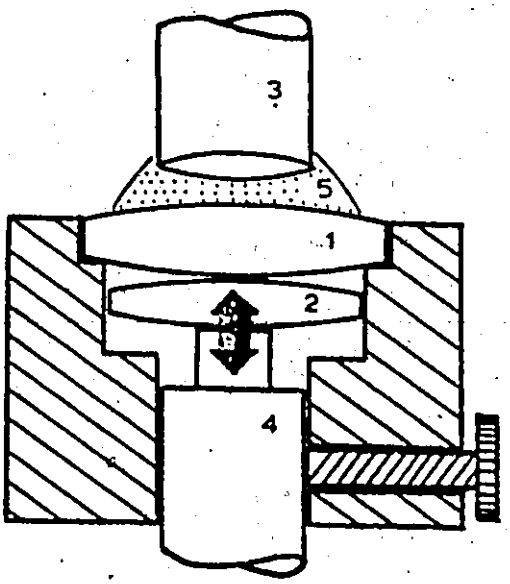

MECHANISM OF INTERFERENCE	APPARATUS
a Light source	1 Upper lens (fixed)
b Transmitted part of (a)	2 Lower lens (movable)
c Reflected part of (a)	3 Microscope and camera
d Reflected part of (b)	4 Micrometer screw
e Reflected part of (b)	5 Immersion oil
(c) and (d) form interference	

Figure 4

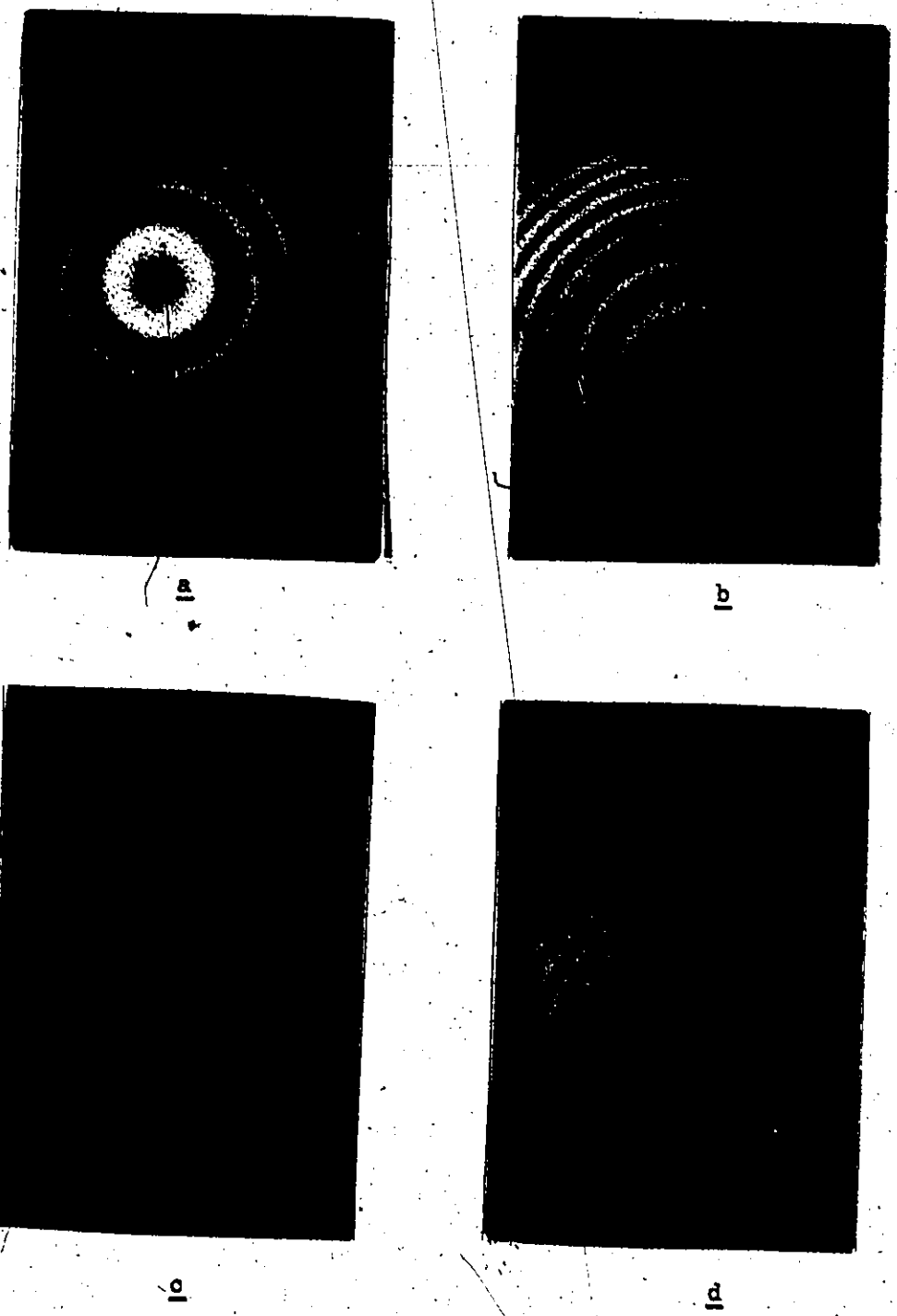

a b c d

APPENDIX D

DETAILS OF THE NUMERICAL SOLUTION OF THE POLYNOMIAL MODEL

This appendix describes the numerical calculation of the solution of the polynomial model which has been left out of the main text Chapter 4. The corresponding sections in Chapter 4 are shown by the numbers in parantheses given at the end of the section headings.

1. The solution of the pressure boundary conditions (4.2.1)

The boundary conditions Eqs. (4-11) to (4-13) can be expressed in terms of the polynomial coefficients by

$$\sum_{n=0}^{N}{}_{e} \frac{2}{n+2} A_n R_p^{n+2} = \psi \qquad (1)$$

$$\sum_{n=0}^{N}{}_{e} A_n R_p^{n} = 0 \qquad (2)$$

$$\sum_{n=2}^{N}{}_{e} n A_n R_p^{n-2} = 0 . \qquad (3)$$

where the subscript e denotes that the summation is taken over even numbers of n.

Because these boundary conditions must always be satisfied, there are only $(\frac{1}{2}N - 1)$ coefficients of A_n which can be chosen independently in the fitting of the film thickness profile. If A_0, A_2 ... A_{N-4} are chosen as the independent coefficients, then the values of A_{N-2}, A_N and R_p can be calculated from Eqs. (1) to (3). Thus all the film thickness

coefficients L_n, needed to satisfy Eq. (4-21) for fitting the film thickness profile, can be calculated from the normal force balance equation Eq. (4-20). In this thesis the value of N = 8 was used and the three-dimensional minimization problem was solved using the Rosenbrock search technique[1].

Consider now the calculation of A_{N-2}, A_N and R_p from Eqs. (1) to (3). Elimination of A_N from Eqs. (2) and (3) gives

$$A_{N-2} = -\frac{1}{R_p^{N-2}} \sum_{n=0}^{N-4}{}_e \frac{1}{2}(N-n) A_n R_p^n \tag{4}$$

Similarly, elimination of A_{N-2} from Eqs. (2) and (3) gives

$$A_N = \frac{1}{R_p^N} \sum_{n=0}^{N-4}{}_e \frac{1}{2}(N-2-n) A_n R_p^n \tag{5}$$

Substitution of Eqs. (4) and (5) into (1) gives the equation for solving R_p. The result is

$$f(R_p^2) = \sum_{n=0}^{N-4}{}_e \left\{ \frac{2}{n+2} - \frac{N-n}{N} + \frac{N-2-n}{N+2} \right\} A_n (R_p^2)^{\frac{n+2}{2}} - \psi = 0 \tag{6}$$

The solution of Eq. (6) by the Newton Raphson method is given by

$$R_p^{2\,(j+1)} = R_p^{2\,(j)} - \frac{f}{f'}\Big|_{R_p^{2\,(j)}} \tag{7}$$

where the superscript j denotes the iteration number and f' is the derivative of f with respect to R_p^2 given by

$$f' = \sum_{n=0}^{N-4}{}_e \frac{n+2}{2} \left\{ \frac{2}{n+2} - \frac{N-n}{N} + \frac{N-2-n}{N+2} \right\} A_n (R_p^2)^{\frac{n}{2}} \tag{8}$$

After R_p is calculated from Eq. (6), the values of A_{N-2} and A_N can be readily calculated from Eqs. (4) and (5) respectively.

2. The initial condition problem: calculation of interface velocities and surface concentrations (4.2.2)

The calculation of the interface velocities and surface concentrations involves the computation of derivatives and integrals of variables which can only be calculated numerically at discrete radial locations in the film. The method used to compute derivatives or integrals is to fit a Chebysev polynomial for the variable and then differentiate or integrate the polynomial. The following section reviews the use of Chebysev polynomials for curve fitting and summarizes the properties which are of interest in this thesis.

2.1. Chebysev polynomials for curve fitting[2]

The n^{th} member of Chebysev polynomial is defined by

$$T_n(r) = \cos n (\cos^{-1} r) \tag{9}$$

which satisfies the recurrence relationship

$$T_{n+1} = 2 r T_n - T_{n-1} \tag{10}$$

From the definition of T_n it can be shown that

$$\begin{aligned} T_0 &= 1 \\ T_1 &= r \end{aligned} \tag{11}$$

and hence the expressions for higher members of T_n can be derived from Eq. (11) and the recurrence relationship Eq. (10)

The properties of interest are:

(i) Integration

$$\int T_n\,dr = \begin{cases} T_1 & , n=0 \\ \frac{1}{4}(T_2+T_0) & , n=1 \\ \frac{1}{2}\left(\frac{1}{n+1}T_{n+1} - \frac{1}{n-1}T_{n-1}\right) & , n>1 \end{cases} \qquad (12)$$

(ii) Differentiation

$$\frac{d}{dr}T_{2n} = 4n\sum_{j=1}^{2n-1}{}'' T_j \quad , \quad n=0,1,2\ldots$$

$$\frac{d}{dr}T_{2n+1} = 4n+2\sum_{j=0}^{2n}{}' T_j \quad n=0,1,2\ldots \qquad (13)$$

where the superscript ' denotes that the first term in the summation is halved.

Consider now the application of Chebysev polynomials for least squares curve fitting. The problem considered is the approximation of a function W (r) in the region of $-1 \leq r \leq 1$ by

$$W(r) = \sum_{n=0}^{N}{}' \omega_n T_n(r) \qquad -1 \leq r \leq 1 \qquad (14)$$

where W (r) can only be calculated at discrete values of r. If the (M+1) values of W (r) are calculated at the following locations

$$r_k = \cos\left(\frac{2k+1}{M+1}\frac{\pi}{2}\right) \qquad k=0,1,2\ldots M \qquad (15)$$

that is, the zeros of an $(M+1)^{th}$ Chebysev polynomial, then the coefficients ω_n given by

$$\omega_n = \frac{2}{M+1} \sum_{k=0}^{M} W(r_k)\, T_n(r_k) \qquad (16)$$

satisfy the least squares criterion defined by

$$\sum_{k=0}^{M} \left[W(r_k) - \sum_{n=0}^{N}{}' \omega_n T_n(r_k) \right]^2 = \text{minimum} \qquad (17)$$

The advantages of using Chebysev polynomials as compared to other polynomials are:

(i) The computation of the coefficients ω_n is easy

(ii) The values of ω_n are independent of the number of terms used in the polynomial and

(iii) The maximum error in the curve fitting can be easily calculated by examining the coefficients of the discarded terms.

When the function to be approximated is even, that is

$$W(-r) = W(r) \qquad (18)$$

the odd terms in Eq. (14) vanish and the coefficients ω_n can be calculated from the values of W (r) in the region $0 \leq r \leq 1$. If M is an even number Eq. (16) becomes

$$\omega_n = \frac{2}{M+1} \sum_{k=0}^{\frac{M}{2}}{}^{e} 2W(r_k) T_n(r_k) \qquad (16a)$$

where the superscript e denotes that the last term is halved. (The last term corresponds to $r_k = 0$, which should not be counted twice)

Similarly, if W (r) is an odd function, that is

$$W(-r) = -W(r) \qquad (19)$$

the even terms in Eq. (14) vanish and again Eq. (16a) can be used to calculate the coefficients ω_n.

Consider now the calculation of the interface velocities and surface concentrations as outlined in Chapter 4.2.2.

2.2. Sum of interface velocities (4.2.2.1)

Eq. (4-25) can be written in terms of the polynomial coefficients for pressure, film thickness profile and rate of thinning as

$$U_1+U_2=\frac{2}{\phi_5}\left[\phi_4\left(\sum_{n=2}^{N} n A_n r^{n-1}\right)\left(\sum_{n=0}^{N-2} L_n r^n\right)^2-\sum_{n=0}^{N-2}\frac{1}{n+2}\frac{dL_n}{d\theta}r^{n+1}\right] \qquad (20)$$

where all the coefficients have been calculated as described in Chapter 4.2.1 and Section 1 of this appendix . The sum of interface velocities can therefore be calculated at the radial locations defined by Eq. (15).

2.3. Calculation of surface concentration at the centre from the boundary conditions

Before the calculation is described, consider first an equivalent boundary condition which can be used more conveniently.

2.3.1. A different form of boundary condition

The boundary conditions Eqs. (4-15) and (4-16) can be written in a general form as

$$\Gamma = \Gamma_s \qquad r = R' \qquad (21)$$

$$\frac{\partial \Gamma}{\partial r} = 0 \qquad r = R' \qquad (22)$$

where Γ_s is the stationary interface concentration and R' is the radial location at the interface where the interface is not influenced by the flow in the film. Eqs. (21) and (22) are general in that for Γ_1 or Γ_2, for example, the same equations can be used by assigning the value of Γ_s to be $\Gamma_s = 1$ or $\Gamma_s = \phi_7$ respectively.

The boundary condition Eq. (22) can be replaced by the following (will be shown in Section 2.5)

$$\int_0^{R'} 2\pi r \Gamma \, dr = \pi R'^2 \Gamma_s \qquad (23)$$

provided that the surfactant is insoluble in the bulk phase or that the rate of adsorption is given by $j_n \alpha (\Gamma_s - \Gamma)$. The boundary condition Eq. (23) states that the total amount of surfactant from r = 0 to r = R' is the same as that of a uniform concentration of Γ_s.

For the purpose of calculating the surface concentration at the centre Γ_o, Eq. (23) is rearranged by subtracting $\pi R'^2 \Gamma_o$ from both sides of the equation. The result is

$$\int_0^{R'} 2\pi r(\Gamma - \Gamma_o) \, dr = \pi R'^2 (\Gamma_s - \Gamma_o) \qquad (24)$$

2.3.2. Parabolic extrapolation for surface concentration in the region of $r > 1$ (4.2.2.2)

Because the film thickness profile can be measured only in the region $r \leq 1$ and because the surface concentration boundary conditions extend beyond r = 1, it is necessary to assume the concentration profile outside r = 1 . Assume that the concentration in the region r>1 can be approximated by

$$\Gamma - \Gamma_o = \sigma_1 + \sigma_2 (r-1) + \sigma_3 (r-1)^2 \qquad (25)$$

From the imposed condition that at r = 1 the function matches (both in value and slope) with the concentration profile inside $r \leq 1$ and the boundary condition Eq. (21), the parameters in Eq. (25) are given by

$$\sigma_1 = \Gamma - \Gamma_o \Big]_{r=1, \text{ for profile inside } r<1}$$

$$\sigma_2 = \frac{\partial \Gamma}{\partial r} \Big]_{r=1, \text{ for profile inside } r<1}$$

$$\sigma_3 = \frac{\Gamma_s - \Gamma_o - \sigma_1 - \sigma_2 (R'-1)}{(R'-1)^2}$$

Consider now the calculation of surface concentration at the centre for the following cases.

2.3.3. Case 1: sum of surface concentrations (4.2.2.2)

The values of σ_1 and σ_2 are calculated from Eqs. (4-28) and (4-27). The results are:

$$\sigma_1 = -\frac{1}{\Phi_9} \int_0^1 h \frac{\partial p}{\partial r} dr = -\frac{1}{\Phi_9} \sum_{n=2}^{2N+2} \frac{1}{n} \Phi_n \qquad (26)$$

$$\sigma_2 = -\frac{1}{\Phi_9} h \frac{\partial p}{\partial r} \Big|_{r=1} = -\frac{1}{\Phi_9} \sum_{n=2}^{2N+2} \Phi_n \qquad (27)$$

where

$$\Phi_n = \sum_{j=0}^{n-2} (n-j)\, L_j A_{n-j} \qquad n = 2,4 \ldots 2N+2 \qquad (28)$$

The value of σ_3 is calculated from the boundary condition Eq. (21):

$$\Gamma_s - \Gamma_o = \sigma_1 + \sigma_2 (R'-1) + \sigma_3 (R'-1)^2 \qquad (29)$$

hence

$$\sigma_3 = \frac{\Gamma_s - \Gamma_o - \sigma_1 - \sigma_2 (R'-1)}{(R'-1)^2} \qquad (30)$$

where $\Gamma_s = 1 + \phi_7$ and $\Gamma_o = \Gamma_1 + \Gamma_2$ at the centre r = 0. To simplify the calculation it is assumed that

$$R' = \beta R_p \qquad (31)$$

where β is treated as a parameter and R_p is the location where the pressure is zero.

Consider now the calculation of Γ_o from the boundary condition Eq. (24). The LHS of Eq. (24) can be written as

$$\int_0^{R'} = \int_0^1 + \int_1^{R'} \qquad (32)$$

where the first and second terms in the RHS of Eq. (32) can be calculated from Eq. (4-28) and (25) respectively. Thus Eq. (24) becomes

$$T + (\sigma_1 - \sigma_2)(R^2-1) + \frac{2}{3}\sigma_2 (R^3-1) + \frac{1}{6}\sigma_3 (3R^4 - 8R^3 + 6R^2 - 1) = R^2 (\Gamma_s - \Gamma_o) \qquad (33)$$

where

$$\Upsilon = \int_0^1 2r(\Gamma-\Gamma_o)dr = -\frac{1}{\Phi_9}\sum_{n=2}^{2N-2}{}_e \frac{2}{n+2}\frac{1}{n}\Phi_n \qquad (34)$$

Substitution of Eqs. (26), (27) and (30) into Eq. (30) gives the solution for Γ_o:

$$\Gamma_o = \frac{\Upsilon + (\sigma_1-\sigma_2)(R'^2-1) + \frac{2}{3}\sigma_2(R'^3-1) + \Phi_\bullet(\Gamma_s-\sigma_1-\sigma_2(R'-1)) - R'^2\Gamma_s}{\Phi_\bullet - R'^2} \qquad (35)$$

where

$$\Phi_\bullet = \frac{3R'^4-8R'^3+6R'^2-1}{6(R'-1)^2} \qquad (36)$$

2.3.4. Case 2: rate of change of the sum of surface concentrations (4.2.2.2)

The rate of change of the sum of surface concentrations at the centre is given by Eq. (35) with the following variables.

$$\Gamma_s = 0 \qquad (37)$$

$$\Upsilon = -\frac{1}{\Phi_9}\sum_{n=2}^{2N-2}{}_e \frac{2}{n+2}\frac{1}{n}\Phi'_n \qquad (38)$$

$$\sigma_1 = -\frac{1}{\Phi_9}\sum_{n=2}^{2N-2}{}_e \frac{1}{n}\Phi'_n \qquad (39)$$

$$\sigma_2 = -\frac{1}{\Phi_9}\sum_{n=2}^{2N-2}{}_e \Phi'_n \qquad (40)$$

where

$$\Phi'_n = \sum_{j=0}^{n-2}{}_e (n-j)\left(L_j\frac{dA_{n-j}}{d\theta} + \frac{dL_j}{d\theta}A_{n-j}\right) \qquad (41)$$

2.3.5. Case 3: surface concentration at interface 1. (4.2.2.3)

Since (U_1+U_2) have been calculated and U_1 assumed, $\partial\Gamma_1/\partial r$ can be calculated numerically from Eq. (4-5). The result is

$$\frac{\partial\Gamma_1}{\partial r} = -\frac{1}{\Phi_9}\left[\Phi_{10}\frac{U_1-U_2}{\sum_{n=0}^{N\cdot2} L_n r_k^n} + \frac{1}{2}\sum_{n=2}^{2N\cdot2} \Phi_n r_k^{n-1}\right] \qquad (42)$$

The integration of Eq. (42) can be carried out by assuming that $\partial\Gamma_1/\partial r$ can be approximated by a Chebysev polynomial given by

$$\frac{\partial\Gamma_1}{\partial r} = \sum_{n=1}^{N^\circ}{}_o\, G_n T_n \qquad (42a)$$

where the subscript o denotes that the summation is taken over odd numbers of n only. The coefficients G_n are calculated from Eq. (16a)

$$G_n = \frac{1}{M+1}\sum_{k=0}^{M/2} 2\frac{\partial\Gamma_1(r_k)}{\partial r} T_n(r_k) \qquad n = 1,3,\ldots N^\circ \qquad (43)$$

Typical results of the approximation for different values of N° are shown in Fig. 1; the eight-term polynomial is adequate.

Integration of Eq. (42a) from r = 0 to r = r can be carried out using Eq. (12). The result is

$$\Gamma_1 - \Gamma_1(r=0) = \sum_{n=0}^{N^\circ\cdot1}{}_e\, \bar{G}_n T_n \qquad (44)$$

where

$$\bar{G}_0 = \frac{1}{4} G_1 + \sum_{j=3}^{N^*}{}_{o} (-1)^{\frac{j-1}{2}} \left(\frac{1}{j-1} + \frac{1}{j+1} \right) G_j$$

$$\bar{G}_n = \frac{1}{2} \left(\frac{1}{n-1} \right) \left(G_{n-1} - G_{n+1} \right) \qquad n = 2,4 \ldots N^*-1 \qquad (45)$$

$$\bar{G}_{N^*+1} = \frac{1}{2} \frac{1}{N^*+1} G_{N^*}$$

It can be verified that the RHS of Eq. (44) is equal to zero at r = 0.

The concentration at the centre is again calculated from Eq. (35) with the following variables.

$$\Gamma_s = 1 \qquad (46)$$

$$\sigma_1 = \Gamma_1(r=1) - \Gamma_1(r=0) = \sum_{n=0}^{N^*+1}{}_{e} \bar{G} \qquad (47)$$

$$\sigma_2 = \left. \frac{\partial \Gamma_1}{\partial r} \right|_{r=1} = \sum_{n=1}^{N^*}{}_{o} G_n \qquad (48)$$

$$\Upsilon = \int_0^1 2r \left(\Gamma_1 - \Gamma_1(r=0) \right) dr = \bar{G}_0 - \sum_{n=2}^{\frac{N^*+1}{2}}{}_{e} \frac{1}{n+1} \frac{1}{n-1} \bar{G}_{2n} \qquad (49)$$

Eq. (49) has been obtained from Eqs. (10) and (12).

2.4. Interface velocity of interface 1 (4.2.2.3)

The equation for calculating the interface velocity U_1 is Eq. (4-34). For covenience, the LHS of Eq. (4-34) can be written as

$$\sum_{n\,o}^{2N-2}{}_{e} q_n r^n \qquad (50)$$

where

$$q_o = \frac{\partial}{\partial\theta}(\Gamma_1+\Gamma_2)_{r=o} - \phi_{12}\left\{1+\phi_7-(\Gamma_1+\Gamma_2)_{r=o}\right\}+2\frac{\phi_6}{\phi_9}\Phi_2$$

$$q_n = \frac{1}{n}\Phi_n' + \phi_{12}\frac{1}{n}\Phi_n + (n+2)\frac{\phi_6}{\phi_9}\Phi_{n+2} \qquad n = 2,4\ldots 2N \qquad (51)$$

$$q_{2N+2} = \frac{1}{2N+2}\left(\Phi_{2N+2}' + \phi_{12}\Phi_{2N+2}\right)$$

Integration of Eq. (4-34) with respect to r from r = 0 to r = r gives

$$r(U_1\Gamma_1 + U_2\Gamma_2) = -\frac{1}{\phi_5}\sum_{n=0}^{2N+2}\frac{1}{n+2}q_n r^{n+2} \qquad (52)$$

The integration constant is equal to zero because $U_1=U_2=0$ at r=0. Both terms in Eq. (52) can be devided by r to give:

$$U_1\Gamma_1 + U_2\Gamma_2 = Q = -\frac{1}{\phi_5}\sum_{n=0}^{2N+2}\frac{1}{n+2}q_n r^{n+1} \qquad (53)$$

which is the equation for calculating the bulk interface velocity U_1.

Once U_1 has been tentatively assumed, U_2 and Γ_1 can be calculated from Eqs. (20) and (42) to (49) respectively and then Γ_2 can be calculated from $\Gamma_1 + \Gamma_2$ given by Eqs. (4-27), (4-28) and (35) and Γ_1 which has already been calculated. Hence the problem becomes the finding of U_1 which satisfies Eq. (53).

The repetitive substitution method was used to solve Eq. (53). That is,

$$U_1^{(j+1)}(r_k) = \frac{Q(r_k) - U_2^{(j)}(r_k)\Gamma_2^{(j)}(r_k)}{\Gamma_1^{(j)}(r_k)} \qquad (54)$$

where the superscript j denotes the j^{th} iteration.

2.5. The equivalence of the two types of boundary condition for surface concentration

This section shows that the boundary conditions Eqs. (22) and (23) are equivalent. Consider the surfactant mass balance at an interface, given by

$$\frac{\partial \Gamma}{\partial \theta} = j_n + \frac{1}{r}\frac{\partial}{\partial r}\left\{r\left(\mathcal{D}\frac{\partial \Gamma}{\partial r} - U\Gamma\right)\right\} \tag{55}$$

with one of the boundary conditions approximated by

$$\Gamma = \Gamma_s \quad \text{at } r = R' \tag{56}$$

where

$$\frac{\partial \Gamma}{\partial r} = 0 \quad \text{at } r = R' \tag{57}$$

Integration of Eq. (55) with respect to r from r = 0 to r = R' with a weighting factor of $2\pi r$ gives

$$\int_0^{R'} 2\pi r \frac{\partial \Gamma}{\partial \theta}\, dr = \frac{\partial}{\partial \theta}\int_0^{R'} 2\pi r\, \Gamma\, dr = \int_0^{R'} 2\pi r\, j_n\, dr + 2\pi r\left(\mathcal{D}\frac{\partial \Gamma}{\partial r} - U\Gamma\right)\Big]_{r=0}^{r=R} \tag{58}$$

Application of Eq. (57) and the condition that at r = R' there is no interface movement U = 0 simplify Eq. (58) into

$$\frac{\partial}{\partial \theta}\int_0^{R'} 2\pi r\, \Gamma dr = \int_0^{R'} 2\pi r\, j_n\, dr \tag{59}$$

The LHS of Eq. (59) is the rate of change of the total amount of surfactant from r = 0 to r = R'.

Consider now the value of the RHS of Eq. (59) for the following cases.

Case 1: non-soluble surfactant

The RHS of Eq. (59) is equal to zero since $j_n = 0$ for a non-soluble surfactant. Hence Eq. (59) becomes

$$\int_0^{R'} 2\pi r \Gamma dr = C = \pi R'^2 \Gamma_s \tag{60}$$

which is the form of boundary condition Eq. (23). The result is physically consistent since there is no transfer between the bulk phase and the interface.

Case 2: linear form of j_n

If j_n is given by

$$j_n = k_3 (\Gamma_s - \Gamma)$$

then Eq. (59) becomes

$$\frac{\partial}{\partial \theta} \int_0^{R'} 2\pi r \Gamma dr = k_3 \int_0^{R'} 2\pi r (\Gamma_s - \Gamma) dr \tag{61}$$

Eq. (61) can be written in the form

$$\frac{dw}{d\theta} = k_3 (C - w) \tag{62}$$

where $w(\theta)$ is defined by

$$w(\theta) = \int_0^{R} 2\pi r \Gamma dr \tag{63}$$

The solution of Eq. (62) is

$$w = C + (w_o - C)\exp(-k_3\theta) \qquad (64)$$

where w_o is $w(\theta)$ at the initial time $\theta = 0$. The initial time can be selected at the instant prior to any interface movement; hence the surface concentration is uniform and equal to Γ_s and thus $w_o = C$. Therefore Eq. (64) reduces into Eq. (60)

In summary, the boundary conditions Eq. (22) can be replaced by a more convenient form Eq. (23) provided that the surfactant is non-soluble or that j_n is linear in Γ.

3. Integration of the film thinning equations (4.2.3)

3.1. Numerical calculation of $\partial\Gamma_1/\partial\theta$

Expansion of the surfactant mass balance equation Eq. (4-7) gives

$$\frac{\partial\Gamma_1}{\partial\theta} = \phi_{12}(1-\Gamma_1) + \phi_6\left(\frac{1}{r}\frac{\partial\Gamma_1}{\partial r} + \frac{\partial^2\Gamma_1}{\partial r^2}\right) - \phi_5\left(\frac{U_1\Gamma_1}{r} + U_1\frac{\partial\Gamma_1}{\partial r} + \Gamma_1\frac{\partial U_1}{\partial r}\right) \qquad (65)$$

The numerical values of U_1, $\partial\Gamma_1/\partial r$ and Γ_1 are known from the solution of Eqs. (54), (42) and (44) to (49) respectively. The other terms are calculated as follows.

Differentiation of Eq. (42a) gives

$$\frac{\partial^2\Gamma_1}{\partial r^2} = \sum_{n=1}^{N^\circ}{}' \left\{ \sum_{j=n}^{N^\circ}{}_o \; 2\,j\,G_j \right\} T_{n-1} \qquad (66)$$

where the superscript ' denotes that the first term in the summation is halved.

The derivative of U_1 is calculated by approximating U_1 by

$$U_1 = \sum_{n=1}^{N^*}{}_{o} B_n T_n \qquad (67)$$

where the coefficients can be calculated from the numerically known values of U_1 as described in Section 2.1. The derivative is given by

$$\frac{\partial U_1}{\partial r} = \sum_{n=1}^{N^*}{}_{o} \left\{ \sum_{j=n}^{N^*}{}_{o} 2\, j\, B_j \right\} T_{n-1} \qquad (68)$$

Typical results of the approximation Eq. (67) for a nine-term polynomial are shown in Fig. 2 and the calculated derivative given by Eq. (68) is shown in Fig. 3.

To calculate the rate of change at the centre, the L'Hopital rule is applied to Eq. (65) to yield

$$\left.\frac{\partial \Gamma_1}{\partial \theta}\right|_{r=o} = \phi_{12}(1-\Gamma_1) + 2\,\phi_6 \frac{\partial^2 \Gamma_1}{\partial r^2} - 2\,\phi_5 \Gamma_1 \left.\frac{\partial U_1}{\partial r}\right|_{r=o} \qquad (69)$$

3.2. The one-dimensional minimization of Davies et al[3]

The method is shown diagramatically in Fig.4. The outline of the method is as follows.

(i) Starting from an initial value x_0, proceed to x_1 and calculate the corresponding objective functions f_0 and f_1

(ii) If $f_1 < f_0$ double the step size and proceed to x_2 and calculate f_2 (as shown in Fig. 4). If $f_1 > f_0$ proceed in the opposite direction

(iii) Repeat the procedure until failure occurs, $f_n > f_{n-1}$ (in Fig. 4 x_4 is a failure)

(iv) Halve the step size, x_5 and calculate f_5

(v) Discard the worst exterior point (x_4 in Fig. 4) and fit a parabola through the remaining points and calculate the minimum

(vi) The calculated minimum and the best point of the three points through which the parabola was fitted become the starting values for the subsequent search

In the calculation of the rate of thinning at time $\theta_o + \Delta\theta$, the starting point x_0 was the rate of thinning at the previous time θ_o.

4. Density difference and interfacial tension of anisole/water (Table 4-Ib)

Burrill[4] measured the density difference and interfacial tension of the oil/water systems used in his coalescence experiments. His results agree with the values published in literature (International Critical Tables) except for anisole/water system. The density difference was measured to be 0.0097 gm/ml as compared to a literature value of 0.00415 gm/ml and the interfacial tension was measured to be 20.5 dn/cm as compared to 25.8 dn/cm. (Note: if the interfacial tension is measured by a method which is based on the balance between buoyancy and surface forces, such as the drop volume method, the value of interfacial tension is not independent of density difference)

To resolve the large discrepancy the following approach has been used. The different values of density difference and interfacial tension were used to fit experimental thickness profiles using the method described in Chapter 4.2.1 and Section 1 of this appendix. The set of values which gave the best fit would be used.

The approach is reasonable since

(i) The equation used for fitting the film thickness profile - the normal force balance equation Eq. (2-41) - contains assumptions which are justifiable and

(ii) The polynomial pressure distribution has proved to be valid for toluene/water system , the system of accurately known density difference and interfacial tension.

Typical results of the film thickness fitting with an eighth order polynomial for the pressure distribution are shown in Fig. 5. The values measured by Burrill produced the best fit; hence his values have been used in this thesis.

5. Literature cited

1. Subroutine program ROSE1, Chemical Engineering Department, McMaster University, Hamilton, Can. (For the theory of Rosenbrock technique, see Ref.3)

2. Fox, L. and I. B. Parker " Chebysev polynomials in numerical analysis " Oxford University Press, London (1965)

3. Box, M. J. et al , I. C. I. Ltd., Monograph No. 5 " Non-linear optimization techniques " Oliver and Boyd, Edinburg (1969)

4. Burrill, K. A., Ph. D. Thesis, McMaster University, Hamilton, Can. (1970):428-436

5. Hodgson, T. D. and D. R. Woods, J. Coll. Int. Sci., 30 (1969):429

Figure captions

1. The Chebysev polynomial approximation of $\partial\Gamma_1/\partial r$, showing the effect of the number of terms in the polynomial. The maximum absolute and relative errors of the eight-term polynomial used are shown in the accompanying table.

2. The Chebysev polynomial approximation of U_1 . The maximum absolute and relative errors of the nine-term polynomial used are shown in the accompanying table.

3. The calculated derivative of U_1 from Fig. 2.

4. The algorithm of the one-dimensional minimization method of Davies et al[5].

5. The selection of density difference and interfacial tension of anisole/water system based on the fitting of experimental film thickness profiles. The values measured by Burrill[4] gave the best fit.

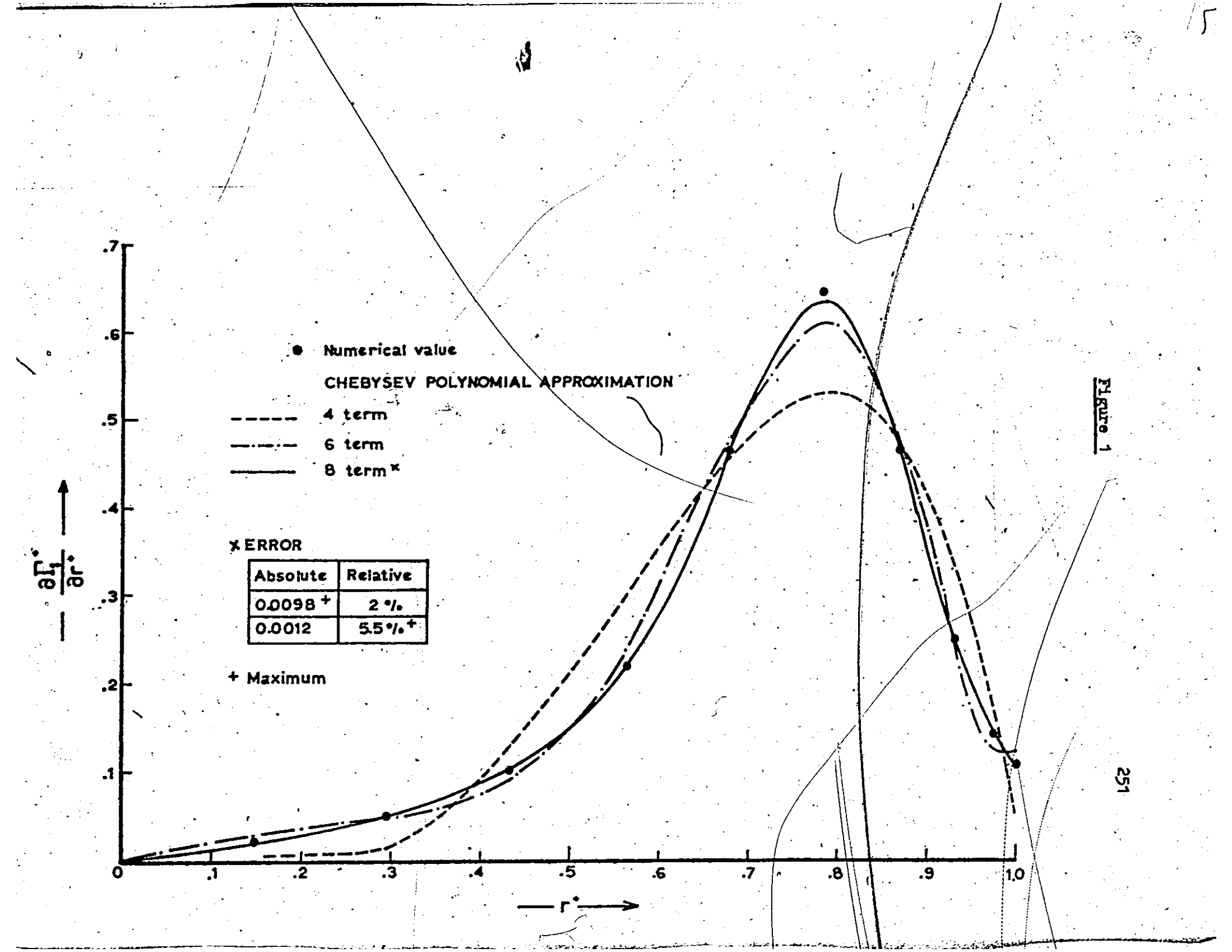
Numerical value
CHEBYSEV POLYNOMIAL APPROXIMATION
4 term
6 term
8 term ×
× ERROR
Absolute | Relative
0.0098 + | 2 %
0.0012 | 5.5 % +
+ Maximum
$\frac{a\Gamma_1^*}{ar^*}$
r^*
0
.1
.2
.3
.4
.5
.6
.7
.8
.9
1.0

Figure 1

Figure 2

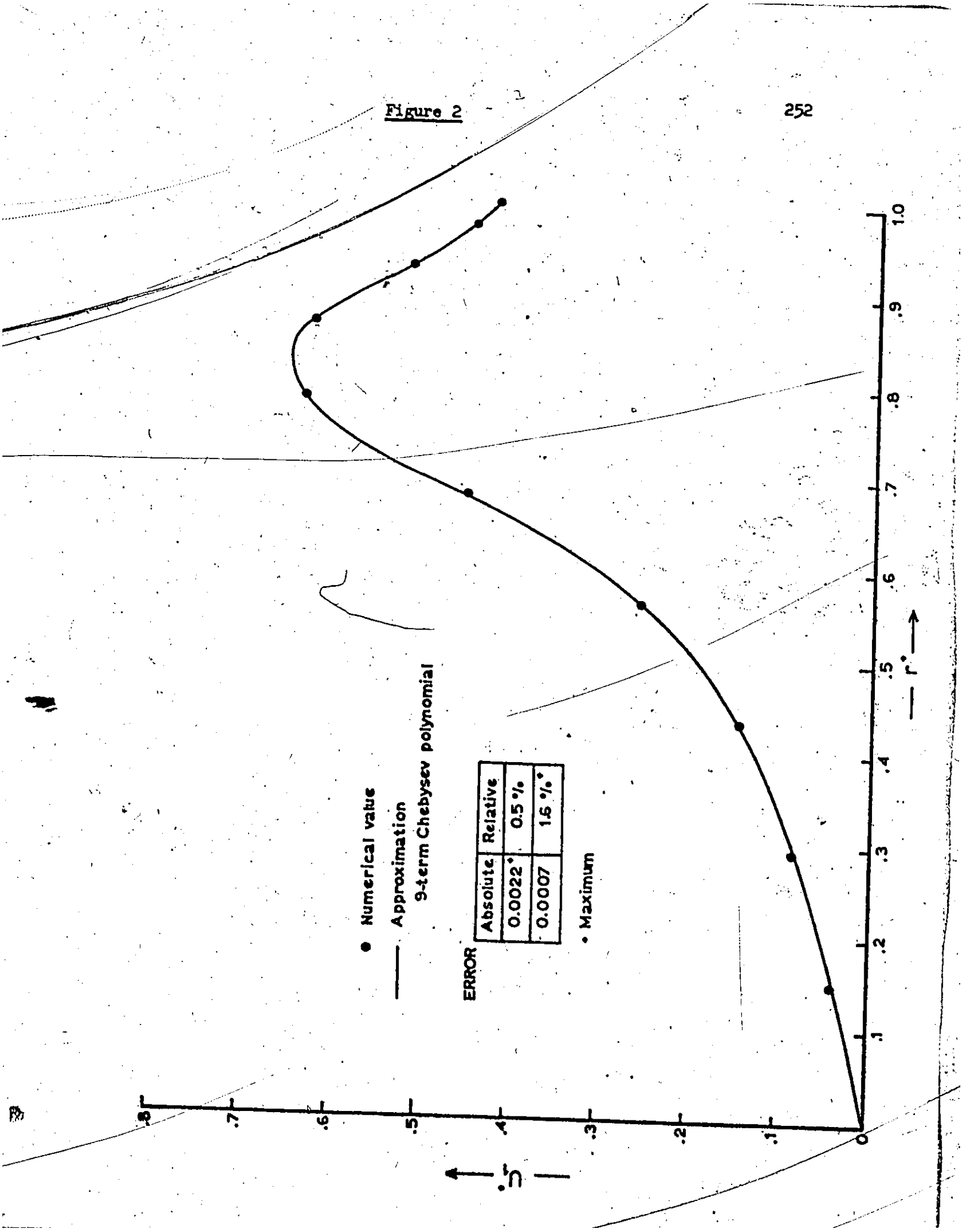
● Numerical value
—— Approximation
9-term Chebyscv polynomial
ERROR
Absolute
Relative
0.0022°
0.5 %
0.0007
1.5 %*
* Maximum
— r* →
← ζ* —
0
.1
.2
.3
.4
.5
.6
.7
.8
.9
1.0

Figure 3

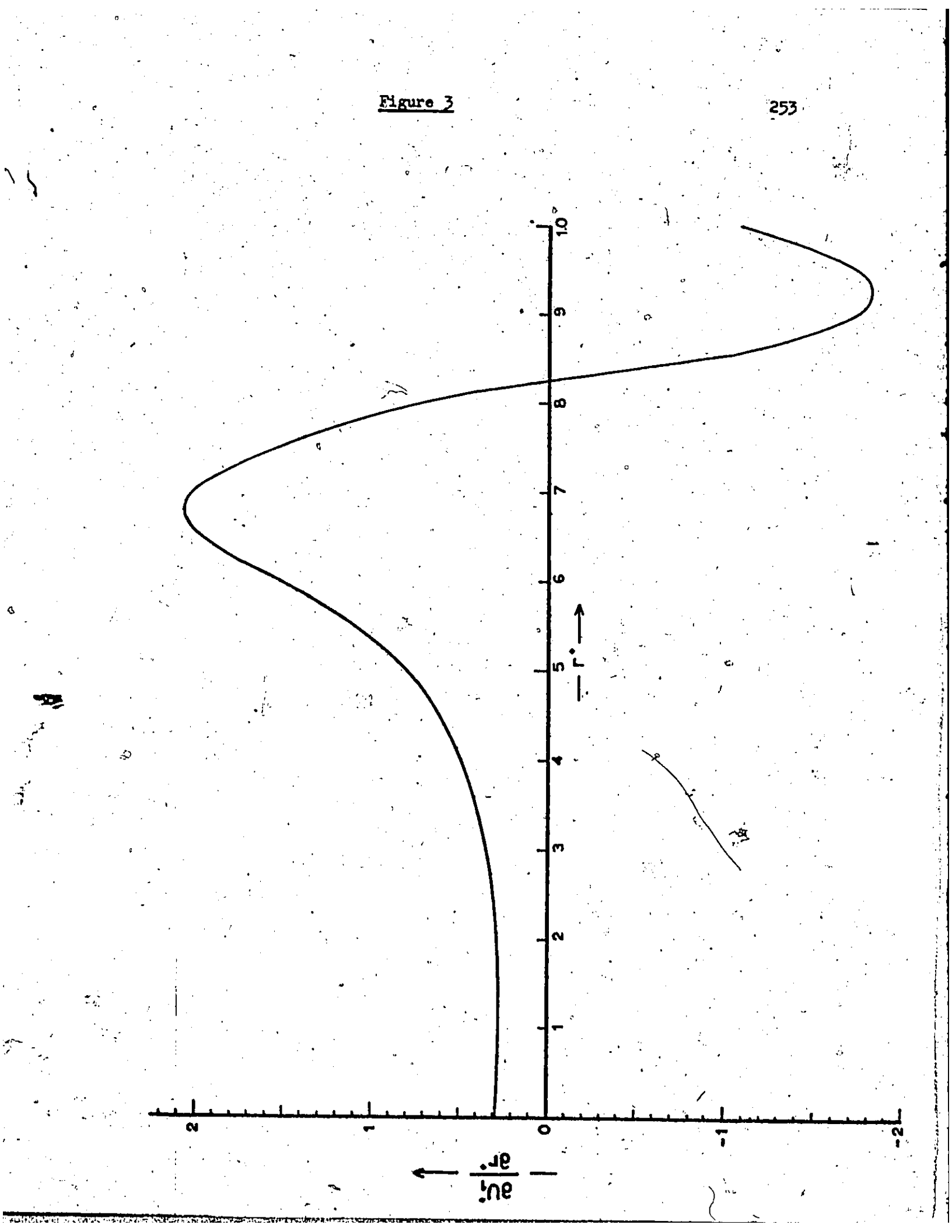

Figure 4

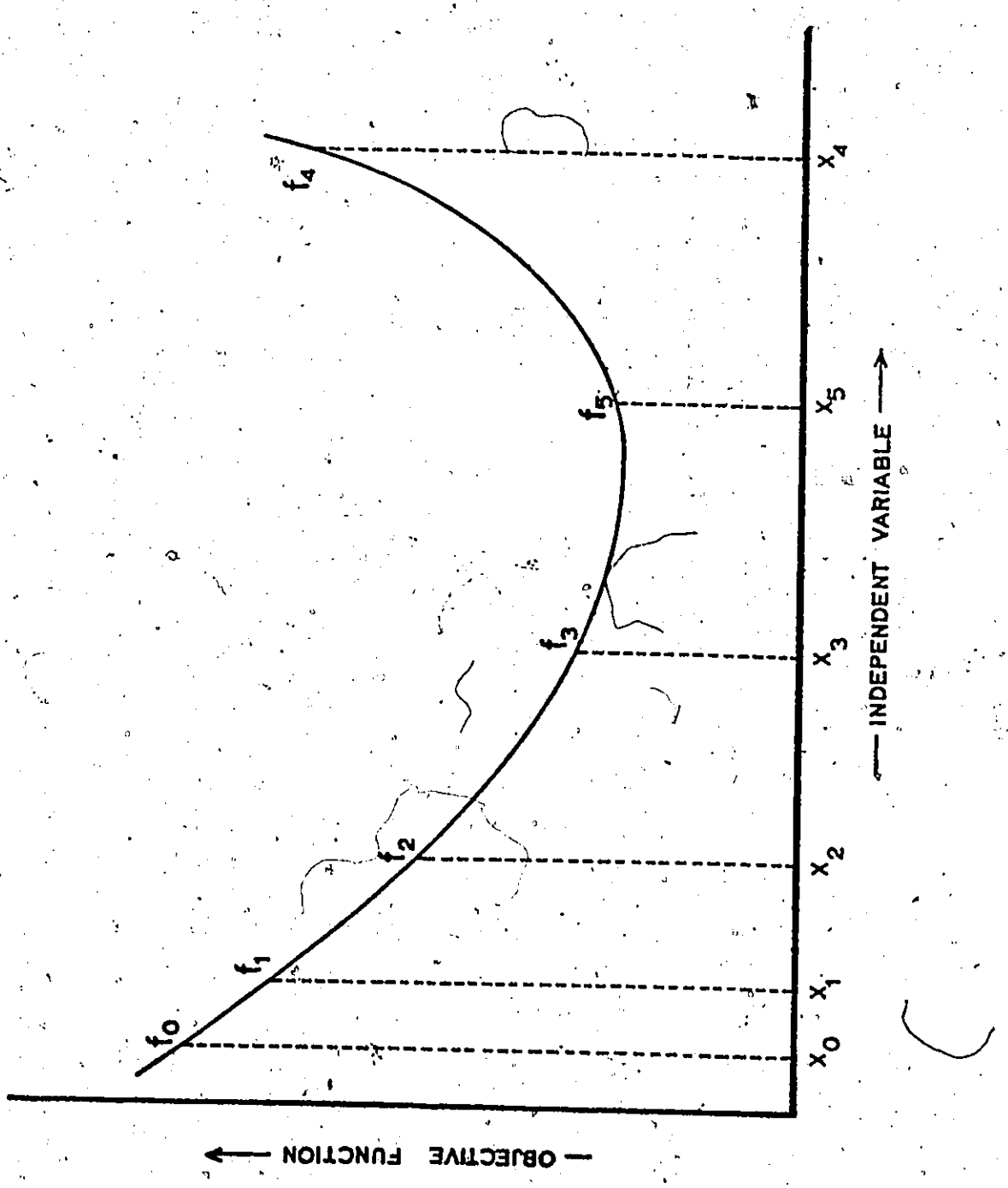
OBJECTIVE FUNCTION
INDEPENDENT VARIABLE
f_0
f_1
f_2
f_3
f_4
f_5
x_0
x_1
x_2
x_3
x_4
x_5

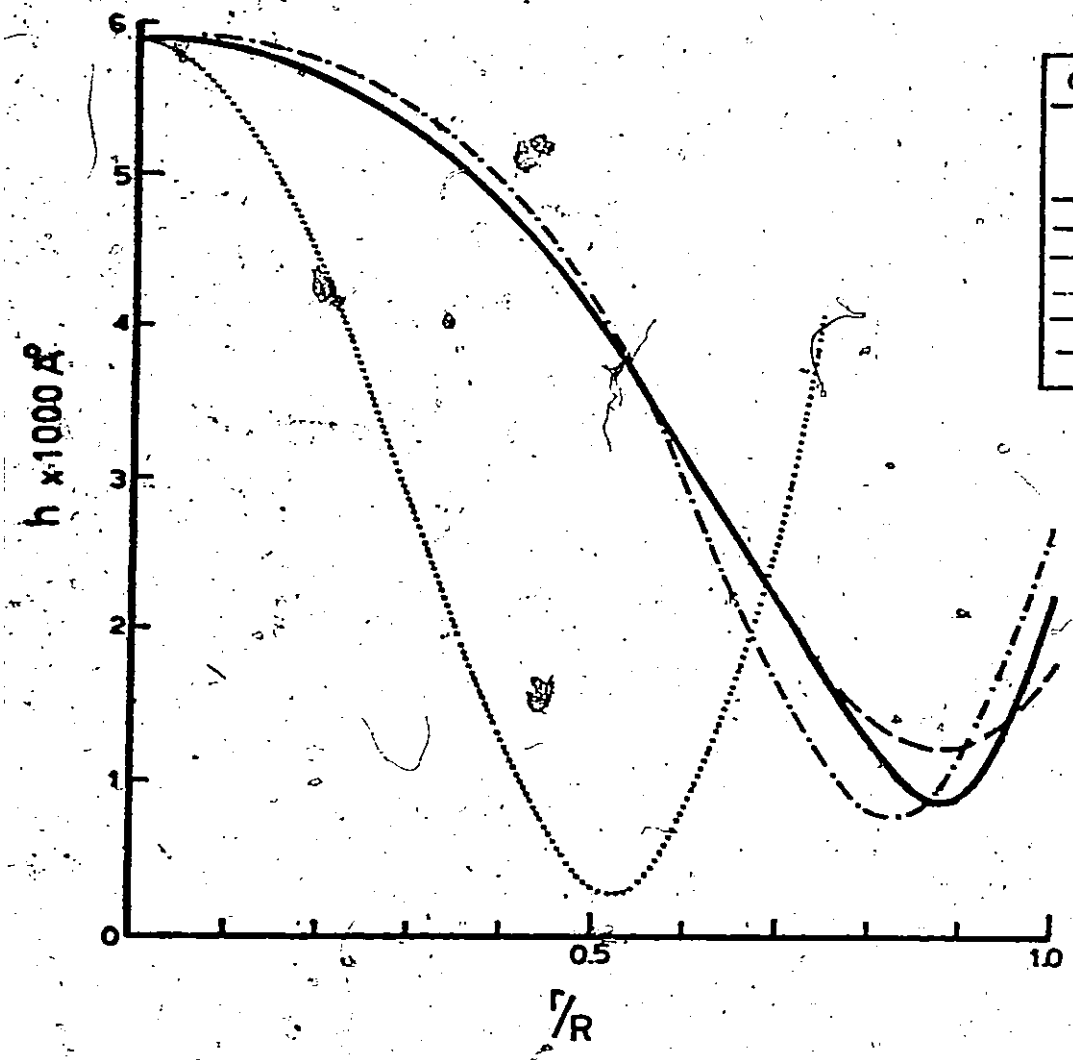

DATA (Ref.5 Fig.10a)
Anisole drop 0.005 ml

CALCULATED FILM THICKNESS		
	$\Delta\rho$	γ
	gm/l	dn/cm
– – – –	0.0097	20.5
.....	0.004	25.0
–·–·–	0.0097	25.0

Figure 5

APPENDIX E

CALCULATION OF THE INTERFACE VELOCITIES AND SURFACE CONCENTRATION DISTRIBUTIONS USING THE PARABOLIC MODEL

This appendix describes the calculation of the interface velocities and surface concentration distributions for a given set of film thickness, rate of thinning and system physical properties, using the parabolic model as outlined in Chapter 2.6. The notation used in this appendix is the same as that used in Chapter 6.

The calculation can be reduced into the calculation of one unknown ζ defined by

$$B_1 = \zeta \ (B_1 + D_1) \tag{1}$$

Eq. (1) can be rearranged into

$$D_1 = (1 - \zeta) \ (B_1 + D_1) \tag{2}$$

where (B_1+D_1) can be calculated from the rate of thinning equation Eq. (6-3) since the film thickness and the rate of thinning are known. The result is

$$B_1 + D_1 = 4 \frac{\Phi_4 A_2}{\Phi_5} L_o^2 - \frac{1}{\Phi_5} \frac{1}{L_o} \frac{dL_o}{d\theta^+} \tag{3}$$

Surface concentration distributions

The surface concentrations can be expressed in terms of ζ by substituting Eqs. (1) to (3) into the tangential force balance equations Eqs. (6-4) and (6-5) and the boundary conditions Eqs. (6-13) and (6-14).

The results are:

$$G_2 = \alpha_1 \left[\frac{1}{2} - \zeta \right] - \alpha_2 \tag{4}$$

$$H_2 = \alpha_1 \left[\zeta - \frac{1}{2} \right] - \alpha_2 \tag{5}$$

where

$$\alpha_1 = \frac{\phi_{10}}{\phi_9} \frac{B_1 + D_1}{L_o} \tag{6}$$

$$\alpha_2 = \frac{A_2}{2\phi_9} L_o \tag{7}$$

and

$$G_o = 1 + \frac{1}{2} R_p^{+2} \left\{ \left(\zeta - \frac{1}{2} \right) \alpha_1 + \alpha_2 \right\} \tag{8}$$

$$H_o = \phi_7 + \frac{1}{2} R_p^{+2} \left\{ \left(\frac{1}{2} - \zeta \right) \alpha_1 + \alpha_2 \right\} \tag{9}$$

Surfactant mass balance

The rate of change of surface concentration can also be expressed in terms of ζ by combining Eqs. (1), (2), (4), (5), (8), (9) and the surfactant mass balance equation Eqs. (6-16) and (6-17). The results are:

$$\frac{dG_o}{d\theta^+} = -\alpha_1^{\bullet} \zeta^2 - \left(\lambda - \frac{\alpha_1^{\bullet}}{2} + \alpha_1^{-} + \alpha_2^{\bullet} + \alpha_2^{x} \right) \zeta + \left(\frac{1}{2} \left[\alpha_1^{-} + \alpha_1^{x} \right] - \alpha_2^{-} - \alpha_2^{x} \right) \tag{10}$$

$$\frac{dH_o}{d\theta^+} = -\alpha_1^{\bullet} \zeta^2 - \left(\lambda \phi_7 + \frac{3}{2} \alpha_1^{\bullet} + \alpha_1^{-} + \alpha_2^{\bullet} + \alpha_2^{x} \right) \zeta$$
$$- \left(\frac{1}{2} \left[\alpha_1^{\bullet} + \alpha_1^{-} + \alpha_1^{x} \right] + \alpha_2^{\bullet} + \alpha_2^{-} + \alpha_2^{x} + \lambda \phi_7 \right) \tag{11}$$

where

$$\lambda = 2\,\phi_5 (B_1 + D_1) \tag{12}$$

$$\alpha_i^{\bullet} = \frac{1}{2} R_p^{+2} \lambda\, \alpha_i \,, \quad i = 1,2 \tag{13}$$

$$\alpha_i^{-} = 4\,\phi_6\, \alpha_i \,, \quad i = 1,2 \tag{14}$$

$$\alpha_i^{x} = \frac{1}{2} R_p^{+} \phi_{12} \alpha_i \,, \quad i = 1,2 \tag{15}$$

The equation for calculating ζ

The equation for calculating ζ, Eq. (6-18), becomes - after the substitution of Eqs. (10) and (11)

$$-2\alpha_1^{\bullet}\zeta^2 + \left\{(\phi_7 - 1)\lambda + 2\,\alpha_1^{\bullet}\right\}\zeta - \left\{\frac{1}{2}\alpha_1^{\bullet} + \alpha_2^{\bullet} + 2(\alpha_2^{-} + \alpha_2^{x}) + \lambda\,\phi_7\right\} = \frac{R_p^{+2} A_2}{2\,\phi_9}\,\frac{dL_o}{d\theta^{+}} \tag{16}$$

Eq. (16) can be rearranged into the following form

$$A^{*}\zeta^2 + B^{*}\zeta + C^{*} = 0 \tag{17}$$

where

$$A^{*} = 2\,\alpha_1^{\bullet} \tag{18}$$

$$B^{*} = (1 - \phi_7)\lambda - 2\,\alpha_1^{\bullet} \tag{19}$$

$$C^{*} = \frac{1}{2}\alpha_1^{\bullet} + \alpha^{\bullet} + 2(\alpha_2^{-} + \alpha_2^{x}) + \lambda\,\phi_7 + \frac{R_p^{+2} A_2}{2\,\phi_9}\,\frac{dL_o}{d\theta^{+}} \tag{20}$$

The solution of Eq. (17) is

$$\zeta = \frac{-B^{*} \pm \sqrt{B^{*2} - 4\,A^{*}C^{*}}}{2\,A^{*}} \tag{21}$$

After ζ has been calculated, the interface velocities and the surface concentrations can then be readily calculated from Eqs. (1) to (9). This completes the calculation of the interface velocities and surface concentration distributions which are consistent with the given set of system physical properties, film thickness and rate of thinning.

APPENDIX F

COMPUTER LISTING OF THE SOLUTION OF THE POLYNOMIAL MODEL

F.1.PROGRAM TST (INPUT,OUTPUT,TAPE5=INPUT,TAPE6=OUTPUT)

```
C
C     ******************************************************************
C     *                                                                *
C     *  FITTING LAMELLA THICKNESS DATA SUBJECT TO                     *
C     *    IMPOSED BOUNDARY CONDITIONS-----                            *
C     *    --  AT R=RR , DP/DR=0 AND P=0, AND TOTAL FORCE BALANCE      *
C     *    (8)TH  ORDER POLYNOMIAL FOR P  IS USED                      *
C     *                                                                *
C     *                                                                *
C     ******************************************************************
C
      COMMON KM,MCYC,MAXK,MKAT,NSTEP,SUMN
      COMMON EPS(20),AKF(20),ALPHA,BETA,V(20,20)
      COMMON/LAB1/FE(20),FM(20),RR,A0,A2,A4,CF0,CF2,CF4,CF6,DELRO,VD,
     1GAMA,RD,DROPR,DRX,NRX,C1,DN1,DN,A6,CF8,PHI,RAD(20),PR(10,20),X11,
     2X12,X13,A8,CF10,X14
      COMMON/LAB2/IFIND,NOB
      DIMENSION PRESS(20),PRESS1(20),TITLE(12)
C
C+++++++++++++++++++++++++++++++++++++++++++++++++++++++++++++++++++++++
C
C     LIST OF SYMBOLS  ********************
C  --
C      KM --- V    CONSTANTS FOR S/R  ROSE1
C  --
C --  DATA TO BE READ IN ****************
C      NDATA      NO OF DATA SETS
C      IDATA      NO OF DIFFERENT FILM THICKNESS PROFILES
C                   IN EACH SET
C      VD         DROP VOLUME, ML
C      DELRO      DENSITY DIFFERENCE, GM/ML
C      GAMA       INTERFACIAL TENSION, DN/CM
C      RD         NORMALIZING RADIAL DISTANCE, CM
C      NRX        NO OF DATA POINTS
C      RAD(I)     DIMENSIONLESS RADIAL DISTANCE
C      TITLE      DATA IDENTIFICATION, 1 TO 72 COLUMNS
C      CF0        FILM THICKNESS AT THE CENTRE, 1000 ANGSTROMS
C      FE(I)      EXPTL FILM THICKNESS, 1000 A
C  --
C  --   **  OTHER SYMBOLS  *********
C    A0 --- A8    PRESSURE COEFFTS
C    CDF          THINNING RATE COEFFTS
C    CF(IC,I), CF0 -- CF8  FILM THICKNESS COEFFTS
C    DN, DN1, PHI  DIMENSIONLESS CONSTANTS
C    F            BUOYANCY FORCE
C    FM(I)        PREDICTED FILM THICKNESS
C    IC, NOB      COUNTERS
C    IFIND        CONVERGENCE INDICATOR
C    PRESS(I)     PREDICTED PRESSURE AT DATA POINTS
C    PRESS(I)     PRESSURE, R=0 TO R=RR AT REGULAR INTERVALS
C    RR           SEE BOUNDARY CONDITIONS
C
C+++++++++++++++++++++++++++++++++++++++++++++++++++++++++++++++++++++++
C
C
C ++++++ READING IN INPUT +++
C
      READ(5,100)NDATA
```

```
      DO 203 IIT=1,NDATA
      IC=1
      READ(5,100)IDATA
   11 READ(5,101)VD,DELRO,GAMA,RD
      DROPR=(VD/4.1888)**0.33333
      F=VD*DELRO*981.0
      PHI=F/(314.0*RD*RD)
      DN1=RD*RD/GAMA*10000000.0
      DN=RD*RD/DROPR*100000.0
      WRITE(6,103)
      WRITE(6,104)GAMA,DELRO,DROPR,VD,RD,F
      READ(5,100)NRX
      READ(5,101)(RAD(I),I=1,NRX)
      X11=-DN1/8.0
      X12=-DN1/18.0
      X13=-DN1/32.0
      X14=-DN1/50.0
      DO 20 I=1,NRX
      PR(1,I)=RAD(I)
      DO 20 N=2,10
   20 PR(N,I)=PR(N-1,I)*RAD(I)
   30 READ(5,99)(TITLE(I),I=1,12)
      READ(5,101)CF0,(FF(I),I=1,NRX)
      IFIND=1
      NOR=0
C
C
C  +++++++ MINIMIZATION BY ROSENBROCK METHOD +++
C  ----- SUBROUTINE S/R ROSE1
C--------- CONSTANTS FOR S/R  ROSE1
C
      ALPHA=1.5
      BETA=0.5
      KM=3
      MCYC=20
      MAXK=25
      MKAT=3000
      AKE(1)=GAMA/DROPR/100.0
      AKE(2)=-0.1
      AKE(3)=0.0
      EPS(1)=0.05*AKE(1)
      EPS(2)=0.01
      EPS(3)=0.02
      V(1,1)=1.0
      V(1,2)=0.0
      V(2,1)=0.0
      V(2,2)=1.0
      V(1,3)=0.0
      V(2,3)=0.0
      V(3,1)=0.0
      V(3,2)=0.0
      V(3,3)=1.0
      RR=3.5
      NSTEP=1
C
      CALL ROSE1
      IF(IFIND.EQ.2)GO TO 160
      CALL OBJECT
```

```
      IF(IFIND.EQ.2)GO TO 160
      WRITE(6,98)(TITLE(I),I=1,12)
C
C PRINTING OUT COEFFTS FOR PRESSURE AND FILM THICKNESS
C
      WRITE(6,105)A0,A2,A4,A6,A8
      WRITE(6,106)CF0,CF2,CF4,CF6,CF8,CF10
      RR=SQRT(RR)
      WRITE(6,107)SUMN,RR
      RX1=0.0
      XNRX=NRX
      DRX1=RR/XNRX
C
C +++++++++ CALCULATION OF PRESSURE
C ++++++ PRINTING OUT RESULTS
C
      DO 30 I=1,NRX
      RX1=RX1+DRX1
      PRESS(I)=A0+A2*PR(2,I)+A4*PR(4,I)+A6*PR(6,I)+A8*PR(8,I)
       PRESS1(I)=A0+A2*RX1*RX1+A4*RX1**4+A6*RX1**6+A8*RX1**8
   30 WRITE(6,108)I,FE(I),FM(I),PRESS(I),PRESS1(I)
      WRITE(6,103)
  999 IF(IC.GE.IDATA)GO TO 203
      IC=IC+1
      GO TO 10
  160 WRITE(6,109)A0,A2,NOB
      IC=IC+1
      GO TO 999
  203 CONTINUE
      STOP
   98  FORMAT(////12A6////)
    99 FORMAT(12A6)
  100 FORMAT(I5)
  101 FORMAT(7F11.6)
  102 FORMAT(5I5)
  103 FORMAT(1H1)
  104 FORMAT(    /8H*RESULTS/8H*GAMA    ,F11.6/8H*DELRO   ,F11.6/
     18H*DROPR   ,F11.6/8H*VD      ,F11.6/8H*RD      ,F11.6/8H*F       ,
     2F11.6//)
  105 FORMAT(6H*CP    ,4F11.6)
  106 FORMAT(6H*CF    ,5F11.6/)
  107 FORMAT(/11H*(ERROR)**2,3X,F11.6,2X,4HRR =,F11.6
     1                                  //8X,4H*EXP,11X,5HMODEL,5X,5HPRESS/
     2)
  108 FORMAT(I3,2X,4F11.6)
  109 FORMAT(31H*NO CONVERGENCE IN PRESSURE DSN,2X,4HA0 =,E12.4,2X,
     14HA2 =,E12.4,2X,4HNO =,I7)
  110 FORMAT(//* CHEB H *,5F13.7)
  111 FORMAT(* CHEB P *,4F13.7//)
      END
      SUBROUTINE OBJECT
C
C +++++++ SUBROUTINE OBJFCT
C         SOLVES THE PRESSURE B.C. - APP. D-1
C          AND CALCULATES THE SUM OF SQUARES OF ERROR  +++
C
C
      COMMON KM,MCYC,MAXK,MKAT,NSTEP,SUMN
```

```
      COMMON EPS(20),AKF(20),ALPHA,BETA,V(20,20)
      COMMON/LAB1/FF(20),FM(20),RR,A0,A2,A4,CF0,CF2,CF4,CF6,DELRO,VD,
     1GAMA,RD,DROPR,DRX,NRX,C1,DN1,DN,A6,CF8,PHI,RAD(20),PR(10,20),X11,
     2X12,X13,A8,CF10,X14
      COMMON/LAB2/IFIND,NOB
C
C ------ CALCULATION OF A6, A8 AND RR ------
C ------  NEWTON RAPHSON METHOD  ------
C
      A0=AKF(1)
      A2=AKF(2)
      A4=AKF(3)
      NIT=0
      NOB=NOB+1
  120 RR2=RR*RR
      FR=0.6*A0*RR   +0.15*A2*RR2+A4/30.0*RR2*RR-PHI
      IF(ABS(FR).LT.0.0000001)GO TO 100
      DFR=0.6*A0+0.3*A2*RR+0.1*A4*RR2
      RNEW=RR-FR/DFR
      IF(ABS(RNEW-RR).LT.0.00001)GO TO 100
      NIT=NIT+1
      IF(NIT.GT.30)GO TO 110
      RR=RNEW
      GO TO 120
  110 IFIND=2
      GO TO 130
  100 IF(RR.LT.0.0)GO TO 110
      A6=-(4.0*A0/RR2+3.0/RR*A2+2.0*A4)/RR
      A8=(3.0*A0/RR2+2.0*A2/RR+A4)/RR2
      CF2=0.5*(DN-A0*DN1)
      CF4=A2*X11
      CF6=A4*X12
      CF8=A6*X13
      CF10=A8*X14
C
C ----- CALCULATION OF OBJECTIVE FUNCTION
C
      SUMN=0.0
      DO 10 I=1,NRX
      FM(I)=CF0+CF2*PR(2,I)+CF4*PR(4,I)+CF6*PR(6,I)+CF8*PR(8,I)+CF10*
     1PR(10,I)
      SS=FF(I)-FM(I)
   10 SUMN=SUMN+SS*SS
  130 RETURN
      END
      SUBROUTINE ROSE1
C     ROSENBROCK SEARCH FOR  1  TO  20  VARIABLES
C   KM        NO OF INDEPENDENT VARIABLES
C   MKAT      NO OF TIMES (VAX) OBJECT IS CALLED
C   MCYC      NO OF ADDITIONAL SEARCHES TO BE MADE AFTER MIN IS 'FOUND'
C   MAXK      MAX NO OF 'ROTATIONS'
C   NSTEP     1
C   EPS(I)    STEP SIZE
C   AKF(I)    STARTING VALUES OF INDEPENDENT VARIABLES
C  ALPHA      RECOMENDED VALUE  1.5
C   BETA      RECOMENDED VALUE  0.5
C   V(I)      RECOMFNDFD VALUF  UNIT MATRIX.
      COMMON KM,MCYC,MAXK,MKAT,NSTEP,SUMN
```

```
      COMMON EPS(20),AKE(20),ALPHA,BETA,V(20,20)
      COMMON/LAB2/IFIND,NOB
C     AJ= INDICATORS
C     AFK=OPTIMIZED VALUES OF PARAMETERS.
C     E = TEMPORARY STORAGE FOR STEP SIZE
C     KAT = NO OF TIMES OBJECT BEING CALLED
C     KK1  =NO OF STAGES
C     OBJECT = SUBROUTINE FOR OBJECTIVE FUNCTION SUMN
C     SUMO = STORAGE FOR MINIMUM SUMN
C     V =ORTHOGONAL UNIT VECTORS
C     THE PROGRAMME TERMINATES AFTER  MAXK STAGES
C             OR AFTER  OBJECT BEING CALLED MKAT TIMES
C             OR AFTER NCYC SUCCESSIVE FAILURES BEINNG ENCOUNTERED
C     MAX NUMBER OF PARAMETERS IS 20
C
C
      DIMENSION D(20),BL(20,20),BLEN(20),AJ(20)
      DIMENSION F(20),AL(20,20),AFK(20)
C
      KAT =1
      CALL OBJECT
      IF(IFIND.EQ.2)GO TO 9001
      SUMO =SUMN
      DO 812 K=1,KM
      AFK(K) =AKE(K)
  812 CONTINUE
      KK1=1
      IF (NSTEP .EQ.1) GO TO 1000
      DO 350 I=1,KM
      E(I)  =EPS(I)
  350 CONTINUE
 1000 DO 250 I=1,KM
      AJ(I) =2.0
      IF (NSTEP .NE.1) GO TO 250
      E(I) =EPS(I)
  250 D(I) =0.0
      III=0
  397 III=III+1
  258 I=1
  259 DO 251 J=1,KM
  251 AKE(J) =AKE(J) +F(I) *V(I,J)
      CALL OBJECT
      IF(IFIND.EQ.2)GO TO 9001
C  ***************************************************************
C    PRINT HERE IF DESIRED NO OF TIMES OBJECTIVE FUNCTION BEING CALLED
C     (KAT), OBJECTIVE FUNCTION(SUMN), VARIBLES(AKE(I))
C  ***************************************************************
      KAT =KAT +1
      IF (KAT .EQ. MKAT ) GO TO 1002
      IF (SUMN .LE. SUMO ) GO TO 253
      DO 254 J=1,KM
  254 AKE(J) =AKE(J) -E(I) *V(I,J)
      E(I) =-BETA*E(I)
      IF (AJ(I) .LT. 1.5) AJ(I) =0.0
      GO TO 255
  253 D(I) =D(I) +F(I)
      E(I) =ALPHA *F(I)
      SUMO =SUMN
```

```
      DO 813 K=1,KM
  813  AFK(K) =AKE(K)
      IF (AJ(I) .GT. 1.5) AJ(I) =1.0
  255 DO 256 J=1,KM
      IF (AJ(J) .GT. 0.5) GO TO 299
  256 CONTINUE
      GO TO 257
  299 IF (I.EQ. KM) GO TO 399
      I=I+1
      GO TO 259
  399 DO 398 J=1,KM
      IF (AJ(J) . LT.2. ) GO TO 258
  398 CONTINUE
      IF (III.LT. MCYC ) GO TO 397
      GO TO 1001
  257 CONTINUE
      IF(KM.EQ.1) GO TO 1000
      DO 290 I=1,KM
      DO 290 J=1,KM
  290 AL(I,J) =0.0
C
C     ORTHOGONALIZATION
C
C     WRITE (6,280 ) KK1
C     WRITE (6,281) SUMO,(AKE(I) ,I=1,KM)
      DO 260 I=1,KM
      KL=I
      DO 260 J=1,KM
      DO 261 K=KL,KM
  261 AL(I,J) =D(K) *V(K,J) +AL(I,J)
  260 BL (I,J)= AL(I,J)
      BLEN(1)=0.0
      DO 351 K=1,KM
      BLEN(1)= BLEN(1) +BL(1,K)*BL(1,K)
  351 CONTINUE
      BLEN(1) =SQRT(BLEN(1))
      DO 352 J=1,KM
      V(1,J) =BL(1,J) /BLEN(1)
  352 CONTINUE
      DO 263 I=2,KM
      II=I-1
      DO 263 J=1,KM
      SUMAVV=0.0
      DO 264 KK=1,II
      SUMAV =0.0
      DO 262 K=1,KM
  262 SUMAV=SUMAV + AL(I,K)*V(KK,K)
  264 SUMAVV =SUMAV*V(KK,J) +SUMAVV
  263 BL(I,J) =AL(I,J) -SUMAVV
      DO 266 I=2, KM
      BLEN(I) =0.0
      DO 267 K=1,KM
  267 BLEN(I) =BLEN(I) +BL(I,K) *BL(I,K)
      BLEN(I) = SQRT(BLEN(I) )
      DO 266 J=1, KM
  266 V(I,J) =BL(I,J) / BLEN(I)
      KK1 =KK1+1
      IF (KK1.EQ.MAXK ) GO TO 1001
```

```
      GO TO 1000
 1002 WRITE (6,910 ) KAT
 1001 WRITE (6, 1003) KK1, KAT ,III
      WRITE (6, 1004) SUMO
      WRITE (6, 1006) (AFK(I),I=1, KM)
  280 FORMAT(/ 3X, 12HNO OF STAGE=, 3X, I5 )
  281 FORMAT (10X, 18HSUMO AND VARIABLES,3X, 6E12.4/)
  910 FORMAT(//3X,25HPROGRAM HAS CALLED OBJECT,2X,I5, 2X,
     1 25HTIMES WITHOUT CONVERGANCE/)
 1003 FORMAT(/3X, 13HNO OF STAGES=,I5, 3X, 23HAND OBJECT BEING CALLED,
     1 I5, 3X, 5HTIMES,3X,26HNO OF SUCCESSIVE FAILURES=,I5/)
 1004 FORMAT(/3X, 7HOBJECT=, E15.5/)
 1006 FORMAT(/3X, 16HTHE VARIBLES ARE, 6E12.5X)
      DO 9000 LX=1,KM
 9000 AKE(LX)=AFK(LX)
      SUMN=SUMO
 9001 RETURN
      END
           END OF RECORD
```

CDTOT 0368

```
F.2PROGRAM TST(INPUT,OUTPUT,PUNCH,TAPE5=INPUT,TAPE6=OUTPUT,TAPE7=PUNC
     1H)
      COMMON/SU1/CHEB(20,11),CHSC1(9),Q(11),RTC,RTD,RT1,RT12,RT2,RT21,
     1RT31C,SC(11),SC1(11),SC2(11),U1(11),U12(11),U2(11),XHP(11),X20(11)
     2,CON1(8),X(8),X1(11)
      DIMENSION CDH(20),CH(20),CP(5),CQ(10),CSC(10),CTSC(10),DP(11),DTP(
     35),
     1H(11),P(11),R(11),RR(11,20),TITLE(12),T1(20),T2(20),T3(20),T4(20),
     2XDN5(10),XDN6(10),XDN8(10),XN1(10),XN2(10),X2N(10),X16(11)
      DIMENSION CHU(9),CDU(9),DU(11),CD2R(9),D2R(11),CTSC1(11)
   96 FORMAT(* DTSC *,11F10.5)
   97 FORMAT(1H1)
   98 FORMAT(3I5)
   99 FORMAT(12A6)
  100 FORMAT(7F11.6)
  101 FORMAT(//16X,*  CH = *,6F12.6)
  102 FORMAT(16X,*  CP = *,5F12.6)
  103 FORMAT(16X,* CDH = *,6F12.6)
  104 FORMAT(*   H = *,11F10.5)
  106 FORMAT(*  U1 = *,11F10.5)
  107 FORMAT(*  U2 = *,11F10.5)
  108 FORMAT(* SC1 = *,11F10.5)
  109 FORMAT(* SC2 = *,11F10.5)
    1 FORMAT(//*  INITIAL CONDITIONS *//)
    3 FORMAT(//* ---------------------------------------- */12A6
     1//)
    4 FORMAT(*  PHYS PROPS          *,5F12.6)
    5 FORMAT(*  PARAMETERS         *,5F12.6)
    6 FORMAT(*  RD (CM)            *,F12.6/
     1        * ----------------------------------------  *//)
    7 FORMAT(*  NO CONVERGENCE IN U1 *)
    9 FORMAT(*  R = *,11F10.5//)
    2 FORMAT(* U12 = *,11F10.5)
C
C
C    ++++++++++++++++++++++++++++++++++++++++++++++++++++++++++++++++++
C    +                                                                +
C    +  ------ CALCULATION OF THE INITIAL CONDITIONS  ------          +
C    +                                                                +
C    +          REPETITIVE SUBSTITUTION FOR U1                        +
C    +                                                                +
C    ++++++++++++++++++++++++++++++++++++++++++++++++++++++++++++++++++
C
C
C    ******************************************************************
C    *                                                                *
C    *  ++++++  INPUT TO BE READ IN  ++++++                           *
C    *                                                                *
C    *  -- U1(I),2 - 11      INITIAL ESTIMATES FOR U1                 *
C    *  -- NDAT              NO OF DATA SETS                          *
C    *  -- R(I),1 - 11       ZEROTH OF 21ST CHEBYSEV POLN, 0 TO 1     *
C    *  -- IDAT              NO OF SETS OF PARAMETERS FOR EACH NDAT   *
C    *  -- TITLE             IDENTIFICATION CARD, COL 1 TO 71         *
C    *  -- RD                NORMALIZING RADIAL DISTANCE, CM          *
C    *     RR                RADIAL DISTANCE WHERE P=0, DP/DR=0       *
C    *  -- VD                DROP VOLUME, ML                          *
C    *     DELRO             DENSITY DIFFERENCE, GM/ML                *
C    *     GAMA              INTERFACIAL TENSION, DYNE/CM             *
C    *     XMU               FILM VISCOSITY, POISE                    *
```

```
C     *  == CH(I)I = 6        FILM THICKNESS COEFFICIENTS                *
C     *                       PRESSURE COEFFICIENTS                      *
C     *  -- CDH(I)1 - 4       RATE OF THINNING COEFFICIENTS              *
C     *  -- BET               PARAMETER FOR SAA CONCN B.C.               *
C     *     DN9               LOWERING OF GAMA AT ONE INTERFACE, DN/CM   *
C     *     DN7               RATIO OF THE TWO SAA CONCNS                *
C     *     RK3               RATE CONSTANT FOR ADS/DES , 1/SEC          *
C     *     DIFFS             SURFACE DIFFUSIVITY, CM*CM/SEC             *
C     *                                                                  *
C     *  ------  PUNCHED CARDS OUTPUT  ------                            *
C     *                                                                  *
C     *  -- BET, DN9(DN/CM), DN7, RK3, DIFFS                             *
C     *  -- U1(I),2 - 11                                                 *
C     *  -- U2(I),1 - 11      DROP INTERFACE VELOCITY                    *
C     *  -- SC1(I),1 - 11     BULK SAA CONCN                             *
C     *  -- SC2(I),1 - 11     DROP SAA CONCN                             *
C     *  -- CTSC1(I)1 - 11    RATE OF CHANGE OF SC1                      *
C     *                                                                  *
C     ********************************************************************
C
      WRITE(6,97)
      CON1(1)=0.25
      CON1(2)=-0.375
      CON1(3)=5.0/24.0
      CON1(4)=-7.0/48.0
      CON1(5)=9.0/80.0
      CON1(6)=-11.0/120.0
      CON1(7)=13.0/168.0
      CON1(8)=-15.0/224.0
      U1(1)=0.0
      U2(1)=0.0
      U12(1)=0.0
      DO 90 N=1,10
      XN=N
      X2N(N)=4.0*XN*XN
      XN1(N)=XN+1.0
   90 XN2(N)=2.0*XN
C
C ++++++  READING IN INPUT  ++++++
      READ(5,100)(U1(I),I=2,11)
      READ(5,98)NDAT
      READ(5,100)(R(I),I=1,11)
      DO 10 I=1,11
      RP(I,1)=R(I)
      DO 10 N=2,19
   10 RP(I,N)=RP(I,N-1)*R(I)
      DO 15 J=1,11
C
C ++++++  NUMERICAL VALUES FOR CHEBYSEV POL
C
      CHEB(1,J)=1.0
      CHEB(2,J)=R(J)
      DO 15 N=2,18
   15 CHEB(N+1,J)=2.0*R(J)*CHEB(N,J)-CHEB(N-1,J)
      DO 700 ND=1,NDAT
      READ(5,98)IDAT
      READ(5,99)(TITLE(I),I=1,12)
      READ(5,100)RD,RR
```

```
      READ(5,100)VD,DELRO,GAMA,XMU
      READ(5,100)(CH(I),I=1,6)
      READ(5,100)(CP(I),I=1,5)
      READ(5,100)(CDH(I),I=1,4)
C ++++++  CALCULATION OF CONSTANTS  ++++++
      DROPR=(VD/4.188888)**0.333333333
      DN=RD*RD/DROPR*1.0E+5
      DN1=1.0E+7*RD*RD/GAMA
      DN4=1.0E-8/(12.0*XMU*RD*RD)
      DN5=0.01/RD
      DN10=XMU*RD*1.0E+6
      X11=-2.0/DN1
      X12=-8.0/DN1
      X13=-DN1/18.0
      X14=-DN1/32.0
      X15=DN/DN5
      X19=2.0/DN5
      DTP(1)=X11*CDH(2)
      DTP(2)=X12*CDH(3)
      RR2=RR*RR
      RR4=RR2*RR2
      RR6=RR4*RR2
      DTP(3)=CDH(4)/X13
      DTP(4)=-4.0/RR6*(4.0*DTP(1)+1.5*DTP(2)*RR2+DTP(3)*RR4/1.5)
      DTP(5)=5.0/RR6/RR2*(3.0*DTP(1)+DTP(2)*RR2+DTP(3)*RR4/3.0)
      CDH(5)=X14*DTP(4)
      CDH(6)=-DN1/50.0*DTP(5)
C
C ------  ( U1+U2 ) -- CH. 4.2.1 AND APP. D-2.2 +++
C
      DO 70 I=1,11
      DP(I)=2.0*CP(2)*RP(I,1)+4.0*CP(3)*RP(I,3)+CP(4)*6.0*RP(I,5)
     1+CP(5)*8.0*RP(I,7)
      H(I)=CH(1)+CH(2)*RP(I,2)+CH(3)*RP(I,4)+CH(4)*RP(I,6)+CH(5)*RP(I,8)
     1+CH(6)*RP(I,10)
      X16(I)=0.5*DP(I)*H(I)
      X17=H(I)*H(I)
      X18=0.5*CDH(1)*RP(I,1)+0.25*CDH(2)*RP(I,3)+CDH(3)*RP(I,5)/6.0+
     1CDH(4)*RP(I,7)/8.0+0.1*CDH(5)*RP(I,9)+CDH(6)*RP(I,11)/12.0
   70 U12(I)=X19*(DN4*DP(I)*X17-X18/H(I))
      T1(1)=2.0*CP(2)
      T1(2)=4.0*CP(3)
      T1(3)=6.0*CP(4)
      T1(4)=8.0*CP(5)
      CALL XMY(T1,CH,T3,4,6)
      CALL XMY(T1,CDH,T4,4,6)
      T1(1)=2.0*DTP(2)
      T1(2)=4.0*DTP(3)
      T1(3)=6.0*DTP(4)
      T1(4)=8.0*DTP(5)
      CALL XMY(T1,CH,T2,4,6)
C ------  PRINTING IN INPUT  ------
      WRITE(6,3)(TITLE(I),I=1,12)
      WRITE(6,4)VD,DELRO,GAMA,XMU,RR
      WRITE(6,9)(R(I),I=1,11)
      WRITE(6,101)(CH(I),I=1,6)
      WRITE(6,102)(CP(I),I=1,5)
      WRITE(6,103)(CDH(I),I=1,6)
```

```
      WRITE(6,104)(H(I),I=1,11)
      WRITE(6,2)(U12(I),I=1,11)
      WRITE(6,6)RD
C
      DO 700 ID=1,IDAT
      READ(5,100)BET,DN9,DN7,RK3,DIFFS
C ------  PARAMETRIC CONSTANTS FOR SAA BC ---
      RT=BET*RR
      RT2=RT*RT
      RT1=RT-1.0
      RT12=RT1*RT1
      RT21=RT2-1.0
      RT31C=(RT*RT2-1.0)/1.5
      RTC=(-1.0+RT2*(6.0+RT*(-8.0+3.0*RT)))/6.0/RT12
      RTD=RTC-RT2
      WRITE(6,5)BET,DN9,DN7,RK3,DIFFS
      DN6=DIFFS/RD/RD
      DN9=DN9*1000.0
      DN12=RK3
      DN109=DN9/DN10
      DN71=DN7+1.0
      DO 91 N=1,10
      XDN5(N)=DN5*XN2(N)
      XDN6(N)=DN6*X2N(N)
   91 XDN9(N)=DN9*XN2(N)
C
C ++++++ SUM OF SAA CONCN -- CH. 4.2.2, APP. D-2.1, 2.3 ++
C        SUM OS RATE OF CHANGE OF SAA CONCN
C
      DO 81 N=1,9
   83 CTSC(N+1)=-(T2(N)+T4(N))/XDN9(N)
   81 CSC(N+1)=-T3(N)/XDN9(N)
C ------  VALUE AT R=0 IS CALCULATED FROM B.C.  ------
      PHI3=0.0
      DPHI3=0.0
      ZA=0.0
      ZB=0.0
      DZA=0.0
      DZB=0.0
      DO 84 N=1,9
      PHI3=PHI3+CSC(N+1)/XN1(N)
      DPHI3=DPHI3+CTSC(N+1)/XN1(N)
      ZA=ZA+CSC(N+1)
      DZA=DZA+CTSC(N+1)
      ZB=ZB+CSC(N+1)*XN2(N)
   84 DZB=DZB+CTSC(N+1)*XN2(N)
      CSC(1)=(PHI3+(ZA-ZB)*RT21+ZB*RT31C+RTC*(DN71-ZA-ZB*RT1)-RT2*DN71)
     1/RTD
      CTSC(1)=(DPHI3+(DZA-DZB)*RT21+DZB*RT31C+RTC*(-DZA-DZB*RT1))/RTD
      DO 85 I=1,11
      SC(I)=CSC(1)
      XHP(I)=X16(I)/DN9
      X20(I)=H(I)*DN109
      DO 85 N=2,10
   85 SC(I)=SC(I)+CSC(N)*RP(I,2*N-2)
C
C ++++++ CALCN OF THE RHS OF EQS. D-53, 51  +++
C ------ CO== U1*SC1+U2*SC2 - IF U1 IS CORRECTLY CHOSEN  ------
```

```
C
      CO(1)=CTSC(1)-DN12*(DN71-CSC(1))-XDN6(1)*CSC(2)
      DO 86 N=2,9
   86 CO(N)=CTSC(N)+DN12*CSC(N)-XDN6(N)*CSC(N+1)
      CO(10)=CTSC(10)+CSC(10)*DN12
      DO 88 N=1,10
   88 CO(N)=CO(N)/XDN9(N)
      DO 87 I=1,11
      Q(I)=0.0
      DO 87 N=1,10
   87 Q(I)=Q(I)+CO(N)*RP(I,2*N-1)
C
C  ++++++  CALCULATION OF U1 -- APP. D.2.4  +++
C
      CALL FU1(ICHECK)
      IF(ICHECK.EQ.2)GO TO 126
      WRITE(6,1)
C
C ------  RATE OF CHANGE OF SC1 -- APP. D-3.1  +++
C         FOR INPUT TO THE SOLN OF DIFF. EQNS.
C
      DO 30 N=1,9
      CHU(N)=0.0
      DO 31 J=1,11
   31 CHU(N)=CHU(N)+2.0*U1(J)*CHEB(2*N,J)
   30 CHU(N)=CHU(N)/10.5
      XNN=34.0
      CDU(9)=34.0*CHU(9)
      DO 32 N=1,7
      NN=9-N
      XNN=XNN-4.0
   32 CDU(NN)=XNN*CHU(NN)+CDU(NN+1)
      CDU(1)=0.5*CDU(2)+CHU(1)
      CD2R(8)=30.0*X(8)
      XNN=30.0
      DO 33 N=1,6
      NN=8-N
      XNN=XNN-4.0
   33 CD2R(NN)=CD2R(NN+1)+XNN*X(NN)
      CD2R(1)=0.5*CD2R(2)+X(1)
      CD2R(9)=0.0
      DO 34 J=1,11
      DU(J)=0.0
      D2R(J)=0.0
      DO 34 N=1,9
      DU(J)=DU(J)+CDU(N)*CHEB(2*N-1,J)
   34 D2R(J)=D2R(J)+CD2R(N)*CHEB(2*N-1,J)
      DO 35 J=2,11
   35 CTSC1(  J)=DN12*(1.0-SC1(  J))+DN6*(X1(J)/R(J)+D2R(J))-DN5*(U1(J)*
     1(SC1(  J)/R(J)+X1(J))+SC1(  J)*DU(J))
      CTSC1(  1)=DN12*(1.0-SC1(  1))+2.0*(DN6*D2R(1)-DN5*SC1(  1)*DU(1))
C
C ------  INITIAL CONDITIONS  ------
C
      WRITE(6,106)(U1(I),I=1,11)
      WRITE(6,107)(U2(I),I=1,11)
      WRITE(6,108)(SC1(I),I=1,11)
      WRITE(6,109)(SC2(I),I=1,11)
```

```
      WRITE(6,96)(CTSC1(I),I=1,11)
C
C ------  PUNCHING INPUT FOR FILM THINNING  ------
C
      DN8=DN8/1000.0
      PUNCH(7,100)RET,DN8,DN7,RK3,DIFFS
      PUNCH(7,100)(U1(I),I=2,11)
      PUNCH(7,100)(U2(I),I=2,11)
      PUNCH(7,100)(SC1(I),I=1,11)
      PUNCH(7,100)(SC2(I),I=1,11)
      PUNCH(7,100)(CTSC1(I),I=1,11)
      GO TO 700
  126 WRITE(6,7)
      DO 900 I=1,11
  900 U1(I)=0.0
  700 WRITE(6,97)
      STOP
      END
      SUBROUTINE FU1(ICHECK)
C
C  ++++++ REPETITIVE SUBSTITUTION METHOD
C         FOR CALCULATING U1 -  APP. D-2.4 +++
C
      COMMON/SU1/CHEB(20,11),CHSC1(9),Q(11),RTC,RTD,RT1,RT12,RT2,RT21,
     1RT31C,SC(11),SC1(11),SC2(11),U1(11),U12(11),U2(11),XHP(11),X20(11)
     2,CON1(8),X(8),X1(11)
      DIMENSION T(11),T1(11)
      ICHECK=1
      NTEST=0
      X1(1)=0.0
   70 DO 10 I=2,11
      U2(I)=U12(I)-U1(I)
   10 X1(I)=-( U1(I)- U2(I))/X20(I)-XHP(I)
      DO 20 N=1,8
      X(N)=0.0
      DO 21 J=1,11
   21 X(N)=X(N)+2.0*X1(J)*CHEB(2*N,J)
   20 X(N)=X(N)/10.5
      A=(X(1)-X(2))/2.0+(X(3)-X(4))/6.0+(X(5)-X(6))/10.0+(X(7)-X(8))/14.
      B=X(1)+X(2)+X(3)+X(4)+X(7)+X(5)+X(6)+X(8)
      CHSC1(1)=0.0
      DO 25 N=1,8
   25 CHSC1(1)=CHSC1(1)+CON1(N)*X(N)
      XN=0.0
      DO 26 N=2,8
      XN=XN+4.0
   26 CHSC1(N)=(X(N-1)-X(N))/XN
      CHSC1(9)=X(8)/32.0
      C=CHSC1(1)-(CHSC1(3)/3.+CHSC1(5)/15.+CHSC1(7)/35.+CHSC1(9)/63.0)
            D=(C+(A-B)*RT21+B*RT31C+RTC*(1.0-A-B*RT1)      -RT2)/RTD
      DO 30 J=1,11
      SC1(J)=D
      DO 31 N=1,9
   31   SC1(J)= SC1(J)+CHSC1(N)*CHEB(2*N-1,J)
   30 SC2(J)= SC(J) -SC1(J)
      CHSC1(1)=CHSC1(1)+D
C
C ------  T(J) IS THE CALCULATED U1 FOR
```

```
C          THE NEXT ITERATION
C
      DO 40 J=2,11
      T(J)=-(Q(J)+ U2(J)* SC2(J))/ SC1(J)
   40 T1(J)=ABS(T(J)- U1(J))
      DO 55 J=2,11
      T2=(ABS(T(J)+  U1(J)))*0.001
      IF(T1(J).GT.T2)GO TO 51
   55 CONTINUE
      GO TO 52
   51 NTEST=NTEST+1
      IF(NTEST.GT.50)GO TO 60
C
C ------  REPETITIVE SUBSTITUTION
C
      DO 53 J=2,11
   53 U1(J)=T(J)
      GO TO 70
   60 ICHECK=2
   52 RETURN
      END
      SUBROUTINE XMY(X,Y,Z,N1,N2)
C
C ------ SUBROUTINE FOR MULTIPLYING TWO POLYNOMIALS
C
      DIMENSION X(20),Y(20),Z(20)
      N3=N1+N2-1
      DO 10 I=1,N3
      Z(I)=0.0
      I1=I
      IF(I1.GT.N1)I1=N1
      I2=1
      IF(I.GT.N2)I2=I-N2+1
      DO 20 J=I2,I1
   20 Z(I)=Z(I)+X(J)*Y(I-J+1)
   10 CONTINUE
      RETURN
      END
        6400 END OF RECORD
```

CDTOT 0388

F.3 PROGRAM TST (INPUT,OUTPUT,TAPE5=INPUT,TAPE6=OUTPUT)

```
      COMMON/SU1/CHFB(20,11),CHSC1(9),D(11),RTC,RTD,RT1,RT12,RT2,RT21,
     1RT31C,SC(11),SC1(2,11),SC2(11),U1(11),U12(11),U2(11),XHP(11),X20(1
     21),CON1(8),X(9),X1(11)
      DIMENSION CDH(2,6),CH(2,6),      CHU(9),CP(5),CQ(10),CSC(10)
     1 ,CTSC(10) ,CTSC1(2,11),      DP(11),DTP(11),H(11),P(11),R(11),
     2RP(11,20),DX(5),     TFST( 11),          TITLE(12),T1(20),T2(20),
     3T3(20),T4(20),USC1(11),XDH(4,6),XDN5(10),XDN6(10),XDN9(10),XN1(10)
     4,XN2(10),X16(11),CD2R(9),D2R(11),DU(11),CDU(9)
      DIMENSION ZH(6),ZP(5),ZDH(6),OBJ(4),QDH(4,4),OB(4),XSM(4)
   97 FORMAT(1H1)
   98 FORMAT(3I5)
   99 FORMAT(12A6)
  100 FORMAT(7F11.6)
  101 FORMAT(//* JETA = *,F8.4,*  CH = *,6F12.6)
  102 FORMAT(16X,*  CP = *,5F12.6,3X,*  RR = *,F12.6)
  103 FORMAT(16X,* CDH = *,6F12.6)
  104 FORMAT(*   H = *,11F10.5)
  105 FORMAT(*   P = *,11F10.5)
  106 FORMAT(*  U1 = *,11F10.5)
  107 FORMAT(*  U2 = *,11F10.5)
  108 FORMAT(* SC1 = *,11F10.5)
  109 FORMAT(* SC2 = *,11F10.5)
    1 FORMAT(*  RUPTURE  *)
    2 FORMAT(*  NEGATIVE CONCN  *)
    3 FORMAT(//* ------------------------------------------------ */12
     1A6//)
    4 FORMAT(*  PHYS PROPS          *,5F12.6)
    5 FORMAT(*  PARAMETERS         *,5F12.6)
    6 FORMAT(*  RD (CM)            *,F12.6/
     1       * ------------------------------------------------ *//)
    7 FORMAT(*  NOCONVERGENCE IN U1 *)
    8 FORMAT(*  NO CONVERGENCE IN CDH *)
    9 FORMAT(* R = *,11F10.5//)
C     ++++++++++++++++++++++++++++++++++++++++++++++++++++++++++++++++++
C     +                                                                +
C     +  ------ PREDICTION OF FILM THINNING                           +
C     +          SEQUENCE OF INITIAL CONDITION  PROBLEMS              +
C     +                                                                +
C     ++++++++++++++++++++++++++++++++++++++++++++++++++++++++++++++++++
C
C
C     ******************************************************************
C     *                                                                *
C     *  ------  INPUT TO BE READ IN  ------                           *
C     *                                                                *
C     *  -- NDAT              NO OF SETS OF PARAMETERS                 *
C     *       NPO             OUTPUT IS PRINTED OUT EVERY              *
C     *                         NPO*DT SECONDS                         *
C     *  -- NTOT              MAX, ALLOWABLE NO OF ITERATIONS          *
C     *  -- DT                STEP SIZE IN TIME, .00405 RECOMMENDED    *
C     *     TEND              MAX ELAPSED TIME, SEC                    *
C     *     RD, RR            SEE I.C. PROGRAM                         *
C     *                  TOL  ACCURACY OF INTEGRATION, 0.01 IS USED    *
C     *  -- VD,DELRO,GAMA                                              *
C     *       XMU             SAME AS IN I.C. PROGRAM                  *
C     *  -- ZH(I),1 - 6       SAME AS CDH IN I.C. PROGRAM              *
C     *  -- ZP(I)1 - 5        SAME AS CP                               *
C     *  -- ZDH(I)1 - 6       SAME AS CDH,(4) AND (5) FROM I.C. PROGRAM *
```

```
C     *  -- TITLE              IDENTIFICATION CARD, COL 1 TO 72          *
C     *                        $$$$$$$$$$                                *
C     *                                  $                               *
C     *  -- U1(I)2 - 11                  $   PUNCHED CARDS               *
C     *  -- U2(I)2 - 11                  $$$  FROM                       *
C     *                                  $   I.C. PROGRAM                *
C     *  -- SC1(I)1 - 11                 $                               *
C     *  -- SC2(I)1 - 11                 $                               *
C     *  -- CTSC1(I)1 - 11               $                               *
C     *                           $$$$$$$$$$                             *
C     *                                                                  *
C     ********************************************************************
C
      ICON=1
      CON1(1)=0.25
      CON1(2)=-0.375
      CON1(3)=5.0/24.0
      CON1(4)=-7.0/48.0
      CON1(5)=9.0/80.0
      CON1(6)=-11.0/120.0
      CON1(7)=13.0/168.0
      CON1(8)=-15.0/224.0
      X1(1)=0.0
      U1(1)=0.0
      U2(1)=0.0
      U12(1)=0.0
C
C ++++++  READING IN INPUT  ++++++
C
      READ(5,98)NDAT,NPO
      READ(5,98)NTOT
      READ(5,100)(R(I),I=1,11)
      READ(5,100)DT,TEND,RD,ZR,TOL
      READ(5,100)VD,DELRO,GAMA,XMU
      READ(5,100)( ZH(I),I=1,6)
      READ(5,100)(ZP(I),I=1,5)
      READ(5,100)(ZDH(I)  ,I=1,6)
      DO 200 IDAT=1,NDAT
      RR=ZR
      DO 13 I=1,5
      DX(I)=0.05
      CP(I)=ZP(I)
      CDH(1,I)=ZDH(I)
   13 CH(1,I)=ZH(I)
      CDH(1,6)=ZDH(6)
      CH(1,6)=ZH(6)
      IT=1
      XDH(1,5)=CDH(1,5)
      XDH(1,6)=CDH(1,6)
      READ(5,99)(TITLF(I),I=1,12)
      WRITE(6,97)
      READ(5,100)BET,DN9,DN7,RK3,DIFFS
      READ(5,100)(U1(I),I=2,11)
      READ(5,100)( U2(I),I=2,11)
      READ(5,100)(SC1(1,I),I=1,11)
      READ(5,100)( SC2(I),I=1,11)
      READ(5,100)(CTSC1(1,I),I=1,11)
C ------  PRINTING INPUT  ------
      WRITE(6,3)(TITLE(I),I=1,12)
```

```
      WRITE(6,4)VD,DELRO,GAMA,XMU,RR
      WRITE(6,5)BET,DN9,DN7,RK3,DIFFS
      WRITE(6,6)RD
      WRITE(6,9)(R(I),I=1,11)
C
C ++++++  CALCULATION OF CONSTANTS  ++++++
C
      F=VD*DELRO*981.0
      PHI=F/(1314.7*RD*RD)
      DROPR=(VD/4.1888888)**0.33333333
      DN=RD*RD/DROPR*1.0E+5
      DN1=1.0E+7*RD*RD/GAMA
      DN4=1.0E-8/(12.0*XMU*RD*RD)
      DN5=0.01/RD
      DN6=DIFFS/RD/RD
      DN9=1000.0*DN9
      DN10=XMU*RD*1.0E+6
      DN12=RK3
      X11=-2.0/DN1
      X12=-8.0/DN1
      X13=-DN1/18.0
      X14=-DN1/32.0
      X15=DN/DN1
      X19=2.0/DN5
      X21=-DN1/50.0
      DN109=DN9/DN10
      DN71=DN7+1.0
      DT05=DT/2.0
      DO 90 N=1,10
      XN=N
      XN1(N)=XN+1.0
      XN2(N)=2.0*XN
      XDN6(N)=4.0*XN*XN*DN6
      XDN9(N)=DN9*XN2(N)
   90 XDN5(N)=DN5*XN2(N)
      DO 10 I=1,11
      U12(I)=U1(I)+U2(I)
C
C ------  CALCN OF POWERS OF R, AND CHEBYSEV POL.
C
      RP(I,1)=R(I)
      DO 10 N=2,19
   10 RP(I,N)=RP(I,N-1)*R(I)
      DO 15 J=1,11
      H(J)=CH(1,1)+CH(1,2)*RP(J,2)+CH(1,3)*RP(J,4)+CH(1,4)*RP(J,6)+CH(1,
     15)*RP(J,8)+CH(1,6)*RP(J,10)
      CHEB(1,J)=1.0
      CHEB(2,J)=R(J)
      DO 15 N=2,18
   15 CHEB(N+1,J)=2.0*R(J)*CHEB(N,J)-CHEB(N-1,J)
      TETA=-DT
      MOP=NPO
C
C ++++++  THE START OF CALCULATION  ++++++
C
   20 TETA=TETA+DT
C
C ++++++  PRINTING OUT RESULTS  ++++++
```

```
      IF(MOP.NE.NPO)GO TO 300
      MOP=0
      DO 140 I=1,11
  140 P(I)=CP(1)+CP(2)*PP(I,2)+CP(3)*RP(I,4)+CP(4)*RP(I,6)+CP(5)*RP(I,8)
      WRITE(6,101)TETA,(CH(1,N),N=1,6)
      WRITE(6,102)(CP(N),N=1,5),RP
      WRITE(6,103)(CDH(1,I),I=1,4),(XDH(IT,J),J=5,6)
      WRITE(6,104)(H(I),I=1,11)
      WRITE(6,105)(P(I),I=1,11)
      WRITE(6,106)(U1(I),I=1,11)
      WRITE(6,107)(U2(I),I=1,11)
      WRITE(6,108)(SC1(I),I=1,11)
      WRITE(6,109)(SC2(I),I=1,11)
  300 MOP=MOP+1
      IF(TETA.GT.TEND)GO TO 200
C
C ++++++ START OF ITERATION  ++++++
C
      NIT=0
      IT=1
      DO 44 N=1,4
      NAL=5-N
   44 QDH(1,NAL)=CDH(1,N)
   40 NV=1
      XDH(1,1)=QDH(1,1)
   50 GO TO (41,42,43,46)NV
   41 XDH(IT,2)=QDH(1,2)
      XDH(IT,3)=QDH(1,3)
      XDH(IT,4)=QDH(1,4)
      GO TO 45
   42 XDH(IT,1)=QDH(2,1)
      XDH(IT,3)=QDH(1,3)
      XDH(IT,4)=QDH(1,4)
      GO TO 45
   43 XDH(IT,1)=QDH(2,1)
      XDH(IT,2)=QDH(2,2)
      XDH(IT,4)=QDH(1,4)
      GO TO 45
   46 XDH(IT,1)=QDH(2,1)
      XDH(IT,2)=QDH(2,2)
      XDH(IT,3)=QDH(2,3)
C ------ FILM THICKNESS AND PRESSURE  ------
   45 DO 60 N=1,4
      NAL=5-N
   60 CH(2,N)=CH(1,N)+DT05*(CDH(1,N)+XDH(IT,NAL))
      CP(1)=X11*CH(2,2)+X15
      CP(2)=X12*CH(2,3)
      CP(3)=CH(2,4)/X13
C
C ++++++  CALCN OF OTHER COEFFTS FROM PRESSURE B.C.
C          APPENDIX D.1
C
      CALL BC(CP,RR,RR2,RR4,RR6,PHI,IND)
      IF(IND.EQ.2)GO TO 200
      CH(2,5)=CP(4)*X14
      CH(2,6)=CP(5)*X21
      DTP(1)=X11*XDH(IT,3)
      DTP(2)=X12*XDH(IT,2)
```

```
      DTP(3)=XDH(IT,1)/X13

      DTP(4)=-4.0/RR6*(4.0*DTP(1)+1.5*DTP(2)*RR2+DTP(3)*RR4/1.5)
      DTP(5)=5.0/RR6/RR2*(3.0*DTP(1)+DTP(2)*RR2+DTP(3)*RR4/3.0)
      XDH(IT,5)=X14*DTP(4)
      XDH(IT,6)=DTP(5)*X21
      RT=BET*RR
C ------  (U1 +U2 )  ------
      DO 70 I=1,11
      DP(I)=2.0*CP(2)*RP(I,1)+4.0*CP(3)*RP(I,3)+6.0*CP(4)*RP(I,5)+
     18.0*CP(5)*RP(I,7)
      H(I)=CH(2,1)+CH(2,2)*RP(I,2)+CH(2,3)*RP(I,4)+CH(2,4)*RP(I,6)+CH(2,
     15)*RP(I,8)+CH(2,6)*RP(I,10)
      X16(I)=0.5*DP(I)*H(I)
      X17=H(I)*H(I)
      X18=0.5*XDH(IT,4)*RP(I,1)+0.25*XDH(IT,3)*RP(I,3)+XDH(IT,2)*RP(I,5)
     1/6.0+XDH(IT,1)*RP(I,7)/8.0+0.1*XDH(IT,5)*RP(I,9)+XDH(IT,6)*RP(I,11
     2)/12.0
   70 U12(I)=X19*(DN4*DP(I)*X17-X18/H(I))
C
C ++++++  RATE OF CHANGE OF SUM OF SAA CONCN -- CH. 4.2.2.3, APP. D-2.1,
C ++++++  SUM OF SAA CONCN -- CH.4.2.2.2., APP. D-2.1, 2.3
C
      T1(1)=2.0*CP(2)
      T1(2)=4.0*CP(3)
      T1(3)=6.0*CP(4)
      T1(4)=8.0*CP(5)
      DO 80 N=1,6
   80 T2(N)=CH(2,N)
      CALL XMY(T1,T2,T3,4,6)
      DO 81 N=1,9
   81 CSC(N+1)=-T3(N)/XDN9(N)
      T1(1)=2.0*DTP(2)
      T1(2)=4.0*DTP(3)
      T1(3)=6.0*DTP(4)
      T1(4)=8.0*DTP(5)
      CALL XMY(T1,T2,T3,4,6)
      T1(1)=2.0*CP(2)
      T1(2)=4.0*CP(3)
      T1(3)=6.0*CP(4)
      T1(4)=8.0*CP(5)
      DO 82 N=1,4
      NAL=5-N
   82 T2(N)=XDH(IT,NAL)
      T2(5)=XDH(IT,5)
      T2(6)=XDH(IT,6)
      CALL XMY(T1,T2,T4,4,6)
      DO 83 N=1,9
   83 CTSC(N+1)=-(T3(N)+T4(N))/XDN9(N)
C ------ VALUE AT R=0 FROM SAA B.C. ---
      RT2=RT*RT
      RT1=RT-1.0
      RT12=RT1*RT1
      RT21=RT2-1.0
      RT31C=(RT*RT2-1.0)/1.5
      RTC=(-1.0+RT2*(6.0+RT*(-8.0+3.0*RT)))/6.0/RT12
      RTD=RTC-RT2
      PHI3=0.0
      DPHI3=0.0
```

```
      ZA=0.0
      ZB=0.0
      DZA=0.0
      DZB=0.0
      DO 84 N=1,9
      PHI3=PHI3+CSC(N+1)/XN1(N)
      DPHI3=DPHI3+CTSC(N+1)/XN1(N)
      ZA=ZA+CSC(N+1)
      DZA=DZA+CTSC(N+1)
      ZB=ZB+CSC(N+1)*XN2(N)
   84 DZB=DZB+CTSC(N+1)*XN2(N)
      CSC(1)=(PHI3+(ZA-ZB)*RT21+ZB*RT31C+RTC*(DN71-ZA-ZB*RT1)      -RT2*
     1DN71)/RTD
      CTSC(1)=(DPHI3+(DZA-DZB)*RT21+DZB*RT31C+RTC*(-DZA-DZB*RT1))/RTD
      DO 85 I=1,11
      SC(I)=CSC(1)
      XHP(I)=X16(I)/DN9
      X20(I)=H(I)*DN109
      DO 85 N=2,10
   85 SC(I)=SC(I)+CSC(N)*RP(I,2*N-2)
C
C +++++++  CALCN OF THE RHS OF EQ. D-53, 51
C           CQ == U1*SC1+U2$SC2 , IF U1 IS CORRECTLY CHOSEN.
C
      CQ(1)=CTSC(1)-DN12*(DN71-CSC(1))-XDN6(1)*CSC(2)
      DO 86 N=2,9
   86 CQ(N)=CTSC(N)+DN12*CSC(N)-XDN6(N)*CSC(N+1)
      CQ(10)=CTSC(10)+DN12*CSC(10)
      DO 88 N=1,10
   88 CQ(N)= CQ(N)/XDN5(N)
      DO 87 I=1,11
      Q(I)=0.0
      DO 87 N=1,10
   87 Q(I)=Q(I)+CQ(N)*RP(I,2*N-1)
C
C +++++++ INITIAL CONDITION PROBLEM AT TETA+DT
C ------- CALCULATION OF U1,U2,SC1,SC2  ------
C
      CALL FU1(ICHECK)
      IF(ICHECK.EQ.2)GO TO 126
C
C ++++++  TESTING IF THE CORRECT RATE OF THINNING
C          HAS BEEN CHOSEN AT TETA+DT
C ------  IS SAA MASS BALANCE SATISFIED  ------
C
C
C ------ CALCN RATE OF CHANGE OF SC1 AT TETA+DT - APP.D-3.1 **
C
      DO 30 N=1,9
      CHU(N)=0.0
      DO 31 J=1,11
   31 CHU(N)=CHU(N)+2.0*U1(J)*CHEB(2*N,J)
   30 CHU(N)=CHU(N)/10.5
      XNN=34.0
      CDU(9)=34.0*CHU(9)
      DO 32 N=1,7
      NN=9-N
      XNN=XNN-4.0
```

```
   32 CDU(NN)=XNN*CHU(NN)+CDU(NN+1)
      CDU(1)=0.5*CDU(2)+CHU(1)
      CD2R(8)=30.0*X(8)
      XNN=30.0
      DO 33 N=1,6
      NN=8-N
      XNN=XNN-4.0
   33 CD2R(NN)=CD2R(NN+1)+XNN*X(NN)
      CD2R(1)=0.5*CD2R(2)+X(1)
      CD2R(9)=0.0
      DO 34 J=1,11
      DU(J)=0.0
      D2R(J)=0.0
      DO 34 N=1,9
      DU(J)=DU(J)+CDU(N)*CHEB(2*N-1,J)
   34 D2R(J)=D2R(J)+CD2R(N)*CHEB(2*N-1,J)
      DO 35 J=2,11
   35 CTSC1(2,J)=DN12*(1.0-SC1(2,J))+DN6*(X1(J)/R(J)+D2R(J))-DN5*(U1(J)*
     1(SC1(2,J)/R(J)+X1(J))+SC1(2,J)*DU(J))
      CTSC1(2,1)=DN12*(1.0-SC1(2,1))+2.0*(DN6*D2R(1)-DN5*SC1(2,1)*DU(1))
      DO 120 N=1,11
  120 TEST(   N)= SC1(1,N)+DT05*(CTSC1(1,N)+CTSC1(2,N))
      DO 121 J=1,11
      IF(ABS(TEST(J)-SC1(2,J)).GT.0.002)GO TO 122
C
C ++++++ 122 -- MINIMIZATION PROGRAM -
C
  121 CONTINUE
C
C ++++++  SOLUTION AT TETA+DT HAS BEEN FOUND  ++++++
C
C ------ TESTING FOR RUPTURE AND NEGATIVE SAA CONCN ------
  473 DO 123 I=1,11
      IF(H(I).LT.0.1)GO TO 124
      IF(SC1(2,I).LT.0.0.OR.SC2(I).LT.0.0)GO TO 125
  123 CONTINUE
C ------  SETTING BACK TETA=TETA+DT  ------
      DO 130 N=1,11
      CTSC1(1,N)=CTSC1(2,N)
  130 SC1(1,N)=SC1(2,N)
      CH(1,5)=CH(2,5)
      CH(1,6)=CH(2,6)
      DO 131 N=1,4
      CH(1,N)=CH(2,N)
      NAL=5-N
  131 CDH(1,N)=XDH(IT,NAL)
      ICON=1
C ------  MOVE TO THE NEXT TIME INTERVAL  ------
      GO TO 20
C ------  TERMINATION OF PROGRAM BEFORE TEND  ------
  124 WRITE(6,1)
      GO TO 200
  125 WRITE(6,2)
      GO TO 200
  126 WRITE(6,7)
      WRITE(6,103)(XDH(IT,N),N=1,6)
      WRITE(6,106)(U1(N),N=1,11)
      WRITE(6,108)(SC1(2,N),N=1,11)
```

```
      GO TO 200
  127 WRITE(6,8)
      GO TO 200
C
C ++++++ START OF MINIMIZATION -- CH.4.2.3, APP. D-3.2 ++
C
  122 OBJ(IT)=0.0
      DO 400 J=1,11
      SS=(TEST(J)-SC1(2,J))*100.0
  400 OBJ(IT)=OBJ(IT)+SS*SS
      GO TO (600,473,603,606,605)ICON
  600 IF(IT.EQ.1.AND.NV.EQ.1)OBJ(1)=OBJ(1)
      GO TO(410,411,412,413)IT
  410 IT=2
      XDH(2,NV)=XDH(1,NV)+DX(NV)
      GO TO 50
  411 IF(OBJ(1).LT.OBJ(2))GO TO 420
  421 IT=3
      XDH(3,NV)=3.0*XDH(2,NV)-2.0*XDH(1,NV)
      GO TO 50
  420 TEM1=XDH(1,NV)
      TEM2=OBJ(1)
      XDH(1,NV)=XDH(2,NV)
      OBJ(1)=OBJ(2)
      XDH(2,NV)=TEM1
      OBJ(2)=TEM2
      GO TO 421
  412 IF(OBJ(3).GT.OBJ(2))GO TO 430
      XDH(1,NV)=XDH(2,NV)
      OBJ(1)=OBJ(2)
      XDH(2,NV)=XDH(3,NV)
      OBJ(2)=OBJ(3)
      GO TO 421
  430 IT=4
      XDH(4,NV)=(XDH(2,NV)+XDH(3,NV))/2.0
      GO TO 50
  413 S=XDH(2,NV)-XDH(1,NV)
      IF(OBJ(1).GT.OBJ(3))GO TO 440
      I1=1
      I2=2
      I3=4
  441 SM=S*(OBJ(I1)-OBJ(I3))/2.0/(OBJ(I1)+OBJ(I3)-2.0*OBJ(I2))
      IF(ABS(SM).LT.TOL)GO TO 450
      XDH(1,NV)=XDH( I2,NV)
      OBJ(1)=OBJ(I2)
      IT=2
      XDH(2,NV)=XDH( I2,NV)+SM
      GO TO 50
  440 I1=2
      I2=4
      I3=3
      GO TO 441
  450 XDH(2,NV)=XDH( I2,NV)+SM
      DX(NV)=SM
      IF(ABS(DX(NV)).LT.TOL )DX(NV)=TOL
      GO TO (460,461,463,462)NV
  460 NV=2
      IT=1
```

```
      GO TO 50
  461 NV=3
      IT=1
      GO TO 50
  463 NV=4
      IT=1
      GO TO 50
  462 DO 471 N=1,4
      IF(ABS(QDH(1,N)-QDH(2,N)).GT.TOL)GO TO 472
  471 CONTINUE
      ICON=2
      GO TO 480
  472 NIT=NIT+1
      IF(NIT.GT.NTOT)GO TO 127
      ICON=3
  480 DO 474 N=1,4
  474 XDH(1,N)=QDH(2,N)
      IT=1
      GO TO 45
  603 OB(2)=OBJ(1)
  830 DO 700 N=1,4
      QDH(3,N)=3.0*QDH(2,N)-2.0*QDH(1,N)
  700 XDH(1,N)=QDH(3,N)
      IT=1
      ICON=4
      GO TO 45
  604 OB(3)=OBJ(1)
      IF(OB(3).LT.OB(2))GO TO 800
      DO 810 N=1,4
      QDH(4,N)=(QDH(2,N)+QDH(3,N))/2.0
  810 XDH(1,N)=QDH(4,N)
      ICON=5
      IT=1
      GO TO 45
  800 DO 820 N=1,4
      QDH(1,N)=QDH(2,N)
  820 QDH(2,N)=QDH(3,N)
      OB(1)=OB(2)
      OB(2)=OB(3)
      GO TO 830
  605 OB(4)=OBJ(1)
      IF(OB(1).GT.OB(3))GO TO 840
      I1=1
      I2=2
      I3=4
  841 DO 850 N=1,4
      XSM(N)=(QDH(2,N)-QDH(1,N))*(OB(I1)-OB(I3))/2.0/(OB(I1)+OB(I3)-2.0*
     1OB(I2))
  850 QDH(1,N)=QDH(I2,N)+XSM(N)
      IT=1
      ICON=1
      GO TO 49
  840 I1=2
      I2=4
      I3=3
      GO TO 841
  200 CONTINUE
      STOP
```

```
      END
      SUBROUTINE FU1(ICHECK)
C
C ++++++ REPETITIVE SUBSTITUTION FOR
C        CALCULATING U1  -- APP. D-2.4 ++
C
      COMMON/SU1/CHEB(20,11),CHSC1(9),Q(11),RTC,RTD,RT1,RT12,RT2,RT21,
     1RT31C,SC(11),SC1(2,11),SC2(11),U1(11),U12(11),U2(11),XHP(11),X20(1
     21),CON1(8),X(9),X1(11)
      DIMENSION J(11),T1(11)
      ICHECK=1
      NTEST=0
   70 DO 10 I=2,11
      U2(I)=U12(I)-U1(I)
   10 X1(I)=-(  U1(I)-  U2(I))/X20(I)-XHP(I)
      DO 20 N=1,8
      X(N)=0.0
      DO 21 J=1,11
   21 X(N)=X(N)+2.0*X1(J)*CHEB(2*N,J)
   20 X(N)=X(N)/10.5
      A=(X(1)-X(2))/2.0+(X(3)-X(4))/6.0+(X(5)-X(6))/10.0+(X(7)-X(8))/14.
      B=X(1)+X(2)+X(3)+X(4)+X(7)+X(5)+X(6)+X(8)
      CHSC1(1)=0.0
      DO 25 N=1,8
   25 CHSC1(1)=CHSC1(1)+CON1(N)*X(N)
      XN=0.0
      DO 26 N=2,8
      XN=XN+4.0
   26 CHSC1(N)=(X(N-1)-X(N))/XN
      CHSC1(9)=X(8)/32.0
      C=CHSC1(1)-(CHSC1(3)/3.+CHSC1(5)/15.+CHSC1(7)/35.+CHSC1(9)/63.0)
            D=(C+(A-B)*RT21+B*RT31C+RTC*(1.0-A-B*RT1)     -RT2)/RTD
      DO 30 J=1,11
      SC1(2,J)=D
      DO 31 N=1,9
   31 SC1(2,J)=SC1(2,J)+CHSC1(N)*CHEB(2*N-1,J)
   30 SC2(J)=  SC(J)-SC1(2,J)
      CHSC1(1)=CHSC1(1)+D
      DO 40 J=2,11
      T(J)=-(Q(J)+  U2(J)*  SC2(J))/SC1(2,J)
   40 T1(J)=ABS(T(J)-  U1(J))
      DO 55 J=2,11
      T2=(ABS(T(J)+  U1(J)))*0.001
      IF(T1(J).GT.T2)GO TO 51
   55 CONTINUE
      GO TO 52
   51 NTEST=NTEST+1
      IF(NTEST.GT.50)GO TO 60
      DO 53 J=2,11
   53 U1(J)=T(J)
      GO TO 70
   60 ICHECK=2
   52 RETURN
      END
      SUBROUTINE XMY(X,Y,Z,N1,N2)
C
C MULTIPLICATION OF TWO POLYNOMIALS
C
```

```
      DIMENSION X(20),Y(20),Z(20)
      N3=N1+N2-1
      DO 10 I=1,N3
      Z(I)=0.0
      I1=I
      IF(I1.GT.N1)I1=N1
      I2=1
      IF(I.GT.N2)I2=I-N2+1
      DO 20 J=I2,I1
   20 Z(I)=Z(I)+X(J)*Y(I-J+1)
   10 CONTINUE
      RETURN
      END
      SUBROUTINE BC(XX,PP,RR2,RR4,RR6,PHI,IND)
C
C ++++++ SOLUTION OF PRESSURE B.C. -- APP. D-1 PP
C ++++++ SOLUTION OF PRESSURE B.C. -- APP. D-1 ++
C
      DIMENSION XX(5)
  200 FORMAT(* BC --- *,7F12.6)
      NIT=0
      IND=1
      A0=XX(1)
      A2=XX(2)
      A4=XX(3)
      RR2=RR*RR
  120 RR4=RR2*RR2
      RR6=RR2*RR4
      FR=0.6*A0*RR2+0.15*A2*RR4+A4/30.*RR6-PHI
      IF(ABS(FR).LT.0.0000001)GO TO 100
      DFR=0.6*A0+0.3*A2*RR2+0.1*A4*RR4
      RNEW=RR2-FR/DFR
      IF(ABS(RNEW-RR2).LT.0.00001)GO TO 100
      NIT=NIT+1
      IF(NIT.GT.30)GO TO 110
      RR2=RNEW
      GO TO 120
  110 IND=2
      WRITE(6,200)(XX(J),J=1,3),RR2,FR,DFR,RR
      GO TO 130
  100 IF(RR2.LT.0.0)GO TO 110
      RR=SQRT(RR2)
      XX(4)=-(4.0*A0/RR4+3.0/RR2*A2+2.0*A4)/RR2
      XX(5)=(3.0*A0/RR4+2.0*A2/RR2   +A4)/RR4
  130 RETURN
      END
         6400 END OF RECORD
```

CDTOT 0628